Vibration and torsion-facilitated interactions in *para-* and *meta*-disubstituted benzenes

David Joseph Kemp

Thesis submitted to the University of Nottingham for the degree of Doctor of Philosophy

May 2020

I.   Abstract:

Intramolecular vibrational (energy) redistribution (IVR) has been a point of discussion in monosubstituted and *para*-disubstituted benzene molecules for some time, with studies drawing comparisons between related molecules in order to understand the factors that influence the rate at which coupling between vibrational and torsional coordinates is seen. The presence of the methyl rotor, such as in *para*-fluorotoluene, greatly increases the number of available internal energy levels such that the rate of IVR is expected to increase. It has been suggested, however, that the density of states is not the only factor that causes increased rates of coupling, but small differences in quantum numbers, and thus similarity in character between two states, must also be observed for efficient coupling to occur. Further to this, barriers to internal rotation can be shown to directly affect the positions of the rotor levels, with electronic structure differences between molecules also expected to induce additional changes to vibrational or torsional levels. The expected result of this is that these levels may shift further from, or closer to other levels that may efficiently couple to them.

A combination of photoionisation, photoelectron and fluorescence techniques are employed to record electronic spectra *via* a number of excited intermediates of three molecules: *para*-fluorotoluene, *meta*-fluorotoluene and *meta*-chlorotoluene. Use of these techniques allows one to probe and understand any interactions occurring between levels, mainly in the S_1 excited state, although potential interactions in other states can also be unpicked. A number of energetic regions of the $S_1 \leftarrow S_0$ transition in *p*FT are studied, allowing one to deduce how the coupling evolves as a function of energy, as well gaining insight into how the character of the vibrations and torsions involved in these interactions affects the efficiency of the observed interactions. Further to this, low energetic regions of the S_1 state for both *m*FT and *m*ClT are discussed, allowing one to gain gauge the changes in torsion-facilitated interactions as a function of not only energy, but also of electronic and mass related properties.

II.   Publications covered in this thesis:

1. "Unravelling overlaps and torsion facilitated coupling using two-dimensional laser-induced fluorescence", **D.J. Kemp**, A.M. Gardner, W.D. Tuttle and T.G Wright, *Mol. Phys.*, 2019, **117**, 3011–3026.

2. "Complexity surrounding an apparently simple Fermi resonance in *p*-fluorotoluene revealed using two-dimensional laser-induced fluorescence (2D-LIF) spectroscopy", **D.J. Kemp**, L.E. Whalley, A.M. Gardner, W.D. Tuttle, L.G. Warner and T.G. Wright, *J. Chem. Phys* **150** (6) 064306 (2019).

3. "Observation of the onset of torsion-induced, mode-specific dissipative intramolecular vibrational redistribution (IVR)", **D.J. Kemp**, W.D. Tuttle, A.M. Gardner, L.E. Whalley and T.G Wright, *J. Chem. Phys* **151** (6) 064308 (2019).

4. "Vibration-modified torsional potentials and vibration-torsion levels in the *m*-fluorotoluene cation", **D.J. Kemp**, E.F. Fryer, A.R Davies and T.G. Wright, J. *Chem. Phys. J. Chem. Phys* **151** (8) 084311 (2019).

5. "Torsions, low-frequency vibrations and vibration-torsion ("vibtor") levels in the *m*-chlorotoluene cation", **D.J. Kemp**, L.G. Warner and T.G. Wright, *J. Chem. Phys.*, 2020, **152**, 064303.

III. Publications not covered in this thesis:[1]

1. "Consistent assignment of the vibrations of symmetric and asymmetric ortho-disubstituted benzenes" W.D. Tuttle, A.M. Gardner, A. Andrejeva, **D.J. Kemp**, J.C.A. Wakefield and T.G. Wright, *J. Mol. Spec.*, **344**, 46-60 (2018)

2. "Consistent assignment of the vibrations of symmetric and asymmetric meta-disubstituted benzenes" **D.J. Kemp**, W.D. Tuttle, F.M.S. Jones, A.M. Gardner, A. Andrejeva, J.C.A. Wakefield and T.G. Wright, *J. Mol. Spec.*, **346**, 46-59 (2018)

3. "Vibrations of the *p*-chlorofluorobenzene cation", **D.J. Kemp**, L.E. Whalley, W.D. Tuttle, A.M. Gardner, B.T. Speake and T.G. Wright, *Phys. Chem. Chem. Phys.,* **20**, 12503-12516 (2018)

4. "Identifying complex Fermi resonances in p-difluorobenzene using zero-electron-kinetic-energy (ZEKE) spectroscopy", **D.J. Kemp**, A.M. Gardner, W.D. Tuttle, J. Midgley, K.L. Reid and T.G. Wright, *J. Chem. Phys,* **149** (9) 094301 (2018).

5. "Effects of symmetry, methyl groups and serendipity on intramolecular vibrational energy dispersal", W.D. Tuttle, A.M. Gardner, L.E. Whalley, **D.J. Kemp** and T.G. Wright, *J. Mol. Spec,* **344**, 46-60 (2019).

6. "Identification of separate isoenergetic routes for vibrational energy flow in *p*-fluorotoluene", A.M. Gardner, L.E. Whalley, **D.J. Kemp**, W.D. Tuttle and T.G. Wright, *J. Chem. Phys.* **151** (15), 1543025 (2019)

7. "Variations in Duschinsky rotations in m-fluorotoluene and *m*-chlorotoluene during excitation and ionization", A.R. Davies, **D.J. Kemp**, L.G. Warner, E.F. Fryer, A. Rees and T.G. Wright, *J. Chem. Phys.,* Submitted (Mar 2020)

---

[1] Explicit discussion of these is not made, although reference to several of the above publications is made throughout the summary and future work.

IV.   Acknowledgements:

Table of Contents:

V. List of Figures:

VI.   List of Tables:

1. Introduction:

This thesis is part of a wider study of the electronic spectroscopy of a range of disubstituted benzenes. Here, the focus is on *para*-fluorotoluene (*p*FT), *meta*-fluorotoluene (*m*FT) and *meta*-chlorotoluene (*m*ClT) – seen in Figure 1:1. Discussion of these molecules will be focused on the vibrations of the ground (S_0), first excited (S_1) and cationic ground (D_0^+) electronic states. Five different techniques are taken advantage of to probe these states. A combination of resonance-enhanced multiphoton ionisation (REMPI) and laser-induced fluorescence (LIF) spectroscopies are used for the S_1 state; zero-electron-kinetic-energy (ZEKE) spectroscopy is used for the D_0^+ state while, for the S_0 state, two-dimensional laser-induced fluorescence (2D-LIF) and dispersed fluorescence (DF) spectroscopies are used. The details of these techniques, and their uses, will be summarised in Chapter 8.

Figure 1:1 Depictions of the three molecules of interest: *m*FT, *m*ClT and *p*FT.
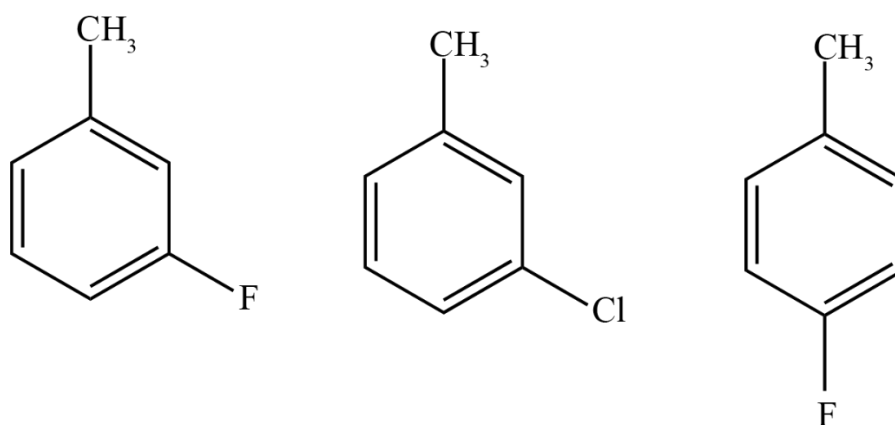
Energy dispersal occurring within molecules is a common and widely studied topic by spectroscopists, as it holds the answers of how molecules behave whilst containing significant internal energy; for example, following the absorption of electromagnetic radiation. Photophysical behaviour, such as photostability, linked to the molecule is of imperative importance for scientists to be able to understand; the survival of biological molecules has a reliance on redistributing energy that has been inputted into them, such as following interaction with ultraviolet (UV) light. If this energy cannot be re-emitted, dissipated or redistributed within a molecule, then reactive photochemistry can occur. A notable example of this is thymine dimerization[1] in DNA shown in Figure 1:2.[2] When DNA is directly exposed to UV light, and if the energy remains localized within the molecule, then the bonds between DNA bases break down, with bonds then reforming between the exposed bases as well as the sugar-phosphate backbone of the double-helix structure.[3] These are known as premutagenic lesions. If these remain uncorrected by natural DNA repair

mechanisms, it can lead to errors in the translation and transcription of new DNA and become the basis of malignant melanomas. Such damage is very common in life, so it can easily be inferred that understanding energy dispersal mechanisms is important, with this field of research acting as a foundation for potential design of new products that may protect against UV light. Current sun creams, for example, often have many problems particularly due to their low photostability as well as being moderately toxic,[4] and spectroscopic research can provide new insight into which molecular systems can alleviate these issues.

Figure 1:2: Schematic depicting the process of dimerization between two thymine bases as a result of ultraviolet impingement. Note that this figure is extracted from Ref (2).
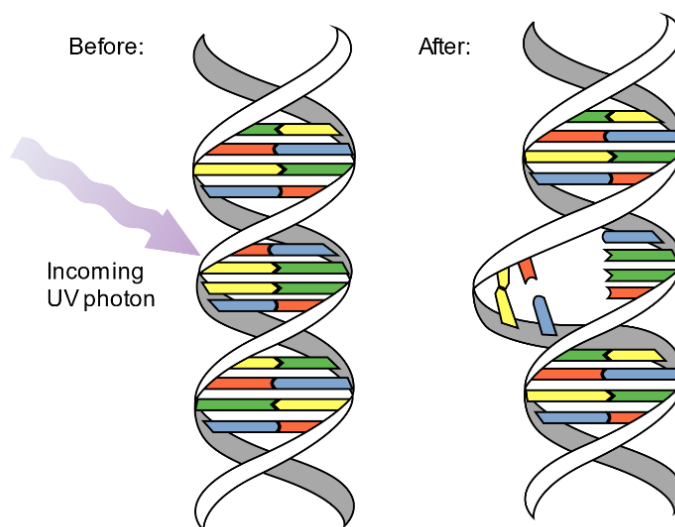
We can begin to understand how large biomolecules interact with high-energy electromagnetic radiation, usually by both mapping out the structure of, and modelling the energetic dynamics of the system. Many of these molecules, such as amino acids, nucleic acids and, to a wider extent, proteins are, however, complex in nature and difficult to understand spectroscopically.

One way around this is to study these molecules with a bottom-up approach. If one isolates individual parts of a large molecule then, in theory, one can try to understand how certain functional groups interact with other parts of the molecule it is connected to. These groups can then be modified, with the properties of each group then analysed in turn. From here, it may then be possible to slowly build up a picture of how more complex molecules, containing a larger number and variety of different groups, present their physical properties. Many biomolecules contain aromatic systems, with these playing a vital role in nature, thus it makes some sense to begin by exploring simple aromatic molecules, such as benzenes.

These molecules have several properties which make them an appropriate choice for this field of study, namely:

(i) They are usually spectroscopically bright, and consequently using the techniques previously mentioned, it is often straightforward to observe the transitions of interest.

(ii) The energy regions of interest are easily accessible with standard spectroscopic equipment (roughly 240–350 nm radiation).

(iii) The design of substituted benzenes is very versatile – there are large numbers of possible substituents that can be attached to the ring, as well as several different positions they can be attached at. More complicated structures can also be created with the ring as a foundation. This allows one to infer the effects of mass, electronic and steric interactions separately as a function of the substituent itself, as well as its location on the ring.

(iv) The energy levels and electronic transitions of a number of simple ring systems are relatively well understood as a result of previous work conducted, so this knowledge can be used as a basis for understanding similar molecules – noted below.

The overarching focus of this thesis will take advantage of the properties of substituted benzenes to aid understanding in how the presence of the methyl rotor, as well as its position relative to other substituents, can have an effect on the internal energy levels of the molecule. This usually occurs through coupling with other levels, such as vibrations, where it will be shown that a number of factors influence the extent of the couplings observed. This work will be split into 5 publication sections. The first three publications will be focussed on three different energetic regions of the $S_1 \leftarrow S_0$ transition in pFT. These isolated regions of interest each have their own nuances relating to mode coupling, and these will be discussed with a focus on the role of the torsions in facilitating these interactions, with further conversation on the factors that cause efficient coupling to be observed.

Parmenter et $al.$[5] have previously discussed differences seen in the rate of energy redistribution when comparing the $sans$ methyl group molecule, $para$-difluorobenzene (pDFB), with both pFT and mFT, initially suggesting that the point group is the prime factor in deciding the rate of IVR. Furthermore, they have debated, across a number of publications,[6–10] the use of chemical timing experiments to elucidate the time-resolved properties of intramolecular vibrational (energy) redistribution (IVR). Reid et $al.$ then employed a

combination of conventional photoelectron, and later picosecond time-resolved photoelectron spectroscopy (tr-PES), to further identify and unpick rotor facilitated interactions, some of which were initially noted by Parmenter. Originally, these ideas were applied through the study of interactions in toluene,[11] and then, after this, many different energetic regions of pFT[11–15], where the wavepacket dynamics observed provided insight into a number of the previously hypothesised interactions, as well as allowing elucidation of interactions towards higher internal energies which had not previously been investigated. In the frequency domain, a series of experimental studies were completed by Ito and coworkers, who used a combination of LIF/DF[16] and ZEKE[17,18] techniques to derive torsional barriers through assignment of low-energy torsional transitions. They also compared and tried to rationalise the different torsional structure seen accompanying electronic transitions as a function of both the barrier height and phase of the torsional potential. Work towards understanding the theory behind the methyl rotor, such as the selection and intensity rules associated with the rotor energy levels was pioneered by Weisshaar et $al.$, with most of this work completed through the study of both pFT and toluene.[19–22] Later, they published a theoretical study improving upon the initial work of Ito, where they examined the reasoning behind the observed torsional barrier heights, [21] which was only discussed briefly by Ito. Work from the Wright group, through some collaboration with Reid with the use of conventional photoelectron spectroscopy, employed a combination of REMPI and ZEKE studies with the aim of understanding the specific factors that lead to increased rates of coupling, and how it is related to the methyl rotor, as well as unpicking further interactions that were not possible to see with the lower-resolution conventional photoelectron spectroscopy experiment. A range of internal energetic regions across a number of different molecules were analysed, these being toluene,[11,23,24] p-xylene,[25,26] and pFT.[11,12,27–31]

In more recent times, the Lawrance group has made use of the 2D-LIF technique in order to quantify and model couplings between vibrations, torsions and vibration-torsional combinations.[32–38] They have also provided theoretical explanations for the observation of forbidden torsional transitions, with these being previously noted by the groups mentioned above, albeit the original explanations were incomplete and did not fully explain certain transition types. The Wright group, with collaboration from Lawrance and co-workers, has used a combination of ZEKE and 2D-LIF spectroscopy to extend these ideas, and apply them to higher energetic regions to elucidate the primary factors that determine the efficiency of methyl-dependent coupling, notably for pFT[39–43], and also now mFT[44], with a number of these studies being the focus of this work. Here, we aim to probe a series of different energetic

regions of the S_1 state of pFT, with the aim of clarifying how the rate of coupling is affected by the density of states, as well as deducing if there is a degree of specificity necessary in order for coupling between states to be efficient *i.e.* do certain modes interact more efficiently than others and, if so, why?

The final two sections involve examinations of the electronic, vibrational and torsional structure seen in both mFT and mClT, with a comparison between the two molecules occurring in the second of these two publications. These molecules can be viewed as being identical in symmetry terms, but with slightly different electronic and mass properties due to the change from a fluorine to a chlorine atom, thus allowing one to ascertain the relationship between the molecular electronic and mass properties and the photobehaviour. This allows us to gain insight into how vibration-torsion coupling is modified as a function of property, compared to the modification as a function of energy seen in the pFT chapters.

Work on *meta* isomers of substituted benzenes has largely gone untouched, although Ito *et al.*[16–18] as well as Weisshaar *et al.*[45] discuss torsional barrier heights of all three electronic states of interest. Further, their discussion is accompanied by some ZEKE spectra, although these are only focused on the low internal energy regions. Similarly, Warren *et al.* have undertaken a 2D-LIF study of mFT[38] but, once again, have only covered interactions in the low energy regions. The aim of this work, with regards to the mFT and mClT molecules, is to also elucidate low-energy interactions between vibrations and torsions using the REMPI and ZEKE techniques – albeit with a focus on a number of low energy vibration-torsion combination bands not previously covered in other work. It will be seen that these will set the foundations upon which we begin to understand interactions at higher internal energies.

The following chapters first begin with an overall description of types of photophysical and energetic dispersal pathways, with specific comment on those for which this work is concerned. Throughout this thesis, the focus will be on interactions occurring specifically between electronic, vibrational and torsional coordinates. A number of scenarios within this work show that vibrational interactions can occur with or without additional interaction from torsional components, hence the theoretical background will be split into two sections with the vibrational and torsional related interactions initially treated independently, with comments later made regarding combinations of the two. The aim is to give a fundamental description of the key parts of electronic spectroscopy required to understand our data prior to presenting the publications.

We begin with a basic introduction to electronic spectroscopy, and the assumptions made in rationalising the collected data. We then discuss the forms of electronic and vibrational transitions that we expect, followed by a commentary on forbidden transitions and their origins. From there, we talk about possible interactions between the vibrational and electronic components of the molecule and what the consequences of these are, followed by a commentary of the vibrational labelling nomenclature employed in our analyses. Although what will be covered here will be adequate for understanding this thesis, the reader is encouraged to read elsewhere for a more detailed insight into the background theory of spectroscopy if interested. Herzberg[46,47] and Hollas,[48] among many others, provide a much more expansive and diverse contribution to the field. Following this, a general overview of methyl-torsion spectroscopy will then be discussed prior to a summary of experimental techniques, the advantages and disadvantages of each technique used, and some theoretical concepts related to them. The publications are then introduced, and shown, where the main body of results and discussion occurs, followed by an overall summary, and the future work that may be considered a natural direction given the conclusions from this work.

2. Photophysical pathways:

In general, understanding what happens to a molecule after absorption of a photon is the core aim for spectroscopists. If a photon strikes a molecule, and the conditions are correct, then the photon may be absorbed, with many possible outcomes. As the molecule has quantised energy levels, for a photon to be absorbed the requirement is that its energy must be an exact match with the energy gap between an initial and final energy level, which is given by:

$$hv = E' - E''$$

<div align="right">Eq. 1</div>

where, traditionally, E'' is the initial state and E' is the final (excited) state.

The main concern in this thesis will be transitions involving photons in the ultraviolet region of the electromagnetic spectrum. In this region, the photon energy is usually enough to promote an electron from a ground state valence orbital to the first unoccupied molecular orbital – termed an electronic excitation. Furthermore, simultaneous population of vibrational and rotational quanta also usually occurs during electronic excitation.

For the majority of molecules, the lowest electronic state is the S_0 state, or the ground state, where all electrons are paired and in their lowest energy configuration, according to Hund's

rules.[49] Once energy is inputted into the molecule, some of the energy becomes localised within the molecular degrees of freedom, and there are many options a molecule has in order to redistribute or remove the energy from its system. The purpose of this is to return to a stable, low energy state. A Jablonski diagram[50] showing the many photophysical pathways a molecule may access after electronic excitation is shown in Figure 2:1. Table 2-1, shown below, also summarises each of the photophysical pathways mentioned herein, each with the timescale in which they are expected to occur.

The two main umbrella terms involving energetic redistribution are radiative and non-radiative processes *i.e.* ones that involve energy loss through photon emission, and ones that involve energy loss by other means.

The two forms of radiative processes discussed are fluorescence and phosphorescence, together known a luminescence. If the multiplicity of the initial and final state is the same ($S_1 \rightarrow S_0$ or $S_3 \rightarrow S_1$ etc), this is fluorescence. If, however, the multiplicity changes between states ($T_1 \rightarrow S_0$), then it is said that phosphorescence occurs. For phosphorescence to occur, a change in spin multiplicity must occur, which is an unfavourable process. As a result of this, the triplet state lifetime is long, thus phosphorescence is often outcompeted by other, much faster, pathways.
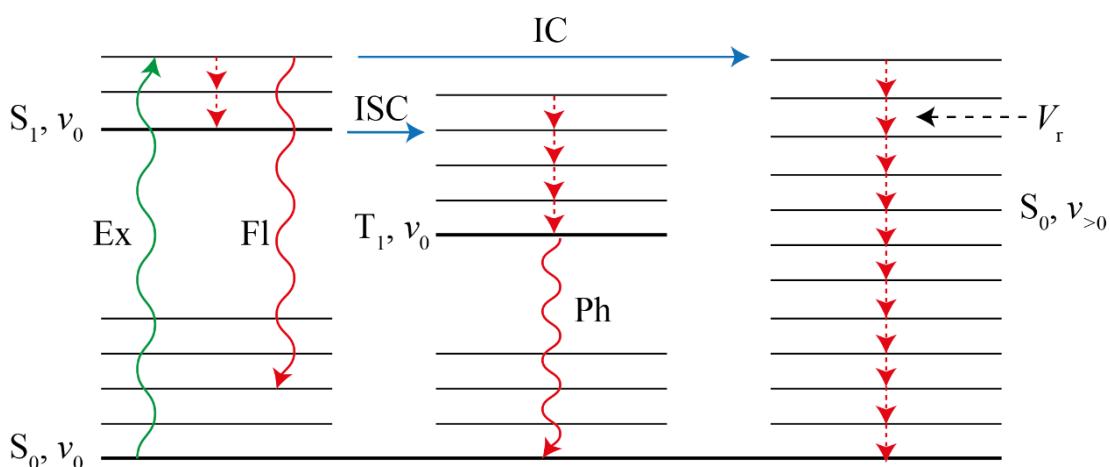
Figure 2:1: Jablonski diagram indicating examples of the types of energetic pathways after an initial photoexcitation to the S_1 state where: S_x = Singlet state, T_x = Triplet state, Ex = Photon absorption, Fl = Fluorescence, Ph = Phosphorescence, ISC = Intersystem Crossing, IC = Internal Conversion, V_r = Vibrational Relaxation. Note that wavy arrows indicate that energy is gained or lost *via* a photon, solid arrows indicate no energy is exchanged, dashed arrows indicate non-radiative energy loss (through collisions).

Non-radiative pathways dispose of energy largely through vibrational relaxation (V_r). This usually involves energy stored in vibrational degrees of freedom of one molecule being spread across a larger range of molecules in a system, largely through collisions. If, however,

a collisionless or near collisionless environment is created *e.g.* a jet expansion, energy redistribution or loss must occur by other means, usually luminescence. Although not a concern in this work, liquid or condensed phase samples often have large numbers of collisions, thus V_r is favoured with luminescence mechanisms become stymied as a result of this. Furthermore, the rate at which V_r (and IC – described below) occurs is often much faster in higher-lying electronic states compared to from the S_1 state. This is known as Kasha's rule,[51] although it will not be necessary to consider this within our studies here, as we only consider the S_1 state.

Table 2-1 - Typical rates at which certain photophysical processes occur at. Note that the scales shown do not always assume that the pathway occurs with the system in the same environment *e.g.* vibrational relaxation will occur at this speed in the liquid phase, whereas fluorescence is likely to occur at this speed in the gas phase.

Pathway	Scale/ s
Photon absorption	10^{-15}
Fluorescence	10^{-7}-10^{-9}
Phosphorescence	10^{1}-10^{-6}
Internal Conversion	10^{-10}-10^{-14}
Intramolecular vibrational (energy) redistribution	10^{-12}
Intersystem crossing	10^{-3}-10^{-8}
Vibrational relaxation	10^{-13}

Photophysical pathways can often work complementarily to open new relaxation pathways that were inaccessible after the initial excitation stage. If two vibronic levels are isoenergetic and have the same multiplicity, for example an S_1 and S_0 vibronic level, a crossing point, or conical intersection, in the potential energy surface (PES) can allow the molecule to surface hop from the S_1 to the S_0 PES . This is known as an internal conversion. Note that no energy is gained or lost in this process although, after surface hopping, excess energy is inputted into the vibrational coordinates of the S_0 state. This can then be lost *via* other pathways. Similarly, intersystem crossings may also occur which are not vastly different to internal conversions. Here, the molecule can surface hop between two isoenergetic vibronic states, albeit occurring between electronic states of different spin multiplicity. Notably, a change in spin multiplicity is an unfavourable mechanism, thus intersystem crossing is usually a significantly slower process than internal conversion.

A final non-radiative process is IVR (intramolecular vibrational (energy) redistribution), not shown on Figure 2:1. This process will be one of the main focusses of this thesis and will be described in more detail in Chapter 5. In general, if certain vibrational states appear close in energy and have the same symmetry then those states may couple, allowing energy to pass between them. The rate at which IVR is observed tends to increase as a function of the density of vibrational states, although other factors are important which are discussed later in this work. IVR is a key tool by which energy becomes dispersed among many vibrational coordinates, thus is an important mechanism which influences the photostability of a system and is therefore a key spectroscopic topic of interest.

3. Introduction to electronic spectroscopy:

3.1 The Born-Oppenheimer approximation:

In the case of diatomic and polyatomic molecules, the Hamiltonian, *H*, may be given as a sum of the kinetic and potential energy terms related to the electrons, *e*, and nuclei, *n*, shown below:

$$H = T_n + T_e + V_{nn} + V_{ee} + V_{en}$$

<div align="right">Eq. 2</div>

where T_n and T_e are the kinetic energy terms of the nuclei and electrons respectively. The V_x terms comprise the nuclear-nuclear repulsions (V_{nn}), electron-electron repulsions (V_{ee}), and the coulombic attractions between the nuclei and electrons (V_{en}).

Initially this equation is too difficult to solve as there are too many variables to consider. In 1927, Born and Oppenheimer[52] highlighted that the vibrations of the nuclei occur on a significantly slower timescale than do the electronic motions, and so (to a good approximation), one can separate the electronic parts of the Hamiltonian from the nuclear part, thus the electronic structure of the molecules can be treated with reasonable accuracy without much consideration of the nuclei. We assume, then, the positions of the nuclei are fixed *i.e.* T_n = 0 and V_{nn} is constant; this is referred to as the Born-Oppenheimer (BO) approximation. The electronic Hamiltonian may then be given as:

$$H_e = T_e + V_{ee} + V_{en}$$

<div align="right">Eq. 3</div>

Notably, the V_{en} term remains in the electronic Hamiltonian after the BO approximation is accounted for, but with this assumption the nuclei will be fixed *i.e.* the molecule is 'stuck' in a particular nuclear configuration. As a result of this, V_{en} can be considered as a parameter,

as opposed to an operator. Notably, if the nuclear motion does change, then the electrons are 'dragged' to accommodate this, and their positions change instantaneously as a function of the nuclear coordinates.

One can then solve the Schrödinger equation using the above Hamiltonian, and then combine this with the remaining terms from Eq. 2, which yields:

$$H = T_n + V_{nn} + E_e \qquad \text{Eq. 4}$$

Thus, the nuclear part of the equation remaining can be interpreted as if it involves the nuclei interacting with an effective potential defined by the electronic energy. Taking into account all of the above, we can say that the nuclear wavefunction can be assumed to be independent of the electronic coordinates, but the electronic wavefunction depends on both electronic and nuclear coordinates. As a result of this, the total wavefunction can then be separated into two components:

$$\Psi = \Psi_n(Q)\,\Psi_e(Q,q) \qquad \text{Eq. 5}$$

where Q are nuclear coordinates and q are electronic coordinates. Then, the overall energy may be given as:

$$E = E_n + E_e \qquad \text{Eq. 6}$$

Although not as good an approximation, the nuclear wavefunction can then be broken down further into subcomponents, each of which involves nuclear motion: the vibrations, rotations and torsions:

$$\Psi_n = \Psi_{vib}\Psi_{rot}\Psi_{tor} \qquad \text{Eq. 7}$$

As a result of this breakdown, the overall wavefunction can then be given as:

$$\Psi_{tot} = \Psi_{elec}\Psi_{vib}\Psi_{rot}\Psi_{tor} \qquad \text{Eq. 8}$$

Separation of the nuclear and electronic wavefunctions is incredibly useful as a basis for deriving transition selection rules involving electronic, vibrational, and torsional coordinates as well as, although not covered to a great extent in this work, rotational motion. Although convenient, breakdown of the BO approximation through coupling between electronic and nuclear motion does occur, and sometimes more in-depth treatments are required.

3.2 The Harmonic Oscillator model:

The BO approximation is useful as it allows us to treat the vibrations independently of the other nuclear motions. In doing so, and in the simplest scenario of a diatomic system, the molecule can be treated as two balls connected by a spring.

If a displacement occurs along the length of the bond, *i.e.* a stretch, it can be treated with Hooke's Law:

$$-\frac{dV(x)}{dx} = -kx \qquad \text{Eq. 9}$$

where V is the potential, k is the force constant and x is the displacement from the equilibrium bond length, r_e. Thus, the potential varies as a function of the bond displacement.

If one then integrates the above equation, the vibrational potential can be given as:

$$V(x) = \frac{1}{2}kx^2 \qquad \text{Eq. 10}$$

The x^2 term indicates that the vibrational potential is in fact parabolic, where the minimum occurs at r_e and the potential increases as function of the absolute value of x.
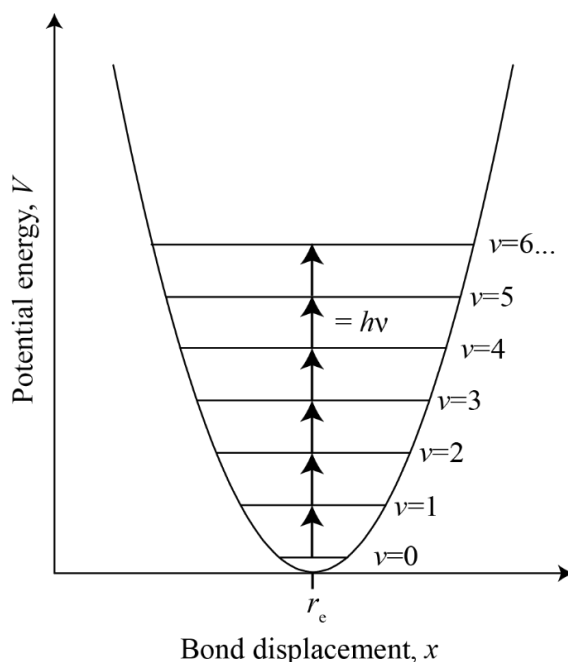
Figure 3:1: Harmonic scheme of the vibrational potential, where the energy levels are given as a function of vibrational quantum number, *v*, and the energy gaps can be seen to be equal between each level, separated by a value corresponding to *hv*.

The one-dimensional harmonic oscillator Hamiltonian can be written as:

$$H = -\frac{\hbar^2}{2\mu}\frac{d^2}{dx^2} + \frac{1}{2}kx^2$$

Eq. 11

where μ is the reduced mass of the nuclei and $\hbar = h/2\pi$.

If one then solves the Schrödinger equation for the above Hamiltonian, then the vibrational energies are yielded:

$$E_{vib} = h\nu\left(v_i + \frac{1}{2}\right)$$

Eq. 12

where v_i is the vibrational quantum number (0, 1, 2, 3 etc.)

The vibrational term value, $G(v)$, in cm^{-1}, can then be given as:

$$G(v) = \omega_e\left(v_i + \frac{1}{2}\right)$$

Eq. 13

where ω_e is the harmonic wavenumber.

As seen in Figure 3:1, the vibrational levels are equally spaced by $h\nu$. Notably, even for a vibrational quantum number of 0, there is a minimum energy associated with the molecule, which is known as the 'zero-point (vibrational) energy' or ZP(V)E.

3.3 Anharmonicity:

As a chemist, intuition comes into play as we know that we need to be able to make and break bonds in order to perform chemical synthesis. We may, therefore, come to the conclusion that not all molecules behave in a harmonic way. We know that after a bond becomes extended by a certain amount, the potential begins to plateau; eventually only very small changes to the potential occur as the bond length increases, and finally the bond dissociates. The harmonic treatment of the bond is, thus, only a good model for small bond displacements away from the equilibrium bond length. This deviation from the parabolic behaviour of the vibrational potential is known as anharmonicity. Hollas[48] has previously described this in detail, and splits the concept of anharmonicity into two components:

(i)   Electrical Anharmonicity

(ii)   Mechanical Anharmonicity.

For (i), the transition dipole moment, R_v, related to an infrared transition from an initial vibrational state, Ψ_v'', to an upper vibrational state Ψ_v', is given by:

$$R_v = \int \Psi_v' \mu \Psi_v'' \, dx \qquad \text{Eq. 14}$$

where x corresponds to the magnitude of displacement from the equilibrium bond length. For a heteronuclear molecule with a dipole moment, μ, its value can be shown to have a dependence on x, which can be modelled as a Taylor series expansion:

$$\mu = \mu_e + \left(\frac{d\mu}{dx}\right)_e x + \frac{1}{2!}\left(\frac{d^2\mu}{dx^2}\right)_e x^2 + \cdots \qquad \text{Eq. 15}$$

Should μ only vary linearly with x, then only the first term is necessary, and a harmonic potential is a satisfactory description. In reality, however, μ contains terms in x to multiple powers above the first. The change in dipole moment of the molecule in question is related to the 'allowedness' of an infrared transition – thus the effect of the higher order terms breaks down traditional selection rules associated with the harmonic oscillator. Furthermore, dipole moment is an electrical molecular property, thus this is referred to as electrical anharmonicity.

For (ii), the vibrational terms derived above assume a Hookean molecule, in that the vibration itself behaves as a perfect spring would. The assumption that this is correct only truly applies to very small displacements from the equilibrium bond length. In reality, as the bond displacement increases the force constant, k, decreases and, as a result, the potential curve begins to flatten, this is particularly noticeable for $x \gg r_e$. As the bond displacement decreases, k begins to increase, such that the wall of the potential becomes much steeper than what is seen in the parabolic potential. As these changes to the shape of the potential are caused by the mechanical properties of the bond itself, it is referred to as mechanical anharmonicity.

Mechanical anharmonicity, unlike its electrical counterpart, also serves to modify the vibrational wavefunctions and the term values corresponding to the overall vibrational potential. The potential terms, at this point, are not accurately described by an x^2 function, but become more accurately described by a power series in $(v + \frac{1}{2})$, or, to a very good approximation, a Morse function, shown in Figure 3:2.

The vibrational term is given as:

$$G(v) = \omega_e \left(v + \frac{1}{2}\right) - \omega_e x_e \left(v + \frac{1}{2}\right)^2 + \omega_e y_e \left(v + \frac{1}{2}\right)^3 + \cdots \qquad \text{Eq. 16}$$

Where ω_e is the vibrational wavenumber for a classical oscillator, and x_e and y_e are anharmonicity constants.

The key differences between the harmonic and anharmonic models are thus (i) the shape of the potential curve due to the abovementioned electronic and mechanical contributions to the anharmonic potential, and (ii) the vibrational energy levels close-up as v increases, which occurs due to the presence of the anharmonicity constants.
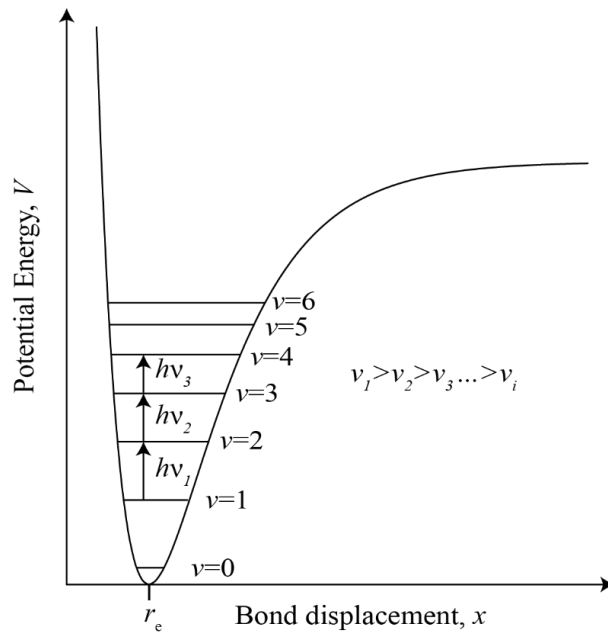
Figure 3:2: Anharmonic scheme of the vibrational potential, modelled by a Morse function. The energy levels are given as a function of the vibrational quantum number, v. Introduction of anharmonicity yields decreasing vibrational energy levels spacings as v increases.

3.4 Polyatomic molecules:

In the case of molecules containing multiple atoms, one can simply extend the ideas of harmonicity and anharmonicity previously derived. We begin by assuming a polyatomic molecule to be a series of point masses linked together by a number of springs with different force constants describing the strength of the bond. For non-linear polyatomic molecules, which will be considered exclusively in this thesis, there will be 3N-6 vibrational modes, where N is the number of atoms. Each of these vibrations is referred to as a normal mode for which are all independent of one another with a fixed centre of mass, if harmonicity is obeyed.

If a force is applied to any of the atoms within the network of springs, one can imagine that the vibration will occur throughout the molecule, and so different parts of the structure will also be displaced as a result of the initially applied force *i.e.* perturbing a single spring will have an effect on closely located springs within that system. It is therefore fair to assume that the overall motion of the molecule can be described as a weighted linear combination of the springs' displacements.

If one carries the ideas from the diatomic scenario through, then one can assume that the overall vibrational potential can be given as a sum of each vibrational term, such that:

$$\sum_i G(v_i) = \sum_i \omega_i \left(v_i + \frac{1}{2}\right) \qquad \text{Eq. 17}$$

This harmonic treatment of polyatomic vibrations can then be extended to encompass the true anharmonic nature of the vibrations. This takes a similar form to the potential seen in the diatomic system shown in Eq. 16. The resulting expression becomes:

$$\sum_i G(v_i) = \sum_i \omega_i \left(v_i + \frac{1}{2}\right) + \sum_{i \leq j} x_{ij} \left(v_i + \frac{1}{2}\right)\left(v_j + \frac{1}{2}\right) + \cdots \qquad \text{Eq. 18}$$

The overall vibrational potential becomes the sum total of a number of converging power terms. Here, the anharmonic constants are given, for example, by x_{ij}. For situations in which $i = j$, the constant is analogous to the $\omega_e x_e$ term seen in the diatomic scenario, in which the anharmonicity is unrelated to any interactions with the other normal modes – often referred to as diagonal anharmonicity. This term accounts for the closing up of vibrational energy levels as a function of vibrational quantum number, *v*.

Cross-terms, *i.e.* when $i \neq j$, take into account anharmonic interactions between, in this case, a pair of vibrational modes, *i* and *j*, such that these modes are no longer truly independent of one another – referred to as off-diagonal anharmonicity. Higher terms in the power series indicate off-diagonal interactions between multiple vibrational levels may occur, although these are expected to be small in magnitude.

4. Electronic and vibrational transitions and their accompanying selection rules:

If a photon has an energy, *hv*, exactly equal to the energy difference between two electronic states, then it is possible to promote an electron from a valence orbital into a higher-lying

unoccupied orbital. Electronic excitation is usually accompanied by population of a vibrational level, termed a vibronic transition, and sometimes torsional levels, which are colloquially known as 'vibtoronic' transitions. The main scope of the present work involves using the observed vibrational and torsional structure accompanying an electronic transition to infer interactions between electronic, vibrational and torsional states. As such, this section will detail the types of allowed and forbidden transitions that may be expected, first describing pure electronic transitions and then also with the inclusion of the accompanying vibrational structure. Torsional structure and their accompanying interactions are treated separately in Chapter 7. Changes to rotational level population also accompany electronic transitions but these are not resolvable with the experiment used in this work, so are not discussed.

In general, for a molecule that absorbs a photon and undergoes a transition to a given state, the equation relating to the transition is given by:

$$R = \langle \psi' | \mu | \psi'' \rangle$$
Eq. 19

Where R is the transition dipole moment, ψ'' is the initial state wavefunction, ψ' is the final state wavefunction, and μ is the electric dipole moment operator. The square of the value of R is directly related to the intensity of the transition and if the value is non-zero, then the transition is said to be allowed. As such, if $R = 0$ then the transition is electric dipole forbidden, and should not be observed experimentally. This principle may be extended to a variety of situations; although we only consider pure electronic, vibronic and also, later on, torsional transitions.

4.1 Pure electronic transitions:

A pure electronic transition is one that exclusively involves a movement of an electron between electronic energy levels, with only the ZPVE levels being populated in the initial and final states. Electronic transitions occur between an initial state with a wavefunction, ψ'', and a final state with a wavefunction, ψ', where the electric component of the incoming photon may interact with a bound electron, causing an energy transfer and, hence, excitation. As a result, the 'allowedness' of a transition is related to the ability of the molecule to interact with the electric component of the incoming photon. The electric transition dipole moment, R_e, can therefore be given as:

$$R_e = \langle \psi'_e | \mu | \psi''_e \rangle$$
Eq. 20

Where μ is the electric dipole moment operator, which has linear function components along the *x,y* and *z* axes. For a transition to be allowed, the value of R_e must be non-zero, and the intensity of the transition is proportional to the square of R_e.

The requirement for $R_e \neq 0$ depends upon the symmetry of the components in the equation above, such that:

$$\Gamma(\psi'_e) \times \Gamma(\mu_{x,y,z}) \times \Gamma(\psi''_e) \supset A \qquad \text{Eq. 21}$$

where *A*, here, represents the totally symmetric symmetry class of the molecule's point group. If the product of the symmetries of each component in Eq. 21 contain the totally symmetric symmetry class, then the transition is said to be allowed, although this statement says nothing about how intense the transition could be. To determine if such a transition is allowed, then, one must first consider the point group of a given molecule. In *p*FT, assuming that the methyl rotor can be treated as a point mass, the point group is C_{2v} (Table 4-1). One must then decide the molecular axis system which will then be employed. Here we place the *z*-axis directly through the C_2 principal axis, with the plane of the ring in the *yz* plane. Consider the $S_1 \leftarrow S_0$ transition which is a $B_2 \leftarrow A_1$ symmetry transition. For the overall transition to be allowed:

$$\Gamma(\psi'_e) \times \Gamma(\mu_{x,y,z}) \times \Gamma(\psi''_e) \supset A_1 \qquad \text{Eq. 22}$$

Table 4-1: C_{2v} symmetry point group table.

C_{2v}	E	$C_2(z)$	$\sigma_v(xz)$	$\sigma_v(yz)$	Linear functions	Rotations
A_1	+1	+1	+1	+1	z	-
A_2	+1	+1	-1	-1	-	R_z
B_1	+1	-1	+1	-1	x	R_y
B_2	+1	-1	-1	+1	y	R_x

With reference to C_{2v} point group elements in Table 4-1, one can see that the symmetry of $\mu_{x,y,z}$ (given by the linear functions column) transforms as B_1, B_2 or A_1 respectively. For an electronic transition to be allowed, the symmetry product of the initial and final electronic wavefunctions must transform as the symmetry components of $\mu_{x,y,z}$ in order for the overall product to be totally symmetric, as shown below.

$$\Gamma(\psi'_e) \times \Gamma(\psi''_e) \supset B_1, B_2 \text{ or } A_1 \qquad \text{Eq. 23}$$

Substituting in the symmetries for ψ'_e and ψ''_e, then:

$$\Gamma(\psi'_e) \times \Gamma(\psi''_e) = B_2 \times A_1 = B_2$$

It can be seen that the product of the symmetries of the wavefunctions above corresponds to the symmetry of the electric dipole operator in the y-axis. Hence, the $S_1 \leftarrow S_0$ transition is said to be allowed and polarised along the y-axis.

4.2 Vibronic transitions:

A similar treatment can be applied for simultaneous electronic and vibrational transitions or a vibronic transition. Here, the vibronic transition moment, R_{ev}, is assessed such that:

$$R_{ev} = \langle \psi'_{ev} | \mu | \psi''_{ev} \rangle \qquad \text{Eq. 24}$$

At this point, one must take into account the symmetries of both the initial and final vibronic states involved in the transition. Here, the symmetry of each vibronic state can be assumed to be the product of the electronic and vibrational wavefunctions. Using pFT as a reference, once again, R_{ev} will be non-zero if:

$$[\Gamma(\psi'_e) \times \Gamma(\psi''_e)] \times [\Gamma(\psi''_v) \times \Gamma(\psi''_v)] \supset B_1, B_2 \text{ or } A_1 \qquad \text{Eq. 25}$$

For the above equation, it is worth noting that there is a large variety of combinations of vibrational and electronic wavefunctions which may give rise to an allowed transition. For example, if the first vibronic state had an electronic and vibrational symmetries of A_1 and B_1 respectively, and the final vibronic state has an electronic and vibrational wavefunction of A_2 and A_2, then the transition is said to be symmetry allowed, even though the both the electronic and vibrational components, separately, would not yield an allowed transition.

These symmetry arguments merely dictate whether a transition is allowed, but they do not give any indication of how much intensity is to be expected following the transition. For a transition to have significant intensity, the degree of overlap between the initial and final wavefunctions must be large, thus one can always decide whether or not a transition is allowed, but it is difficult to say without further analysis if said transition will be seen experimentally.

The above treatment of a vibronic transition assumes that the electronic and vibrational wavefunction components are intrinsically linked. However, the Born-Oppenheimer approximation, mentioned in Chapter 3.1, assumes that, due to the mass difference between

the nuclei and electrons, the vibrational motion is on a much faster timescale than the electronic motion. As a result of this, one may assume separability of the electronic and vibrational wavefunctions yielding the equation below:

$$R_{ev} = \langle \psi'_e | \mu | \psi''_e \rangle \langle \psi'_v | \psi''_v \rangle$$

<div align="right">Eq. 26</div>

The vibronic transition dipole moment now occurs as the product of two integrals; the first component being the electronic term, as previously seen in Eq. 20, and the second being a vibrational overlap integral, for which the square of the $\langle \psi'_v | \psi''_v \rangle$ term is referred to as the Franck-Condon Factor (FCF). The FCF is related directly to the expected intensity of a given vibronic transition, provided the pure electronic integral yields an allowed transition. Here, then, both integrals must be non-zero for the transition to be allowed, in which case it is referred to as a Franck-Condon allowed transition. This assumption can be a more reliable way of inferring whether a transition will have some experimental intensity associated with it, compared to what was seen in Eq. 25. If the pure electronic transition is allowed and is seen experimentally, one can often deduce the structural change accompanying the transition, usually through quantum chemical calculations. Using this information it is possible to calculate the overlap of the vibrational wavefunctions within each electronic state to try and elucidate if a strong transition is expected. For substituted benzenes, this approach works reasonably well, although caution is required as intensity can be gained by other second order coupling mechanisms, which will be discussed in Chapters 4.3.2 and 5.

4.3 Vibrational structure associated with electronic transitions:

4.3.1 Allowed transitions:

Vibrational structure accompanying electronic transitions can take one of many forms, of which examples of each of these can be seen in Figure 4:1. When assigning electronic spectra, one must take into account which types of transitions, and their respective intensities, are expected as getting the assignments correct is important in deducing the properties of the coupling mechanisms observed. This subsection will describe briefly the five types of electronic and vibrational transitions anticipated, assuming all states are non-degenerate, and possible interactions between these levels will be described in Chapter 5. Transition and intensity rules related to torsions will be described at a later point in Chapter 7.

(i) Electronic origin:

Briefly, as was described in Section 4.1, an electronic origin transition, also referred to as a pure electronic transition, is one for which an electron is excited from the ground electronic state, to a higher lying electronic state. The ZPVE level must be populated in the ground state, and no change in vibrational population must occur upon excitation.

(ii) Vibrational Fundamental:

If the energy of the incoming photon is equal to the gap between the ground electronic state in the ZPVE level, and a vibrational state within the higher-lying electronic state, then transitions may also be expected. When seen experimentally, the bands corresponding to these forms of transitions are referred to as vibrational structure. Assuming the electronic part of the transition is allowed, the intensity of vibrational structure is dictated by the square of the overlap between the initial and final vibrational wavefunction, *i.e.* the FCF is non-zero:

$$\text{FCF} = \langle \psi'_v | \psi''_v \rangle^2 \neq 0 \qquad \text{Eq. 27}$$

If there is a singular change in the vibrational quantum number upon excitation, $(v_1 \leftarrow v_0)$, then this is referred to as a vibrational fundamental *i.e.* a single quantum of one of the vibrational modes becomes populated. Note that this terminology is often reserved for IR transitions, although it is common practice to use the same terminology when $v_1 \leftarrow v_0$ transitions occur following electronic excitation. This idea is carried through with the descriptions of overtone and combination bands given with the same assumptions.

Figure 4:1: Scheme to show examples of the expected forms of vibrational transitions accompanying electronic transitions. A transition involving a photon of energy $h\nu_{i,f}$ is shown, where i and f are the initial and final vibronic states respectively. If i or f are numbers (0, 1, 2) it refers to the quantum of a given vibrational mode, whereas the letters, x_1/y_1, indicate a single quanta of two different vibrational modes. Filled circles arbitrarily indicate the of a given vibronic state, whereas an empty circle indicates the 'hole' left behind after excitation. See text for more details.
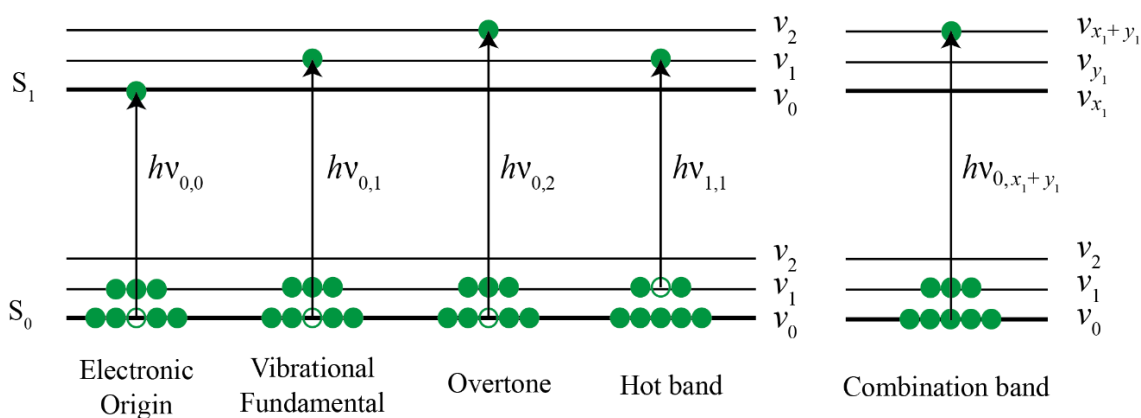
(iii) Vibrational Overtones:

Electronic spectra often display vibrational structure corresponding to transitions that do not match one of the vibrational fundamentals. A number of these transitions correspond to integer combinations of a singular fundamental vibrational mode ($\Delta v = \pm 2, \ \pm 3, \ \pm 4 \ etc$). These are referred to as overtone bands, and often appear in the spectrum roughly at the vibrational frequency of the fundamental multiplied by the number of vibrational quanta of said level.

Here, one must take into account the selection rules to determine if a band is allowed. In the scenario of an allowed electronic transition, and if the ZPVE is populated in the ground state, one would only expect to see totally symmetric vibrational fundamental transitions. What, then, happens to the symmetry selection rules if multiple quanta of a vibration are being excited? If we take an a_1 fundamental vibration in the excited state of *p*FT, once again, the symmetry of the first overtone of the vibration ($\Delta v = \pm 2$) can be given as twice the product of the fundamental:

$$a_1 \times a_1 = a_1$$

The first overtone is therefore allowed. In the case of the 2nd overtone, three times of product of the fundamental is required:

$$a_1 \times a_1 \times a_1 = a_1$$

So, for a symmetric fundamental, every overtone will meet the symmetry requirements and could theoretically be expected to be seen in an electronic spectrum.

It is worth noting that, in this work, the geometry change between the electronic states is often reasonably small, thus the larger the change in vibrational quantum number upon transition, the lesser the expected intensity. Higher order overtones ($\Delta v = \pm 3, \pm 4$ and higher) are therefore not expected to be particularly intense.

A vibrational fundamental that is not symmetry allowed, *e.g.* a b_2 vibration, can be treated in a similar way. For any given odd overtone, such as the 1st overtone:

$$b_2 \times b_2 = a_1$$

The product of any number of wavefunctions in an odd overtone will always be symmetry allowed. For even overtones of a symmetry forbidden vibration however:

$$b_2 \times b_2 \times b_2 = b_2$$

Notably, in every case of an even overtone, the overall symmetry will never transform as A_1, thus should not be expected in an electronic spectrum, disregarding any coupling mechanisms.

(iv) Vibrational combinations:

Vibrational structure can be seen which appears at energies that are sums of multiple fundamental or overtone terms. These can be thought of as two or more different vibrational fundamentals and/or overtones being excited simultaneously. This is known as a combination or summation band.

The symmetry selection rules must also be obeyed for combination bands. Disregarding any second-order mechanisms, and in a simple scenario of a two-vibration combination band, one may imagine four different scenarios:

(i)   A combination of two symmetry allowed vibrations:

$$a_1 \times a_1 = a_1$$

(ii)   A combination of one symmetry allowed and one symmetry forbidden vibration:

$$a_1 \times b_1 = b_1$$

(iii)   A combination of two **same** symmetry forbidden vibrations:

$$b_1 \times b_1 = a_1$$

(iv)   A combination of two **different** symmetry forbidden vibrations:

$$b_1 \times b_2 = a_2$$

As seen from above, so long as the overall product of the vibrational symmetries yields a_1, then the transition is allowed. This can be further extended to combinations involving multiple vibrations. As seen with the overtones, the electronic states discussed in this work have largely unchanged geometries upon excitation or ionisation, thus the larger the change in vibrational quantum number between states, the lower the expected intensity of the transition. As a result of this, a large number of possible combination bands are not expected to have much intensity, if any at all.

(v) Hot Bands:

As will be detailed in Section 8, all experimental data collected and presented in this work employs jet-expansion conditions, thus it is expected that all molecules will initially be in their vibrationless level, *i.e.* the ZPVE level. One would therefore only expect to see transitions originating from the ground electronic state with the ZPVE populated. This greatly decreases the complexity of the spectra, allowing one to more easily deduce the transitions seen as

they all originate from the same starting point. It is possible, however, that some population may remain in the low-lying vibrational energy levels of the ground state as a result of incomplete cooling. As a result of this, and depending on the extent of the cooling, one may see transitions beginning in these low lying levels. These are referred to as 'hot bands'. Once again, these bands must obey the abovementioned symmetry rules, but are often, in our experiment, particularly small as the degree of vibrational cooling is often enough to ensure most population originates in the vibrationless level. For a given transition to the same final vibrational state, *e.g.* $v'_3 \leftarrow v''_0$ vs $v'_3 \leftarrow v''_1$, the hot band will appear on the red side, or at a lower absolute wavenumber than the electronic fundamental band, as the energy gap between the states is smaller due to a higher energy state initially being populated.

4.3.2 Forbidden transitions:

(i) Herzberg-Teller coupling:

In some cases, transitions that are not allowed by Franck-Condon (symmetry) arguments may be observed experimentally in a spectrum. All transitions described so far are allowed to first order, and do not take into account any higher-order coupling interactions. Thus far, we have been using the Born-Oppenheimer approximation, which assumes that the separability of the vibrational and electronic components of the dipole moment is possible. If, however, the nuclear and electronic co-ordinates cannot be separated, then one needs to be able to understand their dependence on one another. One can therefore perform an expansion of the electronic dipole moment, R_e, as a Taylor series in terms of the vibrational co-ordinates, Q_i.

$$R_e = (R_e)_{eq} + \sum_i \left(\frac{\partial R_e}{\partial Q_i}\right)_{eq} Q_i + \cdots \qquad \text{Eq. 28}$$

where $(R_e)_{eq}$ is the electronic transition dipole moment at the equilibrium geometry, and is given by Eq. 20. This allows one to determine the impact, if any, of the vibrational motion on R_e.

If the electronic transition within the BO approximation is symmetry forbidden, such that $(R_e)_{eq} = 0$, then the second, as well as the higher terms in the expansion, need to be considered. The second term in Eq. 28 indicates that if the vibrational coordinate changes, such as when a vibration is excited, it can potentially induce a change in R_e. This can be imagined as the vibration distorting the molecule so that it 'looks like' a symmetry allowed state – thus some 'allowed' character may be seen experimentally. This was first noted by

Herzberg and Teller[53] and is commonly referred to as 'Herzberg-Teller coupling'. This will be referred to as Type (i) HT coupling.

Qualitatively, an alternative mechanism is often provided to explain Herzberg-Teller coupling, although the end result is the same. This second mechanism, or Type (ii) HT coupling, is given as an intensity-stealing mechanism, by which the forbidden vibronic transition 'steals' intensity from an allowed electronic transition. A common example used to describe Herzberg-Teller coupling is the false origin of benzene, for which a schematic is shown in Figure 4:2.

Figure 4:2: Mechanism of Herzberg-Teller coupling, in which the forbidden e_{1u} vibronic level steals intensity from a nearby allowed electronic level of the same symmetry - refer to text to more details.
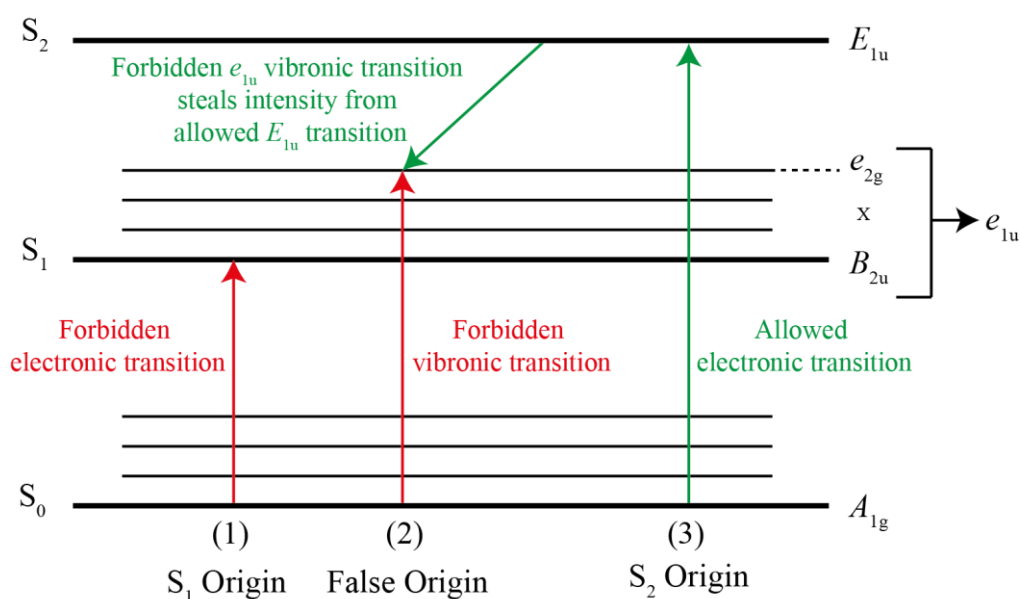
Benzene has D_{6h} symmetry, for which the totally symmetric irreducible representation is A_{1g}, thus, with reference to the linear functions of the point group table (not shown), for a vibronic transition to be allowed then:

$$\left(\Gamma(\psi'_e) \times \Gamma(\psi''_e) \right) \times \left(\Gamma(\psi''_v) \times \Gamma(\psi''_v) \right) \supset A_{2u} \; or \; E_{1u}$$

The first electronic state, S_1, of benzene has B_{2u} symmetry, so assuming separability of the vibrational and electronic wavefunctions, we can first analyse if the electronic transition (Depicted as (1) in Figure 4:2) is allowed, remembering that for this transition to be symmetry allowed then:

$$\langle \psi'_e | \mu_{x,y,z} | \psi''_e \rangle \supset A_{1g}$$

As the ground state is A_{1g}, we can substitute the symmetries of the electronic states and dipole moment vectors into the above equation:

$$\langle B_{2u} | A_{2u} \text{ or } E_{1u} | A_{1g} \rangle \not\supset A_{1g}$$

As the symmetry products do not contain the A_{1g} species, the pure electronic transition is not allowed.

The S_2 electronic state, however, has E_{1u} symmetry:

$$\langle E_{1u} | A_{2u} \text{ or } E_{1u} | A_{1g} \rangle \supset A_{1g}$$

This transition (depicted as (3) on Figure 4:2) is allowed as the x,y components of the electronic dipole moment vector transform as E_{1u}, so the overall symmetry product does contain A_{1g}.

Notably, vibrational structure accompanying the $S_1 \leftarrow S_0$ transition corresponding to e_{2g} symmetry vibrations (depicted as (2) on Figure 4:2) is apparent in the experimental spectrum, originally thought to be the S_1 electronic origin. Referring back to Eq. 26, one sees that the combination of both the electronic and vibrational parts of the vibronic dipole moment must be non-zero in order to witness a vibronic transition. How, then, do we see vibrational structure when the electronic component of the transition is forbidden? If one analyses the vibrational and electronic symmetry products in the S_1 state, then one sees that:

$$\Gamma(\psi'_e) \times \Gamma(\psi'_v) = B_{2u} \times e_{2g} = e_{1u}$$

As the symmetry of the S_1 e_{2g} vibrations within the B_{2u} electronic state have an overall vibronic symmetry of e_{1u}, then, during the oscillation of the vibration, the transition may 'steal' intensity from the allowed $S_2 \leftarrow S_0$ ($E_{1u} \leftarrow A_{1g}$) electronic transition – this takes the form of a vibronic coupling between the e_{1u} vibronic state and the E_{1u} electronic state. Thus, a nominally forbidden transition can be seen.

Both mechanisms of Herzberg-Teller coupling are given above, where the interpretation is slightly different albeit with the end product being the same. Notably, this mechanism is often referred to as 'intensity borrowing' or intensity stealing'. The former, however, is a misnomer as the intensity is never 'returned' to the electronic state.[48] As this second-order mechanism relies on coupling between two different states, the intensity of the interaction is expected to vary as a function of the energy gap between the forbidden vibronic level and the symmetry allowed electronic state. The closer in energy are the forbidden and allowed

states, the greater the interaction; for observable transitions, this gap is usually required to be 1 eV or less.

(ii) Intrachannel coupling:

The abovementioned Herzberg-Teller coupling yields intensity as a direct result of vibronic interactions between levels in two different electronic states, and is therefore referred to as an interchannel coupling mechanism. Franck-Condon forbidden behaviour has been noted that seemingly cannot be explained by intensity stealing mechanisms and, thus, another mechanism is necessary to describe these transitional activities. In our studies, particularly in the ZEKE photoelectron studies of pDFB[54] and mFT,[44] we often note that we see forbidden out-of-plane modes to low energy. Poliakoff *et al.* [55–57] have developed the idea in which there is some form of interaction between an outgoing photoelectron and the vibrational modes, thus a breakdown of the BO approximation is required to explain this. Here, we have extended this to incorporate interactions between the Rydberg states – described shortly – populated in the experiment with the ionic core of the molecule.[54] This is termed an intrachannel coupling mechanism, as it does not require multiple electronic states for its invocation, unlike Herzberg-Teller interactions.

In the case of a standard photoejection of an electron (given with the example of the C_s molecule, mFT), one can first apply the selection rules inside the BO approximation, in a similar way as before, *i.e.:*

$$\langle {\psi'}_e^+ | \mu | {\psi''}_e \rangle \langle {\psi'}_v^+ | {\psi''}_v \rangle \supset A' \qquad \text{Eq. 29}$$

Thus, the products of symmetries of the cationic electronic state and the excited electronic state must transform as one of the components of the dipole moment vector, μ, and the symmetry of both vibrational states must also be the same. In the case of mFT, knowing that the symmetries of the S_1 and D_0^+ state are both A' we know that the electronic transition is allowed. However, we note that we have a tendency of seeing transitions from the ZPVE of the excited state, which has a' symmetry, to a'' vibrations of the cationic ground state, thus the FCF should, in fact, be zero. Initially, one turns to Herzberg-Teller coupling for a reason as to why such a transition exists, however a nearby electronic state of A'' symmetry is required, but not present. Another explanation is therefore necessary.

In the process of the ZEKE experiment (see Chapter 8), one can imagine that as the electron leaves the immediate vicinity of the remaining ionic core and populates a Rydberg orbital, then the instantaneous positions of the nuclear co-ordinates may interact, to some degree,

with the electron, and this interaction is not taken account of in Eq. 29. One would expect that, for such an interaction to occur between the ionic core and the electron, then the electron needs to spend some time close to the core. Note that the Rydberg states are high principal quantum number states that have a largely diffuse character, and thus may be treated as if they have the symmetries of hydrogenic atomic orbitals. For an interaction to occur between the Rydberg electron and the ionic core, one requires the orbital to have a large degree of penetrating character so that the 'closeness' mentioned above is possible. One would expect that the s and p orbital electrons will have the highest degree of penetration. Thus, in the case of mFT, the symmetries of these Rydberg electrons are:

(i)   s, p_y and p_z - a'

(ii) p_x - a''

One can now consider the electronic transition dipole moment with the included dependence on the Rydberg electron, which can be given by:

$$R_{ev} = \left\langle {\psi'}_e^{+} {\psi'}_v^{+} {\psi'}_{Ryd}^{+} \middle| \mu_{x,y,z} \middle| {\psi''}_e {\psi''}_v \right\rangle \qquad \text{Eq. 30}$$

where ${\psi'}_{Ryd}^{+}$ is the wavefunction associated with the Rydberg electron in question.

Bearing in mind that for R_{ev} to be non-zero, the overall symmetry of the products of each component in Eq. 30 must contain A', one can work out the required symmetry of the Rydberg electron in order for interaction to occur between itself and the ionic core:

$$\Gamma\left({\psi'}_{Ryd}^{+}\right) = \Gamma\left({\psi'}_e^{+}\right) \times \Gamma\left({\psi'}_v^{+}\right) \times \Gamma\left(\mu_{x,y,z}\right) \times \Gamma\left({\psi''}_e\right) \times \Gamma\left({\psi''}_v\right) \qquad \text{Eq. 31}$$

If there is an s or p Rydberg orbital with the symmetry of $\Gamma\left({\psi'}_{Ryd}^{+}\right)$, then interaction between the electron and core is possible, and thus the transition becomes 'allowed'.

Seemingly, for molecules with low symmetry, such as mFT, this mechanism appears convenient in that it provides a way, in essence, for any vibration to gain viable intensity in a photoelectron spectrum. One can see by looking at other examples by Rathbone $et\ al.$[56] and also us,[54] that this mechanism is, in fact, fairly rigid for molecules of much higher symmetries (such as D_{2h} in pDFB). Furthermore, and similarly for other transition mechanisms, even if a transition is 'allowed', this does not mean that one should always expect the transition to have observable intensity. For intrachannel coupling to yield sufficient intensity, the degree of interaction between the outgoing Rydberg electron and the vibrational motion associated

with the core must be significant. If a photoionization occurs *via* a vibrational motion that is, for example, a high amplitude (low frequency) out-of-plane motion, one can imagine that, in any instance of time, the outgoing electron can be heavily influenced, and perturbed by the motion of the core. In other instances, such as a low-amplitude (high frequency) in-plane mode, the outgoing photoelectron would have a much less degree of interaction with the atoms associated with the mode.

5. Coupling schemes:

As has previously been mentioned in Section 3.3, the breakdown of the harmonic oscillator model begins to be more evident as the bond lengths become notably different from the equilibrium value, thus an anharmonic model is required in order to more accurately describe the behaviour of the molecule. As a result of anharmonicity, it was noted that the potential terms are no longer merely the sum of those of each individual vibrational state (Eq. 17), but a more complicated sum (Eq. 18) that shows cross-terms in the overall expression. This indicates that the vibrational modes are not completely independent of one another, consequently leading to vibrational coupling.

Coupling between two vibrational states can be viewed as a 'mixing' between the initial states, forming two new states. When probing these coupled states using time-resolved experiments, energy, or population within them, can be seen to be transferred between them, thus providing a mechanism for energy to be redistributed amongst two, or more, vibrational coordinates. This flow of energy is often referred to as intramolecular vibrational (energy) redistribution or IVR, although localised treatments of such interactions are also common such as Fermi resonances. Although one cannot see population transfer within a frequency domain experiment, one can ascertain if there is any coupling occurring, and these experiments often have the added benefit of having a higher resolution. Therefore, using a combination of frequency-resolved and time-resolved experiments, one can elucidate and understand the vibrational coupling mechanisms to a higher degree than using one technique alone. The majority of this work is in the frequency domain, although there is some commentary on time-resolved data from Reid *et al.*[11–15] This section, therefore, aims to describe the types of coupling we see, how they present themselves experimentally, in both frequency-resolved and time-resolved experiments, and what their significance is in the wider picture of internal energy redistribution.

5.1 Fermi resonance:

The simplest case of vibrational coupling will involve two (zero-order) vibrational states. If one of these levels is a vibrational fundamental and the other is either an overtone or combination band, the interaction is termed a Fermi resonance.[58] Sometimes an interaction between two overtones or combination bands can occur, and this is termed a Darling-Dennison interaction.[59]

In the case of a Fermi resonance (FR), depicted in Figure 5:1, one considers two vibrational states of the same symmetry, the first state, $|x\rangle$, being slightly higher in energy than $|y\rangle$ (although the reverse is also commonly observed) – these are referred to as the zero-order states (ZOSs).

Figure 5:1: Schematic illustrating the mechanism of a Fermi Resonance. Two initial ZOSs interact with each other, pushing each other apart and forming two new 'mixed' eigenstates – see text for more details.
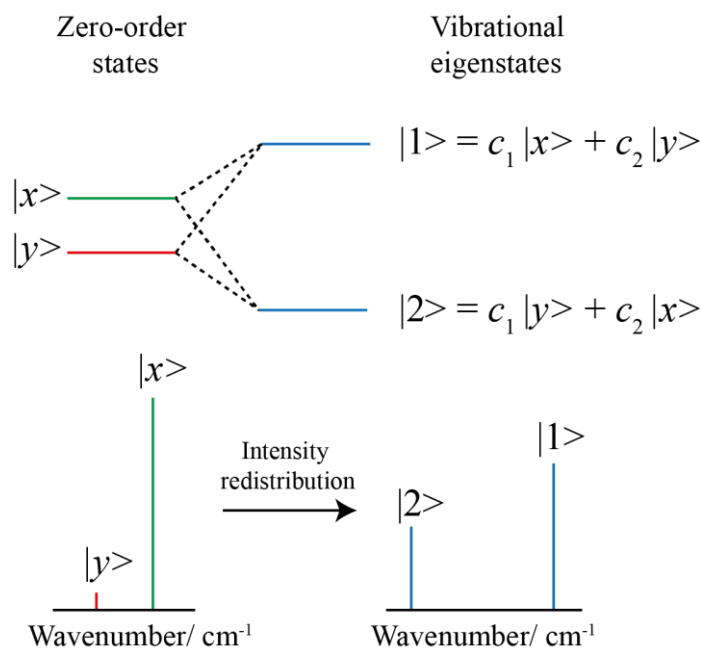
When these states interact, they will induce a perturbation to each other, effectively a repulsion. The result of this is that two new vibrational eigenstates are formed, $|1\rangle$ and $|2\rangle$, where the energy gap between them is now larger than the initial energy gap between $|x\rangle$ and $|y\rangle$. These two vibrational eigenstates each become a linear combination of the initial zero-order states, akin to how the mixing of atomic orbitals in the formation of molecular orbitals is described. This is expressed as:

$$|1\rangle = c_1|x\rangle + c_2|y\rangle$$
$$|2\rangle = c_1|y\rangle + c_2|x\rangle$$

<div style="text-align:right">Eq. 32</div>

where c_1 and c_2 denote the weightings of the initial zero-order states in the final vibrational eigenstates, depending on the extent of the interaction. As the vibrational eigenstates have character from each of the ZOSs, then it is expected that a redistribution of spectral intensity will arise when a transition occurs to them, as the FCFs will be modified as a result of the mixing. This is specifically seen in frequency-resolved experiments and will be described in more detail below.

The magnitude of the coupling between the zero-order states, which must have the same symmetry, is influenced mainly by two factors. These are (i) the energetic separation of the zero-order states, and (ii) the character of the vibrational states:

(i) The smaller the energy gap between the two modes, the greater the expected magnitude of the coupling. Should two ZOSs be essentially coincident, the resulting vibrational eigenstates would be expected to have nearly equal contributions from each ZOS, thus the values for both c_1 and c_2 would both be expected to be close to 0.5. If the ZOSs are energetically far apart, the magnitude of coupling will be reduced, such that the values of c_1 and c_2 will become close to 1 and 0 respectively – these states are no longer coupled.

(ii) The vibrational motions themselves are also an indication as to how strong the expected coupling between two ZOSs should be. One would expect that if the ZOSs each have a vibrational character that is notably different, then interaction between the two modes would not be as efficient. This is mentioned in the thesis by Tuttle[60] as an intuitive extension of the idea that two modes will not couple if their symmetry is different.

The classic example of a simple Fermi resonance is seen in the Raman spectrum of CO_2.[58] The symmetric stretch and the first overtone of the bending mode are expected to appear close to degeneracy, at 1330 and 1334 cm^{-1} respectively. Given the Raman selection rules, and within the harmonic oscillator approximation, one would only expect to see a transition involving the symmetric stretch, whereas transition to the bending mode should be forbidden. In the spectrum, two bands are observed, located at 1285 cm^{-1} and 1385 cm^{-1}. Given the fact that the experimental bands are seen to have an increased energy gap with respect to the expected bands, one can infer that some form of vibrational coupling has occurred.

As previously mentioned, vibrational coupling can also be manifested as an intensity redistribution mechanism. In a hypothetical situation, if one imagines transitions to the ZOSs, it is expected that, as the character of these modes is different from one another, the

transition intensities will also be different. In a FR, one of the ZOSs is usually assumed to have a larger amount of intensity with respect to the other, this being referred to as a zero-order bright (ZOB) state. The other ZOS is usually a state with a forbidden transition associated with it, this is referred to as the zero-order dark (ZOD) state.

In the formation of the vibrational eigenstates, the vibrational wavefunctions of the ZOB and ZOD states mix. As a result of this, a modification to the FCFs is seen – depicted in the bottom half of Figure 5:1. As the ZOB state gains ZOD state character through the coupling, one of the resulting vibrational eigenstates (given by $|1\rangle$) is expected to be less intense than the initial ZOB state, $|x\rangle$. The reverse happens for the ZOD state; as it gains ZOB state character, the resulting vibrational eigenstate, $|2\rangle$, is expected to be more intense than the initial ZOD state, $|y\rangle$. This mechanism, in essence, allows the bending overtone transition to, 'share' intensity with the symmetric stretch transition in the abovementioned case of CO_2.

Although the simplest scenario of vibrational coupling, caution is merited when discussing these forms of interaction. Notably, these mechanisms are often described and interpreted differently depending on whether one is working in a time-resolved environment compared to, such as in this work, a frequency-resolved environment.

First, we begin by looking at time-resolved experiments, particularly those using lasers with a pulse duration in the picosecond or femtosecond domain. A key point of information for working in the time domain is that, due to the uncertainty principle, the pulse width, in terms of frequency, of each laser shot is significantly larger than in the nanosecond lasers employed in our experiments. Furthermore, in a Fermi resonance, the resulting vibrational eigenstates are usually energetically nearby. As a result of these two factors, both (or all if there are multiple) vibrational eigenstates are usually excited coherently with the same laser pulse, thus forming a wavepacket: a superposition of eigenstates.

If one employs a pump-probe type experiment, then it is possible to measure the evolution of the wavepacket as a function of time. Should the probe arrive coincident with the pump at t = 0, then one will see the ZOB state at its maximum intensity, with ZOD state being at its minimum. If one then probes the wavepacket over a series of different time steps, the intensity of the signal arising from the ZOD state will wax, and that of the ZOB state wanes until the intensities have switched. This will then reverse and will continue indefinitely, should no other decay mechanisms be in place. This can be viewed as a population transfer between the ZOB and ZOD states as a function of time, and is referred to as quantum beating.

In a frequency-resolved experiment, a narrower laser pulse, usually in the nanosecond domain is employed. In this case, only one of the two eigenstates is excited, thus no wavepacket is created and no wavepacket dynamics (quantum beating) are observed. Although no time-dependent properties of the eigenstates can be measured, one can infer the nature of the vibrational couplings by other means. For example, if one believes two arbitrary vibrational modes $|x\rangle$ and $|y\rangle$ are intrinsically coupled in the S_1 state forming two eigenstates, $|1\rangle$ and $|2\rangle$, then one can prepare one of the two eigenstates and then project the population of that eigenstate onto another electronic state, such as the D_0^+ (or S_0) states *via* ZEKE (or DF) spectroscopy. In the case of ZEKE, assuming no coupling is present in the D_0^+ state and the vibrational modes are unchanged upon ionisation, one can deduce the make-up of the S_1 eigenstate by analysing the D_0^+ vibrational structure that is present in the ZEKE spectrum. If one assumes that two eigenstates are composed purely from two ZOSs, and, in this example, the coupling has an intermediate strength, then an example of the make-up of the eigenstates can be given as:

$$|1\rangle = 0.7\,|x\rangle + 0.3\,|y\rangle$$
$$|2\rangle = 0.7\,|y\rangle + 0.3\,|x\rangle$$

If one projects from S_1 $|1\rangle$, one expects to see transitions to both D_0^+ $|x\rangle$ as well as D_0^+ $|y\rangle$, with the overall transition intensity to $|x\rangle$ being greater than $|y\rangle$. If one then projects from S_1 $|2\rangle$, the same vibrational structure would be expected, albeit with the intensities of D_0^+ $|x\rangle$ and D_0^+ $|y\rangle$ being reversed. One must be careful, however, as it is possible that the intensity will be affected by other mechanisms, so some intuition may be required to deduce whether two vibrations are indeed coupled or not.

5.2 Intramolecular vibrational (energy) redistribution:

5.2.1 Restricted IVR:

Vibrational coupling is not always as simple as a two-state interaction. The number of zero-order states involved in coupling interactions can be many, with it sometimes being too difficult to experimentally pick out contributions due to the large number of interactions. One can imagine that as a molecule's internal energy increases, the number of possible vibrations, overtones or combinations increases, and the density of states can rapidly rise over relatively small energy ranges.[31]

When the density of states is low, however, only a few states of the correct symmetry are expected to be in close proximity, and thus the degree of coupling is anticipated to be low.

At low internal energies, then, either no coupling occurs, or one can sometimes observe interactions involving two or three zero-order states. In a time-dependent picture, with such a small number of interacting ZOSs, the quantum beating previously described is more complicated, but still oscillates for an indefinite period, in the absence of photophysical losses, showing no obvious signs of decay to the population. These interactions, therefore, are usually termed: restricted IVR

5.2.2 Statistical IVR:

To higher internal energy, as the density of states increases, the potential for coupling between zero-order states greatly increases. If many states couple together then, once again, both frequency and time-domain studies can be used synergistically to understand the mechanism by which the coupling occurs.

If one prepares a large number of coupled eigenstates inside a wavepacket, one can monitor the evolution of the wavepacket as before. Close to $t = 0$, the same pattern is observed in that population loss from the initial bright state occurs and is transferred to the coupled states. If, however, the number of coupled states is particularly large – referred to as a 'bath of states', the oscillations cannot be discerned and re-localisation of the population within the bright state is unlikely to occur on a reasonable timescale. In this case, the signal monitored becomes weaker as population spreads out widely into the bath states and can rapidly decay to insignificance – this is described *via* an exponential term and the process is often referred to as 'statistical' or 'dissipative' IVR.

In the frequency domain one may, as mentioned before, individually prepare the coupled eigenstates and project their population onto another electronic state, such as the S_0 or D_0^+ states *via* DF or ZEKE respectively. As the eigenstate's vibrational wavefunctions are expected to be composed of those from a large number of ZOSs, one would expect to see a large amount of FC vibrational structure in the resulting spectra. The observed structure will correspond to all the ZOSs that provide contributions to the initial eigenstate. If the number of coupled states is particularly large, it is unsurprising that the amount of structure seen in the photoelectron, or fluorescence, spectra will be very high and will start to overlap and become unresolved, thus will appear as a broad, and largely structureless, spectrum.

5.2.3 Doorway state IVR:

In the above, we have described two forms of IVR in which a bright state is either coupled directly and strongly to another state or directly to a large number, or bath, of states. A third, intermediate pathway, is also possible.

If a bright state couples to a dark state, much like in the traditional Fermi resonance, then it is possible that the dark state may then also couple, and more efficiently, with the bath of states. Here, the bright state is not coupled directly to the bath state(s) but is coupled indirectly through an intermediate dark state. The consequence of this is described below. Notably, the efficiency of the population transfer mechanism here strongly relies upon the initial interaction between bright and dark states. Without this step, the dark state does not have any significant population to transfer to the bath state(s). This is therefore referred to as doorway state IVR, as the dark state acts as an intermediate to transfer population from the bright state to the bath of states.

In a time-resolved experiment this is often seen as a combination of restricted and statistical IVR. If one prepares the eigenstates in a wavepacket, the intensity will initially be localised in the ZOB state, as previously seen. As the wavepacket evolves, population transfer to and from the ZOD state begins to take place. However, as the ZOD state begins to populate and the wavepacket continues to evolve, it then begins to transfer some of its population to the bath of states before the population transfers back to the ZOB. As a result of this, the population that the ZOD state has to transfer back is now less than it initially received, hence the ZOB state never receives back its full intensity due to the loss of population to the bath states. This repeats for a number of iterations until almost all of the population is lost to the bath of states, at which point the intensity oscillations become indiscernible.

In a frequency resolved experiment, this mechanism of IVR is more difficult to ascertain due to the inability to see the wavepacket dynamics. If one suspects a doorway state, it is necessary to individually project a number of different eigenstates onto another state, and to look for evidence of both restricted and statistical IVR; this can sometimes present itself as a set of well-structured bands atop a broad and structureless spectrum. Notably, this becomes difficult if there are also interactions occurring in the state the population has been projected onto. Further, certain phenomena related to wavepacket dynamics can also lead to misleading conclusions related to the regime of IVR observed (discussed in Chapters 11 and 12). As such, complementary sets of data, such as through projecting onto multiple

different electronic states, are preferred in order to gain a more reliable and confirmatory idea of the extent of coupling occurring.

The last question we need to ask ourselves is: how do we know we are observing vibrational coupling, specifically IVR? As mentioned earlier in this thesis, if one promotes an electron to a higher lying electronic state then the molecule can sometimes undergo decay or redistribution/relocation mechanisms such as fluorescence, intersystem crossings or internal conversions. A number of these mechanisms occur on very similar timescales (see Table 2-1) depending on the system, and these must be considered in deducing that IVR dynamics have been seen. Recent work by Reid *et al.*,[11,13,14] as well as others, has shown that IVR dynamics often occur on the picosecond timescale. With regards to other mechanisms: the fluorescence lifetime of the molecules discussed in this thesis are usually on the order of around 100 ns, with phosphorescence taking much longer than this. Intersystem crossing lifetimes are on the order of μs or slower as substitutions on the benzenes are light (fluorine/chlorine) thus spin-orbit coupling contributions are expected to be low. Internal conversions also occur on timescales usually outside of the picosecond region so can be ignored. It is therefore worth noting that the processes that could possibly compete with IVR all take significantly longer than IVR itself thus, in a time-resolved experiment, one can usually be certain that all population transfer mechanisms occurring with these types of molecules would be expected to be related to vibrational coupling.

5.3 Centrifugal distortion and Coriolis coupling:

We have seen that the Born-Oppenheimer approximation[52], in some scenarios, breaks down allowing us to see interactions between electronic and vibrational states. Similarly, vibrations cannot always be treated completely separately from rotations, and interactions can occur between them also.

If one imagines a linear molecule, CO_2 for example, rotating about its C_2 axis, a centrifugal force is exerted, pushing the oxygen atoms away from the centre of rotation, this provides a small changes to the equilibrium positions of the atoms, which can affect, albeit only slightly, expected transition intensities. This is known as centrifugal distortion.[61]

If, however, one imagines the bending motion in CO_2 - depicted below in Figure 5:2(a), one can imagine that as the O-C-O bond angle closes and the molecule rotates in an anti-clockwise fashion, then a force is imparted parallel to the direction of the bond, thus

imparting some anti-symmetric stretch character to the bending mode. This is referred to as a Coriolis force[61].

The same can be said of the anti-symmetric stretch (Figure 5:2(b)) in that, as it stretches whilst rotating anti-clockwise, the Coriolis force is perpendicular to the bond, imparting some bending character.

Figure 5:2: Depiction of the effect of the Coriolis force on (a) the bending mode and (b) the anti-symmetric stretching mode of a linear molecule.

(a) Bending mode

(a) Anti-symmetric stretching mode
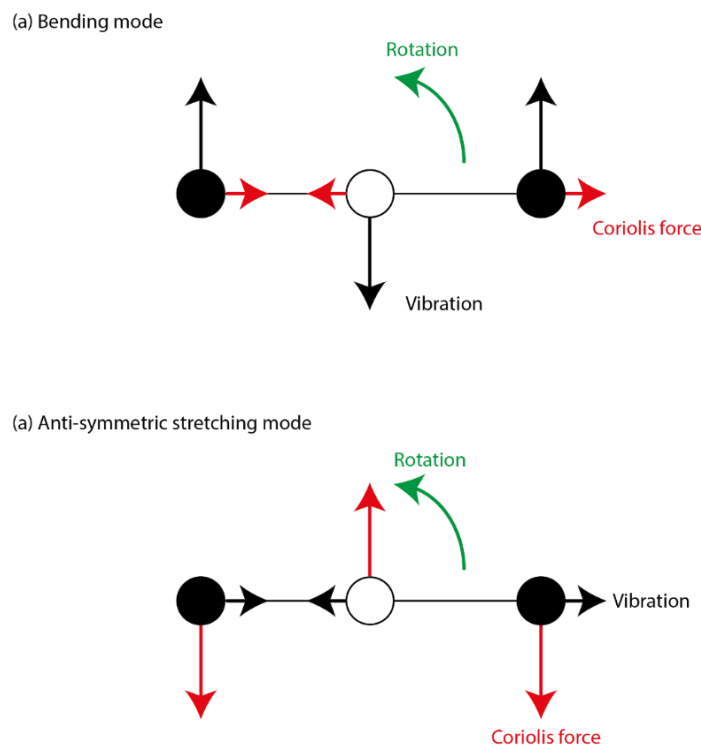
Notably, if either of these vibrations were excited then each of them contains some form of vibrational character from the other as a result of the direction of the Coriolis force; these modes would be said to be Coriolis coupled.

This form of coupling has its own selection rules, much like those previously seen accompanying electronic and vibrational transitions. For a Coriolis interaction, the product of the two vibrations involved must transform as a rotation. In the case of pFT, which can be treated as a C_{2v} molecule (Table 4-1), the rotations R_x, R_y and R_z transform as b_2, b_1 and a_2 respectively. As a result of this, Coriolis interactions may only be seen between two vibrational states with different symmetry, unlike the previous forms of coupling where the symmetries had to be the same.

It is worth noting that in our experiments we employ jet-expansion conditions. As a result of this, we would only expect low energy J levels to be populated. Due to this, the extent of Coriolis coupling is expected to be weak. It is also well known that centrifugal interactions are often prevalent for higher lying J levels, thus it should be safe to ignore these in our experiments. Coriolis coupling has previously been suggested in the literature for molecules similar to the ones mentioned in this work. This is, however, debatable, as there is a need for high-resolution experiments to pick out this form of coupling, which is not always employed in the literature reporting it.

5.4 Mode mixing:

This section has largely described how vibrational modes can couple together and the effect this may have on the structure seen in experimental electronic spectra, although deviations from expectation are not always due to mode coupling.

Upon excitation to a different electronic state, it is expected that the electronic structure will change. This will lead to changes in the properties of the molecule, such as changes to the conformation, bond lengths as well as differences in charge distribution, amongst others. The expected outcome of this is that the character of the vibrations themselves will change upon excitation, such that a one-to-one representation of the initial and final state vibrations is no longer seen. Instead, the vibrations of the final state can be regarded as a weighted linear combination, or mixture, of the initial vibrational states. This is often referred to as Duschinsky mixing, or Duschinsky rotation.[62] Notably, this is completely independent of any anharmonic coupling interactions previously noted but, to some extent, the symptoms of a Duschinsky rotation can be very similar to those seen in a Fermi resonance, so caution is merited when analysing vibrational structure. Note that one can distinguish between Duschinsky mixing and Fermi resonances as the former occurs between vibrational fundamentals, and the latter cannot.

6. Vibrational labelling:

As just mentioned, the vibrational modes of a molecule are heavily dependent upon factors such as electronic structure, as well as steric and mass effects related to each molecule's substituents. For our research interests, comparison between the activities of different molecules is necessary as we want to understand how changing the ring substituents affects the chemical and physical properties of the molecule.

Seen commonly in spectroscopic literature, there are two widely used vibrational labelling schemes: (i) the Herzberg[63]/Mulliken[64] scheme and (ii) the Wilson[65]/Varsányi[66] schemes. Note that the use of either of these schemes is acceptable, should one desire to understand a single system alone, however using them to compare and understand activity between molecules becomes a problem.

(i)   The Mulliken scheme sorts each vibrational mode of the molecule by a certain symmetry order (a_1, a_2, b_1 and b_2 for C_{2v} and a', a'' for C_s) and then orders them by energy in descending order.

(ii)   The Varsányi notation uses the energetically assorted labels afforded to the vibrational modes of benzene in order to describe the motions of a wide range of substituted benzenes.

Starting with the Mulliken notation, problems arise from the way in which the labels are assigned. For two similar molecules, say pDFB and pFT, if each mode is separated by symmetry, and then labelled in descending energetic order then numerous labels will be different, despite the motions being the same. This is due to (i) pFT having more vibrations than pDFB; (ii) the symmetry being different; and (iii) the energetic ordering of the vibrations may be different due to changes in the properties of the molecule. For the sake of comparison, one would like the vibrational motion to be described accurately by a given label, thus this is not a useful scheme for our purposes.

The Varsányi notation presents very different problems. A large number of substituted benzenes have all been assigned labels using the modes of the parent benzene molecule as a default, *i.e.* the best match is attributed between a given benzene mode and a 'corresponding' mode of a given substituted system. There is, however, a large evolution[67–70] in vibrational character as one moves from benzene to a simple substituted benzene, such as pDFB. If the vibrations of pDFB are greatly different from those of benzene, then they cannot be adequately described by Varsányi labels. Furthermore, Varsányi labelled many modes based upon them arbitrarily containing either 'light' or 'heavy' substituents with no intermediate terms, thus it is not always clear how to treat a large number of molecules. Using this labelling scheme, even for comparison between the simplest of molecules, is therefore a difficult task.

Throughout this thesis we will employ the D_i labelling schemes.[67–70] For the molecules considered herein, this scheme uses difluorinated benzenes as a basis for the labelling. For example, in the case of the *meta* molecules, we take a Mulliken-style approach in that we

order the vibrations of *m*DFB by symmetry and in descending energetic order. We obtain 30 labels, each of which corresponds to a specific vibrational motion, and we then apply these to all the *meta*-disubstituted benzenes we study, in this case *m*FT and *m*ClT, and assuming the rotor is a point group. As the vibrational modes are not expected to change significantly with any further change in mass, this allows ease of comparison between vibrational structure across a wide range of molecules. Similarly, for the most part, the labels are also applicable for the excited states and the ground state cation, thus we can compare vibrational structure between different electronic states of different molecules.

An important note is that *m*DFB obviously contains a different number of vibrations to, for example, *m*FT, as it does not contain a methyl rotor. In the scenarios where additional vibrations are present, these are labelled separately to the 30 ring-localised vibrations. A similar labelling scheme has also been designed for *para*[68] and *ortho*-disubstituted[69] as well as monosubstituted[67] ring systems, although only the *para* and *meta*[70] systems are used in this work.

The D_i notation was designed specifically to be used as a tool for comparison between a wide range of similar molecules, so the labels are given with the lowest possible symmetry for a given isomer. For example, with *meta*-disubstituted benzenes, if both substituents are the same, and are both single atoms, then the symmetry would be C_{2v}, whereas if they are different it would be C_s. Due to this, all labels are ordered with respect to the symmetries of the C_s point group. This then allows for direct comparison between molecules of the same isomer, but with different symmetries.

Finally, it is also worth noting that direct comparisons between different isomers is somewhat difficult using the current schemes. The vibrations between, say, *para* and *meta*-disubstituted systems are somewhat different,[70] thus a given label for a mode in *p*FT will not necessarily correspond to the same motion in *m*FT, so this must be taken into account when comparing between the activity of isomer.

7. The role of the methyl rotor and torsional spectroscopy:

A large amount of work has been completed on methylated benzene rings using a variety of techniques and studying a range of electronic states. It was noted by Timbers *et al.*[5] that, if a single fluorine atom in *p*DFB is substituted for a methyl rotor, the rate of IVR increases by a factor of 40, and if the methyl rotor is then moved to the *meta* position, the rate of IVR increases by a further factor of 12; thus, the rotor must have a significant role in affecting the

rate of coupling observed. For one to understand the role the methyl rotor plays, then it is imperative to first understand how to treat the rotor theoretically, which shall be discussed in further detail in this section. For additional information, the review by Spangler[71] discusses the theory behind, and the role of the torsions within the context of electronic spectroscopy.

Weisshaar[14-16,50–52] instigated a lot of early theoretical work behind the torsions, and played a large role in the derivation of the selection and intensity rules governing torsional transitions. More recent work has been carried out by the Lawrance[32–37] group, who have applied 2D-LIF spectroscopy, as well as in-depth theoretical studies, to analyse rotational band profiles of fluorescence features to comprehend, to a greater extent than was already known, how the torsional energy levels interact with other vibrational and vibtor states. Further to this, they have contributed investigations towards understanding prominent forbidden transitions that had previously been observed, but not well understood. Both the Lawrance group[38] and the Wright group[44,73] have, in more recent times, started to tackle different isomers of well-studied substituted benzenes. This has been attempted in order to begin to comprehend the effect of electronic and steric contributions on the torsional barriers, torsional energy levels, and how, specifically, these factors modify the rate of coupling.

This section aims to summarise much of the working knowledge of methyl rotors, specifically including derivation of the torsional energy levels and symmetries, as well as the selection and intensity rules governing the torsional transitions. All discussion in this work focusses on the case of a single rotor, given in the context of *p*FT, *m*FT and *m*ClT.

7.1 The free rotor:

A starting point for understanding the role of a rotor is to treat it in the simplest possible scenario: a methyl group bonded to a point mass. The rotor, here, can be treated as a rigid group which rotates about the single bond attaching it to the point mass. If there are no electronic or steric hindrances to the internal rotation, then it can be treated and solved as a particle on a ring problem.

The Hamiltonian of the problem can be given as:

$$H = F \frac{\partial^2}{\partial \phi^2}$$

<div align="right">Eq. 33</div>

Where *F* is the internal rotation constant, and ϕ is the torsional angle.

F can be represented as:

$$F = \frac{-\hbar^2}{2I}$$

<div align="right">Eq. 34</div>

Where I is the reduced moment of inertia of the molecule. This can be further broken down to:

$$I = \frac{I_{CH_3} I_{Molecule}}{I_{CH_3} + I_{Molecule}}$$

<div align="right">Eq. 35</div>

where I_{CH_3} is the moment of inertia of the rotor, and $I_{Molecule}$ is the moment of inertia of the remaining part of the molecule which is, in this case, the point mass. As both the methyl group and the point mass are rotating about the same axis, it is fair to assume a reduced moment, given above. We have previously noted that, in this scenario, the methyl group rotates freely whilst attached to a point mass and, if we assume that the latter has infinite mass, then $I_{CH_3} \ll I_{Molecule}$. The overall moment of inertia, *I,* is therefore is roughly equal to I_{CH_3}. As a result of this assumption, then:

$$F = \frac{-\hbar^2}{2I_{CH_3}} \cong 5.4 \text{ cm}^{-1}$$

<div align="right">Eq. 36</div>

This approximation is reasonable for calculating the torsional levels of simple substituted ring systems as the value is not expected to change much, and any small changes that may be expected will not drastically affect the free rotor levels.

If one then solves the particle on a ring problem, the resulting eigenvalues yield the free rotor energy levels:

$$E = m^2 F \text{ where } m = 0, \pm1, \pm2, \pm3 \dots$$

<div align="right">Eq. 37</div>

where *m* is the torsional quantum number and, notably, can be either positive or negative, thus the free rotor energy levels are all doubly degenerate. An important point is that these rotor levels do not have a ZPE and, as $E \propto m^2$, the spacings of the energy levels increases with a quadratic dependence. These, therefore, behave similarly to rotational levels, and thus are often referred to as internal rotations. The corresponding eigenfunctions are given by:

$$\psi = \frac{1}{\sqrt{2\pi}} e^{(im\phi)}$$

<div align="right">Eq. 38</div>

Note that the above expression is often given without the normalisation factor.

7.2 The hindered rotor:

In nearly all cases in which a methyl rotor is present, there will be some degree of interaction between the rotor and the rest of the molecule, which leads to a hindering potential. This interaction arises from several different factors, including steric interactions between rotor and ring, as well as electronic effects due to resonance and hyperconjugation interactions, amongst others. Related to the potential is the barrier height: the difference in energy between the rotor in its energetically most favourable, and least favourable positions. If one assumes that the three C-H bonds of the methyl rotor have the same bond lengths and each H atom is energetically equivalent, then it is expected that the hindering potential will be periodic and will have an integer multiple of three minima, within a 360° turn.

The overall potential of the system can be given as an expansion of cosine terms:

$$V = \frac{V_3}{2}[1 - cos(3\phi)] + \frac{V_6}{2}[1 - cos(6\phi)] + \frac{V_9}{2}[1 - cos(9\phi)] + \cdots \qquad \text{Eq. 39}$$

where V is the overall torsional potential, V_n are contributory potential terms where 'n' takes an integer multiple of three, and ϕ is the angle of rotation of the rotor with respect to the rest of the molecule.

The above expansion is a rapidly converging series of terms; it is expected that the magnitude of each term will decrease in turn, such that the V_9 terms, and above, are sufficiently small to be ignored. The term which has the largest impact on the overall potential is dependent upon the symmetry of the molecule. If one takes *p*FT, for example, then one can imagine that the overall hindering potential will have 6 minima. These correspond to three from the rotor itself, and this must then be multiplied by two to take into consideration the two-fold rotational symmetry of the ring – thus the V_6 term is the first, and leading term in the expansion. If *m*FT is taken, however, the first non-zero term is the V_3 term as there is no longer a two-fold rotational symmetry of the ring.

Depending on the preferred geometry of the rotor with respect to the ring, the value of the V_n terms can also be either positive or negative. For *p*FT, or molecules with a leading V_6 term, the value is said to be positive if the methyl rotor is eclipsed with respect to the ring, and negative if staggered. For molecules with a V_3 leading barrier, such as *m*FT, the definition is slightly different in that the barrier is positive if the rotor is eclipsed, with the in-plane C-H bond pointing in the direction of the *meta* substituent – this is referred to as *pseudo*-cis. The barrier is then negative if the rotor is eclipsed with the in-plane C-H bond pointing away from

the substituent – known as *pseudo*-trans. Notably, a 30° angle is required to change from eclipsed to staggered with a V_6 leading term, thus the potential oscillates from positive to negative every 30°, but 60° is required with a V_6 term, to change from *pseudo*-cis to *pseudo*-trans.

Figure 7:1 depicts an arbitrary example of a molecule with a leading V_3 term. Here, the V_3 term has its first minimum when the dihedral angle is 0°, thus is defined as *pseudo*-cis. The V_3 term therefore has a positive value associated with it. The V_6 term, however, has its first minimum at 30°, out-of-phase with the V_3 term, thus has a negative value associated with it. Looking at the overall potential, comprising both the V_3 and V_6 terms, the overall barrier height, here, is seen to be given largely by the V_3 potential, whereas the V_6 component merely works to shape the torsional barrier.

Figure 7:1: Schematic depicting an example of the shape and role of the V_3 and V_6 torsional potential terms on the overall torsional potential, V_3+V_6. Note that the V_3 and V_6 terms are out of phase which each other, indicating that the preceding signs are different.
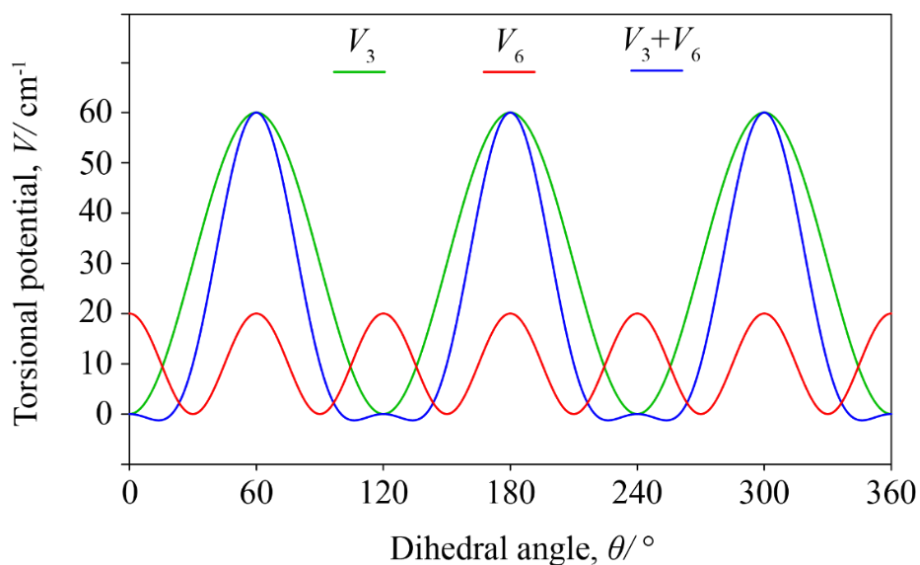
It is of note that the sign of the V_3 term does not affect the torsional energy levels in any way, and is not deducible experimentally, but can be derived from the quantum chemical calculations. The sign of the V_6 term, however, as well as being an indication of the conformation, does affect the ordering of some hindered rotor levels, which will be discussed later in this section.

One may expect that if the internal methyl rotation becomes hindered, then the torsional levels will also be affected. The question is, however, what happens to the levels and how much are they affected by the hindering potential?

A standard approach is to construct a Hamiltonian matrix in a basis set of free rotor eigenfunctions, where the corresponding hindered rotor eigenvalues, are deduced by numerical methods. It can be shown that the hindered rotor levels can be given as a perturbation to the free rotor levels, such that:

$$\int e^{-im\phi} \left\{ \frac{V_n}{2} [1 - cos(n\phi)] \right\} e^{im\phi} d\phi = -\frac{V_n}{4} \delta_{m,m'\pm n} \qquad \text{Eq. 40}$$

If one then follows through for each V_n term, then the matrix elements, A_m, are given, inclusive of V_3 and V_6 potential terms only:

$$A_m = \left(m^2 F + \frac{V_3 + V_6}{2} \right) \delta_{m,m'} - \frac{V_3}{4} \delta_{m,m'\pm3} - \frac{V_6}{4} \delta_{m,m'\pm6} \qquad \text{Eq. 41}$$

where the $m^2 F$ term corresponds to the free rotor levels, and the $\frac{V_3+V_6}{2}\delta_{m,m'}$ term, is a perturbation to all of the free rotor states occurring as a result of the torsional hindrance. Both the $-\frac{V_3}{4}\delta_{m,m'\pm3}$ and $-\frac{V_6}{4}\delta_{m,m'\pm6}$ terms are coupling elements that serve to perturb individual levels that have a difference in torsional quantum number dependent on the V_n term *i.e.* the $-\frac{V_6}{4}$ term couples torsional levels with a difference in torsional quantum number of 6. If one then diagonalises the matrix, then the hindered rotor levels are yielded.

In this work, we will consider the torsional energy levels for both *meta* and *para*-disubstituted molecules. Due to the differences in the leading torsional potential terms, coupling between individual torsions occurs in a noticeably different way.

Figure 7:2 shows how the rotor levels are affected in three different scenarios. Scenario (a) depicts the rotor level evolution purely as a function of V_6, with the value of V_3 being set to 0 cm^{-1} – such as for G_{12} symmetry molecules like pFT (discussed later). For small, negative V_6, one sees that the $m = \pm3$ levels begin to split, with one moving towards degeneracy with $m = \pm2$, and the other moving towards degeneracy with $m = \pm4$ levels. The $m = 3$ level which moves lower in energy with respect to the other is termed the $m = 3(-)$, with the other being termed the $m = 3(+)$ level. In the absence of any other interactions, the value for V_6 can be derived through the experimentally determined spacings between the $m = 3(+)$ and $m = 3(-)$ levels, should one be able to observed transitions involving them. The levels are perturbed from their corresponding free rotor energy levels by $\frac{V_6}{4}$, thus the spacing between the hindered rotor levels will correspond to $\frac{V_6}{2}$. Importantly, in terms of splitting of the levels, the sign of the V_6 barrier here must not be ignored as the directionality of the

splitting is different. Depicted in Figure 7:2(a), if, for example, the V_6 barrier is positive then what we termed the $m = 3(-)$ above, actually moves towards degeneracy with the $m = \pm 4$ levels and, instead, the $m = 3(+)$ moves towards degeneracy with $m = \pm 2$ levels, thus the energetic ordering of the hindered rotor levels becomes reversed with respect to the negative barrier scenario. This is of great importance as the symmetry of the $m = 3(+)$ and the $m = 3(-)$ levels is different, thus are expected to behave differently in the experiment. If one can observe and assign transitions involving these hindered rotor levels, then it is possible to determine the preferred conformation of the methyl rotor from this using the symmetry selection rules.

A similar interaction occurs with the $m = \pm 6$ levels in that, if the barrier is high enough, splitting is observed, as seen with the $m = \pm 3$ rotor levels. Here, one level moves towards the $m = \pm 5$, and the other towards the $m = \pm 7$ levels. Notably, the $m = \pm 6$ levels are not separated by $\Delta m = 6$, but they may couple indirectly *via* the $m = 0$ level. The extent of coupling between these is observed to be much smaller, as a result of its indirect nature.

Figure 7:2: Depiction of the effect of different torsional potential terms on the energetics of the torsional energy levels. Note that the colours of the lines refer to the symmetry of the torsional levels using G_6 symmetry labels – there are more symmetry subcategories if the molecule has G_{12} symmetry, but this will not affect the splitting pattern observed.
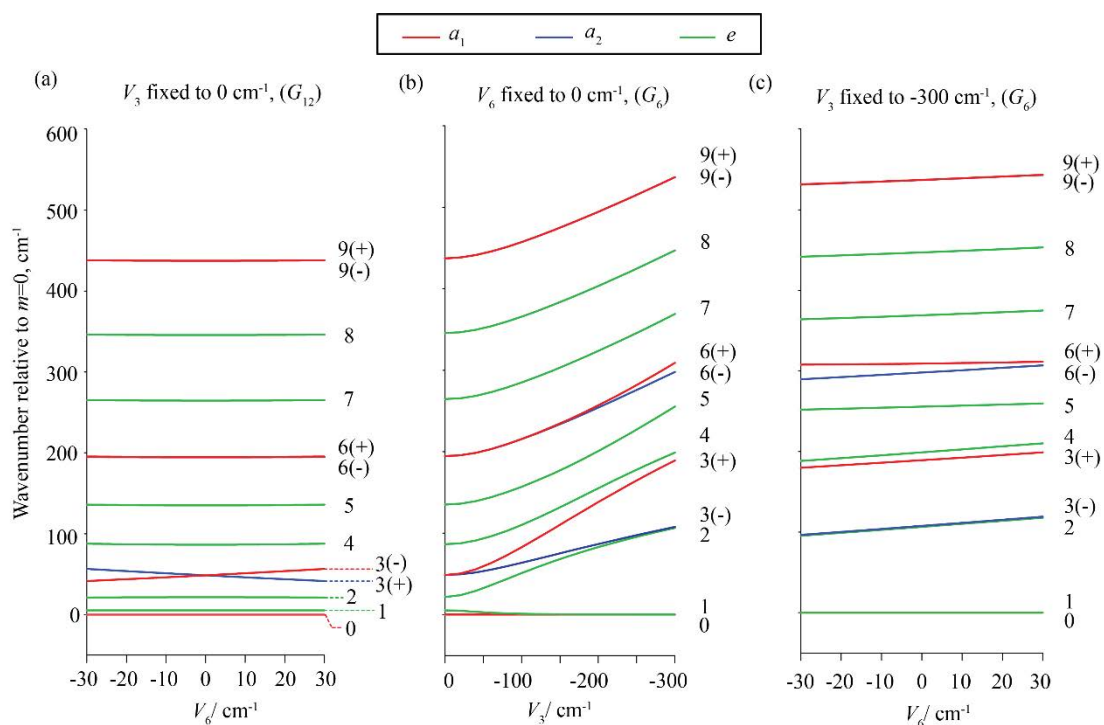
By looking at the other rotor levels in Figure 7:2(a), it can be seen that only the $m = \pm 3$ and $m = \pm 6$ levels (albeit by a very small amount) have split. If one takes, for example, the $m = -2$ and $m = +4$ levels, one may expect splitting to occur between these as they have a $\Delta m =$

45

6. So why, then, do the other m levels not also split? The splitting of the rotor levels requires the energy gap between levels to be low, much like what is seen in a Fermi resonance. Some of the doubly degenerate levels, particularly the lower energy levels, are close enough in energy that they will interact, although this will only occur weakly. Notably, each level within a doubly degenerate pair interacts to the same degree as the other, *i.e.* $m = -2$ and $m = +4$ will interact to the same degree as $m = +2$ and $m = -4$; the result of this is that both of the levels are perturbed by the same amount, thus splitting is not observed.

By analogy, molecules with a V_3 barrier (such as for G_6 symmetry molecules - *m*FT and *m*ClT) work in a similar way. The V_3 barrier is often much higher than the V_6 barrier, as it is the first term in the converging series, thus the splitting between the rotor levels is expected to be much higher. In a similar way, only splitting between the $m = \pm 3 \; or \pm 6$ is seen. The $m = \pm 3$ levels split indirectly *via* the $m = 0$ level, similar to the $m = \pm 6$ levels with the V_6 potential. The resulting perturbations to those levels will then induce further perturbations to the $m = \pm 6$ levels, thus the splitting of these is lower with respect to the $m = \pm 3$. Referring back to Figure 7:2(b), if one assumes that the V_6 term is 0 and allows the potential to vary purely as a function of V_3, the $m = \pm 3$ components move towards degeneracy with the $m = \pm 2$ or $m = \pm 4$ levels, and this begins to be fully realised at a barrier height of 250 cm^{-1}, much faster than would be seen with a V_6 barrier . Similarly, although the degree of splitting of the $m = \pm 6$ levels is much smaller, these, again, move towards degeneracy with the $m = \pm 5 \; or \pm 7$ levels, but require a significantly higher barrier to fully converge. As a result of the more complicated perturbations, one cannot simply derive the value of V_3 through the energetic differences between transitions involving the $m = 3(+)$ and $3(-)$ but, instead, must perform a fit of the experimental data to the terms given in the energetic expression (Eq. 41).

In the case of an infinite barrier, the splitting of the levels leads to a set of triply degenerate states being formed. Notably, if one compares the free-rotor levels with the levels in this case then it is seen that they have transitioned from looking like rotational levels *i.e.* an increasing energy gap as a function of *m*, to behaving much more like harmonic vibrations, where the energy gap between each set of levels is close to constant.

In practice, for molecules such as *m*FT, both the V_3 and V_6 terms are often non-zero. This makes it difficult to accurately determine the true values of each of these terms, as both work in tandem to split the free-rotor levels. Referring to Figure 7:2(c), one can see that if the V_3 barrier is fixed to -300 cm^{-1} and the V_6 parameter is varied, then the levels continue to evolve.

As with the V_3 barrier, one can perform a fit of the data to the terms given in Eq. 41. In estimating the barrier heights in this way, however, we have been assuming that no further interactions are occurring between rotor levels or any of the other degrees of freedom, and that F is also constant. This, however, is not always a reality, as these levels can be perturbed in a similar way to the vibrations which will be seen later in the publication section of this thesis.

7.3 Molecular symmetry:

For molecules such as pFT and mFT, it is convenient to employ the point groups C_{2v} and C_s respectively. Although this can be a fair assumption for considering the vibrations, it neglects treatment of the methyl group and the internal rotations associated with it. In order to be able to fully describe the motions of the system, and treat the symmetry of the torsions correctly, one must use molecular symmetry groups (MSGs). This is of great importance as it allows one to determine the torsional structure associated with transitions to the rotor levels, and allows deductions to be made with regards to which levels can interact together. This approach of labelling non-rigid, or 'floppy' molecules was initially detailed by Longuet-Higgins,[74] but has been expanded upon in more recent times by Bunker and Jensen,[75] thus the reader is ushered in this direction should they desire a wider understanding of the topic.

Where point groups comprise a series of reflections, rotations and inversions, the MSGs differ in that they involve the permutations of identical nuclei as well as the inversions of the coordinates. A complete series of the possible inversions and permutations is referred to as the complete nuclear permutation and inversion group, also known as the CNPI group. This set of elements will be able to fully treat any system, including those with rotors. They are, however, particularly unwieldly as the size of CNPI groups can become very large for reasonably small molecules *i.e.* benzene has 1036800 symmetry operations. If one analyses each possible symmetry operation within the full CNPI group, it is noted that a large number of these are not feasible operations in the instance where one is treating internal rotations of a methyl group. If one cuts out these operations, then what remains is referred to as a molecular symmetry group.

7.3.1 The G_{12} and G_6 MSGs:

The MSGs for pFT and mFT/mClT are G_{12} and G_6 respectively, given in the book by Bunker and Jensen.[75] Each MSG character table is given below (Table 7-1 and Table 7-2). The orientation of the molecule is given using the a,b and c notation to define the axis, as is convention,

where the linear functions are given with the molecule being oriented such that the *a*-axis runs through the centre of the internal rotation, with the *c*-axis being normal to the plane of the page. Note the overall layout of the table is similar to that of a point group, although the symmetry elements here correspond to permutation-inversion (PI) operations, as opposed to standard point group symmetry operations.

With reference to the table, one can determine the symmetry of each torsional level based upon how the rotor transforms under the symmetry operations, but it is necessary to first understand what these individually correspond to. As the operations in G_6 are encompassed in the G_{12} MSG, we will run through examples for the G_{12} group only, shown below in Figure 7:3:

Table 7-1 - Symmetry operations for the G_{12} molecular symmetry group.

G_{12}	E	(123)	$(23)^*$	(AB)	$(123)(AB)$	$(23)(AB)^*$	
$A_1{'}$	1	1	1	1	1	1	T_a
$A_1{''}$	1	1	1	-1	-1	-1	T_b, J_c
$A_2{'}$	1	1	-1	1	1	-1	J_a
$A_2{''}$	1	1	-1	-1	-1	1	T_c, J_b
$E{'}$	2	-1	0	2	-1	0	
$E{''}$	2	-1	0	-2	1	0	

Table 7-2 - Symmetry operations for the G_6 molecular symmetry group.

G_6	E	(123)	$(23)^*$	
A_1	1	1	1	T_a, T_b, J_c
A_2	1	1	-1	J_a, T_c, J_b
E	2	-1	0	

Starting with *E,* this is the same as the identity operation of a point group. This symmetry element merely corresponds to the untreated molecule.

(123) is a hydrogenic interchange mechanism within the rotor, where each number corresponds to a rotor H atom. If one imagines a Newman projection style, shown in Figure 7:3, H atom 1 is moved to the position of H atom 2, with atom 2 moved to position 3 and atom 3 moved to position 1, thus this is a cyclic permutation operation.

(23)* corresponds to a hydrogenic interchange of H atoms 2 and 3, such as in the above, followed by an inversion (*) of all atomic coordinates.

(AB) refers to permutation of the ring hydrogens *i.e.* a ring flipping motion. This occurs in G_{12} molecules as a result of the two-fold rotation of the ring, with respect to the *a*-axis. The asymmetry in the ring for G_6 molecules eliminates this symmetry operation in its corresponding character table. Here, A and B refer to the different sides of the ring with respect to the C_2 axis (ignoring the rotor).

The final two operations are merely combinations of what is already mentioned in the above and are shown in Figure 7:3.

Figure 7:3 - Depiction of the conformation of the methyl rotor with respect to the ring after undergoing the 6 operations in the G_{12} molecular symmetry group.
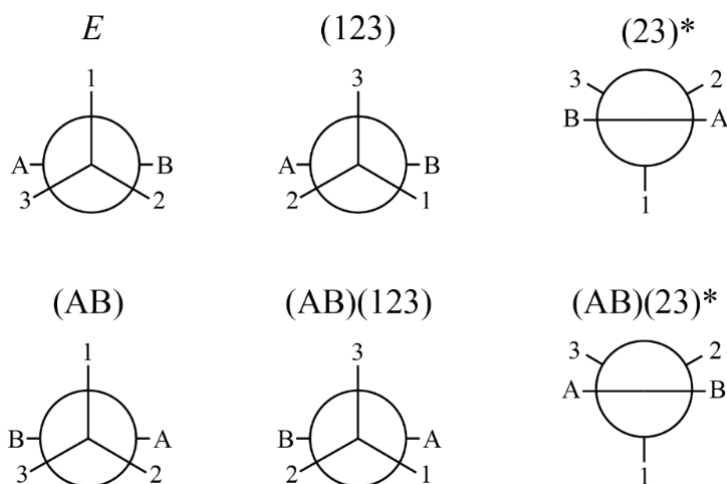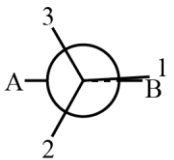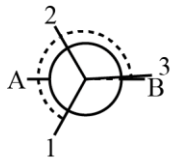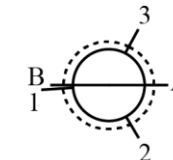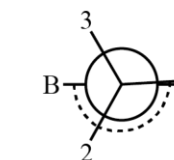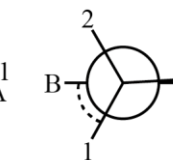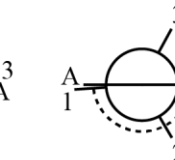
With these operations in mind, one can then begin to apply them to deduce the symmetry of each torsional level within the molecule's corresponding MSG. If one sets up a reference configuration of the rotor with respect to the ring, it is possible to deduce how the torsional angle, ϕ, varies as a function of the MSG operations. The torsional wavefunctions can be evaluated, in turn, as a cosine function, as the symmetry will be the same as that of the particle on a ring basis set eigenfunctions. This can be seen, since:

$$e^{+im\phi} + e^{-im\phi} = 2\cos(m\phi)$$
Eq. 42

We begin by using a reference configuration where H(1) is eclipsed with respect to B, with a torsional angle, ϕ, of 0°, as shown in Table 7-3. We then take the symmetry operations in turn. If one then applies the *E* operation, then ϕ changes by 0°. Similarly, with the (123) operation, ϕ changes by $\frac{4\pi}{3}$, and π for (AB). If one deduces the angle change for every operation it can then be substituted into the $2\cos(m\phi)$ term, where *m* is the torsional level. The reducible representations of the MSG are thus yielded, and if the reduction formula is then applied, the symmetries for each *m* level are then returned.

Table 7-1 – Depiction of the free rotor basis sets being treated with the symmetry operations. The resulting angles, given by the arc lines, are substituted into the $2\cos(m\phi)$ term for each m level, yielding the reducible representations. These are then reduced to give the symmetry for each torsional level for both the G_6 and G_{12} MSGs - see text for more details. Note that this figure is adapted from Table 2 in Ref 71.

Angle, ϕ	E	(123)	(23)*	(AB)	(AB)(123)	(AB)(23)*	Torsional symmetries	
	0	$\dfrac{4\pi}{3}$	2π*	π	$\dfrac{\pi}{3}$	π*		
m							G_6	G_{12}
0	1	1	1	1	1	1	a_1	a_1'
1	2	-1	0	-2	1	0	e	e''
2	2	-1	0	2	-1	0	e	e'
3	2	2	0	-2	-2	0	$a_1 + a_2$	$a_1'' + a_2''$
4	2	-1	0	2	-1	0	e	e'
5	2	-1	0	-2	1	0	e	e''
6	2	2	0	2	2	0	$a_1 + a_2$	$a_1' + a_2'$

Note that as an inversion has occurred, it is no longer possible to express these purely as a cos term, thus the reducible representations are given as zero

7.4 Torsional energy levels populations:

With this information regarding torsional symmetries in mind, one can now begin to look at the expected properties of the torsional structure in electronic spectra.

Before one begins to think about torsional transitions, it is first a good idea to understand which torsional levels are initially populated, remembering that jet-expansion conditions (see Chapter 8) are employed in our experiments.

It is often stated that the populations of the torsional levels may be calculated using the Boltzmann distribution given below:

$$\frac{N_i}{N} = \frac{g_i \times e^{\left(\frac{-E_i}{k_b T}\right)}}{\sum_i \left[g_i \times e^{\left(\frac{-E_i}{k_b T}\right)}\right]}$$

Eq. 43

Where N corresponds to the total number of molecules in the expansion; N_i is the population of a quantum level, i; E_i is the energy of the quantum level, and g_i is the degeneracy of the level. For the purpose of this calculation, the sum in the denominator is truncated after the $m = \pm 5$ torsional levels; we would not expect any significant population in torsional levels higher than these, as a jet-cooled beam should have rotational and vibrational temperatures of roughly 5 K and 50 K respectively. The percentage population of the first 11 torsional states are shown below in Table 7-4. Note that the barriers of mFT, mClT and pFT in the S_0 state are roughly the same, hence the % population in each torsional coordinate is expected to be similar.

Table 7-4 – Expected Boltzmann populations for the torsional energy levels assuming jet-expansion conditions. Note that the S_0 torsional wavenumbers for pFT are used, although the values for mFT and mClT are expected to be similar. The population is calculated assuming a temperature of 5 K, as the torsional temperature is assumed to be similar to the rotational temperature.

m	Wavenumber/ cm^{-1}	Population/ %
0	0	48.82
± 1	5.14	46.19
± 2	21.44	4.88
3(-)	48.1	0.07
3(+)	50.4	0.05
± 4	86.74	0.00
± 5	134.74	0.00

What we note is that roughly equal populations are expected in the $m = 0$ and $m = 1$ torsions, with a small amount in the $m = \pm 2$, and negligible population across any of the

other torsions. Notably, if one starts to change the expansion conditions, such as making them cooler, then it would be expected that the relative population between $m = 0$ and $m = 1$ would change, and more population would shift into the $m = 0$. Experimentally, this does not seem to be the case, with roughly 50 % of the population always residing in *a* symmetry levels ($m = 0, 3(-), 3(+)$ *etc*), with the other 50 % residing in *e* symmetry levels ($m = \pm1, \pm2, \pm4, \pm5$). There must, therefore, be another explanation for the relative population of the torsional levels under these conditions. One can go back to the wavefunction of the system, Ψ_{tot}, and, assuming the BO approximation, can break it down into its component wavefunctions, given below:

$$\Psi_{\text{tot}} = \psi_{\text{elec}}\psi_{\text{vib}}\psi_{\text{rot}}\psi_{\text{tor}}\psi_{\text{ns}}$$
<div align="right">Eq. 44</div>

For G_{12} and G_6 molecules, one can decide which symmetries are allowed for Ψ_{tot} as the Pauli principle states that the wavefunction must be symmetric with respect to exchange of even pairs of equivalent nuclei, and antisymmetric with respect to exchange of odd pairs of equivalent nuclei. With reference to Table 7-1 and Table 7-2, the (123) and (AB) operations for G_{12}, and the (123) operation for G_6 involve exchange of even pairs of H atoms. If one then looks down the column for the (123) and (AB) operations, it can be seen that the only two symmetric wavefunctions that are common to both groups (*i.e.* have values of 1) correspond to $A_1{'}$ and $A_2{'}$. Similarly, for G_6, both A_1 and A_2 are symmetric under the (123) operation. Thus, these are the only allowed symmetries for Ψ_{tot}.

Knowing this, we must then consider the symmetries of each individual wavefunction, in turn, to deduce the allowed symmetries for the torsional levels. Given the jet-expansion conditions, we expect to be in the ground electronic state, as well as the zero-point level for all vibrations, thus both ψ_{elec} and ψ_{vib} should each have $A_1{'}$ and A_1 symmetry for G_{12} and G_6 respectively. For ψ_{rot}, multiple rotational levels will be populated at 5 K, thus the symmetry of ψ_{rot} can be either $a_1{'}, a_1{''}, a_2{'}$, or $a_2{''}$ for G_{12}, and a_1 or a_2 for G_6. The overall symmetry for $\psi_{\text{elec}}\psi_{\text{vib}}\psi_{\text{rot}}$ will therefore have the same symmetry as ψ_{rot}. The torsional wavefunctions have previously been derived, and have been shown to be $a_1{'}, a_1{''}, a_2{'}, a_2{''}, e{'}$ or $e{''}$ for G_{12}, and a_1, a_2 or e symmetry for G_6. Knowing the symmetries of the first 4 terms of Eq. 44, one must then look at the nuclear spin wavefunctions. Longuet-Higgins[74] provides a detailed explanation of the derivation of the nuclear spin symmetries, but this will not be discussed in detail here – the symmetries of the nuclear spin functions can be $a_1{'}, a_1{''}, e{'}$ or $e{''}$ in G_{12}, and a_1 or e symmetry for G_6. One can then summarise all

possible symmetry combinations for the wavefunctions, $\psi_{\text{elec}}\psi_{\text{vib}}\psi_{\text{rot}}$, ψ_{tor} and ψ_{ns} – provided below in Table 7-5 (G_6) and Table 7-6 and Table 7-7 (G_{12}).

Table 7-5 – Summary of possible wavefunctions for each subcomponent of Ψ_{tot} within the G_6 MSG. Note that the product: $\psi_{elec}\psi_{vib}\psi_{rot} \times \psi_{tor} \times \psi_{ns} \supset A_1$ or A_2 for an allowed Ψ_{tot}.

G_6			
Ψ_{tot}	$\psi_{\text{elec}}\psi_{\text{vib}}\psi_{\text{rot}}$	ψ_{tor}	ψ_{ns}
A_1	a_1	a_1	a_1
		a_2	-
		e	e
A_2	a_2	a_1	a_1
		a_2	-
		e	e

Table 7-6 – Part 1 of summary of possible wavefunctions for each subcomponent of Ψ_{tot} within the G_{12} MSG. Note that the product: $\psi_{elec}\psi_{vib}\psi_{rot} \times \psi_{tor} \times \psi_{ns} \supset A_1'$ for an allowed Ψ_{tot}.

G_{12}			
Ψ_{tot}	$\psi_{\text{elec}}\psi_{\text{vib}}\psi_{\text{rot}}$	ψ_{tor}	ψ_{ns}
A_1'	A_1'	a_1'	a_1'
		a_1''	a_1''
		a_2'	-
		a_2''	-
		e'	e'
		e''	e''
	A_1''	a_1'	a_1'
		a_1''	a_1''
		a_2'	-
		a_2''	-
		e'	e'
		e''	e''
	A_2'	a_1'	a_1'
		a_1''	a_1''
		a_2'	-
		a_2''	-
		e'	e'
		e''	e''
	A_2''	a_1'	a_1'
		a_1''	a_1''
		a_2'	-
		a_2''	-
		e'	e'
		e''	e''

Table 7-7: Part 2 of summary of possible wavefunctions for each subcomponent of Ψ_{tot} within the G_{12} MSG. Note that the product: $\psi_{elec}\psi_{vib}\psi_{rot} \times \psi_{tor} \times \psi_{ns} \supset A_2'$ for an allowed Ψ_{tot}.

Ψ_{tot}	$\psi_{\text{elec}}\psi_{\text{vib}}\psi_{\text{rot}}$	ψ_{tor}	ψ_{ns}
A_2'	A_1'	a_1'	a_1'
		a_1''	a_1''
		a_2'	-
		a_2''	-
		e'	e'
		e''	e''
	A_1''	a_1'	a_1'
		a_1''	a_1''
		a_2'	-
		a_2''	-
		e'	e'
		e''	e''
	A_2'	a_1'	a_1'
		a_1''	a_1''
		a_2'	-
		a_2''	-
		e'	e'
		e''	e''
	A_2''	a_1'	a_1'
		a_1''	a_1''
		a_2'	-
		a_2''	-
		e'	e'
		e''	e''

For both G_{12} and G_6 molecules, in general, we can see that the only possible combinations of $\psi_{\text{elec}}\psi_{\text{vib}}\psi_{\text{rot}}$ are all a symmetry wavefunctions[2], thus for the overall wavefunction to be allowed, the product of ψ_{tor} and ψ_{ns} must also be an a symmetry component. For this to occur, the symmetries of ψ_{tor} and ψ_{ns} must both either be an a symmetry component, or both be an e symmetry component. Should one be an a, and the other be an e, then there are no wavefunction combinations that will yield an allowed Ψ_{tot}. As a result of this, conversion between levels of a and e symmetry is forbidden, and both the a and e symmetry torsions are thus fated to both be populated in the jet expansion.

---

[2] Note that we are referring only to 'a' and 'e' symmetry to be inclusive of both G_6 and G_{12} molecules, for which the argument made is the same.

This explanation shows why both *a* and *e* symmetry torsions are populated in the jet expansion but does not explain why they have a 50/50 population split. If one takes a series of all the possible nuclear spin conformations, *i.e.* if one allocates each H atom a spin of $+\frac{1}{2}$ or $-\frac{1}{2}$, and shows how each of these conformations changes under the symmetry operations of the MSG, then one can see that there are twice as many *a* symmetry spin functions as there are *e*. Notably, however, the *e* symmetry levels are each doubly degenerate, thus these factors cancel out, resulting in an approximately equal split of the population in the jet-expansion.

7.5 Torsion-related selection rules and transition intensities:

The transitions one expects to see involving torsions is gleaned from a similar mechanism by which one can understand the vibrational structure. Here, one can express the overall electronic transition dipole moment, M_e, as a function of the torsional angle.

$$G_{12} \rightarrow M_e = \langle \psi_{t''} | \psi_{e''}(q,\phi) | \mu | \psi_{t'} | \psi_{e'}(q,\phi) \rangle \supset A_1{'} \qquad \text{Eq. 45}$$

$$G_6 \rightarrow M_e = \langle \psi_{t''} | \psi_{e''}(q,\phi) | \mu | \psi_{t'} | \psi_{e'}(q,\phi) \rangle \supset A_1$$

where q is the electronic coordinate, and ϕ is the torsional angle.

Referring to the MSG symmetry tables, one first treats the electronic part of the transition:

$$G_{12} \rightarrow M_e = \langle \psi_{e''}(q,\phi) | \mu | \psi_{e'}(q,\phi) \rangle \supset A_1{'}, A_1{''} \text{ or } A_2{''} \qquad \text{Eq. 46}$$

$$G_6 \rightarrow M_e = \langle \psi_{e''}(q,\phi) | \mu | \psi_{e'}(q,\phi) \rangle \supset A_1 \text{ or } A_2$$

Thus, the electronic transition will be allowed if the overall symmetry of the associated terms transforms as $A_1{'}, A_1{''}$ *or* $A_2{''}$ for G_{12}, and A_1 *or* A_2 for G_6.

One must then consider the torsional wavefunctions, assuming an allowed electronic transition, where the allowed torsional transitions and intensities can be given as a converging Fourier series of the electronic transition dipole moment, M_e, in terms of the torsional angle.

$$M_e(\phi) = M_0 + M_3 cos(3\phi) + M'_3 sin(3\phi) + M_6 cos(6\phi) + M'_6 sin(6\phi) \qquad \text{Eq. 47}$$

where M_n are the expansion coefficients, and ϕ is the torsional angle. Here, each of the terms drives a different form of transition; the question being, which of the terms drives which transition? Note that each of the terms above corresponds to the expansion *via* each

component of the dipole moment ope, with the $M'_3 sin(3\phi)$ being the exception to this case. This term only becomes non-zero if affiliated with a vibration i.e. a combination of the m = 3(-) torsion with a vibration where the product of symmetries must be totally symmetric.

If one defines ϕ=0 as the eclipsed conformation, and knowing the symmetries of the initial and final electronic state, as well as the symmetries of each component of the dipole moment operator, one can deduce the allowed symmetries of torsional wavefunctions, $\langle \psi_{t''}|\psi_{t'}\rangle$, driven by each of the Fourier terms, shown in Table 7-8.

Table 7-8 – Symmetries of each Fourier expansion term for both G_{12} and G_6 MSGs.

Term	G_{12} $\langle \psi_{t''}|\psi_{t'}\rangle$ symmetry	G_6 $\langle \psi_{t''}|\psi_{t'}\rangle$ symmetry
$M_3 cos(3\phi)$	a_1''	a_1
$M_0 + M_6 cos(6\phi)$	a_1'	a_1
$M'_6 sin(6\phi)$	a_2'	a_2

Remembering that 50% of the initial state population is in the lowest energy a symmetry state, (a_1' for G_{12} and a_1 for G_6) and the other 50% is in the lowest e symmetry state (e'' for G_{12} and e for G_6), one can then deduce which of the above symmetries corresponds to which torsional transition, $\langle \psi_{t''}|\psi_{t'}\rangle$ - Table 7-9 (G_{12}) and Table 7-10 (G_6).

Table 7-9 – Allowed torsional transitions given by each Fourier expansion term for the G_{12} MSG.

Term	$\psi_{t''}$	$\psi_{t'}$	$\langle \psi_{t''}|\psi_{t'}\rangle$	Transition
$M_3 cos(3\phi)$	a_1'	a_1''	a_1''	$m_0^{3(+)}$
$M_0 + M_6 cos(6\phi)$	a_1'	a_1'	a_1'	$m_0^0, m_0^{6(+)}$
$M'_6 sin(6\phi)$	a_1'	a_2'	a_2'	$m_0^{6(-)}$
$M_3 cos(3\phi)$	e''	e'	e''	m_1^2, m_1^4
$M_0 + M_6 cos(6\phi)$	e''	e''	e'	m_1^1, m_1^5, m_1^7
$M'_6 sin(6\phi)$	e''	e''	e'	m_1^5, m_1^7

Note that in Table 7-9 and Table 7-10, the 'm_x^y' nomenclature is used, with m indicating that this is a torsional transition, x being the initial torsional state, and y being the final torsional state.

Table 7-10 - Allowed torsional transitions for each Fourier expansion term for the G_6 MSG.

	G_6			
Term	$\psi_{t''}$	$\psi_{t'}$	$\langle\psi_{t''}|\psi_{t'}\rangle$	Transition
$M_3 cos(3\phi)$	a_1	a_1	a_1	$m_0^{3(+)}$
$M_0 + M_6 cos(6\phi)$	a_1	a_1	a_1	$m_0^0, m_0^{6(+)}$
$M'_6 sin(6\phi)$	a_1	a_2	a_2	$m_0^{6(-)}$
$M_3 cos(3\phi)$	e	e	e	m_1^2, m_1^4
$M_0 + M_6 cos(6\phi)$	e	e	e	m_1^1, m_1^5, m_1^7
$M'_6 sin(6\phi)$	e	e	e	m_1^5, m_1^7

Referring back to Eq. 47, the expansion coefficients are given by a converging series. These terms correspond to the expected intensities relating to the change in torsional quantum number following an electronic transition, where the M_0 term corresponds to $\Delta m = 0$ transitions, M_3 corresponds to $\Delta m = \pm 3$ transitions, M_6 to $\Delta m = \pm 6$ transitions and so on. It is therefore expected that the intensities will be as follows:

$$\Delta m = 0 > \Delta m = \pm 3 \gg \Delta m = \pm 6$$

Note that the relative symmetries of the initial and final torsional states are important in deducing if the transition is expected to be intense or not. If the symmetry is different between torsional states, then the transition must gain intensity *via* other means. Notably, the a symmetry transitions corresponding to the $M_3 cos(3\phi)$, $M'_3 sin(3\phi)$ and $M'_6 sin(6\phi)$ terms for G_{12} molecules, and $M'_3 sin(3\phi)$ and $M'_6 sin(6\phi)$ for G_6 molecules do not follow the symmetry selection rules. These terms therefore correspond to transitions that may gain intensity from second order mechanisms, such as Herzberg-Teller, Intrachannel or Coriolis coupling.

Taking the above into account, what torsional structure would we then expect to see following an electronic transition between two states that have similar torsional potentials? Using a G_{12} molecule as an example, and assuming that we are starting in the lowest energy

$a_1{}'$ level, then one can combine the transition types from Table 7-10 with the expansion coefficients from Eq. 47 to decide what should be seen. Here, one would expect to see the FC active m_0^0 and $m_0^{6(+)}$ with the latter being significantly weaker than the former. An $m_0^{3(+)}$ band would also be expected *via* a second order mechanism, but its intensity would be dependent on the strength of the coupling that induces the band. An $m_0^{6(-)}$ may also be expected, although a combination of the fact that it is a $\Delta m = 6$ transition, as well as being induced through a second order mechanism means that very little, if any, intensity will be seen.

What if, then, the torsional barrier is radically different between an initial and final electronic state? As will be seen at a later point, the preferred torsional conformation changes during the $D_0^+ \leftarrow S_1$ transition in both *m*FT and *m*ClT; this causes the maximum of the potential to shift by 60°. If one then imagines a transition between two torsional energy levels, the maximum of one potential now corresponds to the minimum of the other, hence the overlap of the torsional wavefunctions is expected to be modified. The symmetry selection rule relating to the transitions is shown to hold although, as expected, the intensity distribution between 'FC' allowed transitions will change, more of which will be seen in the Chapters 13 and 14.

7.6 Interactions involving torsions:

Every time a pure electronic or vibronic state is populated, there will always be an accompanying populated torsional quantum state, assuming *m* = 0 is also labelled as a torsional state. This is denoted simply with the letter '*m*' followed by the torsional quantum number, for example *m* = 3(+). Torsions can also be accompanied by vibrations, thus forming vibration-torsion combinations, colloquially known as vibtor levels. This is denoted by the vibrational mode, followed by the torsional quantum number e.g. D_{30} *m* = 3(-).

Where we have previously seen interactions between two or more vibrations, such as the cases of the Fermi Resonance and different manifestations of IVR, torsions may play a very similar role. The vibtor levels behave in a comparable way to vibrations in that, if they are close by to other fundamentals, vibtors, combination levels or overtones, and the symmetries are the same, then they may perturb them in the same way as seen in Section 5. The presence of the vibtor bands can be seen to drastically increase the density of states at all internal energies within the molecule, thus they greatly increase the potential for coupling

to occur. A clear example of this can be seen in the 1015 cm^{-1} of pFT,[41] although numerous examples will also be seen in Chapters 10-14.

8. Experimental:

The experimental data sets published within this thesis have been collected using a combination of two sets of apparatus. The first experimental apparatus is capable of performing experimentation in order to aid the understanding of both the excited and cationic states – this is the resonance-enhanced multi-photon ionisation (REMPI) spectroscopic set-up, which is paired with the zero-electron-kinetic energy (ZEKE) experiment.

The second experimental set-up combines the laser-induced fluorescence (LIF) setup with the dispersed fluorescence (DF)/two-dimensional laser induced fluorescence (2D-LIF) experiments. These two experiments work to provide complementary sets of results which allow for a more complete understanding of the vibrational coupling and mixing elements seen within our samples. This section will outline both sets of experiments, as well as the individual advantages and disadvantages of each technique. We also discuss the equipment and set-up of each experiment, with further discussion of the theory behind them at the end of the section.

8.1 REMPI spectroscopy:

REMPI spectroscopy is a technique usually employed and utilised to understand the structure of excited electronic states. This form of spectroscopy is well suited to the study of gas phase systems, thus one requires the sample of interest to have a reasonable vapour pressure or, at least, there must be a way to form reasonable vapour either by heating or some form of ablation or shock mechanism. Liquid jets are also possible, although discernible vibrational structure is lost as a result of the energetic distribution within the degrees of freedom.

The REMPI technique can be used to study a wide range of stable molecules, as well as clusters and complexes, and is sometimes used in tandem with another form of spectroscopy. REMPI is used to map out the spectroscopic structure in an excited state, and another technique can then be used to project the population of each of those levels from the excited state onto another. We combine the REMPI and ZEKE techniques in order to first probe the excited, usually S_1, state and then use ZEKE to project the S_1 population onto the

D_0^+ state in order to build up an idea of the structure and interactions occurring in both S_1 and D_0^+ states.

Traditionally, a gaseous sample is pulsed into an interaction region where the output of a tuneable laser is then directed towards, and intersects, the pulsed sample. Should the energy of the laser be suitable, a transition will occur promoting an electron from the ground state to the excited state. This step usually involves single-photon absorption, although it is possible to do this with absorption of multiple photons – a schematic of some of the possible REMPI pathways is given in Figure 8:1, with these being discussed in greater detail below.

Figure 8:1 – Schematic of some possible REMPI pathways.
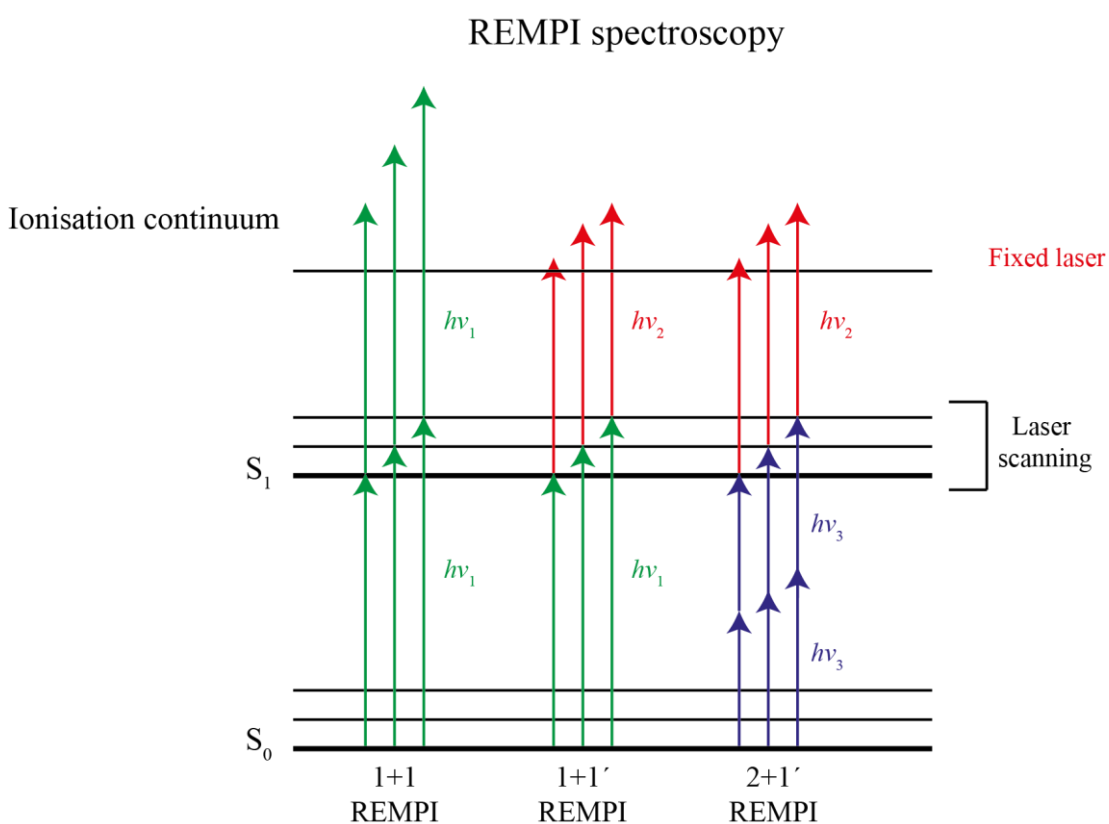
REMPI experiments typically employ tuneable laser sources such as a dye laser, which require a pump source, for instance an Nd:YAG laser. Depicted in Figure 8:1, if one varies the energetic output of the dye laser, then one can begin to scan through the levels of the excited state. Each time an S_1 resonance is reached, an absorption between the ground and excited states occurs. This greatly increases the probability for a second photon to further excite the molecule into the ionisation continuum, thus generating many ions which can be recorded by a detector. If one measures the ion signal as a function of photon energy, one can map out the Franck-Condon active vibrational (and torsional) structure within the excited electronic state – a REMPI spectrum. If the photon density is particularly high *i.e.* the laser

power is high, or the beam is tightly focussed, then it is possible to prepare the molecule in a virtual state, and then ionise *via* this. The resulting ions can also be detected, and this is known as non-resonant ionisation. Notably, signals due to a non-resonant transition are not always related to the vibrational energy levels in the electronic state of interest.

The resulting ions are directed down a time-of-flight tube and detected on a set of microchannel plates (MCPs). In the case of an imaging experiment, the MCPs are paired with a phosphor screen and a CCD camera, although this setup is not used in this work. The time-of-flight tube allows for mass resolution of the ions; the speed in which they travel down the tube will be inversely proportional to the mass of the ion, thus allowing fragments, complexes, clusters and even isotopologues of the sample to be detected separately.

When one describes the REMPI process, the number of photons used to excite and ionise is often indicated. In this work, we take advantage of the 1+1 and 1+1′ REMPI processes – shown in Figure 8:1. In a scenario where the energy gap between the initial state and the intermediate state is larger than the gap between the intermediate and the final state (*i.e.* the intermediate is over half way towards the ionisation energy), one can use 2 photons of the same energy to populate the intermediate state and then ionise. This is referred to as a 1+1 process, or a 'one-colour' process. In the scenario where the gap between the initial and intermediate states is less than the gap between the intermediate and ionisation continuum, two photons of different energies may be required to be able to ionise from the intermediate, this is known as a 1+1′ or 'two-colour' process, where the ′ (prime) symbol indicates a photon of different energy to the initial photon. Note that a two-colour process can also be used in order to lower the effect of power broadening.

Additionally, one can take advantage of multi-photon absorption from the initial to the excited state. Figure 8:1 also depicts 2+1′ REMPI, where two photons of the same energy initially excite to the intermediate state, with another photon of different energy then ionising. The first photon prepares the molecules in a virtual quantum state, awaiting the subsequent photon which can then promote the electron into the bound electronic state of interest. This process becomes more difficult with increasing numbers of photons and, further to this, using different numbers of photons to promote to an excited state modifies the selection rules; this can be useful if one is trying to study forbidden electronic transitions or reach high-lying electronic states. This will not, however, be discussed further in his work, which comprises 1+1 and 1+1′ REMPI processes only.

Notably, all REMPI spectra collected and presented in this work have a resolution which is limited mainly by the jet-expansion conditions. Depending on the temperature of the expansion, and thus the rotational levels populated, the highest resolution achieved in this work yields REMPI bands of roughly 2-4 cm^{-1} full-width-half-max (FWHM).

8.2 ZEKE spectroscopy:

Where REMPI allows one to map out the vibrational and torsional structure in an electronic excited state (S_1), ZEKE then allows us to project the population of excited state intermediates onto the cationic ground state, D_0^+. In essence, this helps us record the structure within the cation as a function of each S_1 intermediate which, in turn, aids our understanding of the magnitude of the vibrational coupling or mixing elements in the excited state. This also, to some extent, gives us some insight into whether or not interactions are occurring in the cationic state, although this is more difficult to ascertain.

For this technique, one usually requires at least 2 photons of different colour. One laser will provide the excitation step to a known intermediate, with its energy being fixed. A second tuneable laser is then used to scan through the internal energy levels in the cation. This is depicted in Figure 8:2 below.

Figure 8:2 – Schematic of the ZEKE operating mechanism.
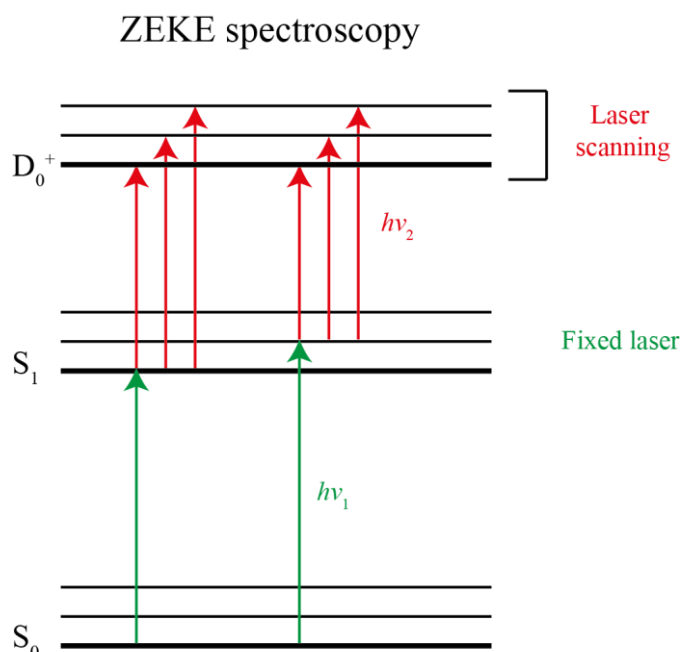
Traditionally, when one scans the second laser through the vibronic levels in the cation and the laser comes into resonance, electrons of zero-kinetic-energy are produced. If one waits for a small amount of time for the kinetic-energy-electrons to move away and then applies a

pulsed electric field, then the zero-kinetic-energy electrons can be extracted in isolation. In practice, this is particularly difficult to achieve, with signal often being quite low due to stray electric and magnetic fields impacting the zero-kinetic-energy electrons. This technique is often referred to as 'true' ZEKE.

If the technique is slightly modified, then it is possible to manoeuvre around the problem relating to the stray fields which can greatly increase the signal. Very slightly below the ionisation energy lies a series of high principal quantum number, n, energy levels, known as Rydberg states. If one excites through to the Rydberg states, as opposed to the cationic level itself, then it is then possible to apply a pulsed field to extract the Rydberg-bound electrons. Here, stray fields do not pose a problem, as they are typically not large enough in magnitude to extract many of the electrons below the ionisation energy. This technique is referred to as ZEKE-PFI or zero-electron-kinetic-energy pulsed-field-ionisation spectroscopy.

'True' ZEKE and ZEKE-PFI both have their own advantages and disadvantages. We have previously discussed the fact that stray electric fields cause issues with the zero-kinetic energy electrons. Collecting the electrons in this way, however, only extracts information from the D_0^+ vibrational level itself, thus the resolution of the spectrum should be limited by the theoretical maximum for the laser, as well as expansion conditions. In ZEKE-PFI an issue is encountered in that, due to the fact that there is a high density of Rydberg states within a small energy range, when the pulse is applied electrons are extracted from a variety of states creating a spread of electron kinetic energies. As a result, the resolution appears lower than it does in 'true' ZEKE, and is related to the field strength of the pulse. Taking this into account, we often see that the ZEKE bands are resolved roughly on the order of 7-10 cm^{-1}, although this is still significantly higher than standard photoelectron techniques which can yield resolutions of up to 100 cm^{-1} or more.

8.3 LIF spectroscopy:

Laser-induced fluorescence (LIF) spectroscopy usually combines a tuneable laser source with either a pulsed gaseous sample or a cuvette-contained liquid sample. A laser is first used to excite through a number of vibrational levels in an excited state of interest, similar to the first step of REMPI. After exciting to a resonant level, one can then wait for a certain amount of time after which the molecule will fluoresce, with the excited electronic state population being projected onto a wide range of FC allowed levels in the lower state. This technique is used widely in the field of spectroscopy and is often seen as the 'fluorescence equivalent' of the REMPI photoionisation technique.

One usually employs a detection mechanism which couples a collection optic with a photo-multiplier tube (PMT). As the fluorescence is isotropic around the interaction region, inevitably some of the photons will pass through the optic, be focused and then impinge upon the PMT, thus creating a measurable current. If one scans the laser through a series of vibrational and torsional levels in the excited state, one can then measure the current, due to fluorescence, as a function of laser energy, thus mapping out the internal structure of the excited state. Note that, if this experiment is not paired with a monochromator, one can only detect when photons are emitted when the laser reaches a resonance, but no information about the S_0 levels is achieved with this technique.

Similar to REMPI, the initial $S_1 \leftarrow S_0$ transition can be achieved as either a single photon excitation or as a multi-photon absorption. We only consider single-photon excitation in this work - a schematic representing this is shown in Figure 8:3(a).

The fact that ionisation is not necessary means that this technique is possible with only a single laser, thus such an experiment is, technically, easier and cheaper to set-up than a REMPI experiment. Notably, one is relying on the fluorescence properties of the molecule to detect any signal. If there are any outcompeting processes, such as internal conversion or intersystem crossings, one would expect to see a significantly reduced amount of fluorescence, or sometimes even lifetime broadening, which can make the structure more difficult to interpret compared to photoionisation techniques, which are inherently much quicker. For molecules such as *m*FT and *p*FT, however, the fluorescence lifetime is on the order of about 100 ns and there are no obvious outcompeting processes, this makes this technique ideal to use for these systems.

Figure 8:3 – Schematic depicting the LIF and DF techniques.
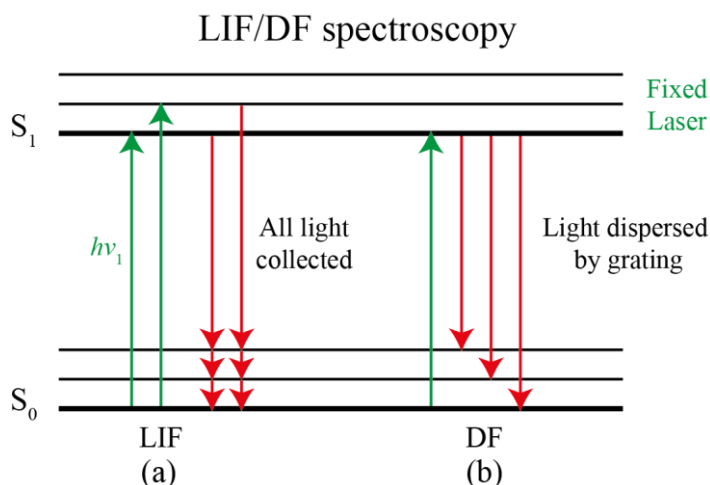
Similarly to the REMPI technique, one expects that the resolution of the experiment will be dictated by a number of factors. Competitive decay processes, jet-expansion conditions (and the resulting populated rotational levels) and power broadening (as a high photon yield can be required for good signal) often make the width of the experimental bands slightly wider than what one sees in the REMPI experiment, with bands often being on the order of 4-7 cm^{-1} in our experiment.

8.4 DF and 2D-LIF spectroscopy:

As seen with the REMPI/ZEKE experiment, one often combines LIF with a complementary technique to further probe the activity of a sample of interest. If a fluorescence experiment is combined with a monochromator, the user has the ability to disperse the fluorescence from the excited state, thus allowing the mapping out of the S_0 vibrational and torsional levels as a function of a given S_1 intermediate.

Two techniques are combined with the LIF experiment in our set-up, with these being dispersed fluorescence (DF) spectroscopy, and two-dimensional laser-induced fluorescence (2D-LIF) spectroscopy. Similar to LIF, if the laser becomes resonant with an excited vibrational level, the molecule may fluoresce. The fluorescence can be focused *via* a collection optic coupled to a monochromator. The light is dispersed by a grating, with this light then directed towards a detector, usually a CCD camera. The schematic of this is shown in Figure 8:3(b). Notably, the active area of the CCD camera is usually quite small with respect to the width of dispersed light. As a result of this, only a small portion of the dispersed wavelengths of light (~300 cm^{-1} window in our experiment) can be detected at a given grating angle. If one changes the angle of the grating, it is then possible to collect different windows of the dispersed light.

2D-LIF repeats the elements of the DF experiment, but differs in the fact that the laser is not fixed, but scanned through the excited state vibrations. The laser is set just below a resonance of interest and the fluorescence is collected for a set number of laser shots at this position. The laser is then stepped in very small increments over the excited state feature, collecting the fluorescence at each position - this is depicted below in Figure 8:4. This process is then repeated for a number of different grating angles, collecting a number of fluorescence windows. Each overlapping window is spliced together, thus building up a figure of the intensity vs both fluorescence wavenumber and laser wavenumber.

Both DF and 2D-LIF have similar advantages to ZEKE in that they allow for the interrogation of any coupled or mixed excited state vibrational/torsional modes. The advantage of these techniques, compared to ZEKE, is that the transitions are all from excited to ground state. Here, the selection rules are more rigorous than they are in photoelectron spectroscopy techniques, arguably allowing one to understand the extent of the interactions more clearly. Furthermore, the S_0 levels are, for a large range of molecules, already known from previous Raman/IR studies which makes understanding the structure significantly easier. As with LIF, one is relying on the fluorescence properties, so lifetime and decay processes can interfere with the fluorescence yield to a degree, although this is not a noticeable issue in this work.

Figure 8:4 – Depiction of the mechanism of 2D-LIF.
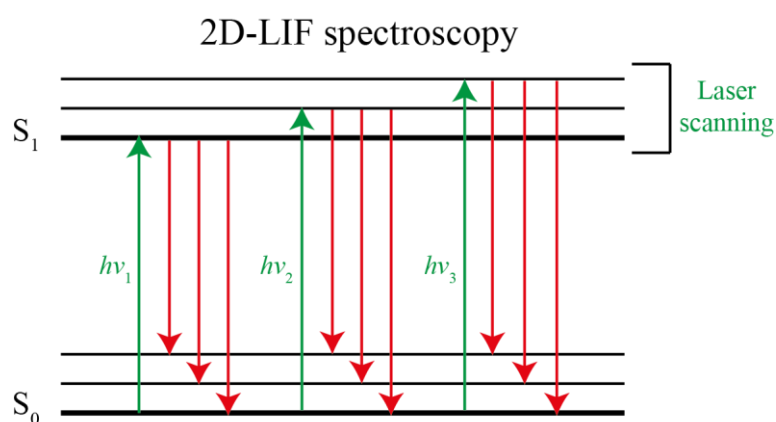
The LIF and DF fluorescence techniques, when combined, allow for complementary information to the REMPI/ZEKE experiment to be obtained which can be useful, particularly in the instances where interactions between the intermediate levels is complicated. The 2D-LIF technique, however, is where fluorescence spectroscopy begins to offer more than the other mentioned techniques. With traditional 1D techniques, it can sometimes be difficult to ascertain whether two close-by/overlapping features are intrinsically coupled or not; in some cases, it is even difficult to determine the identity of the overlapping levels. The profiles and positions of 2D-LIF bands may help overcome these issues. If two excited state intermediates are overlapped, but not coupled, then one would expect to see two series of fluorescence features, each with different emission profiles to the other. However, if the features are indeed coupled then one would expect to see common structure in the emission profiles as, if the wavefunctions are mixed, similar fluorescence profiles should be expected. Examples of this will be seen in greater detail later in this work, specifically in the 400 cm^{-1} and 800 cm^{-1} regions of pFT and, although not discussed in the main body of this work, a prime example of this can be seen in the 1015 cm^{-1} region of the S_1 state of pFT.[41]

This experiment has further limitations than does the LIF experiment, in that the resolution is expected to be related to the expansion conditions, the laser, as well as the properties of the monochromator and the camera coupled to it. If the resolution of either the laser or the monochromator is vastly different from the other, then one of the components can, in essence, 'bottleneck' the maximum resolution capable of the other. Optimally our monochromator/CCD combination, for UV photons of roughly 250 nm, has an operating resolution of under 2 cm^{-1} FWHM. This resolution, however, depends on several properties: the width of the entrance slits, the groove density of the grating, and the pixel density of the camera. The latter two are fixed and cannot be changed without replacing the grating or camera. The width of the entrance slits, however, can be modified in order to alter the amount of light entering the monochromator, and, notably, is inversely proportional to the resolution obtained, thus a balance is required in order to achieve an acceptable signal:resolution ratio. Due to a combination of the chosen entrance slit widths, as well as the expansion conditions, the FWHM of the DF and 2D-LIF is seen to be closer to 5-7 cm^{-1}, which is suitable for our purposes.

8.5 Apparatus:

The previous section has outlined the basic theory behind each technique used in this work, and what they can be used for. This section will describe in more detail the apparatus used, as well as the experimental conditions employed in order to collect the data described in this report.

8.5.1 REMPI/ZEKE:

A schematic for this experiment is shown in Figure 8:5, and is adapted from Ref 60.

The conditions specific to each sample considered in this work will be clearly stated in their respective publication, however a general overview will be given here. The vapour of the room temperature sample of interest (heated to ~50°C for *m*ClT) is seeded in 99% purity argon gas, between 0.5–1 bar above atmospheric pressure. The sample/argon mixture passes through a steel nozzle tube and, after equilibration, is allowed to expand through the orifice of a solenoid pulse valve. The valve operates with a 0.79 mm diameter orifice at a 10 Hz rep rate, and with an opening time of 150-200 μs, optimised to maximise the signal whilst avoiding hot jet-expansion conditions. The resulting gas expands into the interaction region of a vacuum chamber operating at roughly 10^{-7} mbar. Here, it is intersected by the outputs of the lasers – described below.

Two Nd:YAG lasers, a Continuum Surelite I and Surelite III, each pump a Sirah Cobra-Stretch dye laser. The Nd:YAG laser functions at either the 532 nm second harmonic or the 355 nm third harmonic, depending on the photon energy required to pump the required laser dye. The dye laser output is frequency doubled using either BBO or KDP crystals, depending on the energetic output of the laser. The resulting UV output from each laser is steered and focused into the interaction chamber *via* a series of prisms and lenses. The laser beams are each overlapped spatially and temporally with each other, as well as with the expanded gaseous mixture containing the sample.

Figure 8:5 – Schematic of the experimental apparatus employed for the REMPI/ZEKE techniques.
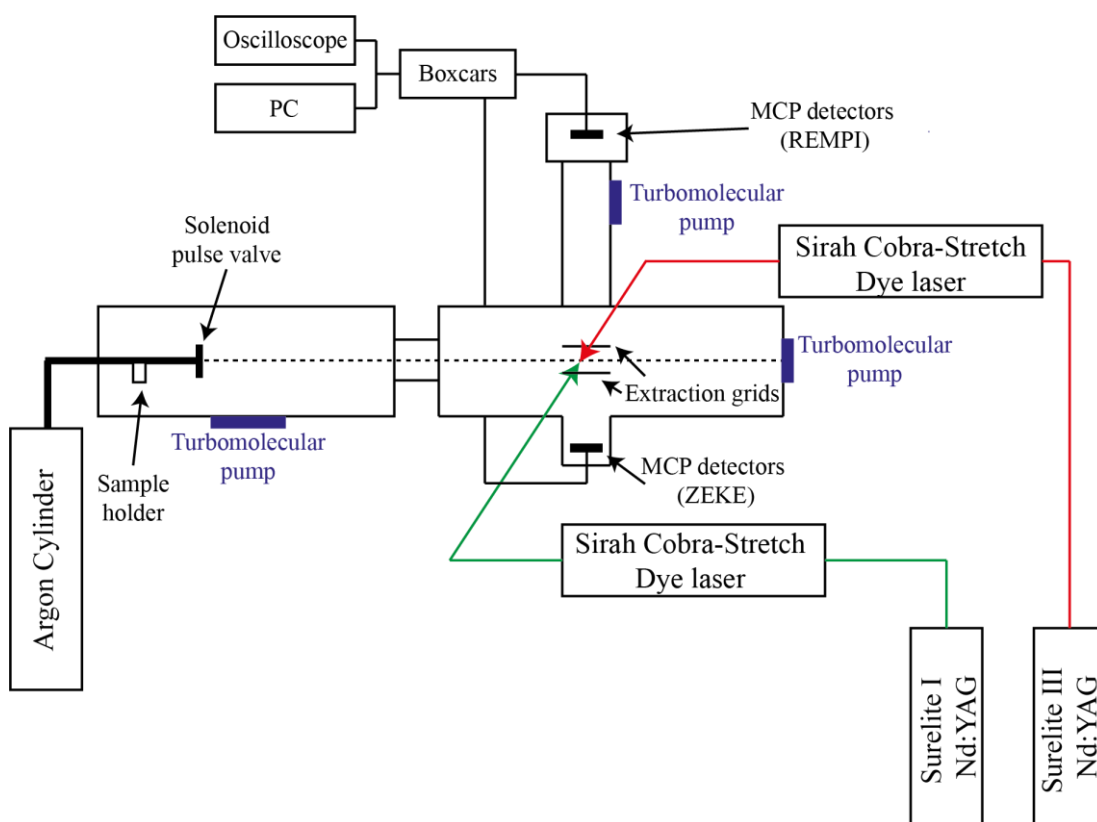
The interaction region occurs halfway between two electrical ion extraction grids. When ionisation occurs, both plates are positively charged. The lower plate has a greater voltage applied than does the upper in order to drive the resulting ions upwards, towards the Wiley-McLaren type time-of-flight mass spectrometer. This set up allows for good mass resolution between ions with mass differences usually within an atomic mass unit (assuming the same charge). The resulting ions then strike the microchannel plate (MCP) detectors. The signal is then sent to a SR250 gated integrator, which is connected to an oscilloscope, for visualisation. The signal is then gated, integrated, averaged and sent to a PC for collection. For the ZEKE experiment, the top ion extraction grid is grounded, and a small positive charge is applied to

the bottom plate after roughly 1.5-2 µs after the laser pulse, thus extracting the Rydberg electrons towards a bottom set of MCPs whilst minimising any signal due to non-zero-kinetic-energy electrons. The signal is processed in the same way as mentioned above.

8.5.2 LIF and DF/2D-LIF:

A schematic for this experiment is shown in Figure 8:6. Note that a side-on view of the apparatus is given for all components apart from the monochromator, where a 'top-downwards' approach is taken.

Similar to the REMPI/ZEKE experiment, the vapour of the room temperature sample is seeded in 99% purity argon gas at 0.5-4 bar above atmospheric pressure. The sample/argon mixture passes through a steel nozzle tube , where it is equilibrated and then allowed to expand through the orifice of a solenoid pulse valve. The valve operates with a 0.79 mm orifice diameter at a 10 Hz rep rate, and with an opening time of ~200-300 µs, optimised to maximise the signal whilst avoiding hot jet-expansion conditions. The resulting gas expands into the interaction region where it is intersected by the laser system.

Figure 8:6 - Schematic of the experimental apparatus employed for the LIF/DF/2D-LIF techniques.
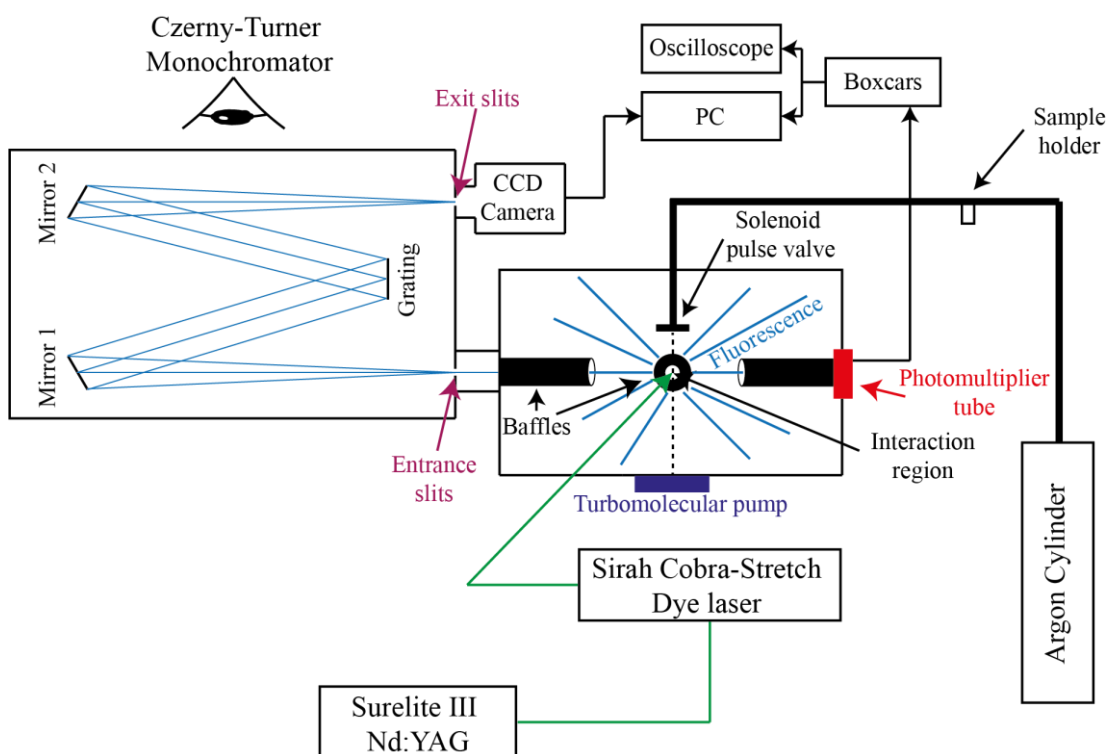
A Surelite III Nd:YAG laser, pumping at 355nm, pumps a Sirah Cobra-Stretch dye laser. The dye laser output is frequency doubled using BBO crystals, and the resulting UV output is directed into the interaction chamber where it perpendicularly intersects and is temporally

overlapped with the expanded sample mixture. The path of the laser beam inside the chamber is partially enclosed inside a pair of baffles, this helps prevent any scatter from the laser striking the photomultiplier tube or entering the monochromator. These are also useful in the process of alignment, as they pass directly down the centre of the chamber, with the orifices of the baffles lined up with the centre of the jet expansion.

Inside the chamber, either side of the interaction region, there are two identical sets of collection optics. These act to focus the fluorescence and direct it towards either the active region of the photomultiplier tube (PMT), or the entrance slits of the monochromator. Each of these optics are enclosed in a set of baffles to contain the fluorescence, as well as also preventing laser scatter reaching the detectors and yielding spurious signals. After a resonance is reached and the molecule fluoresces, part of the isotropic fluorescence will pass down one of the baffles towards the PMT where a current due to the photon flux is created. The signal is then sent to a SR250 gated integrator, which is connected to an oscilloscope, for visualisation, where the signal is gated, integrated, averaged and collected by a PC. The gate is usually positioned slightly off centre from the signal, at a later point in time. The exponential fluorescence decay profile occurs over a longer time period compared to the sharp, narrow laser pulse scatter. By suitable selection of the gate, it is possible to minimise the laser scatter signal with respect to the fluorescence signal, while still obtaining good signal-to-noise.

The fluorescence can also be collected and passed into a Sciencetech 9150 monochromator, in the Czerny-Turner design. The fluorescence is directed through the entrance slits of the monochromator, which are positioned at the focal point of the collection optic. The focussed light travels towards an angled collimating mirror which redirects the, now collimated, light towards the grating. The grating disperses and deflects the light towards a focussing mirror. The focal length of the mirror is such that the light is focussed upon the exit slits, which are paired with an Andor Solis iStar CCD camera. The fluorescence is then detected by a camera, which has internal gating and integrating systems, thus the data is transmitted directly to the PC for analysis.

8.6 Jet expansions:

As mentioned earlier, all spectroscopic measurements in this work have been undertaken with jet-expansion conditions. This greatly aids in cooling the internal degrees of freedom of the system. As a result, the majority of transitions occur from an electronic state in the vibrational zero-point energy, massively reducing the congestion of the spectra.

Jet-expansion experiments, such as ours, rely on having a large pressure differential between the part of the experiment containing the sample: the nozzle, and the part where the sample interacts with the laser: the interaction region. At the end of the nozzle is the pulse valve containing a small pinhole. This pinhole separates the 'high pressure' nozzle from the interaction region, which is under vacuum conditions roughly on the order of 10^{-7} mbar. Should the diameter of the valve orifice be significantly larger than the mean free path of the gas molecules then, when the valve opens, the gas molecules will travel through and undergo a large number of collisions, leading to adiabatic cooling. The molecules that are moving faster will have a lower mean free path than the molecules moving slower, thus the faster molecules undergo more collisions. Further to this, as the molecules are all flowing through a small pinhole, the directionality of the molecules at the centre of the expansion becomes almost identical, thus the translational temperature of the sample, as judged by the narrowness of the speed distribution, may be viewed as being incredibly low. Additionally, the enthalpy of the gas remains identical on both sides of the pinhole as no exchange of energy is occurring between it and the surroundings. As the molecules pass through the pinhole, however, there is a large gain in momentum towards the region of lower pressure such that the internal energy must be reduced to obey energy conservation principles. This is converted to translational energy, hence the average molecular speed is slightly higher on the low-pressure side of the pinhole. Overall, a Maxwell-Boltzmann distribution that is significantly narrower than a standard distribution, but faster on average is yielded.

Importantly, and as noted above, equilibrium of the translational momenta is not the only process occurring. The collisions also allow vibrational and rotational cooling, with these conditions often cooling directly into the zero-point vibrational energy of the sample (about 50 K), and into only a very small number of rotational levels (5 K). A good estimate of the expansion temperature can be measured by performing a fit to the rotational contours, although this is not performed for this work.

8.7 A note on computational chemistry:

To fully understand the spectra we collect, assigning the vibrational and torsional structure is of paramount importance. In general, one can closely infer what type of vibration is likely to be in each energetic region *i.e.* high amplitude out-of-plane modes are likely to be at low internal energy, whereas in-plane stretches appear at high internal energy. As the molecule become more complicated, the number of vibrational modes increases and it can, at this

point, be difficult to ascertain which experimental band corresponds to which mode. Here, computational chemistry can be used to aid the assignments of these bands.

Computational techniques can be used to calculate both vibrational modes and their respective harmonic energies, which are useful tools for assigning spectra. In this work, the Gaussian 16[76] software package is used. Typically, all geometry optimisation and vibrational frequency calculations are performed using the density functional theory (DFT) method with the B3LYP functional. Dunning-style basis sets, specifically aug-cc-pVTZ are preferred throughout this work as this pairing of theory and basis set has been found to give fairly good agreement with experimental vibrational wavenumbers for both the ground state, S_0, and cationic ground state, D_0^+ (note that UB3LYP is used in D_0^+). Similarly, the TD-DFT method is used with the B3LYP functional and the aug-cc-pVTZ basis set for S_1 calculations. Comparatively, the vibrational wavenumbers from the latter are usually less good than the respective S_0 and D_0^+ values for reasons that are not entirely understood. All calculated vibrational frequencies are scaled by a factor of 0.97, to account for the anharmonicity of the system and other deficiencies in the theoretical method. Use of this scaling factor has been found to be a reasonable approximation, and is significantly quicker than performing explicit anharmonic calculations, which have been found to yield very similar, and slightly worse, results.

9. Introduction to Publications:

In the upcoming chapters, the publications that form the results and discussion of this work are presented. Five publications are shown and are split into two sections with separate aims to one another.

We first begin with the publications related to *para*-fluorotoluene. Here, we present 3 separate publications, each covering one of the 400, 800 and 1200 cm^{-1} regions of the S_1 state of *p*FT. The primary focus of this work is to deduce the key factors affecting methyl-facilitated interactions, and we do this through the use of multiple electronic spectroscopic techniques, such as 2D-LIF (S_0), REMPI (S_1), and ZEKE (D_0^+) spectroscopies. Here we present a large range of spectra from each energetic region where, from the observed vibrational and torsional structure, we illuminate a number of restricted or widespread dissipative IVR interactions. We focus mainly on interactions between vibrational, torsional and vibtor levels within the S_1 state although, sometimes, coupling between other states also becomes apparent. The main objective is to understand the aspects that lead to the interactions mentioned above, and to improve our understanding on which factors induce the most efficient forms of coupling. Ideally we will try to understand, as a function of internal energy, whether it simply is a density of states argument - where serendipitous coincidence of multiple levels causes interaction - or whether the states need a strong degree of compatibility, as well as a distinct locality with respect to each other, in order for efficient coupling to be observed. Presenting our assignments at three separate energetic locations, where each is noticeably higher than the last, will effectively allow us to address each of these potential factors in isolation, such that we may conclude which has the greatest ability to induce such interactions.

The last section comprises two further publications, specifically applying to the two *meta*-disubstituted molecules: *m*FT and *m*ClT. Here, our primary objective involves determining the differences in vibrational and torsional structure seen as a function of the halogen substituent. We initially present a series of spectra, corresponding to transitions to the S_1 and D_0^+ states of *m*FT *via* REMPI and ZEKE spectroscopy, respectively. From this information, we gain insight into the geometry changes that occur upon excitation or ionisation, whilst also gaining information regarding the barrier height associated with the torsional motion - both of which can be shown to directly affect the local interactions between the energy levels. We then perform the

same set of experiments for *m*ClT, comparing the vibrational and torsional structure to *m*FT, hence allowing us to rationalise the extent, if any, of the effect of the electronic and mass differences on the couplings observed. This differs from our initial objective for *p*FT in that it will allow us to deduce the effects on torsion-facilitated interactions as a primary function of property, as opposed to a function of energy, and should be a good precursor to understanding higher energetic regions within these molecules in future undertakings.

10. Unravelling overlaps and torsion-facilitated coupling using two-dimensional laser-induced fluorescence:

Contributions:

Authors: David J. Kemp, Adrian M. Gardner, William D. Tuttle, and Timothy G. Wright[*]

This article is redacted from this work and can be found through the above DOI.

This work includes a large number of REMPI, ZEKE, DF and 2D-LIF spectra, a number of which were originally collected by Adrian Gardner and William Tuttle. Upon analysis, it was noted that a number of additional spectra would be required, all of which were gathered by myself.

The largest part of my work on this publication was in the analysis, trying to elucidate the potential coupling pathways and the FC activity associated with each intermediate. This this was performed mostly between myself and Timothy Wright, with small contributions from Adrian Gardner.

Figure production was done exclusively by myself, with collaboration from Timothy Wright, who suggested a number of changes or additional parts to figures.

11. Complexity surrounding an apparently simple Fermi resonance in *p*-fluorotoluene revealed using two-dimensional laser-induced fluorescence (2D-LIF) spectroscopy:

Contributions:

Title: Complexity surrounding an apparently simple Fermi resonance in *p*-fluorotoluene revealed using two-dimensional laser-induced fluorescence (2D-LIF) spectroscopy[40]

Authors: David J. Kemp, Laura E. Whalley, Adrian M. Gardner, William D. Tuttle, Lewis G. Warner and Timothy G. Wright

Submitted to: Journal of Chemical Physics, 30th November 2018; accepted 19th January 2019; published 11th February 2019

Reproduced from 'Complexity surrounding an apparently simple Fermi resonance in *p*-fluorotoluene revealed using two-dimensional laser-induced fluorescence (2D-LIF) spectroscopy', with the permission of AIP Publishing. This article can be located at https://aip.scitation.org/doi/10.1063/1.5083682

This work comprises analysis of REMPI, DF and 2D-LIF spectra of a given energetic region of *p*FT. All of the spectra were collected by myself, with some aid from a summer project student, Lewis Warner, under my supervision. Reference is also made to several ZEKE spectra, which were collected by both Adrian Gardner and William Tuttle before the start date of my project.

The majority of my work on this publication was in the assignments and analysis of the observed spectral bands. Many discussions were had with Timothy Wright regarding the unexpected intensity distributions of a number of features within the 2D-LIF spectra, and some discussion was had with Katherine Reid regarding the unusual beating patterns in the tr-PES. Initial analysis of the ZEKE spectra was performed mostly by Adrian Gardner and William Tuttle, although some reanalysis and reinterpretation by myself and Timothy Wright occurred closer to publication. Figures were all created by myself, with frequent discussions on assignments and inclusions occurring between myself and Timothy Wright.

Complexity surrounding an apparently simple Fermi resonance in p-fluorotoluene revealed using two-dimensional laser-induced fluorescence (2D-LIF) spectroscopy

David J. Kemp, Laura E. Whalley, Adrian M. Gardner,[a] William D. Tuttle, Lewis G. Warner, and Timothy G. Wright[b] (iD)

AFFILIATIONS

School of Chemistry, University of Nottingham, University Park, Nottingham NG7 2RD, United Kingdom

[a]**Present address:** Stephenson Institute for Renewable Energy, University of Liverpool, Liverpool L69 7ZF, United Kingdom.
[b]Tim.Wright@nottingham.ac.uk

ABSTRACT

Two-dimensional laser-induced fluorescence (2D-LIF) spectroscopy is a powerful tool allowing overlapped features in an electronic spectrum to be separated, and interactions between vibrations and torsions to be identified. Here the technique is employed to assign the 790–825 cm^{-1} region above the origin of the S$_1$ ← S$_0$ transition in $para$-fluorotoluene, which provides insight into the unusual time-resolved results of Davies and Reid [Phys. Rev. Lett. **109**, 193004 (2012)]. The region is dominated by a pair of bands that arise from a Fermi resonance; however, the assignment is complicated by contributions from a number of overtones and combinations, including vibration-torsion ("vibtor") levels. The activity in the 2D-LIF spectra is compared to the recently reported zero-electron-kinetic-energy spectra [Tuttle et al., J. Chem. Phys. **146**, 244310 (2017)] to arrive at a consistent picture of the energy levels in this region of the spectrum.

Published under license by AIP Publishing. https://doi.org/10.1063/1.5083682

I. INTRODUCTION

Understanding the internal energy level structure in molecules is a key quest of chemical and molecular physicists. In particular, vibrations underpin our knowledge of the motion of the nuclei, which drives the making and breaking of bonds in chemistry. Chemistry can be further affected by the rotation of the molecule and the torsional motion of hindered rotor groups. All of these motions can couple, although this coupling can usually be treated as a perturbation on the overall vibrational energy structure. Building on work by Parmenter and co-workers,[1-4] recent work by the Lawrance group and ourselves has identified that vibration-torsional ("vibtor") coupling is of key importance in the following molecules that contain methyl groups: toluene,[5-11] $para$-fluorotoluene (pFT),[12-17] and $para$-xylene (pXyl).[17-19] Both a combination of an increasing density of states (DOS) and symmetry-allowed vibtor

coupling have been invoked to rationalize the rapid increase in interactions that occur in such molecules,[17] which drives energy dispersal through a molecule.

In previous work, we have studied the lower-wavenumber regions of the S$_1$ ← S$_0$ transition in $para$-fluorotoluene (pFT) using resonance-enhanced multiphoton ionization (REMPI) and zero-electron-kinetic-energy (ZEKE) spectroscopy,[12,13,17,20] while both we[13,20] and the Lawrance group[16] have also employed the technique of two-dimensional laser-induced fluorescence (2D-LIF).[21] The low-wavenumber region has been shown to be rich in interactions, involving torsional, vibrational, and vibrational-torsional levels. (Since we work under jet-cooled conditions, and since we only partially resolve rotational structure, we do not directly consider interactions involving rotations.)

Earlier work on the S$_1$ ← S$_0$ transition in pFT has been reported by Cave and Thompson,[22] Cvitaš and

Hollas,[23] Seliskar et al.,[24] and Okuyama et al.[25] The latter two studies presented laser-induced fluorescence (LIF) spectra under jet-cooled conditions, giving assignments of some of the vibrational bands. Some of the low-wavenumber bands have been reassigned to vibration-torsion (vibtor) levels by Zhao[3] and confirmed in a recent work by our group[15] and that of Lawrance et al.[16] In an earlier paper from our group,[14] we had used the assignments of Okuyama et al.[25] in assigning ZEKE spectra recorded via various levels, unaware that some of the assignments of the lower-wavenumber features had been superseded by those in Zhao's thesis[3]—some of those latter reassignments are implicit in Ref. 2. In our earlier work,[14] we assigned the two levels at ~800 cm^{-1} to different totally symmetric fundamentals on the basis of Okuyama et al.'s work,[25] but one of these was reassigned to an overtone level in Ref. 26. In Ref. 27, time-resolved photoelectron spectroscopy (tr-PES) was employed, and these same two features were assigned as a Fermi resonance (FR), involving the same levels noted in Ref. 26, although it was suggested that at least one other state might be interacting.

II. EXPERIMENTAL

The 2D-LIF apparatus has been described recently.[13] The vapour above room temperature *para*-fluorotoluene (99% purity, Alfa Aesar) was seeded in ~5 bars of Ar and the gaseous mixture passed through a General Valve pulsed nozzle (750 μm, 10 Hz, opening time of 180–210 μs) to create a free jet expansion. This was intersected at X/D ~ 20 by the frequency-doubled output of a dye laser, operating with C540A. The fluorescence was collected, collimated, and focused onto the entrance slits of a 1.5 m Czerny Turner spectrometer (Sciencetech 9150) operating in single-pass mode, dispersed by a 3600 groove/mm grating, and ~300 cm^{-1} windows of the dispersed fluorescence (DF) collected by a CCD camera (Andor iStar DH334T). At a fixed grating angle of the spectrometer, the excitation laser was scanned, and at each excitation wavenumber, the image was accumulated for 2000 laser shots. This produced a 3D surface of fluorescence intensity versus the excitation laser wavenumber and the wavenumber of the emitted and dispersed fluorescence, termed a 2D-LIF spectrum.[21]

We have also recorded separate dispersed fluorescence (DF) spectra with higher averaging to get better signal to noise than simply taking a vertical slice through the 2D-LIF image. These DF spectra were recorded with the same spectrometer as for the 2D-LIF spectra, and were recorded three times accumulating over 5000 shots each time, and an average taken of these.

III. RESULTS AND ASSIGNMENTS

A. Nomenclature and labelling

1. Vibrational and torsional labelling

Since neither Wilson[28]/Varsányi[29] nor Mulliken[30]/Herzberg[31] notations are appropriate for the vibrations of

TABLE I. Correspondence of the C_{2v} point group symmetry classes with those of the G_{12} molecular symmetry group. Also indicated are the symmetries of the D_i vibrations and the different pure torsional levels.[a]

C_{2v}	G_{12}	D_i[b]	m
a_1	a_1'	D_1–D_{11}	0, 6(+)
a_2	a_2'	D_{12}–D_{14}	6(−)
b_1	a_2''	D_{15}–D_{20}	3(−)
b_2	a_1''	D_{20}–D_{30}	3(+)
	e'		2,4
	e''		1,5

[a]Symmetries of vibtor levels can be obtained by combining the vibrational symmetry (in G_{12}) with those of the pure torsional level, using the D_{3h} point group direct product table.
[b]The D_i labels are described in Ref. 33, where the vibration mode diagrams can also be found.

pFT,[32,33] we shall employ the D_i labels from Ref. 33. (In other papers, we have included the labels used in previous work to aid the reader in referring to the different studies.[12,20]) Since the G_{12} molecular symmetry group (MSG) is appropriate for vibtor levels, we shall use these symmetry labels throughout. In addition, torsional levels will be labelled via their m quantum number. (The reader may find it useful to refer to previous work[9–11,15,18] if they are not familiar with these labels.) The correspondence between the C_{2v} point group labels and the G_{12} MSG ones is given in Table I. To calculate the overall symmetry of a vibtor level, it is necessary to use the corresponding G_{12} label for the vibration and then find the direct product with the symmetry of the torsion (Table I), noting that a D_{3h} point group direct product table can be used, since the G_{12} MSG and the D_{3h} point group are isomorphic.

Under the free-jet expansion conditions employed here, the molecules are all expected to be cooled to their zero-point vibrational level and thus all $S_1 \leftarrow S_0$ pure vibrational excitations are expected to be from this level. In contrast, owing to nuclear-spin and rotational symmetry, the molecules can be in one of the $m = 0$ or $m = 1$ torsional levels.[18,34]

2. Coupling and transitions

If an anharmonic fundamental is close in wavenumber to one or more combination or overtone vibrational levels that has the same overall symmetry, then "off-diagonal" anharmonic interactions can occur. The non-interacting levels are termed zero-order states (ZOSs), and their interaction leads to the formation of eigenstates that are linear combinations of these, and will be at different wavenumbers to the original ZOSs.[31] The simplest example of two interacting states is the classic Fermi resonance,[35] while for more than two levels, we term this a complex Fermi resonance. For molecules that contain a hindered internal rotor, then the ZOSs can also be torsional or, if vibration-torsional coupling occurs, "vibtor" levels. The end result of such interactions is the formation of eigenstates which facilitate delocalization of energy through widespread motion of the molecule. Such couplings are only

expected to be significant for small changes, $\Delta v \leq 3$, of the vibrational quantum number and also for changes, Δm, of 0, ± 3 or ± 6 in the torsional quantum number in descending order of likely strength.[10,15,18,36,37]

In electronic spectroscopy, if we assume a non-coupled picture initially, then a zero-order vibrational, torsional, or vibtor level can be bright (i.e., it has a significant transition intensity) or dark (i.e., it has no, or a very small transition intensity); these are often termed a zero-order bright (ZOB) state and a zero-order dark (ZOD) state, respectively. Following interaction, the resulting eigenstates will be composed of mixtures of ZOB and ZOD state character and so more transitions will become observable in the spectrum as a result of the interaction.

When designating excitations, we shall generally omit the lower level, since it will be obvious from the jet-cooled conditions; similarly, for emissions, we shall omit the upper level, as that will be obvious from the excitation and context. In the usual way, vibrational transitions will be indicated by the cardinal number, i, of the D_i vibration, followed by the number of quanta; torsional transitions will be indicated by m, followed by its value. Finally, vibtor transitions will be indicated by a combination of the vibrational and torsional transition labels. If no m values are specified, then the transition refers to both $m = 0$ and $m = 1$ levels, whose transition wavenumbers are expected to be coincident at the present resolution. We give two examples: (i) When accessed via emission from the origin, $20_1 m_2$ represents an excitation from the S_0 zero-point $m = 1$ level to the $m = 1$ level in the S_1 state, followed by emission to the $m = 2$ level of the D_{20} level in S_0 and (ii) $(29^2, 9_1)$ represents a dual excitation from the $m = 0$ and $m = 1$ levels of the S_0 zero-point level to both m levels of the S_1 state D_{29} overtone level, followed by dual emission to the corresponding m levels of the D_9 level in the S_0 state–note that these two transitions will be coincident with our resolution.

The wavenumbers of the levels will be given with respect to the relevant zero-point level in each state, but noting that some excitations will originate from the $m = 1$ level in S_0 and those transition energies are given with respect to that level, as usual; the $S_1 \leftrightarrow S_0$ origin is located at 36 860.0 cm^{-1} (Ref. 16). Very frequently, the most intense transition is expected to be that for which no change in the vibrational or both vibrational and torsional quantum numbers occurs; these will be designated $\Delta v = 0$ and $\Delta(v, m) = 0$ transitions. As has become common usage, we will generally refer to a level using the notation of a transition, with the level indicated by the specified quantum numbers, with superscripts indicating levels in the S_1 state and subscripts indicating levels in the S_0 state; since we will also occasionally be referring to levels in the ground state cation, D_0^+, we shall indicate those levels with a preceding superscripted + sign. Also, the eigenstates will usually be referred to by the dominant contribution from one of the ZOSs, with the context implying if an admixture of other ZOSs is present. 2D-LIF band positions can be indicated by a pair of (excitation, emission) wavenumbers and corresponding transitions similarly, as indicated in the preceding paragraph.

B. Assignment of the spectra

1. Overall comments on the $S_1 \leftarrow S_0$ spectrum

In Fig. 1, we show an overview of the excitation spectra across the region of interest recorded using both REMPI and fluorescence spectroscopies. To lower wavenumber, it may be seen that there are two dominant features at 797 cm^{-1} and 804 cm^{-1}, with two other weaker features to higher wavenumber (one of which is not so clear in the integrated image, but features are evident in the 2D-LIF image in Fig. 2). In Ref. 12, we discussed the assignment of this spectrum in detail, with the aid of ZEKE spectra and calculated vibrational wavenumbers, although some of the assignments were tentative. The two intense bands have been assigned as arising from eigenstates that are dominated by one of 9^1 and 29^2 (Refs. 12, 26, and 27). Further, our ZEKE study[12] indicated a number of contributions to this region from overtones, combinations, and vibtor levels, with many of these involving the three main levels (14^2, 29^1, and 11^1) that give rise to features seen in the spectrum at ~400 cm^{-1}, whose assignments were deduced from ZEKE[15,16] and, more recently, 2D-LIF spectra.[20] As well as 29^2, the other overtones and combinations of these three levels, and also transitions involving combinations with the vibtor level $14^1 m^{6(-)}$, and possibly others, are expected. In the ZEKE study,[12] it was also concluded that, as well as 9^1, the $12^1 14^1$ and $12^1 m^{6(-)}$ $S_1 \leftarrow S_0$ transitions contribute to this spectral region. Clearly, 2D-LIF spectroscopy will provide further evidence for or against these assignments and, as will be seen, give further insight into the activity and coupling.

(a)

(b)
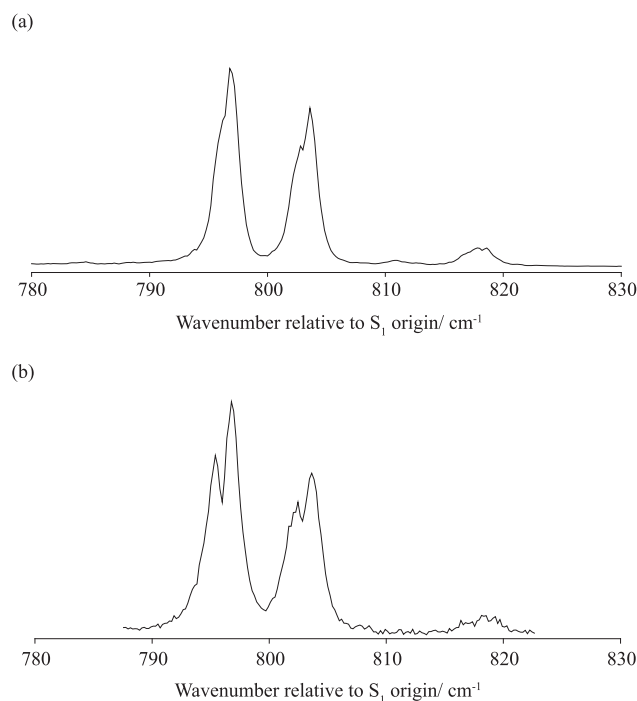
FIG. 1. Overview of the (a) REMPI spectrum and (b) integrated 2D-LIF spectrum over the range of interest—see text.
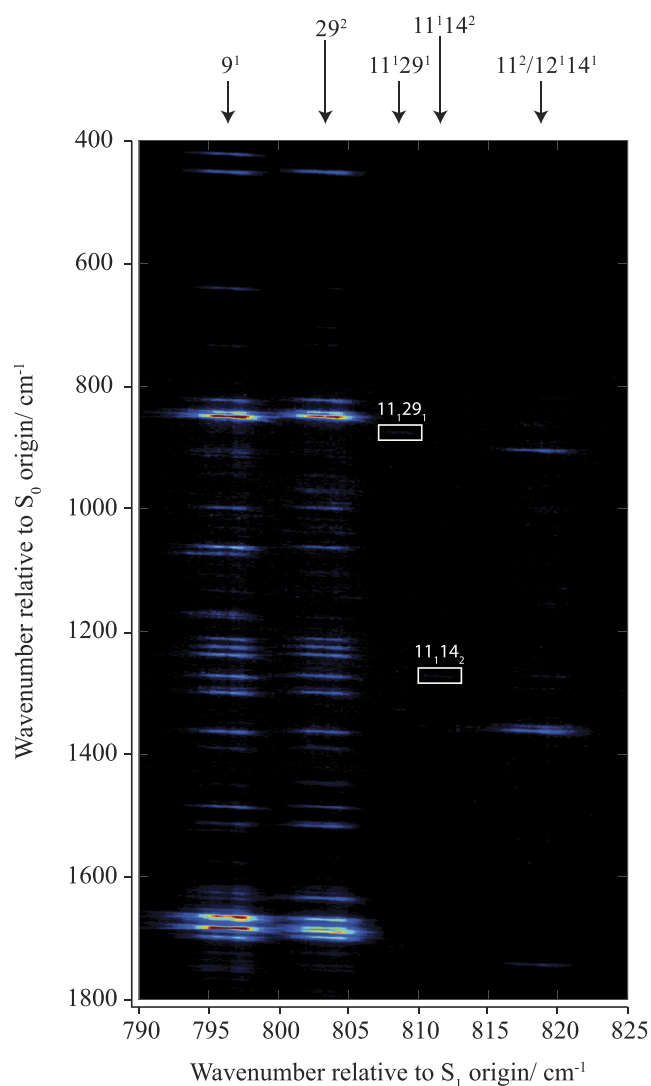
FIG. 2. Overview of the 2D-LIF spectrum across the whole range of interest. The spectral intensities are represented by colours, with red being the most intense through to blue being the least; black represents the zero background.

In Fig. 2, we present an overview of the recorded 2D-LIF spectrum across the 790–825 cm^{-1} excitation region. Vertical integration of the whole of this window of the spectrum gives a standard "LIF" spectrum, which is shown in Fig. 1 where it is compared to the REMPI spectrum; it may be seen that both traces are very similar, indicating that the activity in this window of the 2D-LIF spectrum is a good representation of the overall activity of the transition. The 2D-LIF spectrum also shows a wealth of structure in the 0–300 cm^{-1} region, which is shown in Fig. 3. In Fig. 2, it will be noticed that there are two main vertical stripes of activity, corresponding to excitation via each of the two most intense bands in Fig. 1–this is in line with emissions arising from eigenstates that are composed of the same ZOSs. However, there are also cases where

there is a pronounced difference in activity following excitation of one band and not the other, and such features are expected not to be associated with the two main eigenstates, but to arise from separate overlapping transitions. In addition, there is a third main stripe of emission activity to higher excitation wavenumber, with some common activity across the three main excitation features, with some weaker bands in between. Since we already have the assignments from our earlier ZEKE study,[12] we ought largely be able to assign the 2D-LIF spectrum by reference to the known S_0 and S_1 vibrational wavenumbers,[16,20,33] together with a knowledge of the positions of the torsional and low-wavenumber vibtor levels in the different states.[15,16]

Although we can obtain a conventional DF spectrum at a particular excitation wavenumber by taking a vertical cut through the 2D-LIF spectrum, we have often recorded such DF spectra separately, covering a wider range of emission wavelengths with an increased number of shots. In Figs. 4–8, we show expanded sections of the 2D-LIF spectra, together with the corresponding sections of the DF spectra, recorded via the centre of each of the 797 cm^{-1} and 804 cm^{-1} bands. Much of the activity is very similar from both of the bands, again confirming that these mainly arise from eigenstates that are largely made up from the same ZOSs.

2. Assignment of the main spectral activity

In our earlier ZEKE study,[12] a selection of spectra were recorded at excitation positions across the observed REMPI bands that are shown in Fig. 1. From the changing activity, the make-up of the S_1 levels was deduced. However, the activity was not always as expected and the present 2D-LIF spectra should be able to shed some light on this. If we assume that we can just sum the band positions of the levels seen at 400 cm^{-1}, then we can predict the excitation wavenumber at which we expect to see the relevant combination and overtone 2D-LIF bands. It is likely, however, as the ZEKE study confirmed, that levels are interacting with each other and also with the bright fundamental, 9^1, that appears in this spectral region; as such, the excitations could appear at shifted positions. We will now briefly discuss both the positions of the observed 2D-LIF bands and their activity.

Previous ZEKE,[12] fluorescence,[26] and tr-PES[27] studies agree that the two main excitation bands at 797 cm^{-1} and 804 cm^{-1} (Fig. 1) correspond to eigenstates that largely correspond to contributions from 9^1 and 29^2, and this is confirmed by the present DF and 2D-LIF spectra in Fig. 5. At first sight, the $\Delta v = 0$ region shown at the top of Fig. 5 is perplexing, as it indicates large contributions from 29^2 to both levels, with the spectra being consistent with those of Zhao and Parmenter.[26] Similar behaviour was seen in the ZEKE spectra,[12] but an explanation was found in that the Franck-Condon factors (FCFs) when exciting via 9^1 were non-diagonal. Thus, it was observed that the $^+9^2$ ZEKE band was the most intense when exciting via the 797 cm^{-1} eigenstate, supporting the fact that it was dominated by 9^1, while the 804 cm^{-1} eigenstate is dominated by 29^2. Similar behaviour is seen here–see the next paragraph. Also, there are contributions from other ZOSs

FIG. 3. Expanded view of the 2D-LIF spectrum of pFT in the 0–310 cm^{-1} region exciting via the 797 cm^{-1} and 804 cm^{-1} eigenstates. The spectral intensities are represented by colours, with red being the most intense through to blue being the least; black represents the zero background. We also show the corresponding DF spectra from these two levels and the origin. This region covers the main torsion and vibtor levels associated with the D_{20}, vibration. The appearance of the spectrum via the origin is very similar to that recently published by Gascooke *et al.* in Ref. 16, where it is discussed in detail. The relative intensities in the 2D-LIF spectrum are as recorded, while the DF spectra have been adjusted to be qualitatively in agreement with the 2D-LIF spectrum, but with some regard to presentational clarity. Thus, the relative intensities within the same DF trace will be reliable, but not necessarily when comparing between two traces.

to the spectrum, some of which may contribute to form the main eigenstates−see later in this subsection. Additionally, the ZEKE study[12] concluded that there were two overlapping features at 818 cm^{-1}: 11^2 and $12^1 14^1$, but that these are not obviously in FR−these will be discussed later. Many of the other strong features in the 2D-LIF spectrum in Fig. 2 may be deduced to arise from FC activity of the four main eigenstates dominated by each of 9^1, 29^2, 11^2, and $12^1 14^1$, with a particularly rich structure apparent at both of the 797 cm^{-1} and 804 cm^{-1} excitation regions. Indeed, occasionally the strong FC activity for certain features can obfuscate the assignment of the $\Delta v = 0$ band; however, considering the activity across the spectrum enables this to be achieved.

We first look at the $\Delta v = 0$ region of the 2D-LIF spectrum, at the top of Fig. 5, together with the relevant sections of the DF spectra. The three pairs of bands here may be seen to correspond to three main emissions from each of the excitations, which may be assigned[16] to 14_2 (823 cm^{-1}), 9_1 (843 cm^{-1}), and 29_2 (850 cm^{-1}). Furthermore, it is also pertinent to observe that in the S_0 state, the two eigenstates made up from 9_1 and 29_2 are at 843 cm^{-1} and 850 cm^{-1}, while in the D_0^+ state, the two eigenstates are at 824 cm^{-1} and 832 cm^{-1}.[12] These levels are all close enough to be expected to be in

Fermi resonance in each of the three electronic states, potentially complicating conclusions from DF or ZEKE spectroscopy regarding the make-up of the S_1 eigenstates. This means that, in any of the electronic states, the given labels merely reflect the dominant contribution of a ZOS to the eigenstate. However, we have found that emissions from totally symmetric fundamentals, such as 11^1 (see Ref. 20), and levels in other unpublished work, give a higher intensity for the 9_1 band than the 9_2 and 14_2 bands. From such spectra, we can conclude that the 843 cm^{-1} S_0 eigenstate is made up of predominantly 9_1 character, but with some contribution from 29_2, and that the 850 cm^{-1} S_0 eigenstate is dominated by 29_2, with some contribution from 9_1. It is difficult to be sure of the mixings with the 14_2 state, for which the emissions could also simply be arising from FC activity from the totally symmetric fundamentals.

The immediate observation from Fig. 5 is that the activity of the main emission bands is very similar, with the 850 cm^{-1} emission band dominating from both the 797 cm^{-1} and 804 cm^{-1} levels. If the ZOSs were not interacting in the S_0 state, and if the FC intensity is dominant in the $\Delta v = 0$ region, then we would expect the emissions to the two S_0 levels to switch intensity from the two S_1 eigenstates, in contrast to

FIG. 4. Expanded views of the 2D-LIF and DF spectra for the 390–790 cm^{-1} region, exciting via the 797 cm^{-1} and 804 cm^{-1} eigenstates. The spectral intensities are represented by colours, with red being the most intense through to blue being the least; black represents the zero background. See text for discussion of the assignments. The relative intensities in the 2D-LIF spectrum are as recorded, while the DF spectra have been adjusted to be qualitatively in agreement with the 2D-LIF spectrum, but with some regard to presentational clarity. Thus, the relative intensities within the same DF trace will be reliable, but not necessarily when comparing between two traces.

the observations in Fig. 5. As can be seen from Fig. 7, however, the $(9^1, 9_2)$ emission is much stronger than $(29^2, 9_2)$, and hence the $\Delta v = 0$ intensities in Fig. 5 are somewhat misleading. Overall, we concur with the previous conclusions from our ZEKE work[12] and the tr-PES study[27] that the main S_1 state eigenstates are each dominated by 9^1 and 29^2, but that, as implied above, there is also the possibility of further interactions involving other ZOSs expected to be in this wavenumber region—see below.

A number of 2D-LIF bands appear with intensities that suggest they do not simply arise from FC activity. For example, we see significant non-totally symmetric 29_1 and 28_1 bands (Fig. 4) when exciting at 797 cm^{-1}, with the (totally symmetric) $28_1 29_1$ band being seen in Fig. 5—this is similar to behaviour seen when exciting via the origin (see Ref. 20). As we noted in Ref. 20, some caution is merited with the intensity of the 28_1 band, as this is at the expected wavenumber of the totally symmetric $18_1 20_1$ level, which was concluded to be FC active via the origin, and likely also to be active via totally symmetric fundamentals; the $28_1 29_1$ band may also therefore have a contribution from $18_1 20_1 29_1$. It is clear that the 29_1 band arises from Herzberg-Teller (HT) vibronic activity, and this would also apply to $18_1 20_1 29_1$. Since these bands are seen to

be present, but much weaker, when exciting at 804 cm^{-1}, the HT activity appears to be associated with the smaller 9^1 contribution to the latter eigenstate.

We now highlight the 1636 cm^{-1} emission band (Fig. 7), which appears strongly when exciting at 804 cm^{-1}, but is much weaker when exciting at 797 cm^{-1}. This is assigned to 14_4 and indicates that the $14^2/29^1$ overlap seen at ~400 cm^{-1} is analogously present at 804 cm^{-1}, now involving 14^4 and 29^2; these are shifted up in wavenumber from the expected excitation positions, and this is consistent with interactions with 9^1. We might, therefore, also expect to see one or more 2D-LIF features corresponding to $14_2 29_1$, which is expected at 1248 cm^{-1}. We see $14_2 29_1$ clearly at 1243 cm^{-1} when exciting via 29^1 (see Ref. 20), but unfortunately such features are likely to be obscured by the strong 5_1 band seen in this region of the present spectra (see Fig. 6), precluding definitive deductions regarding $14_2 29_1$ activity.

Other excitations being seen to contribute to the ~400 cm^{-1} region[20] were $14^1 m^{6(-)}$ and $14^1 20^2 m^x$ and so we might expect to see combinations of these with 14^2, 29^1, and 11^1. (Note that the assignment of the m level associated with $14^1 20^2$ was unclear, but was thought to be 1 or 2—see Ref. 20.)
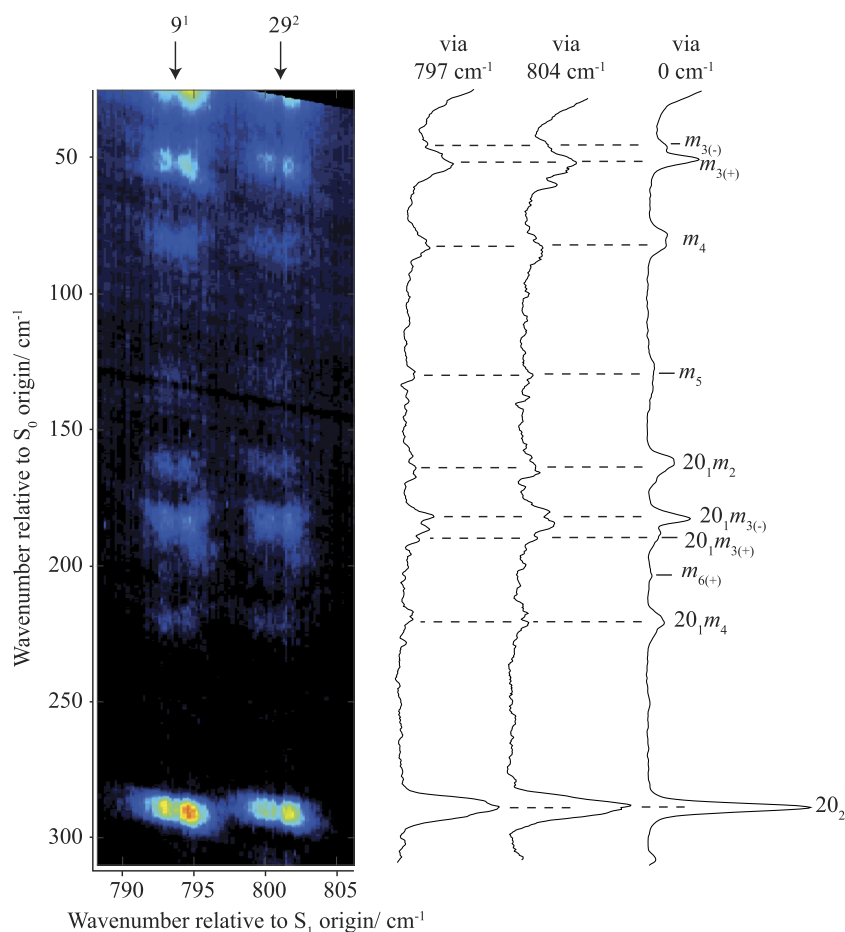
FIG. 5. Expanded views of the 2D-LIF and DF spectra for the 790–1190 cm^{-1} region exciting via the 797 cm^{-1} and 804 cm^{-1} eigenstates. The spectral intensities are represented by colours, with red being the most intense through to blue being the least; black represents the zero background. See text for discussion of the assignments. The relative intensities in the 2D-LIF spectrum are as recorded, while the DF spectra have been adjusted to be qualitatively in agreement with the 2D-LIF spectrum, but with some regard to presentational clarity. Thus, the relative intensities within the same DF trace will be reliable, but not necessarily when comparing between two traces.

Considering this, $14_3 m_{6(-)}$ would be expected at 1443 cm^{-1} and can be assigned to a band seen at 1449 cm^{-1} when exciting via 804 cm^{-1} (see Fig. 6) which appears more weakly at 797 cm^{-1}; $14_2 29_1 m_{6(-)}$ is expected at 1043 cm^{-1} and can be assigned to a weak feature seen at 1040 cm^{-1} when exciting via 804 cm^{-1} (see Fig. 5). The $11_1 14_1 m_{6(-)}$ vibtor band is expected at 1072 cm^{-1} (which is at the same wavenumber as a weak feature seen[20] when exciting at 398 cm^{-1}). Although a clear emission band is seen at 1071 cm^{-1} (Fig. 5), it is unexpectedly only seen when exciting at 797 cm^{-1}–indeed, this band will be assigned to a different transition below.

We note that the 11_1 band is more intense via the 804 cm^{-1} eigenstate (Fig. 4) and associate this with additional FC activity from the various other levels contributing to this feature, as well as that from the 9^1 ZOS contribution.

There are three other ZOSs expected to contribute to this spectral region: 11^2, $11^1 14^2$, and $11^1 29^1$. We see a clear (11^2, 11_2) band at (818, 906) cm^{-1} (Fig. 8) which is slightly shifted up from the expected excitation position of ~816 cm^{-1}. Exciting at 818 cm^{-1}, it is also possible to see extremely weak 11_1 activity on expanded views of Fig. 8, but more sizeable 11_3 activity is evident. There is some 11_2 activity when exciting at 797 cm^{-1},

with very faint activity at 804 cm^{-1}, which is consistent with FC activity.

Weak $11_1 29_1$ emission is seen at 877 cm^{-1}, as expected (see Fig. 8), and has two islands of activity: one at 809 cm^{-1} and the other at 797 cm^{-1}. The latter is likely related to the 29_1 HT activity at that wavenumber, suggesting the former is the $\Delta v = 0$ band, and this is close to the expected position. Note that the $11^1 29^1$ level is of a_1'' symmetry, and so unable to couple to the 9^1 band anharmonically, explaining its weakness; there are, however, possibilities of other vibtor levels with which it could interact and this, together with intrinsic anharmonicity in forming the combination band, could explain the slightly shifted position.

The $11_1 14_2$ band is expected at ~1277 cm^{-1}, and clear features are seen at 1276 cm^{-1} (see Figs. 6 and 8). There are four islands of activity, at 797, 804, 811, and 818 cm^{-1}, with the first two being far stronger than the latter two. We note that the latter may contain some contribution from 29_3, which can be seen when exciting via 29^1 (Ref. 20), but this is expected to be significantly weaker for the present excitation, owing to symmetry. The ZEKE spectra[12] show $^+11^1 14^2$ activity at 804 and 818 cm^{-1}, but not obviously so at 797 cm^{-1}. One complicating
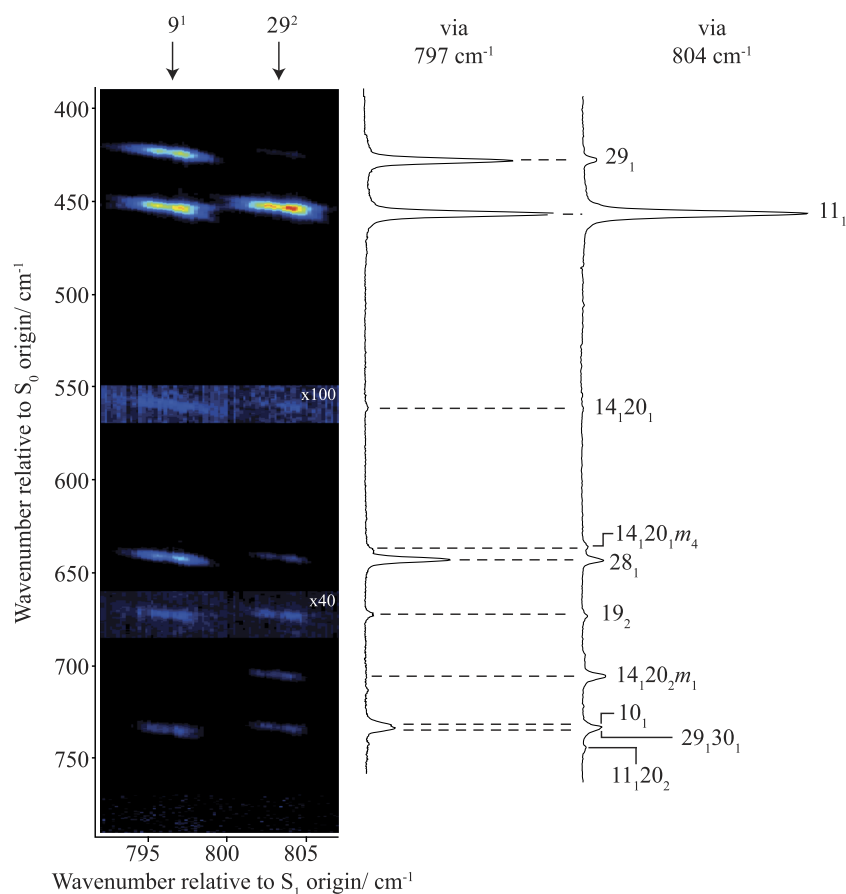
FIG. 6. Expanded views of the 2D-LIF and DF spectra for the 1190–1590 cm^{-1} region exciting via the 797 cm^{-1} and 804 cm^{-1} eigenstates. The spectral intensities are represented by colours, with red being the most intense through to blue being the least; black represents the zero background. See text for discussion of the assignments. The relative intensities in the 2D-LIF spectrum are as recorded, while the DF spectra have been adjusted to be qualitatively in agreement with the 2D-LIF spectrum, but with some regard to presentational clarity. Thus, the relative intensities within the same DF trace will be reliable, but not necessarily when comparing between two traces. For the $14_3 20_2 m_x$ level, we are unable to be definitive of the value of x, which is thought to be 1 or 2—see text and Ref. 20.

factor is FC activity from the two main 797 cm^{-1} and 804 cm^{-1} eigenstates, and it can be seen that there are clear 14_2 bands at these excitation positions (Fig. 5), and so it is not unexpected to see $11_1 14_2$ bands also; hence, these are assigned to FC activity, together with the (818, 1276) cm^{-1} band. These arguments are also supported by the clear FC activity from 18_2 at the two lower wavenumber positions (see Fig. 5); this emission is also seen weakly when exciting at 818 cm^{-1}–see Fig. 8). From this, we conclude that the $11_1 14_2$ band is demonstrating FC activity from 9^1, 29^2, and $12^1 14^1/11^2$. We thus conclude that the band at (811, 1276) cm^{-1} is likely to be the $\Delta v = 0$ band.

The reasons noted above for the very weak $11_1 29_1$ band also apply to $14_2 29_1$ and explain why it is not obviously seen in our spectra, although, as noted, it could be overlapped with the strong 5_1 band. These reasons do, however, make it surprising that the $14_1 29_1 m_{6(-)}$ band is seen at 1042 cm^{-1}, suggesting that this could arise by other coupling mechanisms, perhaps involving 29^2.

We now discuss the $12_1 14_1$ activity–see Fig. 8. This appears at three positions with the $\Delta v = 0$ band clearly seen at 818 cm^{-1} and the other islands of emission activity being via excitations at 797 and 804 cm^{-1}. It is seems likely these last two features

must arise from FC activity from the two main eigenstates, as it is difficult to see that 9^1 and 29^2 are interacting so strongly with $12^1 14^1$ that the resulting eigenstates end up so far apart; moreover, we do not see any evidence of 9_1 nor 29_2 activity when exciting via $12^1 14^1$–see Fig. 8. Interestingly, the same islands of activity for $12_1 14_1$ occur with the much weaker 11_3, although the activity at 804 cm^{-1} seems stronger than that at 797 cm^{-1}, which is the opposite of the $12_1 14_1$ activity. The 11_3 activity can be contrasted with that of 11_2, which is actually stronger when exciting at 797 cm^{-1} than 804 cm^{-1}. We also remark that there is a curious coincidence here, whereby in the S_1 state the 11^2 and $12^1 14^1$ levels are almost isoenergetic, while in the S_0 state, the 11_3 and $12_1 14_1$ levels almost coincide; it is also the case that the latter corresponding cation levels are similarly very close in energy.[12] There is not, however, any unambiguous evidence of interactions between the noted levels in any of the three electronic states.

The relatively strong 1518 cm^{-1} emission band (Fig. 6) when exciting at 804 cm^{-1} can be assigned as $14_3 20_2 m_x$ and would be the counterpart of the $14_1 20_2 m_x$ band (702 cm^{-1}) seen when exciting at ~400 cm^{-1};[20] this would be consistent with the clear 702 cm^{-1} emission seen at this excitation position
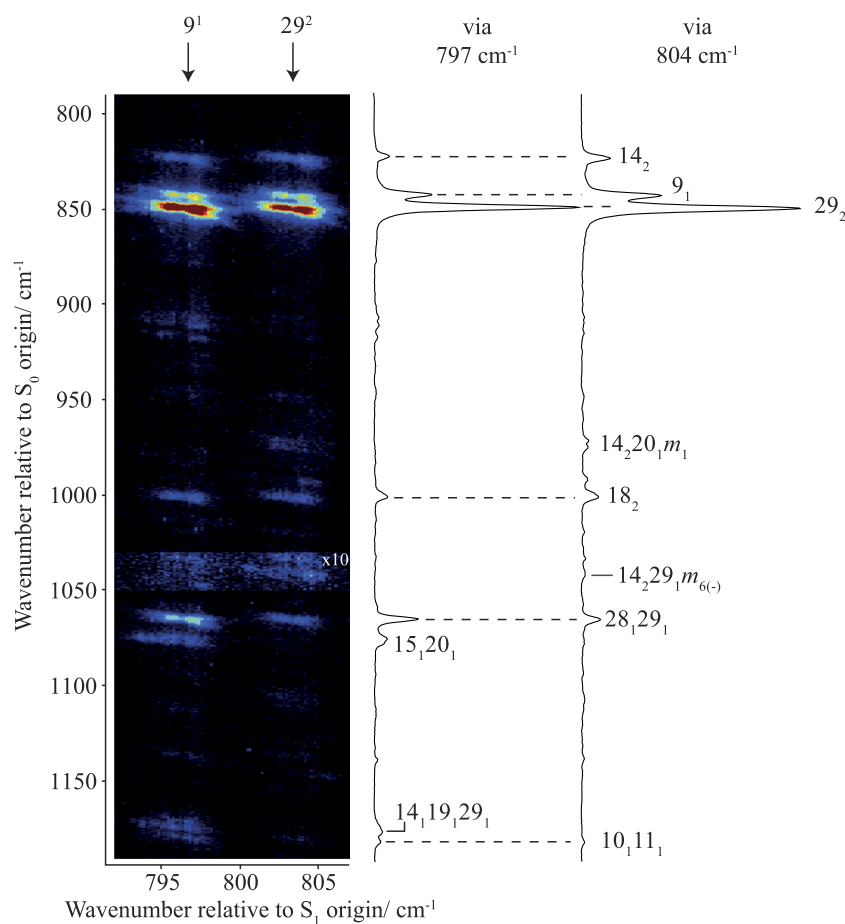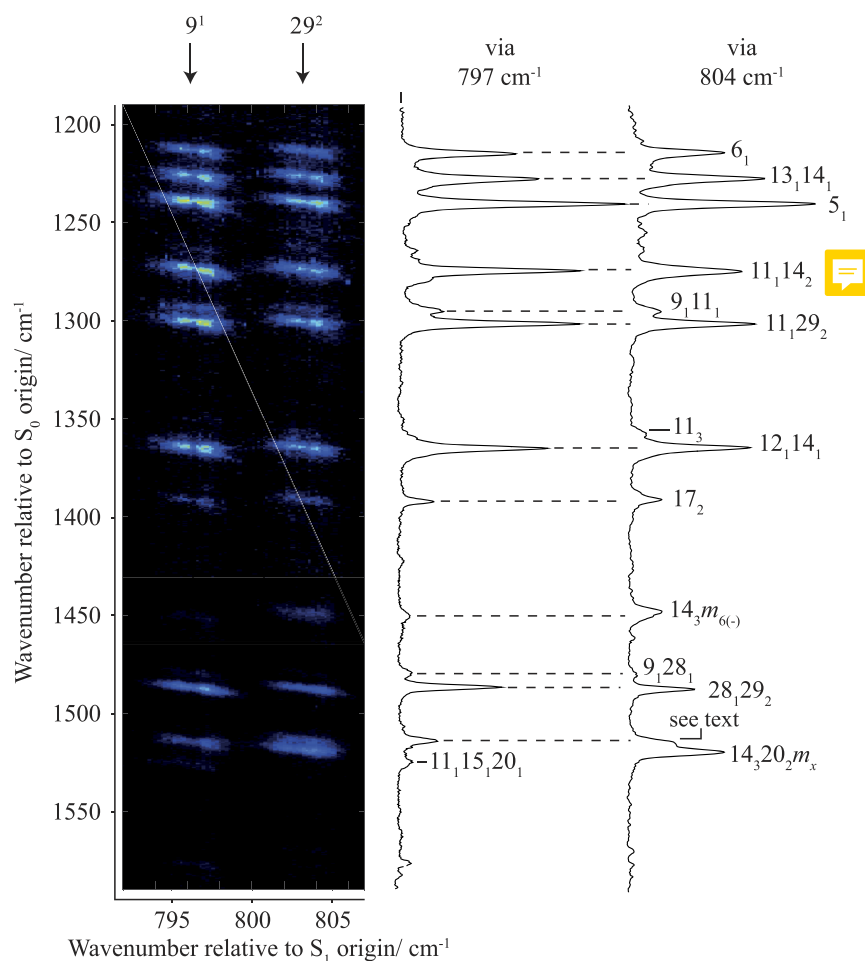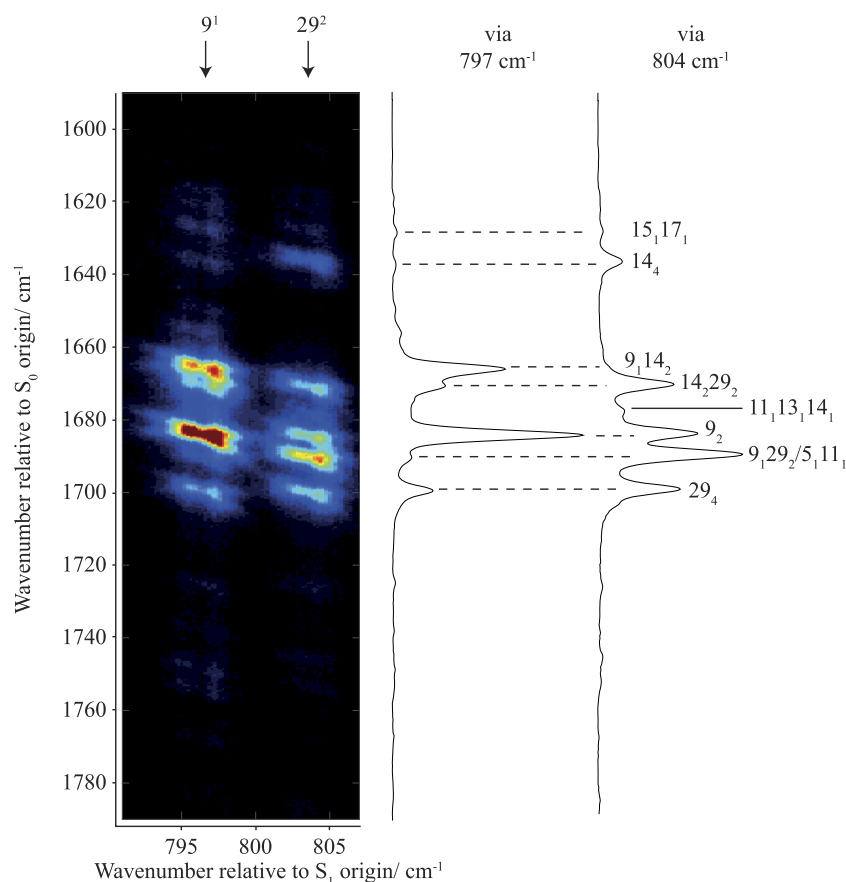
FIG. 7. Expanded views of the 2D-LIF and DF spectra for the 1590–1790 cm^{-1} region exciting via the 797 cm^{-1} and 804 cm^{-1} eigenstates. The spectral intensities are represented by colours, with red being the most intense through to blue being the least; black represents the zero background. See text for discussion of the assignments. The relative intensities in the 2D-LIF spectrum are as recorded, while the DF spectra have been adjusted to be qualitatively in agreement with the 2D-LIF spectrum, but with some regard to presentational clarity. Thus, the relative intensities within the same DF trace will be reliable, but not necessarily when comparing between two traces.

(Fig. 4). (Recall that in Ref. 20 we could not definitively decide on the associated m level.)

In Section III B 2, we have seen that most of the bands we observed[20] when exciting at ~398 cm^{-1} also appear in this region, each in combination with 14_2 and 29_1, but with their $\Delta(v, m)$ bands at 804 cm^{-1}. This is particularly surprising, since the expected band positions might suggest that these would appear close to 797 cm^{-1}. This appears to be the result of a remarkable coincidence caused by the movement of the various levels via their interaction with 9^1, and possibly in tandem with the positive anharmonicity of the 14^n progression, seen for pDFB.[38,39] It is also evident that there is greater 14_2 activity when exciting at 804 cm^{-1} than there is at 797 cm^{-1} (see Fig. 5), which would be consistent with these other S_1 levels arising from 14^2 combinations lying at this wavenumber.

In Section III B 2, we have noted that the 1071 cm^{-1} emission band (Fig. 5) is at the expected position for $11_1 14_1 m^{6(-)}$, but that it is unexpected that this would be almost exclusively localized at 797 cm^{-1}, particularly given the spread of activity of $11_1 14_2$ across the spectrum (and noting that the 14^2 and $14^1 m^{6(-)}$ levels are almost isoenergetic and interacting[12,16,20]). Since we would expect $11^1 14^1 m^{6(-)}$ to appear at an excitation position of 806 cm^{-1}, it seems unlikely that any interaction would be enough to cause it to lie very close to

the 797 cm^{-1} eigenstate and would not be consistent with the localized activity. Further, close inspection of the $14_1 m_{6(-)}$ band profile (seen at 618 cm^{-1} in Refs. 16 and 20) shows these to be somewhat different, and additionally the 1071 cm^{-1} band is found not to be enhanced when exciting via 11^1. Since the band appears relatively localized in excitation position, and being totally symmetric, this is likely to be the $\Delta v = 0$ band; hence, we sought another assignment of this band, with the most likely candidate being $15_1 20_1$. This would suggest that the wavenumber of D_{15} in the S_1 state is 687 cm^{-1}, which is still in reasonable agreement with the calculated value, but would require our previous value[12] of 678 cm^{-1} to be revised. The latter came from a very tentative assignment of a $\Delta(v, m) = 0$ ZEKE band to $^+15^1 m^{3(-)}$. If we then cross-check with the ZEKE spectrum, we would expect the $^+15^1 20^1$ level to lie at ~1109 cm^{-1} using the calculated value for D_{15} in the cation, which would excellently match the ZEKE band at 1112 cm^{-1} seen when exciting at these corresponding wavenumbers;[12] pleasingly, this also matches the extent of this feature to lower wavenumber where the 1112 cm^{-1} ZEKE band is prominent. That ZEKE feature was assigned to $^+14^2 29^1$ in Ref. 12, but as we have noted, we are unable to discern $14_2 29_1$ emission in our 2D-LIF spectra, but it may be masked by the strong 5_1 features−we shall come back to this later. Since we expect $11^1 14^1 m^{6(-)}$ to be interacting
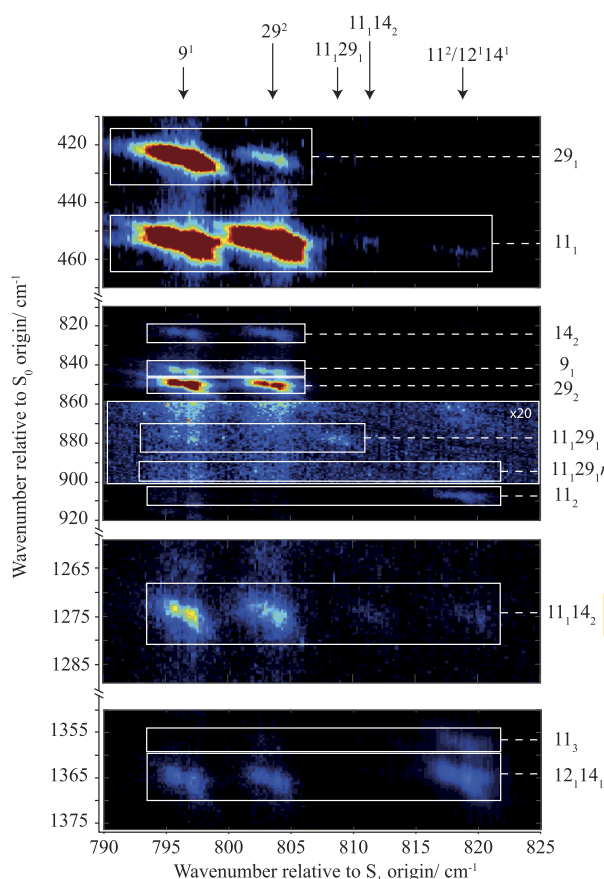
FIG. 8. Expanded views of sections of the 2D-LIF spectra across the 790–825 cm^{-1} region demonstrating the activity when exciting via 797 cm^{-1}, 804 cm^{-1}, and 818 cm^{-1}. The spectral intensities are represented by colours, with red being the most intense through to blue being the least; black represents the zero background. See text for discussion of the assignments.

with $11^1 14^2$, and since the $\Delta v = 0$ band of the latter is weak, then the $11_1 14_1 m_{6(-)}$ band is also expected to be weak, and presumably this is the reason for its non-observation; further, if it were interacting, then we would expect to see activity at different excitation wavenumbers.

In our previous ZEKE study,[12] we also assigned a band at 1171 cm^{-1} to $^+12^1 m^{6(-)}$, seen clearly when exciting at 794 cm^{-1} and at various positions across the 797 cm^{-1} band. The corresponding 2D-LIF band would be expected to have an emission of ~1161 cm^{-1}, but there is no such band seen when exciting at 797 cm^{-1}. (The only possible candidate is a feature at ~1174 cm^{-1}, which lies just above the $10_1 11_1$ band, and appears to be wholly localized around 797 cm^{-1}, but this seems too distant in wavenumber to be likely; further, the S$_1$ excitation position for $12^1 m^{6(-)}$ would be expected to be significantly higher than 797 cm^{-1} in the absence of any significant interactions.) There are a number of pure vibrational assignments for the 1174 cm^{-1} feature, with $14_1 19_1 29_1$ perhaps being the most likely on the grounds that it is totally symmetric (and so could be FC active) and contains 29_1 character (given the

activity of 29_1 at this excitation position). Although we find little enhancement of this feature when exciting via 29^1, this may be because of the difference in symmetry. Alternatives such as a HT-active a_1'' symmetry level, e.g., $14_1 20_1 30_2$, would not be expected to be so intense. Either way, the reassignment of the ZEKE band meets the expectation that the $12^1 m^{6(-)}$ state would not be expected to lie so far from $12^1 14^1$, since the 14^1 and $m^{6(-)}$, and 14^2 and $14^1 m^{6(-)}$, pairs of levels are each close together in the S$_1$ state,[12,16] and so it is difficult to see what could displace the $12^1 m^{6(-)}$ level so far away from $12^1 14^1$. Further inspection of the spectra reveals a very weak 2D-LIF feature at (820, 1159) cm^{-1} that would be consistent with being the ($12^1 m^{6(-)}$, $12_1 m_{6(-)}$) band. We now, however, would need to reassign the 1171 cm^{-1} ZEKE band. One possibility is $^+7^1$ FC activity from totally symmetric levels such as $15^1 20^1$ and 9^1. However, this ZEKE band appears clearly across the 797 cm^{-1} and 804 cm^{-1} excitation regions and it is unclear why it would be so relatively intense when exciting at ~797 cm^{-1}. Another possibility is $^+9^1 14^1$, which would tie in with the activity of $^+14^1$ commonly seen in ZEKE spectra of substituted benzenes, and discussed in our recent paper on p-difluorobenzene;[39] additionally, the $^+9^1 14^1 m^1$ level is possible as it is symmetry allowed from $m = 0$ levels of totally symmetric vibrations.

We summarize the comparison of the present 2D-LIF and DF spectra with the ZEKE spectra of Ref. 12 as follows. First, the main 2D-LIF assignments are consistent, with the 797 cm^{-1} level giving non-diagonal FCFs for the 9_1 and 9_2 bands and confirming the 797 cm^{-1} level is made up predominantly of 9^1; similarly, the ZEKE and 2D-LIF spectra are both strongly indicative of the 804 cm^{-1} band being dominated by 29^2. Also clear in both sets of spectra are the contributions from 11^2 and $12^1 14^1$ at 818 cm^{-1}, $11^1 29^1$ at 807 cm^{-1}, and $11^1 14^2$ at 811 cm^{-1}. We have noted the reassignment of the 1112 cm^{-1} ZEKE band, previously associated with $^+14^2 29^1$, as now being indicative of $15^1 20^1$ activity at 797 cm^{-1}; while the 1171 cm^{-1} ZEKE band, rather than indicating $12^1 m^{6(-)}$ activity at 797 cm^{-1}, is merely reflecting FC activity of $^+7^1$ or $^+9^1 14^1 m^1$. The 14^4 activity was difficult to pin down in the ZEKE study, but there was evidence for the $^+14^4$ ZEKE band appearing across the 804 cm^{-1} excitation region, and this seems to be confirmed in the 2D-LIF. It is difficult to pick out ZEKE bands arising from $^+14^3 m^{6(-)}$, expected at 1237 cm^{-1}, $^+29^1 14^1 m^{6(-)}$ expected at 953 cm^{-1}, nor $^+11^1 14^1 m^{6(-)}$ expected at 977 cm^{-1}. The lack of $^+11^1 14^2$ ZEKE bands in the 797 cm^{-1} excitation region are consistent with the S$_1$ level not interacting significantly with 9^1, but with other ZOSs that are contributing to the 804 cm^{-1} band.

Note that in our recent paper on the 400 cm^{-1} region,[20] we assigned a 489 cm^{-1} 2D-LIF emission band to $20_2 m_{6(+)}$ arising from interaction with 14^2. We can see a weak feature at (805, 1308) cm^{-1}, which can be assigned to $14_2 20_2 m_{6(+)}$ expected at 1311 cm^{-1}. The $14^2 20^2 m^{6(+)}$ level would analogously be expected to interact with 14^4, but we noted in Ref. 20 that such an interaction is likely to be weak and be highly dependent on the levels being extremely close in energy; indeed, this feature does have a localized intensity.

3. Comments on other selected features

In Fig. 4, we see a very weak feature at (797, 558) cm^{-1}, assigned to $14_1 20_1$, that is barely visible when exciting at 804 cm^{-1}; this is consistent with a corresponding emission observed in Ref. 16. A weak band at 633 cm^{-1} seems to be the same band seen when exciting at 364 cm^{-1},[20] assigned to $14_1 20_1 m_4$ and can be expected to be active from $14^3 20^2 m^1$. The band at 670 cm^{-1} is 19_2 consistent with an emission reported by Gascooke et al.[16]

An emission band at 731 cm^{-1} is seen clearly when exciting at 797 and 804 cm^{-1} (see Fig. 4) and was also seen via the origin,[20] and it has been assigned to 10_1. A second very close emission feature is evident at 733 cm^{-1} when exciting via 797 cm^{-1}, which can be discerned in the DF spectra; the most likely assignment is $29_1 30_1$ and ties in with the observed stronger $28_1 29_1 / 18_1 20_1 29_1$ band when exciting at 797 cm^{-1}. It is interesting to note that $29_1 30_1$ is not enhanced when exciting via 29^1 (Ref. 20), which can be attributed to its different symmetry; this could thus be evidence for the enhancement of the $28_1 29_1 / 18_1 20_1 29_1$ band when exciting via 29^1,[20] as being due to a significant $18_1 20_1 29_1$ contribution.

There is a weak emission band at 863 cm^{-1} that is active across the three main regions of the spectrum. A possible assignment is $29_2 m_2$, accessed via a $\Delta m = 3$ transition, but this would be expected to be weak. Other possibilities are $14_1 20_3 m_2$ or $11_1 14_1 m_1$, and we favour the latter as there is a weak secondary feature at 870 cm^{-1}, which seems likely to be $11_1 19_1 m_4$. Then these two bands are analogous to the $14_1 m_1$ and $19_1 m_4$ interaction seen by Gascooke et al.[16] and the $14_2 m_1$ and $14_1 19_1 m_4$ interaction seen in our recent work.[20]

A weak emission band at 895 cm^{-1} also appears at the three main excitation positions and suggests assignments as $9_1 m_{3(+)}$ or $11_1 29_1 m_2$, with the latter favoured as the band is more intense when exciting at 797 cm^{-1}, as is the 29_1 band; also, since the level has e'' symmetry, it is symmetry-allowed at the three main positions from the $m = 1$ levels of the dominant ZOSs; the absence of 9_1 emission when exciting at 818 cm^{-1} makes the $9_1 m_{3(+)}$ assignment unlikely. There are several weak bands around 900 cm^{-1}, and although one of these is clearly 11_2, as noted in Section III B 2, the assignments of the others are uncertain, with vibtor levels related to 9_1 and 29_2 being candidates for some of these.

In the 1200–1300 cm^{-1} emission region (see Fig. 6), there are a series of bands that are straightforwardly assigned. The first three bands at 1210, 1223, and 1236 cm^{-1} have assignments of 6_1, $13_1 14_1$, and 5_1. These assignments are consistent with bands observed via other levels and presented in Ref. 20; the appearance of $13_1 14_1$ is consistent with the observed activity of the 14_2 and $12_1 14_1$ bands. To slightly higher wavenumber are the overlapped $11_1 14_2$ and 29_3 bands, whose presence can be ascertained from the differing activity when exciting via different intermediate levels.[20] We find that the $11_1 14_2$ band is more intense via 11^1 and 797 cm^{-1}, while the 29_3 band is more intense via 29^1,[20] but we expect the contributions from the latter to be minimal in this excitation region. At 1294 cm^{-1} is $9_1 11_1$, and at 1301 cm^{-1}, we see $11_1 29_2$, with the latter being most intense when exciting via 797 cm^{-1} and 804 cm^{-1}, consistent

with the $\Delta v = 0$ region. There are three other prominent features to higher wavenumber in this region: 1364 cm^{-1}, which is assigned to $12_1 14_1$; 1394 cm^{-1}, which is assigned to 17_2; and 1487 cm^{-1}, which is assigned to $28_1 29_2$, and can be seen to intense via both 797 cm^{-1} and 804 cm^{-1}, as for the 29_2 band (refer to Figs. 5 and 6). Finally, there appears to be a double band with maxima at 1515 cm^{-1} and 1519 cm^{-1}; the latter has already been assigned to $14_3 20_2 m_x$ (see above). Taking into consideration the expected activity of various combination bands via different intermediates, our favoured assignment of the 1515 cm^{-1} band is to $11_1 28_1 29_1$, but this is tentative.

The 1600–1750 cm^{-1} emission region (see Fig. 7) is not initially straightforward to assign as there are multiple overlapping bands, with possible interactions between the contributing S$_0$ levels. DF spectra recorded from different intermediate levels (see Figs. 7 and 9) are, however, very useful. This region is complicated since it is expected to show overtones
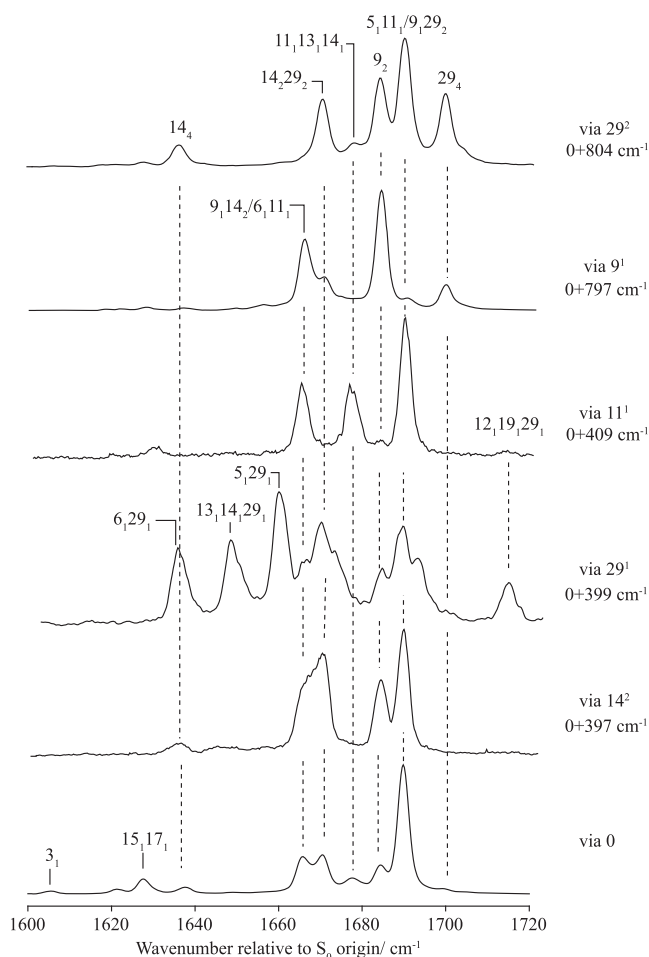

FIG. 9. DF spectra of 1600–1720 cm^{-1} regions via different intermediate levels. See text for discussion of the assignments. Each trace has been normalized to the most intense band; thus, the relative intensities within the same DF trace will be reliable, but to compare intensities between traces, refer to Fig. 7.

and combination bands of the levels that contribute to the Δv = 0 (~800 cm^{-1}) region; it is also where 11_1 and 29_1 combinations with the S_0 levels seen at 1200–1300 cm^{-1} are expected to appear; and there is also the possibility of new fundamentals and other combinations and overtones. Furthermore, there is a likelihood of overlapping features and interactions between levels. In Fig. 9, we show the spectra recorded via six different intermediate levels: 0^0, 14^2, 29^1, 11^1 and the 797 cm^{-1} and 804 cm^{-1} levels. The 11_1 combinations with the 1200–1300 cm^{-1} features are easy to pick out: $6_1 11_1$, $11_1 13_1 14_1$, and $5_1 11_1$, as are the corresponding combinations with 29_1. The strong 9_2 band is also easy to identify and shows clearly that the $(9^1, 9_2)$ band is significantly more intense than $(9^1, 9_1 29_2)$ and $(9^1, 29_4)$, confirming that the 9^1 contribution to the 797 cm^{-1} eigenstate is dominant. (Note that the $9_1 29_2$ and $5_1 11_1$ bands are very close in wavenumber and partially overlapped, but have very different activities via different intermediate levels.) Interestingly, although the $(29^2, 9_1 29_2)$ band is more intense than the $(9^1, 9_2)$ and $(9^1, 9_1 29_2)$ bands, we see that the $(9^1, 29_4)$ band is more intense than $(29^2, 29_4)$—see Fig. 7. Also clear are the $9_1 14_2$ and $14_2 29_2$ bands at 1664 and 1668 cm^{-1}. It can be seen that the $6_1 29_1$, $13_1 14_1 29_1$, and $5_1 29_1$ bands are all enhanced via 797 cm^{-1} compared to 804 cm^{-1}, consistent with the HT activity of 29_1 when exciting at 797 cm^{-1}.

IV. DISCUSSION

In Fig. 3, we show the 0–310 cm^{-1} region of the DF spectra obtained when exciting via the origin, and each of the 797 cm^{-1} and 804 cm^{-1} bands. The features have been assigned and discussed in depth in Ref. 16, to which the reader is referred. It may be seen that the structure is very similar in all three cases and, in particular, that there are features that arise from both the $m = 0$ and $m = 1$ levels, with similar relative intensities in each case.

We have noted that in the picosecond tr-PES[27] study, the two S_1 eigenstates at 797 cm^{-1} and 804 cm^{-1} were concluded to arise from a Fermi resonance, as deduced from monitoring the time-dependent signal from ionization to the origin using photoelectron spectroscopy, and that is consistent with the deductions here and in Ref. 12. Of particular interest, however, is the observation that a large amount of the intensity was lost rapidly (over 30 ps) when these two eigenstates were excited coherently—this was interpreted as rotational dephasing involving one of the torsional levels in each of the two vibrational eigenstates.

Those time-resolved experiments made use of picosecond lasers, whose linewidth is ~15 cm^{-1}. As such, more than one eigenstate is excited coherently, forming a wavepacket—i.e., a coherent superposition of more than one eigenstate. As with the nanosecond experiments, projection of the excited state eigenstates (in that case, a wavepacket) onto those of another state (in that case, the cation) can, in principle, allow the ZOS make-up to be ascertained, particularly if the corresponding ZOSs are well-separated in the cation. (It should be noted that in the picosecond experiments, the populations of the eigenstates do not change with time, unless there is some additional photophysical process occurring: the

variations one sees in the time-resolved photoelectron spectra are caused by the moving in and out of phase of the eigenstates in the wavepacket.) If such variations can be recorded over a large enough time scale, then Fourier transformation can be used to obtain the energy separations between the component eigenstates,[27] and these should, of course, be consistent with the separation of corresponding bands seen in a REMPI or LIF experiment. Such a Fourier transform was performed in that work,[27] and two peaks were seen, one at 6.7 cm^{-1} and the other at 6.2 cm^{-1}, with the former being the more intense and sharp, while the latter was much weaker with a broader structure. The 6.7 cm^{-1} separation matches that between the 797 cm^{-1} and 804 cm^{-1} excitation bands in Fig. 1. The 6.7 cm^{-1} separation was hypothesised as arising from a particular m level of the two vibrations, with the 6.2 cm^{-1} separation arising from the other populated m level in the same levels (recalling that both m = 0 and m = 1 levels will be populated). The separation was suggested as being caused by the $m = 0$ and $m = 1$ levels having slightly different rotational constants. It was then suggested that the rapid loss of intensity within the first 30 ps arose from rotational dephasing, which was suggested as arising from a rotational-level dependent coupling term—it was noted that such a coupling could not be simply anharmonic, since this would not have a rotational dependence. The rotational dephasing would occur as a result of destructive interference between the many coherently excited rotational levels corresponding to the same m level in the two different vibrational eigenstates, caused by an m-specific (and J, K-dependent) interaction. Since this effect is expected to be very small, it would be consistent with the small difference in the two spacings of the eigenstates reported in Ref. 27. Further, this would explain why, in Fig. 3, we see the whole set of torsional levels via both the 797 cm^{-1} and 804 cm^{-1} levels at what appear to be identical emission wavenumbers—the dephasing *only* occurs as a result of the two eigenstates being coherently excited. At the resolution in our spectra, we are unable to see any obvious difference in spacings of the various torsional levels in Fig. 1, nor in the separation of the various $\Delta(v, m) = 0$ bands. As noted in Ref. 27, what is required is for there to be one or more interactions with nearby ZOSs that is m specific, and which causes a sufficient perturbation to lead to a J, K-dependent perturbation to the rotational energy levels, which we now explore.

In Section III B 2, we have noted several levels that are coincident with one or more of the main two eigenstates at 797 cm^{-1} and 804 cm^{-1}; however, we also require the levels to be interacting for the m-specific interaction to occur. Hence, for example, the $15^1 20^1$ level could not be a cause of the perturbation in rotational constants as it is not interacting to any noticeable extent, and there would be no reason why the interaction would not take place in both m levels. The latter comment also applies to levels such as $11^1 14^2$, 14^4, 11^2, and $12^1 14^1$. However, the $14^3 m^{6(-)}$ or $14^3 20^1 m^x$ levels would each be expected to interact only with one of the m levels and so could cause the required perturbation. This seems most likely to happen for the 804 cm^{-1} eigenstate(s), where the activity from these levels is localized. One possibility would be the

interaction between 14^4 and $14^3 m^{6(-)}$, which is analogous to the 14^1 and $m^{6(-)}$ and 14^2 and $14^1 m^{6(-)}$ interactions discussed in Refs. 12, 16, and 20; in particular, this interaction has been noted in Ref. 16 as being sensitive to the rotational levels moving in and out of resonance, and so perturbing the rotational structure. Thus, the interactions between $14^4 m^0$, $14^3 m^{6(-)}$ and $9^1 m^0$ may well have a rotational dependence and cause $m = 0$ rotational levels to have slightly different wavenumber separations than the corresponding $m = 1$ ones. We also observe that it is possible that some of the complications discussed in the analysis of the time-resolved data in Ref. 27 could be attributable to contributions from the various ZOSs to this region, which would also be excited in those experiments. It is clear, however, that the loss of intensity in the tr-PES study cannot be incipient dissipative intramolecular vibrational redistribution (IVR), as then we would expect a significant, broad underlying background in the present nanosecond excitation spectra, but this is not seen.

Coming back to our recent work[20] on the bands at ~400 cm^{-1}, we there noted that there are a significant number of bands involving the low-wavenumber, out-of-plane modes, D_{14} and D_{20}, commensurate with these modes coupling to the torsional motion of the methyl group, and this is also the case in the higher wavenumber region focused on in the present work. These modes, and to some extent D_{19}, seem to be key in providing routes for the methyl group to couple to the vibrational motions. Because of symmetry constraints, the main routes are coupling with the $m = 3(-)$ level for D_{20} and D_{19} and the $m = 6(-)$ level for D_{14}. Coupling between in-plane vibrations also occurs—for example, D_{29} with $m = 3(+)$.

In Refs. 13 and 20, we also highlighted the role of the $m = 1$ levels in enhancing the coupling between levels, something that is implicit in the energy level diagrams of Ref. 16. These open up routes to coupling between vibtor levels arising from vibrations of different C_{2v} symmetry, which lead to a rapid rise in the possibilities for interactions, albeit somewhat sporadically at low energy.[17]

We have seen that there is strong evidence for the interaction between 9^1 and 29^2, both from the tr-PES study[27] and also from the corresponding FC activity, but with differing intensities in both the ZEKE study[12] and the present 2D-LIF study. Furthermore, other activity in the ZEKE and 2D-LIF spectra indicates that there are contributions from other ZOSs and that these have moved from their expected positions, providing evidence of interactions. We also see that for "clean" emission features, such as 1518 cm^{-1} and 1636 cm^{-1}, there is weak activity at 797 cm^{-1} as well as the very dominant activity at 804 cm^{-1}, and this confirms the interactions of some of the ZOSs with 9^1. In contrast, although we see clear $12_1 14_1$ activity when exciting at 797 cm^{-1} and 804 cm^{-1}, the lack of any partnering activity of 9_1 or 29_2 when exciting via $12^1 14^1$ suggests no interaction with those levels, and the former activity is FC in nature. Although a quantitative picture is not straightforward to extract, we believe the picture of the interactions is qualitatively as follows. The 29^2 ZOS lies above 9^1, and this is the main interaction. The 14^4 level also lies above 9^1, which may arise as part of the overall set of interactions, including 9^1 and 29^2, or because of positive anharmonicity in the 14^n

progression; either way, the 14^4 and 9^1 levels also interact. The result is that 29^2-dominated and 14^4-dominated eigenstates are essentially at the same energy (804 cm^{-1}). Since 14^2 and $14^1 m^{6(-)}$ interact strongly,[12,15,16] then this gives some rationale as to why the $14^3 m^{6(-)}$ level also appears at 804 cm^{-1} (since 14^2 and $14^1 m^{6(-)}$ are almost isoenergetic)[16,20] although there is no *a priori* reason to expect the interactions of different ZOSs with 14^4 and $14^3 m^{6(-)}$ to be the same. In contrast, the $11^1 14^2$ level appears at a lower wavenumber, implying that the interactions between 9^1 and this level are weaker; the appearance of $11^1 29^1$ to lower wavenumber is consistent with its different symmetry from 9^1. It is surprising that the $14^1 29^1 m^{6(-)}$ level also appears at 804 cm^{-1}, and this is likely the result of a number of interactions. We cannot be definitive about the positions of $11^1 14^1 m^{6(-)}$ and $14^2 29^1$, as unambiguous emission bands are not seen for these. We might expect $11^1 14^1 m^{6(-)}$ to be close to $11^1 14^2$ and $14^1 29^1 m^{6(-)}$ to be close to $14^2 29^1$, but the interactions could be different for these ZOSs. We assigned an emission band at 1071 cm^{-1} to $15_1 20_1$, even though this was at the wavenumber expected for $11_1 14_1 m_{6(-)}$, and noted that the $15^1 20^1$ level does not appear to be interacting with 9^1 or 29^2. As commented in Section III B 2, via the 797 cm^{-1} and 804 cm^{-1} eigenstates we see $12_1 14_1$ FC emission, and we conclude the $12^1 14^1$ level is not interacting with 9^1. Moreover, even though 11^2 and $12^1 14^1$ are almost degenerate, they do not seem to be interacting in S$_1$, as their activity across the spectra is different; similar comments apply to $12_1 14_1$ and 11_3 in S$_0$. Finally, we have concluded that the $^+12^1 m^{6(-)}$ band was misassigned in our previous ZEKE study[12] and we tentatively conclude that the corresponding S$_1$ level may be located close to $12^1 14^1$.

V. CONCLUSIONS

In this work, it has been seen that, although at first sight the REMPI/LIF excitation spectra appear to indicate a rather straightforward pairwise classic Fermi resonance interaction, in fact the picture is significantly more complicated, in agreement with the conclusions of the ZEKE study[12] and, in part, consistent with the conclusions of the tr-PES study.[27] It is clear, however, that although there are a fair number of ZOSs contributing to the 790–825 cm^{-1} region, the present results and those of Ref. 27 indicate that we are still in the restricted IVR regime, but with the situation being far more complicated than a simple Fermi resonance. In a previous work,[40] we have discussed the factors that affect experimental observations relating to IVR, and one of these was the temperature of the molecules. This, we believe, underlies the indications of wider-ranging IVR implicit in the DF spectra obtained via 9^1 and even via the ~400 cm^{-1} levels in a 300 K sample of pFT,[41] probably driven by thermally populated torsional and rotational levels.

Finally, as with the 14^2 and $14^1 m^{6(-)}$ interaction which has localized rotation-level dependent coupling,[16] we find that several other bands appear to show unexpected intensity profiles (e.g., bands at 973 cm^{-1} and 993 cm^{-1}), and this may be evidence for similar effects.

In summary, we have shown that 2D-LIF is a powerful tool in revealing overlapping bands in an excitation spectrum and separating these to facilitate their assignments. The spectra

also help to reveal interacting levels via the different intensities seen when exciting at different positions. In some cases, complications arise from separating FC activity from cross-activity arising from interacting ZOSs, but considering other activity can often clarify this. The technique is particularly useful in cases such as here, where a (not too large) number of ZOSs are interacting in complex Fermi resonances, and where the anharmonic shifts in levels cause levels to move, making it more difficult to identify them in a simple excitation spectrum. Further, the much more complete dataset represented by a 2D-LIF spectrum provides greater reliability regarding the interpretation of the activity; however, the "2D-ZEKE" spectra we have published[12] are complementary, as they project the S_1 levels onto a different electronic state, and so help to confirm assignments.

ACKNOWLEDGMENTS

REFERENCES

[1] Z.-Q. Zhao and C. S. Parmenter, *Mode Selective Chemistry*, edited by J. Jortner, R. D. Levine, and B. Pullman (Kluwer, 1991), Vol. 24, p. 127.

[2] Z.-Q. Zhao, C. S. Parmenter, D. B. Moss, A. J. Bradley, A. E. W. Knight, and K. G. Owens, J. Chem. Phys. **96**, 6362 (1992).

[3] Z.-Q. Zhao, Ph.D. thesis, Indiana University, 1992.

[4] Q. Ju, C. S. Parmenter, T. A. Stone, and Z.-Q. Zhao, Isr. J. Chem. **37**, 379 (1997).

[5] J. A. Davies, A. M. Green, A. M. Gardner, C. D. Withers, T. G. Wright, and K. L. Reid, Phys. Chem. Chem. Phys. **16**, 430 (2014).

[6] A. M. Gardner, A. M. Green, V. M. Tamé-Reyes, K. L. Reid, J. A. Davies, V. H. K. Parkes, and T. G. Wright, J. Chem. Phys. **140**, 114308 (2014).

[7] A. M. Gardner, A. M. Green, V. M. Tamé-Reyes, V. H. K. Wilton, and T. G. Wright, J. Chem. Phys. **138**, 134303 (2013).

[8] E. A. Virgo, J. R. Gascooke, and W. D. Lawrance, J. Chem. Phys. **140**, 154310 (2014).

[9] J. R. Gascooke, E. A. Virgo, and W. D. Lawrance, J. Chem. Phys. **142**, 024315 (2015).

[10] J. R. Gascooke, E. A. Virgo, and W. D. Lawrance, J. Chem. Phys. **143**, 044313 (2015).

[11] J. R. Gascooke and W. D. Lawrance, J. Mol. Spectrosc. **318**, 53 (2015).

[12] W. D. Tuttle, A. M. Gardner, L. E. Whalley, and T. G. Wright, J. Chem. Phys. **146**, 244310 (2017).

[13] A. M. Gardner, W. D. Tuttle, L. E. Whalley, and T. G. Wright, Chem. Sci. **9**, 2270 (2018).

[14] V. L. Ayles, C. J. Hammond, D. E. Bergeron, O. J. Richards, and T. G. Wright, J. Chem. Phys. **126**, 244304 (2007).

[15] A. M. Gardner, W. D. Tuttle, L. Whalley, A. Claydon, J. H. Carter, and T. G. Wright, J. Chem. Phys. **145**, 124307 (2016).

[16] J. R. Gascooke, L. D. Stuart, P. G. Sibley, and W. D. Lawrance, J. Chem. Phys. **149**, 074301 (2018). This work contains considerable extra information in its supplementary information. Note, however, that the excitation wavenumber axis is incorrect in Fig. S9.

[17] W. D. Tuttle, A. M. Gardner, L. E. Whalley, D. J. Kemp, and T. G. Wright, "Effects of symmetry, methyl groups and serendipity on intramolecular vibrational energy dispersal," Phys. Chem. Chem. Phys. (in press).

[18] A. M. Gardner, W. D. Tuttle, P. Groner, and T. G. Wright, J. Chem. Phys. **146**, 124308 (2017).

[19] W. D. Tuttle, A. M. Gardner, K. B. O'Regan, W. Malewicz, and T. G. Wright, J. Chem. Phys. **146**, 124309 (2017).

[20] D. J. Kemp, A. M. Gardner, W. D. Tuttle, and T. G. Wright, "Unravelling overlaps and torsion-facilitated coupling using two-dimensional laser-induced fluorescence," Mol. Phys. (in press).

[21] J. R. Gascooke and W. D. Lawrance, Eur. Phys. J. D **71**, 287 (2017).

[22] W. T. Cave and H. W. Thompson, Faraday Soc. Trans. **9**, 35 (1950).

[23] T. Cvitaš and J. M. Hollas, Mol. Phys. **20**, 645 (1971).

[24] C. J. Seliskar, M. A. Leugers, M. Heaven, and J. L. Hardwick, J. Mol. Spectrosc. **106**, 330 (1984).

[25] K. Okuyama, N. Mikami, and M. Ito, J. Phys. Chem. **89**, 5617 (1985).

[26] Z.-Q. Zhao and C. S. Parmenter, Ber. Bunsenges. Phys. Chem. **99**, 536 (1995).

[27] J. A. Davies and K. L. Reid, Phys. Rev. Lett. **109**, 193004 (2012).

[28] E. B. Wilson, Jr., Phys. Rev. **45**, 706 (1934).

[29] G. Varsányi, *Assignments of the Vibrational Spectra of Seven Hundred Benzene Derivatives* (Wiley, New York, 1974).

[30] R. S. Mulliken, J. Chem. Phys. **23**, 1997 (1955).

[31] G. Herzberg, *Molecular Spectra and Molecular Structure. II. Infrared and Raman Spectra of Polyatomic Molecules* (Krieger, Malabar, 1991).

[32] A. M. Gardner and T. G. Wright, J. Chem. Phys. **135**, 114305 (2011).

[33] A. Andrejeva, A. M. Gardner, W. D. Tuttle, and T. G. Wright, J. Mol. Spectrosc. **321**, 28 (2016).

[34] P. J. Breen, J. A. Warren, E. R. Bernstein, and J. I. Seeman, J. Chem. Phys. **87**, 1917 (1987).

[35] E. Fermi, Z. Phys. **71**, 250 (1931).

[36] J. R. Gascooke and W. D. Lawrance, J. Chem. Phys. **138**, 134302 (2013).

[37] N. T. Whetton and W. D. Lawrance, J. Phys. Chem. **93**, 5377–5384 (1989).

[38] A. E. W. Knight and S. H. Kable, J. Chem. Phys. **89**, 7139 (1988). Note that this work includes a significant number of further spectra and comments as part of the supplementary information.

[39] D. J. Kemp, A. M. Gardner, W. D. Tuttle, J. Midgley, K. L. Reid, and T. G. Wright, J. Chem. Phys. **149**, 094301 (2018).

[40] C. J. Hammond, V. L. Ayles, D. E. Bergeron, K. L. Reid, and T. G. Wright, J. Chem. Phys. **125**, 124308 (2006).

[41] C. S. Parmenter and B. M. Stone, J. Chem. Phys. **84**, 4710 (1986).

12. Observation of the onset of torsion-induced, mode-specific dissipative intramolecular vibrational redistribution (IVR):

Contributions:

Title: Observation of the onset of torsion-induced, mode-specific dissipative intramolecular vibrational redistribution (IVR)[42]

Authors: David J. Kemp, William D. Tuttle, Adrian M. Gardner, Laura E. Whalley, and Timothy G. Wright

Submitted to: Journal of Chemical Physics, 17th June 2019; accepted 24th July 2019; published 13th August 2019

This work includes a series of both REMPI and ZEKE spectra, all collected by a combination of William Tuttle, Adrian Gardner and Laura Whalley. DF and 2D-LIF spectra were all collected and processed by myself.

As with the previous publications, my contribution to the work focused mainly on analysing and drawing conclusions from the sets of data collected. Numerous discussions occurred between myself and Timothy Wright. Other members who contributed to this work, namely in the data collection, had departed long before we started to analyse and produce the paper.

Figure production on both 2D-LIF and ZEKE spectra, complete with assignments was done by myself. Once again, collaboration with Timothy Wright occurred where he suggested changes to the figures before initial submission to the journal.

Observation of the onset of torsion-induced, mode-specific dissipative intramolecular vibrational redistribution (IVR)

View Online   Export Citation   CrossMark

David J. Kemp, William D. Tuttle, Adrian M. Gardner,[a)] Laura E. Whalley, and Timothy G. Wright[b)] (iD)

AFFILIATIONS

School of Chemistry, University of Nottingham, University Park, Nottingham NG7 2RD, United Kingdom

[a)]**Present address:** Stephenson Institute for Renewable Energy, University of Liverpool, Liverpool L69 7ZF, United Kingdom.
[b)]Tim.Wright@nottingham.ac.uk

ABSTRACT

Evidence is found showing that coupling with vibration-torsion ("vibtor") levels of both in-plane and out-of-plane vibrations is instrumental in causing dissipative intramolecular vibrational redistribution (IVR). Both zero-electron-kinetic-energy (ZEKE) spectroscopy and two-dimensional laser-induced fluorescence (2D-LIF) spectroscopy are employed to investigate a series of bands located ~1200 cm^{-1} above the $S_1 \leftarrow S_0$ origin in p-fluorotoluene. Transitions in this wavenumber region have been the focus of a number of studies probing IVR. By recording both ZEKE and 2D-LIF spectra, a prepared S_1 population is projected onto both the ground state cation and ground state neutral energy states, respectively, giving added confidence to the assignments. The spectral region under discussion is dominated by a pair of fundamental bands, but for the first time, we present explicit evidence that this is complicated by contributions from a number of overtones and combinations, including vibtor levels. We deduce that very different extents of coupling are present across a 60 cm^{-1} window of the spectrum, even though the density of states is similar; in particular, one of the fundamentals couples efficiently to the increasing bath of levels, while one does not. We explain this by the influence of serendipitous near-coincidences of same-symmetry levels.

Published under license by AIP Publishing. https://doi.org/10.1063/1.5115329

I. INTRODUCTION

The ability to describe the making and breaking of chemical bonds and the flow of energy through a molecule necessitates a knowledge of the internal energy level structure, in particular, vibrations and torsions. Building on the work by Parmenter and co-workers,[1–7] and the group of Weisshaar,[8–10] recent work by the Lawrance group and ourselves has identified that vibration-torsional ("vibtor") coupling is of key importance in the following *para*-substituted molecules that contain methyl groups: toluene,[11–17] *p*FT,[11,18–27] and *para*-xylene (*p*Xyl).[25,28,29] Some of the most recent work has employed the technique of two-dimensional laser-induced fluorescence (2D-LIF), which has been reviewed recently.[30]

Following on from earlier work on *p*FT,[31,32] Seliskar *et al.*[33] and Okuyama *et al.*[34] presented laser-induced fluorescence (LIF) spectra under jet-cooled conditions, giving assignments of some of the

vibrational bands. A number of low-wavenumber bands have been reassigned to vibtor levels by Zhao,[5] which was confirmed in the recent work by our group[21] and that of Lawrance *et al.*[22] An overview of the lowest 1250 cm^{-1} of the $S_1 \leftarrow S_0$ resonance-enhanced multiphoton ionization (REMPI) spectrum is shown in Fig. 1. Recently, we have examined the bands close to 400 cm^{-1} (Ref. 26) and those at ~800 cm^{-1} (Ref. 27) using 2D-LIF and compared the results to our earlier zero-electron-kinetic-energy (ZEKE) work.[18,21,23] The assignments of the 2D-LIF spectra indicated that both vibrational interactions and vibration-torsional coupling were occurring.

In the present work, we examine the 1200 cm^{-1} region of the spectrum—see Fig. 1. This region of the spectrum contains two strong fundamental transitions, and these have been assigned by Okuyama *et al.*[34] with LIF and confirmed by our later ZEKE study.[18] What was remarkable about the ZEKE spectra was that the one recorded from the lower fundamental (1196 cm^{-1}) was highly structured, with very limited broadness in the baseline, while the one
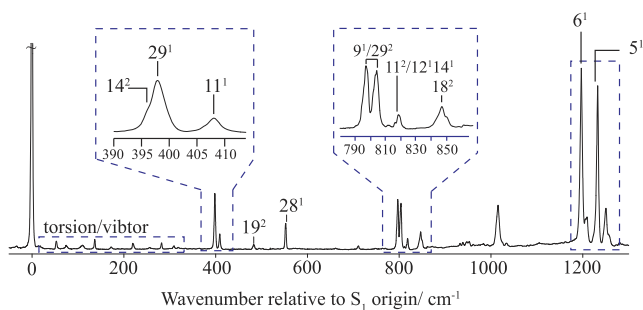
FIG. 1. Overview of the 0–1250 cm^{-1} region of the REMPI spectrum of the S$_1 \leftarrow$ S$_0$ transition in pFT. See text for further comments.

recorded via the higher one (1232 cm^{-1}) had a very large amount of complicated overlapped structure across a wide range. This was interpreted as a significant increase in intramolecular vibrational redistribution (IVR) in the latter, despite it being only 36 cm^{-1} higher in wavenumber. These spectra were further discussed in Refs. 11 and 19 in tandem with additional time-resolved data from the Reid group at Nottingham. In particular, it was noted therein that there has been some ambiguity in the labeling of vibrational levels previously studied, and effects of different experimental conditions were discussed;[19] also, comparisons between observations for toluene, toluene-d_3, and pFT were made.[11] Finally, more-recent work from the Reid group[35] has looked at the same fundamentals, although the focus of that work was on combination levels involving these, located higher in wavenumber.

Both a combination of an increased density of states (DOS) and symmetry-allowed vibtor coupling have been invoked to rationalize the rapid increase in interactions that occur in such molecules driving energy dispersal.[25] In the present work, we consider a ~60 cm^{-1} region close to 1200 cm^{-1} internal energy of the S$_1$ state of pFT. Very different intramolecular vibrational redistribution (IVR) behavior has been observed for two fundamental vibrations located here. It has been hypothesized that the presence of a methyl group is responsible, but over such a narrow range the DOS is not expected to change enormously, and so the reason for the difference is unclear. Here, we examine both the above-mentioned fundamental levels and other levels that are located in the 1190–1250 cm^{-1} range. In this region, we expect to see combinations involving levels on which we have recently reported, at ~400 cm^{-1} (Ref. 26) and ~800 cm^{-1} (Ref. 27); additionally, combinations involving the levels at ~400 cm^{-1} and those at ~845 cm^{-1} (Ref. 24) may be expected to lie toward the higher wavenumber end of this region—see Fig. 1. We piece together evidence from the 2D-LIF and ZEKE spectra presented in the present work to assign this region more completely than has been done before. We conclude that one of the fundamentals is able to couple efficiently to the increasing number of levels, via interactions with vibtor levels, while the other is not. We discuss the rationale for this.

II. EXPERIMENTAL

The 2D-LIF apparatus is the same as that employed recently.[24] The vapor above room temperature $para$-fluorotoluene (pFT)

(99% purity, Alfa Aesar) was seeded in ~5 bars of Ar, and the gaseous mixture passed through a general valve pulsed nozzle (750 μm, 10 Hz, an opening time of 180–210 μs) to create a free jet expansion. This was intersected at X/D ~20 by the frequency-doubled output of a single dye laser (Sirah CobraStretch), operating with C540A. The fluorescence was collected, collimated, and focused onto the entrance slits of a 1.5 m Czerny Turner spectrometer (Sciencetech 9150) operating in the single-pass mode, dispersed by a 3600 groove/mm grating, and ~300 cm^{-1} windows of the dispersed fluorescence (DF) collected by a CCD camera (Andor iStar DH334T). At a fixed grating angle of the spectrometer, the excitation laser was scanned, and at each excitation wavenumber, the camera image was accumulated for 2000 laser shots. This allowed a plot to be produced of fluorescence intensity vs both the excitation laser wavenumber and the wavenumber of the emitted and dispersed fluorescence, termed a 2D-LIF spectrum.[30]

We have also recorded some separate dispersed fluorescence (DF) spectra with higher averaging to get a better signal-to-noise ratio than simply taking a vertical slice through the 2D-LIF image. These DF spectra were recorded with the same spectrometer as for the 2D-LIF spectra and were recorded three times accumulating over 5000 shots each time and an average taken of these.

The REMPI/ZEKE apparatus was the same as that used in earlier work.[18] The focused, frequency-doubled outputs of the two dye lasers (Sirah CobraStretch) were overlapped spatially and temporally and passed through a vacuum chamber coaxially and counterpropagating, where they intersected a free jet expansion of pFT in Ar between two biased electrical grids located in the extraction region of a time-of-flight mass spectrometer, which was employed in the REMPI experiments. These grids were also used in the ZEKE experiments by application of pulsed voltages, giving typical fields (F) of ~10 V cm^{-1}, after a delay of up to 2 μs, where this delay was minimized while avoiding the introduction of excess noise from the prompt electron signal. The resulting ZEKE bands had widths of ~5–7 cm^{-1}. Electron and ion signals were recorded on separate sets of microchannel plates.

The excitation laser operated with C503 and was pumped with the third harmonic (355 nm) of a Surelite III Nd:YAG laser. The ionization laser operated with Pyrromethene 597 and was pumped with the second harmonic (532 nm) of a Surelite I Nd:YAG laser. The fundamental outputs produced by each dye laser were frequency doubled.

III. RESULTS AND ASSIGNMENTS

A. Nomenclature and labeling

1. Vibrational and torsional labeling

Since neither Wilson[36]/Varsányi[37] nor Mulliken[38]/Herzberg[39] notations are appropriate for the vibrations of pFT,[40,41] we shall employ the D_i labels from Ref. 41. In other papers, we have provided correlations with the labels used in previous work to aid the reader in referring to earlier studies.[23,26] Note that we shall refer to previously calculated values (B3LYP/aug-cc-pVTZ) of the vibrational wavenumbers in the three electronic states pertinent to the present study, presented in our previous work—those for the S$_1$ and D$_0^+$ states are taken from Ref. 23, while those for the S$_0$ state are from Ref. 41.

Although referred to in terms of the Wilson nomenclature in earlier work, in fact a detailed analysis of the vibrational motions of various symmetric and asymmetric disubstituted benzenes[41] showed that the D_5 and D_6 vibrations were in-phase and out-of-phase motions of the C–X stretches, where X is the substituent in the symmetrically substituted molecules. In the asymmetrically substituted analogs, these vibrations evolve into localized stretches: in the halotoluenes, D_5 was assigned as the C–Hal stretch, while D_6 was identified as the C–CH$_3$ stretch, where Hal represents a halogen atom.[41]

Since the G_{12} molecular symmetry group (MSG) is appropriate for vibtor levels in pFT, we shall use these symmetry labels throughout. In addition, torsional levels will be labeled via their m quantum number. (The reader may find it useful to refer to previous work[15–17,21,28] if they are not familiar with these labels.) The correspondence between the C_{2v} point group labels and the G_{12} MSG ones is given in Table I. To calculate the overall symmetry of a vibtor level, it is necessary to use the corresponding G_{12} label for the vibration and then find the direct product with the symmetry of the torsion (Table I), noting that a D_{3h} point group direct product table can be used since the G_{12} MSG and the D_{3h} point group are isomorphic.

Under the free-jet expansion conditions employed here, almost all of the molecules are expected to be cooled to their zero-point vibrational level, and thus, essentially all $S_1 \leftarrow S_0$ pure vibrational excitations are expected to be from this level. In contrast, owing to nuclear-spin and rotational symmetry, the molecules can be in one of the $m = 0$ or $m = 1$ torsional levels.[28,42]

2. Coupling and transitions

If an anharmonic vibration is close in wavenumber to one or more combination or overtone vibrational levels that have the same overall symmetry, then "off-diagonal" anharmonic interactions can occur, with the simplest example of two interacting states being the classic Fermi resonance (FR).[43] The noninteracting levels are termed zero-order states (ZOSs), and their interaction leads to the formation of eigenstates that are linear combinations of these and will be at different wavenumbers to the original ZOSs.[39] For molecules that contain a hindered internal rotor, and

if vibration-torsional coupling occurs, then the ZOSs can also be torsional or vibtor levels. The end result of such interactions is the formation of eigenstates which facilitate delocalization of energy through widespread motion of the molecule. Such couplings are only expected to be significant for small changes, $\Delta v \approx 3$, of the vibrational quantum number and also for changes, Δm, of 0, ± 3, or ± 6 in the torsional quantum number in descending order of likely strength.[16,21,28,44,45]

In electronic spectroscopy, if we assume a noncoupled picture initially, then a vibrational, torsional, or vibtor ZOS can be bright (i.e., it has a significant transition intensity) or dark (i.e., it has no or a very small transition intensity); these are often termed a zero-order bright (ZOB) state and a zero-order dark (ZOD) state, respectively. Following interaction, the resulting eigenstates will be composed of mixtures of ZOB and ZOD state contributions and so more transitions will become observable in the spectrum as a result of the interaction, by virtue of the ZOB character.

When designating excitations, we shall generally omit the lower level since it will be obvious from the jet-cooled conditions; similarly, for emissions, we shall omit the upper level as that will be obvious from the excitation and context. In the usual way, vibrational transitions will be indicated by the cardinal number, i, of the D_i vibration, followed by a super/subscript specifying the number of quanta in the upper/lower states, respectively; torsional transitions will be indicated by m followed by its value. Finally, vibtor transitions will be indicated by a combination of the vibrational and torsional transition labels. For example, $5^1 m^0$ implies an excitation from the torsionless (implied by symmetry) zero-point vibrational level in the S_0 state to the S_1 level with one quantum of D_5

TABLE I. Correspondence of the C_{2v} point group symmetry classes with those of the G_{12} molecular symmetry group. Also indicated are the symmetries of the D_i vibrations and the different pure torsional levels.[a]

C_{2v}	G_{12}	D_i[b]	m
a_1	a_1'	D_1–D_{11}	0, 6(+)
a_2	a_2'	D_{12}–D_{14}	6(−)
b_1	a_2''	D_{15}–D_{20}	3(−)
b_2	a_1''	D_{20}–D_{30}	3(+)
	e'		2, 4
	e''		1, 5

[a]Symmetries of vibtor levels can be obtained by combining the vibrational symmetry (in G_{12}) with those of the pure torsional level, using the D_{3h} point group direct product table.
[b]The D_i labels are described in Ref. 41, where the vibration mode diagrams can also be found.
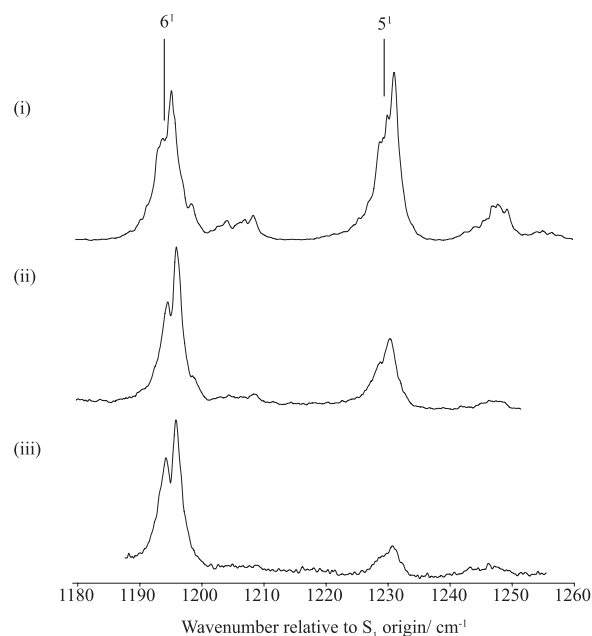
FIG. 2. The 1190–1250 cm^{-1} region of the $S_1 \leftarrow S_0$ transition in pFT: Recorded (i) using REMPI spectroscopy, (ii) using laser-induced fluorescence, and (iii) by vertical integration of the 2D-LIF spectrum. See text for further comment.

excited and no torsional excitation, while $5^1 m^1$ implies an excitation from the zero-point vibrational level, but with one quantum of torsion (implied by symmetry), in the S_0 state to the S_1 level with one quantum of D_5 excited and one quantum of torsion. If no m values are specified, then the transition label refers to transitions involving both $m = 0$ and $m = 1$, whose transition wavenumbers are expected to be coincident at the present resolution.

The wavenumbers of the levels will be given with respect to the relevant zero-point level in each electronic state but noting that some excitations will originate from the $m = 1$ level in S_0 and those transition energies are given with respect to that level, as usual.

The $S_1 \leftrightarrow S_0$ origin is located at 36 860.0 cm^{-1} (Ref. 22). The most intense transition is generally expected to be that for which no change in the vibrational, or both vibrational and torsional, quantum numbers occurs; these will be designated as $\Delta v = 0$ or $\Delta(v, m) = 0$ transitions. As has become common usage, we will generally refer to a level using the notation of a transition, with the level indicated by the specified quantum numbers, with superscripts indicating levels in the S_1 state and subscripts indicating levels in the S_0 state; since we will also be referring to levels in the ground state cation, D_0^+, we shall indicate those levels with superscripts with a preceding superscripted + sign. Also, the eigenstates will often be referred to by the dominant contribution from one of
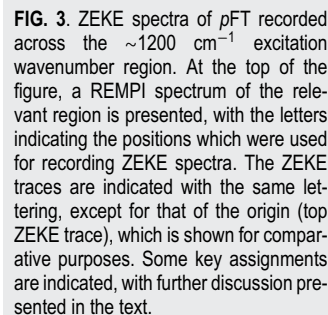
FIG. 3. ZEKE spectra of pFT recorded across the ~1200 cm^{-1} excitation wavenumber region. At the top of the figure, a REMPI spectrum of the relevant region is presented, with the letters indicating the positions which were used for recording ZEKE spectra. The ZEKE traces are indicated with the same lettering, except for that of the origin (top ZEKE trace), which is shown for comparative purposes. Some key assignments are indicated, with further discussion presented in the text.

the ZOSs, with the context implying if an admixture of other ZOSs is present. 2D-LIF band positions will be indicated by a pair of (excitation and emission) wavenumbers and the corresponding transitions similarly.

B. Overall comments on the spectra

1. The $S_1 \leftarrow S_0$ spectrum

In Fig. 1, we show a REMPI spectrum of pFT up to 1250 cm^{-1}. Indicated are a set of bands at ~400 cm^{-1} that are dominated by 14^2, 29^1, and 11^1 transitions[18,21,22,26] but where there are also additional, including vibtor, transitions.[21,22,26] At ~800 cm^{-1}, there are a further set of transitions, dominated by a pair of levels that largely comprise a FR between the 9^1 and 29^2 levels,[23,27,46,47] but again, there are other transitions in this region, including those involving vibtor levels (see Refs. 23 and 27). At ~845 cm^{-1}, there is the 18^2 transition, which has been shown to be interacting strongly with several vibtor levels at this wavenumber (see Ref. 24), while at ~1015 cm^{-1}, there is a band that is the subject of ongoing work. At ~1200 cm^{-1}, there are a series of bands which are dominated by two fundamental transitions, assigned as 6^1 and 5^1; in earlier work, these have mainly been referred to with Wilson labels ν_{13} and ν_{7a}, respectively.[11,18,54] It is clear, however, that further bands are present and expanded views of this wavenumber region are presented in Fig. 2, recorded using three different techniques: REMPI, LIF, and integration of the 2D-LIF spectrum (see Sec. III B 3). Immediately apparent is the relative similarity of the LIF and integrated 2D-LIF spectra. However, the relative intensities of the two most intense bands are clearly different to those in the REMPI spectrum, and indeed, the higher-wavenumber feature has an even greater relative intensity in some REMPI scans.[18] This is supportive of there being some time-dependent effect on the 5^1 band, with REMPI being a far faster technique than LIF, and higher laser power densities favoring ionization over S_1 population-loss mechanisms.

We shall now present the ZEKE spectra and the 2D-LIF spectrum, each recorded across the spectral region shown in Fig. 2. We shall then discuss these together in deducing the detailed assignments.

2. ZEKE spectra

In Fig. 3, we show ZEKE spectra recorded at each of the indicated positions; the ZEKE spectrum recorded via the origin is shown for comparison purposes. The indicated transitions arise from the overall assignment to be discussed in Sec. III C. We highlight that the ZEKE spectrum via the origin has a flat baseline throughout. The spectrum recorded at 1196 cm^{-1} has a largely flat baseline until ~1000 cm^{-1}, and then a small amount of underlying complicated, overlapped structure is seen thereafter. The strong ZEKE bands in this spectrum can be assigned as $^+6^1$, $^+6^111^1$, and $^+6^19^1$. All other spectra have significant contributions from a wide range of underlying overlapped structure, although some caution is required for ZEKE spectra that were recorded via levels corresponding to weak bands in the REMPI spectrum, where the background can be relatively significant. We highlight the spectrum recorded via the level corresponding to the intense band at 1232 cm^{-1}, which shows this broad structure, but there are clear bands seen on top of this, notably those assigned to $^+5^1$, $^+5^111^1$, and $^+5^19^1$. The ZEKE spectra recorded at 1196 cm^{-1} and 1232 cm^{-1}

are very similar to those reported and discussed previously.[11,18,19] Other bands and indicated assignments will be discussed in Sec. III C.

3. 2D-LIF spectrum

In Fig. 4, we show a composite overview of the 2D-LIF spectra recorded across the excitation range corresponding to that of Fig. 2, and covering emissions to the origin up until ~2550 cm^{-1} of the S_0 state, selected to cover the $\Delta v = 0$ regions of transitions that might be contributing to the spectrum in Fig. 2. Integrating the 2D-LIF spectrum vertically gives an excitation spectrum similar to the REMPI and LIF spectra—see Fig. 2. It is evident that there are two main vertical "stripes" of activity located around the 1196 cm^{-1} and 1232 cm^{-1} excitations, i.e., as a result of exciting 6^1 and 5^1, respectively. It is also clear that there is a significant amount of Franck-Condon (FC) emission activity as a result of these two excitations and that there is more intensity associated with the 6^1 excitation than with the 5^1 excitation. In Fig. 5, we show DF spectra recorded through the centers of the 6^1 and 5^1 excitations and, for comparative purposes, also through the origin. Expanded relevant sections of the 2D-LIF spectra in Fig. 2 are given in Fig. 6. From Fig. 5, it is clear that there is much more broad underlying emission structure when exciting 5^1 than there is for 6^1, consistent with the behavior seen in the ZEKE spectra (see Fig. 3). As indicated by the additional structure seen in Figs. 2 and 4, there is additional activity at other excitation wavenumbers, located both
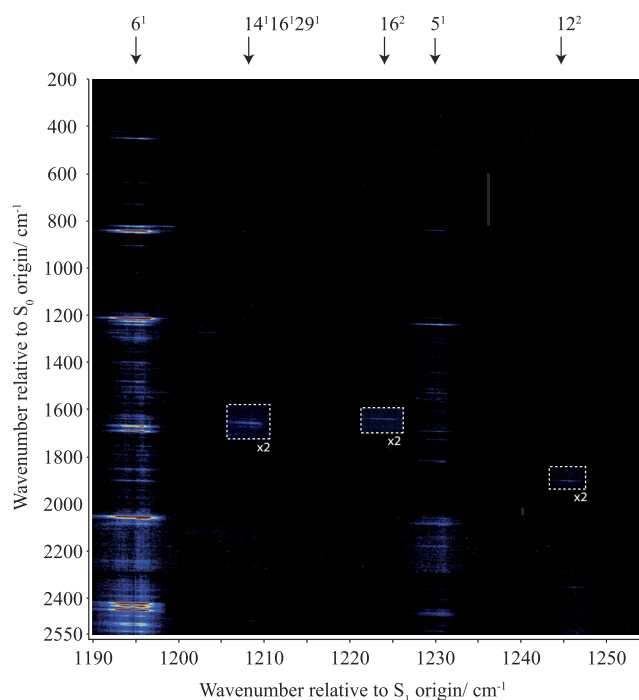
FIG. 4. Composite 2D-LIF spectrum including all regions recorded as part of the present work. Further discussion and expansion of various regions are found elsewhere in the paper. The main excitations are indicated at the top of the spectrum.
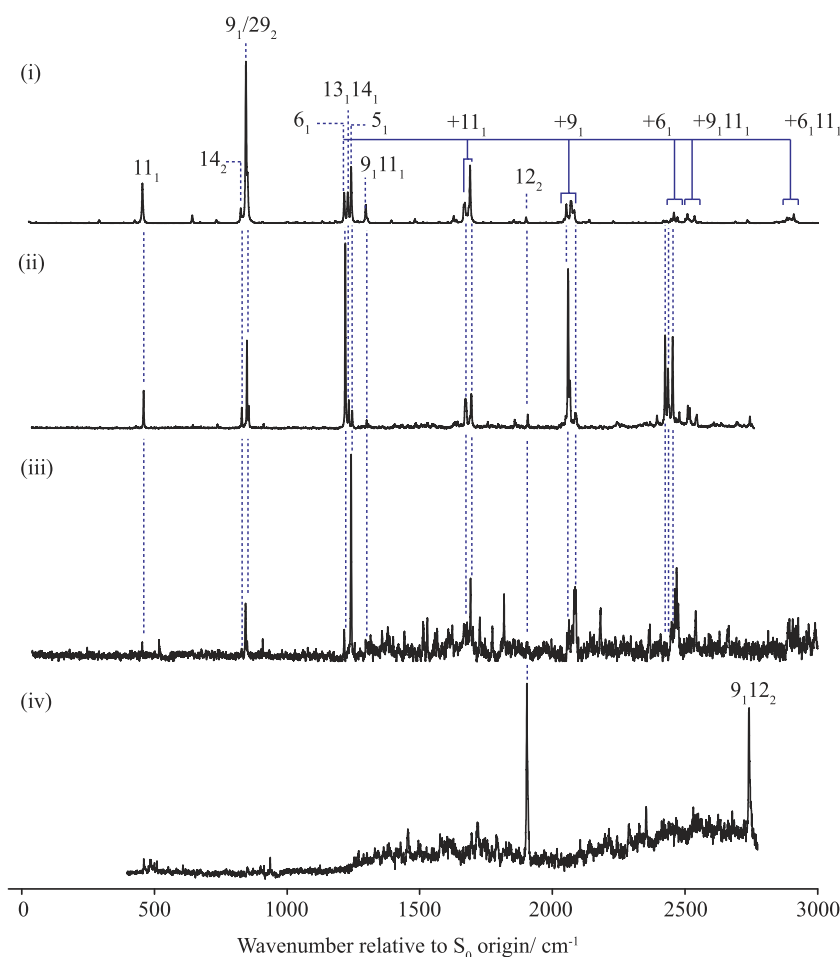
FIG. 5. Dispersed fluorescence spectra recorded via (i) 0^0, (ii) 6^1, (iii) 5^1, and (iv) 12^2. Of note is the almost completely flat baseline for (i), a small amount of rising background with widespread activity to high wavenumber in (ii), and a significant amount of rising background with widespread activity in (iii) and (iv).

between 6^1 and 5^1, as well as to higher wavenumber than 5^1, and this will be discussed and assigned in tandem with the ZEKE spectra in Subsection III C.

C. Assignments

We commence by noting that the previous[11,18,19] and present ZEKE spectra (Fig. 3) are consistent with the main two bands in Fig. 2 being 6^1 and 5^1. The 2D-LIF spectrum is also consistent with this, with outline assignments indicated in the DF spectra in Fig. 5 (further assignments are given in Fig. 6). Thus, the $(6^1, 6_1)$ and $(5^1, 5_1)$ $\Delta v = 0$ bands are located at (1196, 1215) cm^{-1} and (1232, 1241) cm^{-1}, respectively. A series of other intense Franck-Condon (FC) active combination and overtone bands involving the main transition can be seen to higher wavenumber in each case. As well as 11_1 (see Fig. 5), there are also other emissions, with those in the range ~840–855 cm^{-1} being assigned as 14_2, 9_1, and 29_2. (Note that there was some indication that, as well as 9^1 and 29^2 being in Fermi resonance in the S_1 state,[27,47] the 9_1 and 29_2 levels may be in Fermi resonance in S_0, and the same was true of $^+9^1$ and $^+29^2$ in D_0^+.[27]).

We now consider the combination bands involving one of the S_1 levels previously discussed[24,26,27] at ~400 cm^{-1} and others

located at ~800 cm^{-1} and ~845 cm^{-1} (see Fig. 1) that are expected to lie in the 1190–1250 cm^{-1} range. To aid the reader, in Fig. 7, we show the expected positions of various combinations, indicated by shifting the region of the spectrum at ~400 cm^{-1} to positions that indicate where the various combinations are expected. If these combinations have significant intensity, we should be able to identify activity from them in the 2D-LIF and ZEKE spectra, although we need to consider that interactions may shift levels from the expected position. In addition, it is possible for additional ZOB states to contribute to this region of the spectrum, analogous to some of those seen at similar wavenumbers in our recent studies of p-difluorobenzene (pDFB)[48] and p-chlorofluorobenzene (pClFB)[49,50] but noting that the higher symmetry of pDFB means that some transitions are symmetry forbidden, notably 6^1. Between different molecules, however, the brightness of any transition can vary, as can its wavenumber, with the latter potentially causing levels to move, affecting the possible interactions. Furthermore, the presence of the methyl group in pFT leads to vibtor levels built on each vibrational level, dramatically increasing the possibilities for coupling—see the discussion in Ref. 25 concerning comparison between the above-mentioned three molecules and also pXyl.
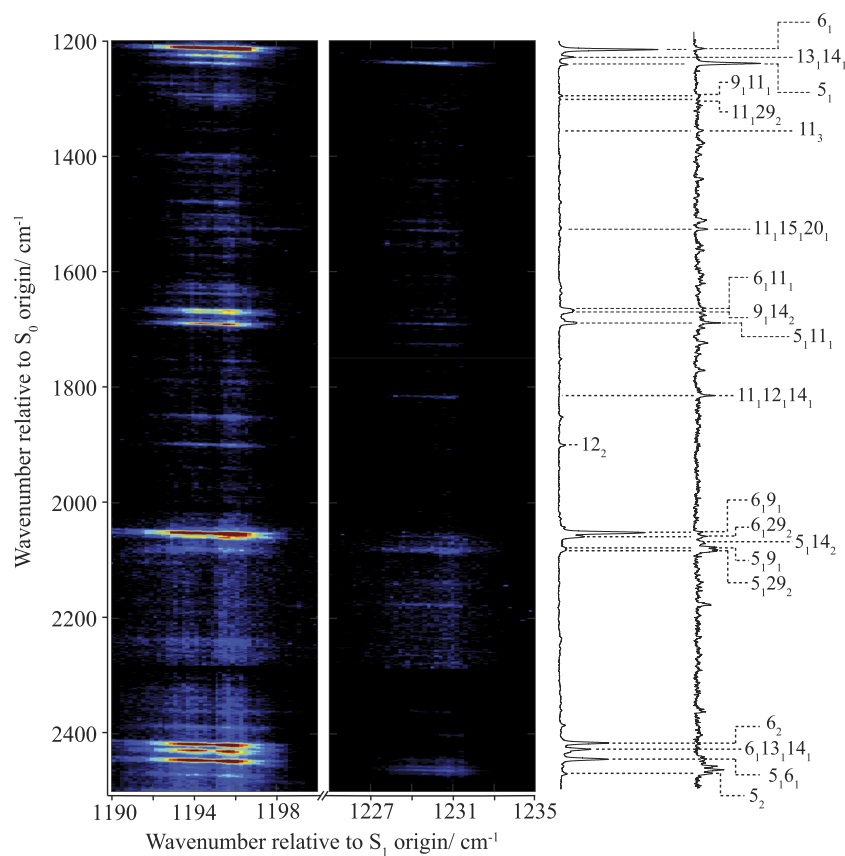
FIG. 6. Slices of the 2D-LIF spectrum showing the key activity following excitation of 6^1 and 5^1. Selected assignments are given, with a number of these discussed in the text.
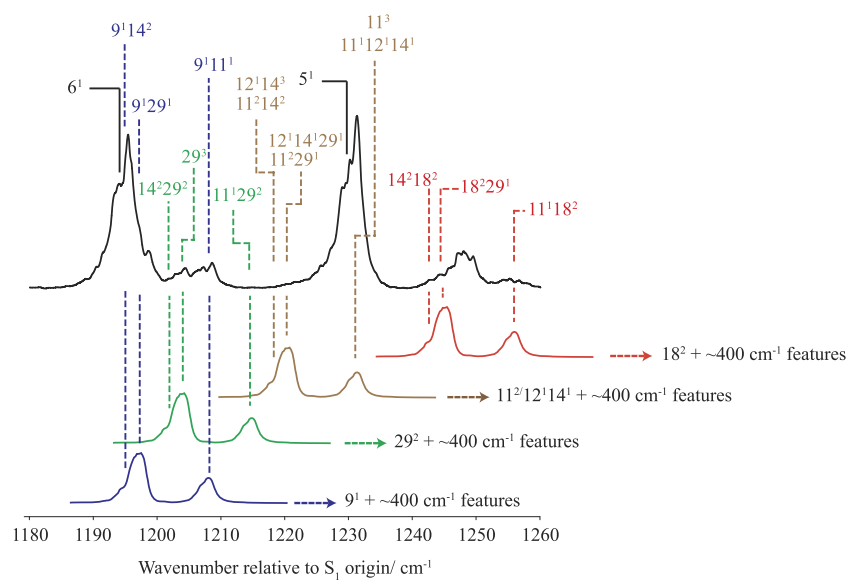
FIG. 7. Indications of the expected $S_1 \leftarrow S_0$ activity arising from combinations of features at ~400 cm^{-1} and ~800 cm^{-1}. The former region of the spectrum is shown offset by amounts corresponding to the three main bands of the latter region. The approximate positions of the various vibrational combination bands is given, although not all are observed; further movement of levels as a result of interactions is expected to occur—see text for further discussion.

1. Combinations of (14^2, 29^1, and 11^1) with (9^1 and 29^2)

We first consider the levels expected to arise from the two $9^1/29^2$ FR levels (located at ~800 cm^{-1}) in combination with the three main ~400 cm^{-1} transitions, 14^2, 29^1, and 11^1—see Figs. 1 and 7.

Although there is an emission to $9_1 14_2$ (1673 cm^{-1})—see Fig. 6—this is particularly intense via 6^1. One explanation for this would be FC activity, but it could also indicate that the $9^1 14^2$ level is coincident with 6^1. Since this coincidence would imply that there was very little interaction between these two levels, and combined with the fact that we see no clear $^+9^1 14^2$ band in the ZEKE spectrum when exciting via 6^1, we favor FC activity.

In Fig. 8, it can be seen that, as well as the clear FC (6^1, 14_2) emission, there is also a secondary 14_2 emission when exciting at 1198 cm^{-1} (see also the integrated trace in the lower half of this figure), and we suggest that this could be associated with the $9^1 14^2$ $\Delta v = -1$ transition, with there being a ZEKE band at the correct position (Fig. 3), as well as a clear $^+14^2$ band when exciting at this

FIG. 8. The top of the figure shows the 2D-LIF features considered, while the bottom traces show integrated activity of the emission of some key 2D-LIF features activity across the excitation region indicated. Integration was carried out over a range of emission wavenumbers that included the main activity whilst avoiding overlap with neighboring features.

wavenumber. (Although 14^6 and $14^4 29^1$ are expected close to this excitation wavenumber, neither $^+14^6$ nor $^+14^4 29^1$ bands are clearly evident, although there is a $^+14^4$ band at 1403 cm^{-1}; in addition, the corresponding emission bands are not definitively seen in the 2D-LIF spectrum, and so evidence for activity involving these levels is weak.) We also cannot rule out a possible contribution to the ~1530 cm^{-1} ZEKE band from $^+14^2 29^2$, which would also be consistent with the FC activity of the $^+14^2$ band. Although there is no definitive $14_2 29_2$ emission band seen, the 14_2 band could also be associated with emission from $14^2 29^2$. In summary, although there is some evidence for $9^1 14^2$ and $14^2 29^2$ (and possibly $14^4 29^1$ and 14^6) activity when exciting at 1198 cm^{-1}, it is not wholly conclusive.

We now move on to $9^1 29^1$ and 29^3, recalling that these are more correctly thought of as combinations of 29^1 with each of the ($9^1 \ldots 29^2$) and ($29^2 \ldots 9^1$) FR pair. The clearest evidence for this activity is from the 29_1 emission, which shows two significant areas of activity at excitations of 1193 cm^{-1} and 1203 cm^{-1} (see Fig. 8). These regions of activity are identified as the (29^3, 29_3) $\Delta v = 0$ band at (1203, 1275) cm^{-1}, with the band at (1193, 1264) cm^{-1} being ($9^1 29^1$, $9_1 29_1$); furthermore, there is some evidence for cross activity between these bands, consistent with FR between the $9^1 29^1$ and 29^3 levels as there was[27,47] between the 9^1 and 29^2 levels. In both cases, the 29_3 emission is the strongest, consistent with the 29_2 band being the stronger when exciting via both of the $9^1/29^2$ FR levels.[27] The weak (6^1, 29_1) activity at (1196, 424) cm^{-1} is assigned as Herzberg-Teller (HT) activity associated with the 6^1 transition, similar to that seen via the origin.[21,22,26]

We expect the combinations of 11^1 with the $9^1/29^2$ FR pair at excitation wavenumbers of around 1205 cm^{-1} and 1211 cm^{-1}. There is clear FC activity for both $9_1 11_1$ (1295 cm^{-1}) and $11_1 29_2$ (1302 cm^{-1}) following 6^1 excitation so that the emission wavenumber is secure. We thus assign the weak band at (1204, 1302) cm^{-1} as ($9^1 11^1$, $11_1 29_2$), in line with the expected greater intensity of $11_1 29_2$ emission when exciting via both FR components, and the very weak (1204, 1296) cm^{-1} band to ($9^1 11^1$, $9_1 11_1$). Surprisingly, we only see the faintest traces of the partner ($11^1 29^2$, $11_1 29_2$) band, expected at around (1211, 1302) cm^{-1}, and no clear evidence for $11^1 14^4$ activity was seen. The ZEKE activity (Fig. 3) shows slightly more convincing evidence of the activity of both of these S_1 levels, although there was no ZEKE spectrum recorded following excitation at 1211 cm^{-1}.

Finally, a weak band at (1198, 1528) cm^{-1} is a reasonably good match for ($11^1 15^1 20^1$, $11_1 15_1 20_1$), expected at (1203, 1524) cm^{-1}—see Fig. 6; however, it is not possible to identify the corresponding $^+11^1 15^1 20^1$ ZEKE band definitively, owing to a number of transitions being expected at this wavenumber in the spectrum—see Fig. 3; on the other hand, the FC-allowed $^+15^1 20^1$ band is seen, supporting the activity of the $11^1 15^1 20^1$ level.

In summary, the main expected combinations between the ~400 cm^{-1} and 800 cm^{-1} set of lines do seem to appear in this wavenumber region, and although they were sometimes weak in the 2D-LIF spectrum, they were often more apparent in the ZEKE spectrum. More clear in the 2D-LIF spectrum is the $9^1 29^1/29^3$ FR interaction (Fig. 8), while the separate bands are less easy to discern in the ZEKE spectra. Part of the explanation for these intensity variations may be different Franck-Condon factors (FCFs) for the ionization and emission processes.

2. Combinations of (14^2, 29^1, and 11^1) with (11^2 and $12^1 14^1$)

Higher in excitation wavenumber, at ~1215 cm^{-1}, we expect to find the combinations of the excitation bands that appear at ~818 cm^{-1}, $12^1 14^1$ and 11^2, with each of 29^1 and 14^2, at excitation wavenumbers of ~1215 cm^{-1}. However, no clear evidence of bands corresponding to these levels could be found.

Slightly higher than this, at 1226 cm^{-1}, we would expect $11^1 12^1 14^1$ and 11^3. We see an unexpectedly bright (compared to the corresponding FC-active band via 6^1) emission at (1230, 1816) cm^{-1}, i.e., essentially coincident with excitation at 5^1, which we assign to $11_1 12_1 14_1$—see Fig. 6. Because of this unexpected brightness, we assign this band as the ($11^1 12^1 14^1$, $11_1 12_1 14_1$) $\Delta v = 0$ band, which is coincident, but apparently not interacting, with 5^1. Note that in the cation, the expected wavenumber of $^+5^1 11^1$ (1772 cm^{-1}) is almost identical to $^+11^1 12^1 14^1$ (1775 cm^{-1}) and so both could be contributing to the ZEKE band seen at 1781 cm^{-1}, when exciting at 1232 cm^{-1}—see Fig. 3. Weak 11_3 activity is also seen when exciting close to 5^1, but such activity is also seen via 6^1, and so these may simply be attributed to FC activity.

3. Other $\Delta v = 0$ bands

In Fig. 9, we show another expanded view of the 2D-LIF spectrum where other $\Delta v = 0$ bands are located. Quite an intense band at (1208, 1654) cm^{-1} is assigned as ($14^1 16^1 29^1$, $14_1 16_1 29_1$), which is at the expected wavenumber in both S_0 and S_1; we would thus expect a ZEKE band at 1608 cm^{-1} when exciting at 1208 cm^{-1}, and indeed, a band is seen at 1607 cm^{-1}—see Fig. 3. We are comfortable with this assignment since the wavenumbers of this combination are consistent across three electronic states, and we observe that its three components are all active in the spectrum in different guises.

The band at (1224, 1639) cm^{-1} is assigned as (16^2, 16_2) and is in fairly good agreement with both the S_1 and S_0 values (unfortunately, no ZEKE spectrum was recorded at this excitation wavenumber);

the 16^2 band was also active in pDFB.[48] A weak band at (1226, 1770) cm^{-1} can be assigned as ($12^1 16^1$, $12_1 16_1$).

The assignments above yield a wavenumber for D_{16} in the S_1 state of ~610 cm^{-1}. Although this value is somewhat different to the calculated value[23] of 651 cm^{-1}, it is in excellent agreement with the experimentally derived value of 609 cm^{-1}, obtained from an assignment of the $16^1 20^1$ combination band.[23] (Note that the tabulated experimental value of 607 cm^{-1} in Ref. 23 is incorrect.) This consistency of the wavenumber for D_{16} in the S_1 state for the three above-mentioned bands adds weight to this value and suggests that an alternative, less favored, value of 621 cm^{-1} that was discussed in Ref. 23 is incorrect.

To a higher excitation wavenumber in Fig. 9, there is a band at (1245, 1900) cm^{-1}, which is consistent with being the (12^2, 12_2) band; the 12^2 band was also active in pDFB.[48] We also see in the ZEKE spectrum in Fig. 3 that when exciting at 1248 cm^{-1}, a strong band was seen at 1977 cm^{-1} assignable to $^+12^2$. Interestingly, there is significant, overlapped underlying structure here, suggesting widespread coupling, which will be commented on in Subsection III D. It is also interesting to see the $^+12^1$ band in this ZEKE spectrum, which is reminiscent of the activity of $^+14^1$ in other ZEKE spectra, despite being nontotally symmetric. Activity in such bands was discussed in relation to pDFB in Ref. 48.

We also saw very weak 2D-LIF bands (not shown), plausibly assignable as combinations of 18_2 with 11_1 and 29_1, suggesting that the activity of the corresponding S_1 levels is low.

4. Vibtor levels

In examining the emission when exciting from 5^1, a band is seen at 518 cm^{-1}, which is the same band seen in our earlier study[24] of the S_1 levels at ~845 cm^{-1} and assigned to $18_1 m_2$, i.e., a vibtor level of e'' symmetry—see Fig. 10. This band was a signature that combinations of the $18^1 m^2$ vibtor level were coupled to $18^2 m^1$ in the S_1 state, also of e'' symmetry. In the present case,
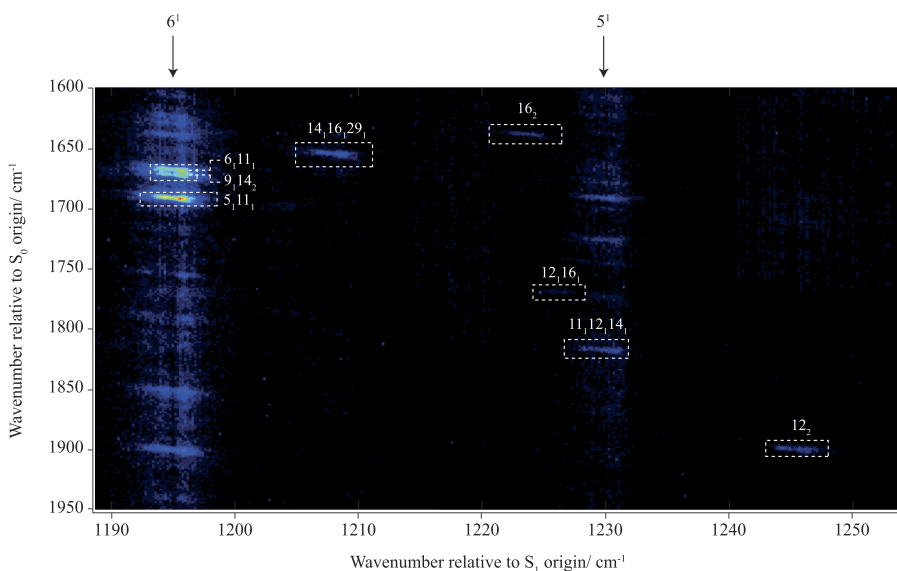
FIG. 9. Region of the 2D-LIF spectrum that shows various $\Delta v = 0$ bands (boxed) that show activity in this region. A couple of bands arising from Franck-Condon activity following 6^1 excitation is shown for orientation purposes with Figs. 4 and 6 and to allow judgment of the relative intensities.
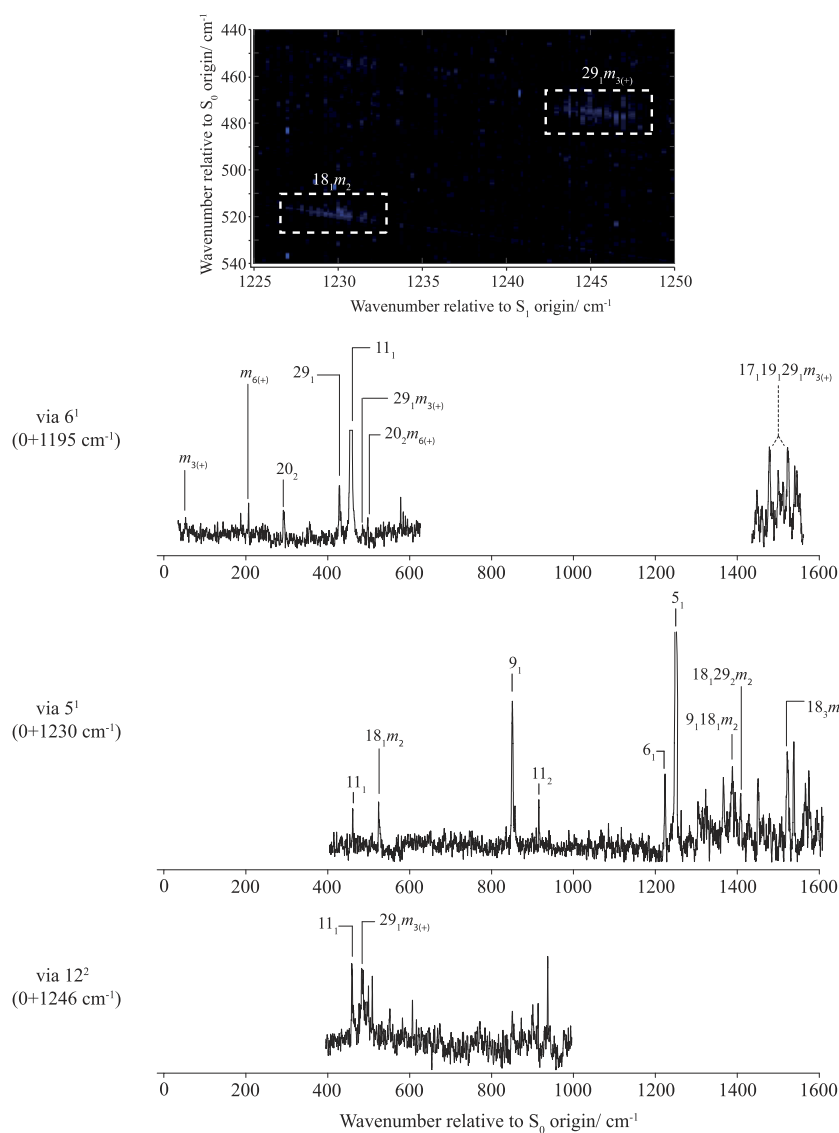
FIG. 10. Vibtor activity seen in the 2D-LIF spectra. The top image shows the $\Delta(v, m) = 0$ 2D-LIF bands of two of the main vibtor levels. The bottom traces show portions of the three dispersed fluorescence spectra where the $\Delta(v, m) = 0$ and/or associated activity is most clearly seen. Note that since the associated vibtor levels are acting as doorway states, their $\Delta(v, m) = 0$ activity is low, being spread through the coupled levels. See text for further discussion.

$9^1 18^1 m^2$ would be expected at ~1238 cm^{-1} and so very close to 5^1; we thus conclude that $9^1 18^1 m^2$ is coupled to $5^1 m^1$, both being of e'' symmetry. There is a weak band that is tentatively assigned to $9_1 18_1 m_2$ at around 1358 cm^{-1} (Fig. 10), with the weakness being explained as being due to this level being a doorway state and so coupled to many other levels, explaining the rich emission coming from a range of different so-formed eigenstates: the $18_1 m_2$ emission band is the resultant sum of FC-active emissions from all of these.

There is also clear weak background emission when exciting at 1246 cm^{-1}, and some clue as to its origin comes from the observation of a 2D-LIF band at (1246, 476) cm^{-1}—see Fig. 10. The emission can be assigned to $29_1 m_{3(+)}$, and so it is then straightforward to deduce that the coupled level in the S$_1$ state is likely to be $9^1 29^1 m^{3(+)}$, which is expected to be close in wavenumber to

12^2 and so may couple to its $m = 0$ level. Indeed, the extent of the 12_2 emission band suggests coupling between these levels. A weak band at (1245, 1325) cm^{-1} (not shown) is the likely $9^1 29^1 m^{3(+)}$ $\Delta(v, m) = 0$ band.

In discussing the levels at ~400 cm^{-1},[26] we identified $20^2 m^{6(+)}$ vibtor activity, and the $9^1 20^2 m^{6(+)}$ level would lie very close in energy to 6^1; this would couple to only the $m = 0$ level. Further evidence for this is provided by some weak emission bands observed when exciting at wavenumbers corresponding to 6^1: 204 cm^{-1} ($m_{6(+)}$), 350 cm^{-1} ($20_1 m_{6(+)}$), and 492 cm^{-1} ($20_2 m_{6(+)}$)—see Fig. 10. The $\Delta(v, m) = 0$ band would be expected at around 1332 cm^{-1}, and there are bands close to this value, and although it was not possible to associate one definitively with this transition, significant coupling would explain this being weak. We also see weak $29_1 m_{3(+)}$ and $m_{3(+)}$ bands, which may be associated with another vibtor level

coupling—a plausible candidate is $17^1 19^1 29^1 m^{3(+)}$, which would appear at this wavenumber, and there are clear emissions close to 1505 cm^{-1}, expected for the $\Delta(v, m) = 0$ band (see Fig. 10), but other levels, such as $6_1 20_2$, are also expected in this wavenumber region, and so it is not possible to associate a particular band with each transition. The $17^1 19^1 29^1 m^{3(+)}$ level can only couple to the $6^1 m^0$ level.

We also did look for activity associated with combination bands associated with emission or ionization from combination bands involving $14^1 m^{6(-)}$, since this transition is observed at ~400 cm^{-1} (Ref. 26), but could not unambiguously identify any such.

In Sec. IV, we shall discuss the above vibtor levels further and their role in promoting IVR.

IV. DISCUSSION

Referring to Fig. 1, in previous work on the S$_1$ state, evidence for Fermi resonances and coupling to vibtor levels has been found in the low wavenumber region (<400 cm^{-1}),[21,22] the bands at ~ 400 cm^{-1},[21] the bands at ~800 cm^{-1},[23,47] and the bands at ~845 cm^{-1}.[24] However, it is the bands at ~1200 cm^{-1}, as studied in the present work, where evidence for widespread coupling is first apparent.[11,18,19,35] The evidence from previous work is somewhat confusing, with uncertainties and apparent contradictions in the deductions. We thus briefly discuss that work while rationalizing it in terms of the present data.

We first note that, as commented on in Refs. 11 and 19, some of the time-domain experiments by Parmenter's group[1,2,6] have some inconsistencies as to the cited wavenumber employed in those studies and also the designation of the vibration being excited. We also recall that D_6 is predominantly the C–CH$_3$ stretch, while D_5 is the C–F stretch.[41] As such, with the large amplitude motion (the CH$_3$ torsion) being the likely perpetrator of any acceleration, the expectation would be[51,52] that the D_6 mode would be subject to more-widespread coupling than D_5, and this can clearly be seen not to be the case from the spectra and assignments discussed above. Furthermore, the ZEKE (see Fig. 3), 2D-LIF, and DF (see Figs. 4, 5, and 6) spectra show that there is only a very small amount of underlying broad structure when exciting 6^1, while, in contrast, the time-resolved data in Refs. 11 and 35 indicate that there is significant loss of signal for this level, which would be consistent with widespread coupling. The data in Ref. 35 are in agreement that there is widespread coupling for 5^1, and furthermore, it is deduced that the IVR lifetime for 5^1 is about a quarter of that for 6^1, consistent with the more significant underlying unresolved structure in the ZEKE, 2D-LIF, and DF spectra. Moreover, the time-dependent plots shown in Ref. 35 show only the faintest signs of quantum beating and mostly are described by an exponential decay. Of particular interest is that the 6^1 signal decays to about 50% of its original value by 100 ps, while the 5^1 signal has reached about 10%. The former observation is highlighted in Refs. 11 and 35, where it is suggested that only one of the m levels efficiently facilitates vibtor coupling. No explicit comments are made in Ref. 35 regarding the remnant 5^1 signal, but being less than 50%, it would have to imply that both $m = 0$ and $m = 1$ levels undergo losses in intensity. The higher resolution of the ZEKE spectra in the present work, together with the added information from the 2D-LIF

spectra on the nature of the S$_1$ vibrations and vibtor levels in the ~1200 cm^{-1} region, provides more insight into the time-resolved observations.

First, we note that the picosecond laser used in the time-resolved slow-electron velocity-map imaging (SEVI) studies in Refs. 11 and 35 had a FWHM of ~13 cm^{-1}. Hence, when centered on the 6^1 transition, this could be exciting a number of eigenstates, amongst which are $11^1 15^1 20^1$, $9^1 29^1$, $9^1 14^2$, 29^3, with other possibilities being 14^6, $14^5 m^{6(-)}$, $9^1 14^1 m^{6(-)}$, and $14^5 m^{6(-)}$; in addition, in the SEVI spectrum, unresolved from the main $^+6^1$ band are likely to be $^+9^1 29^1$, $^+9^1 11^1$, $^+29^3$ and a number of others. Thus, the time-dependent SEVI signal that was monitored may well comprise a number of different contributions. That said, the fact that the intensity dropped to 50% after a few hundred picoseconds would be consistent with only one of the m levels of the main 6^1 transition undergoing widespread coupling. (Vibration-vibration anharmonic coupling to other totally symmetric levels would occur for both $m = 0$ and $m = 1$ vibtor levels and consequently would not explain the loss in intensity of just one of the m levels.) Additionally, the growth in intensity of the 1370–1550 cm^{-1} region of the SEVI spectrum observed in Ref. 11 is consistent with a ZOB state coupling to a wide range of levels, and similar broad underlying structure is also evident in the ZEKE spectrum in Fig. 3.

We have noted above that the $9^1 20^2 m^{6(+)}$ and $17^1 19^1 29^1 m^{3(+)}$ levels would lie very close in energy to 6^1 and that these would couple to the $m = 0$ level only. Also, once such vibration-torsional coupling has occurred, further interactions with other levels open up and this, together with couplings involving other ZOSs in this region, would explain the underlying structure seen in the ZEKE and DF spectra in Figs. 3 and 5. That said, it does not seem that the ZEKE and 2D-LIF/DF spectra recorded when exciting 6^1 are consistent with a 50% loss in intensity, suggesting that there may be another mechanism causing the time-dependent SEVI signal[11] to decay. One such would be rotational dephasing[53] occurring between the $6^1 m^0$ rotational levels, caused by an m- and J, K-dependent vibtor interaction.[27,47] Such dephasing in pFT was put forward with regard to the two main levels at ~800 cm^{-1} by Davies and Reid[47] and commented on further in our recent study of the same levels.[27] As noted above, the suggested vibtor interactions would be with just the $6^1 m^0$ level and so could cause the rotation-dependent coupling required for dephasing. If the dephasing were complete in a few 100 ps (as was in the case of the levels at ~800 cm^{-1}),[47] then this would be an explanation for the decay in the 6^1 signal in Refs. 11 and 35. As discussed in Ref. 27, the rotational dephasing does not lead to a population change, and so in the frequency-resolved experiments, no effect is seen from this; it only arises from the simultaneous excitation of the perturbed rotational levels. This explanation would then explain the very small unstructured background seen in the present work and the very significant (~50%) drop in the "$^+6^1$" SEVI signal. Given that the amount of unstructured background appears to be comparable in those SEVI spectra[11,35] as in the present ZEKE and 2D-LIF/DF spectra, we conclude that the two sets of results are consistent within this explanation.

For the 5^1 level, the situation is somewhat different, with only ~10% of the $^+5^1$ SEVI signal remaining after 100 ps.[35] We have seen that we observe the $18_1 m_2$ emission band when exciting at the wavenumber of 5^1 (Fig. 10), and from this, we conclude that the

$9^1 18^1 m^2$ level is coupled to $5^1 m^1$ in a similar way that $11^1 18^1 m^2$ and $14^2 18^1 m^2$ are coupled to $18^2 m^1$ (Ref. 24). Assuming that the coupling to $9^1 18^1 m^2$ opens up efficient routes for second-order coupling of $5^1 m^1$ to a significant set of bath states, then this could be a rationale for a loss of 50% of the $^+5^1$ SEVI signal in Ref. 35. Although there are a wealth of bands seen in the 2D-LIF/DF spectra at the wavenumber of 5^1 (for example, see Figs. 5, 6, and 10), it is difficult to assign them all uniquely, but there are various emission bands that can be assigned as analogous FC-active bands, now in combination with $18_1 m_2$, seen via 9^1, but now active close to the 5^1 wavenumber (Fig. 10). In contrast to the ZEKE spectra in Ref. 24, we did not observe the $^+18^1 m^2$ ZEKE band in the present work, but the UV intensity of the ionization laser was poor in the spectral region where this band is expected; for the same reason, other torsional levels were also not always seen in the ZEKE spectra that were seen here in emission. Overall, though, on the basis of earlier work and the 2D-LIF results, we are confident that the $5^1 m^1$ level is strongly coupled to a background bath of states, with $9^1 18^1 m^2$ acting as a doorway state. With this in mind, looking back at the ZEKE and 2D-LIF/DF spectra recorded via 5^1, we see that there is still significant intensity in the $^+5^1$ and 5_1 bands, respectively; indeed, the amount is consistent with the majority of the $5^1 m^0$ intensity remaining. We thus conclude that, similar to the $6^1 m^1$ case above, in the time-resolved experiments,[35] rotational dephasing causes the loss of essentially all of the remaining $^+5^1 m^0$ SEVI signal, with a possible interacting level being $11^1 12^1 m^{6(-)}$. In our ZEKE study of the ~800 cm^{-1} bands,[23] we assigned a ZEKE band to $^+12^1 m^{6(-)}$ but reassigned this on the basis of our recently reported 2D-LIF spectrum.[27] A large aspect of this reassignment was that we would expect the $12^1 m^{6(-)}$ and $12^1 14^1$ levels to be close in wavenumber, in the same way that the 14^2 and $14^1 m^{6(-)}$ levels are close in wavenumber,[21,22,26] as are 14^1 and $m^{6(-)}$.[22] Hence, here we would expect the $11^1 12^1 14^1$ and $11^1 12^1 m^{6(-)}$ levels to be close together, with the $11^1 12^1 14^1$ level already having been deduced to be almost coincident with 5^1 (Subsection III C 2). What then of the remaining SEVI signal seen when exciting at ~1230 cm^{-1}? Again, we note that the resolution of the SEVI experiment is not sufficient to resolve all contributions, and so we suspect that there are underlying FC-active contributions to this SEVI signal that are independent of $^+5^1$, with $^+11^3$ and $^+11^1 12^1 14^1$ being possibilities at this wavenumber. Hence, we conclude that the residual signal of the decay of the "$^+5^1$" SEVI signal (~10% remaining) may be assigned to activity arising from uncoupled levels.

In summary, the 5^1 SEVI signal is lost by two mechanisms, with the $^+5^1 m^1$ intensity being rapidly lost mainly via coupling to a bath of levels (dissipative IVR)—seen in both frequency- and time-resolved studies, while the $^+5^1 m^0$ intensity is lost to rotational dephasing in the time-resolved experiments (the $^+5^1 m^1$ signal could also be partially affected by rotational dephasing). The IVR causes the unstructured background in the SEVI, ZEKE, and 2D-LIF/DF spectra, which arises from activity originating from a large number of bath states; the dephasing only occurs as a time-dependent interference effect and consequently means that half the intensity is still present, as the $^+5^1 m^0$ or $5_1 m_0$ ZEKE or 2D-LIF/DF signals, respectively. The residual signal in the time-resolved SEVI spectrum when exciting via 5^1 is concluded to arise from FC activity from overlapped, but uncoupled, S$_1$ levels.

Consistent with the comments above, we ruled out an assignment of the ZEKE band at 1606 cm^{-1}, seen when exciting at 1208 cm^{-1}, to $^+11^1 12^1 m^{6(-)}$, since the excitation position is 25 cm^{-1} away from the $11^1 12^1 14^1$ transition, which has been deduced to be almost coincident with 5^1 (Subsection III C 2). Instead, the 1606 cm^{-1} band has been assigned to $^+14^1 16^1 29^1$ on the basis that this fits the observed bands in the S$_0$, S$_1$, and D$_0^+$ states. Close to the $14^1 16^1 29^1$ band is the 16^2 band (Fig. 9), whose assignment is secure (despite the lack of a ZEKE spectrum) on the basis of the excellent agreement with the expected position of the 16_2 band; furthermore, this is also in agreement with the observation of the 16^2 band in pDFB.[48] We can see a weak band that corresponds to $(14^1 16^1 29^1, 16_2)$ but do not see the partner $(16^2, 14_1 16_1 29_1)$ band, from which we conclude that it is unlikely these levels are in FR but that 16_2 is FC active via $14^1 16^1 29^1$. We note that there is some FC activity of these when exciting 5^1 and, most clearly, 6^1.

Finally, we discuss the excitation region close to ~1250 cm^{-1} where the 12^2 band is located. We have noted the observation of the $29_1 m_{3(+)}$ band and have associated this with $9^1 29^1 m^{3(+)}$. We conclude that this level is likely interacting with the $12^2 m^0$ level since 12^2 appears to be the only bright level in this region (and is a transition also seen for pDFB).[48] Although we do not see the $18_1 m_2$ band, it is likely that there are some interactions with vibtor combinations involving this level, as we see evidence of weak emissions from $18^2 29^1$ and $11^1 18^2$ levels (not shown), and our earlier work[24] has indicated interactions between $18^2 m^1$ levels and levels such as $11^1 18^1 m^2$. However, the interaction with the $29^1 m^{3(+)}$ combination levels is the most likely explanation of the unstructured background that is present in the ZEKE (Fig. 3) and 2D-LIF/DF (Figs. 2 and 5) spectra when exciting at 1248 cm^{-1}. In Figs. 3 and 8, we see that there are still substantial $^+12^2$ and 12_2 ZEKE and 2D-LIF signals in the respective spectra, attributable to the $12^2 m^1$ level.

In Table II, we present the number of levels of different types that have the correct symmetry and lie close in wavenumber to the 6^1 and 5^1 levels, while in Fig. 11 we show the rise in the number of S$_1$ vibrational and vibtor levels with increasing internal energy. The stark difference between the coupling of 6^1 and 5^1 cannot be straightforwardly related to the density of vibrational states since,

TABLE II. Numbers of vibrations and vibtor levels that can interact with D_6 or D_5.[a]

Vibrational subset	D_6	D_5
Totally symmetric vibrations	20	22
All vibrations	49	92
A_1' vibtors[b]	67	77
E'' vibtors[c]	102	132
$A_1' + E''$ vibtors	169	209
All vibtors	426	585

[a]Numbers of S$_1$ levels calculated within a ±20 cm^{-1} window of each fundamental, based upon calculated harmonic vibrational wavenumbers[23] and approximate energies of the torsional levels. It is clear that both anharmonicity and vibration-torsional coupling will produce minor changes in these numbers but are not expected to be large.
[b]Symmetry-allowed coupling to $m = 0$ levels of totally symmetric vibrations.
[c]Symmetry-allowed coupling to $m = 1$ levels of totally symmetric vibrations.
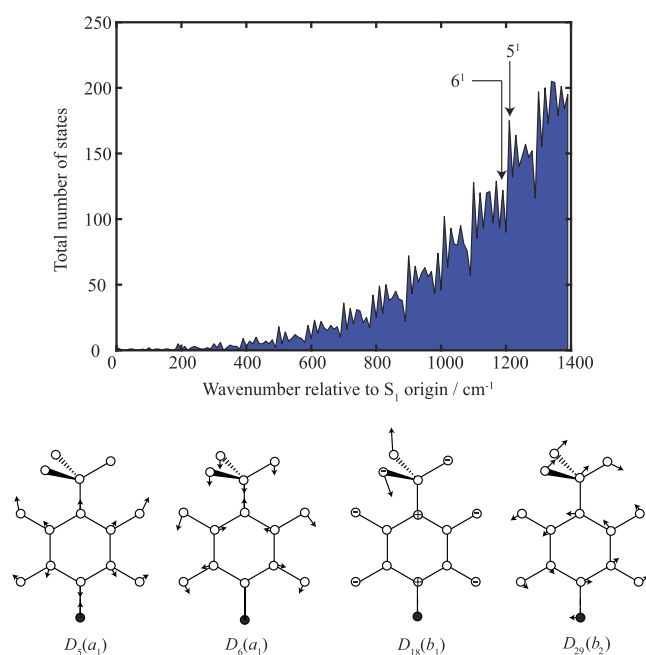
FIG. 11. In the upper part of the figure, the number of states within 10 cm^{-1} windows is plotted as a function of the S_1 state internal energy. The positions of 6^1 and 5^1 are indicated. Below this, the mode diagrams of the D_6 and D_5 fundamentals are shown, as are those for D_{18} and D_{29}. In the latter two cases, it can be seen how the motion can cause the vibrations to interact with the torsional motion of the methyl group.

as Table II and Fig. 11 indicate, there are only a handful of extra totally symmetric levels for the latter. There are more vibtor levels, with ~25% more levels that have the correct symmetry (a' and e'') that could interact (see Table II and Fig. 11), but this is unlikely to explain the marked difference in behavior between these two close-lying fundamentals. As such, and as discussed in Ref. 25, there is a certain amount of serendipity required, in that not only must there be levels of the correct symmetry to interact but the coupling must also be efficient—with at least one doorway state.

We concluded in Ref. 25 that such coupling is aided by torsional motion, which allows out-of-plane (and so nontotally symmetric) vibrations to become coupled to totally symmetric vibrations, which will be FC-active. This idea was explored in Ref. 35 by Davies et al., building on the ideas of Moss et al.,[54] by modeling the van der Waals interaction between the methyl group and the closest phenyl hydrogen atoms. It was found that, on the basis of the calculated vibrational motion, the D_5 vibration produced a larger interaction than did D_6. This is in apparent contrast to the localized motions, which are C–F stretch for D_5 and C–CH$_3$ stretch for D_6, with the latter then being expected to cause more interaction.[51,52] The explanation lies in the relative motions of the in-plane wags of the two closest phenyl C–H bonds and the CH$_3$ stretch. Referring to Fig. 11, these may be seen to be in-phase in the case of D_6 so that the methyl group moves away from the phenyl ring, in sync with the two neighboring C–H bonds, and vice versa, so that the interaction between the sets of hydrogen atoms remains very similar; in contrast, since the C–CH$_3$ bond remains largely stationary in the D_5 motion (Fig. 11),

then the same C–H wagging motions cause a greater interaction than in D_6. This shows that there is vibrational mode specificity in determining the efficiency of IVR, as concluded by Davies et al.[35] The analysis here emphasizes that the whole vibrational motion should be considered when examining this, not just looking at localized motions.

Also, Fig. 11 shows that the D_{18} mode has out-of-plane "wagging" of the two C–H bonds closest to the methyl group, suggestive of their being able to "waft" the methyl group (see also Ref. 24). Also, the motion of D_{29} indicates significant methyl motion, causing it to come into closer contact with a phenyl C–H bond, causing interaction. Hence, both vibrations may reasonably be expected to cause motion of the methyl group.

V. CONCLUDING REMARKS

In this work, we have presented further explicit evidence that vibration-torsion interactions are a key factor in facilitating IVR in molecules that contain a methyl group. Furthermore, we have shown that there is a certain amount of serendipity involved, particularly at moderately low internal energy, in doorway states being present close to a ZOB state and which can enable efficient coupling to the background bath states, whose density is increasing rapidly with increasing internal energy. The efficiency of a doorway state in effecting IVR is dependent on having the correct symmetry, being energetically close to the ZOB state, and being well-coupled both to the ZOB state and a significant number of the bath states—this is likely to be linked to its motion and how this interacts with other motions in the molecule, particularly the methyl group. In this regard, we have suggested that the whole vibrational motion should be considered and not simply local motions.

The above conclusions have been obtained from both fluorescence and ZEKE spectroscopies, with consistent activity in both producing the most reliable results. The 2D-LIF spectra, in particular, have aided in the identification of overlapped activity and particularly allowing the extraction of the vibtor activity. We have been further aided by earlier analyses[26,27] of the lower wavenumber regions that underpin much of the energy level structure in the present wavenumber region. The detailed knowledge of the wavenumbers of the vibrational and vibtor levels in the S_0, S_1 and D_0^+ states (present work and Ref. 23 and the work cited therein) provides great insight into the couplings that occur. Notably, the greater detail of the present study has allowed further insight into the results of time-resolved studies.

It is clear that many of these ideas will be more generally applicable, with coupling between chromophore-localized vibrations and wide-amplitude motions that will provide routes for IVR in a range of molecules, with one key set being biomolecules which often contain NH$_2$ and CH$_3$ groups, as well as other flexible side chains.

REFERENCES

[1] C. S. Parmenter and B. M. Stone, J. Chem. Phys. **84**, 4710 (1986).

[2] D. B. Moss and C. S. Parmenter, J. Chem. Phys. **98**, 6897 (1993).

[3] Z.-Q. Zhao and C. S. Parmenter, in *Mode Selective Chemistry*, The Jerusalem Symposia on Quantum Chemistry and Biochemistry, edited by J. Jortner, R. D. Levine, and B. Pullman (Kluwer, 1991), Vol. 24, p. 127.

[4] Z.-Q. Zhao, C. S. Parmenter, D. B. Moss, A. J. Bradley, A. E. W. Knight, and K. G. Owens, J. Chem. Phys. **96**, 6362 (1992).

[5] Z.-Q. Zhao, Ph.D. thesis, Indiana University, 1992.

[6] P. J. Timbers, C. S. Parmenter, and D. B Moss, J. Chem. Phys. **100**, 1028 (1994).

[7] Q. Ju, C. S. Parmenter, T. A. Stone, and Z.-Q. Zhao, Isr. J. Chem. **37**, 379 (1997).

[8] R. A. Walker, E. C. Richard, K.-T. Lu, and J. C. Weisshaar, J. Phys. Chem. **99**, 12422 (1995).

[9] E. C. Richard, R. A. Walker, and J. C. Weisshaar, J. Chem. Phys. **104**, 4451 (1996).

[10] S. H. Feldus, M. J. Schroeder, R. A. Walker, W.-K. Woo, and J. C. Weisshaar, Int. J. Mass Spectrom. Ion Proc. **159**, 231 (1996).

[11] J. A. Davies, A. M. Green, A. M. Gardner, C. D. Withers, T. G. Wright, and K. L. Reid, Phys. Chem. Chem. Phys. **16**, 430 (2014).

[12] A. M. Gardner, A. M. Green, V. M. Tamé-Reyes, K. L. Reid, J. A. Davies, V. H. K. Parkes, and T. G. Wright, J. Chem. Phys. **140**, 114308 (2014).

[13] A. M. Gardner, A. M. Green, V. M. Tamé-Reyes, V. H. K. Wilton, and T. G. Wright, J. Chem. Phys. **138**, 134303 (2013).

[14] E. A. Virgo, J. R. Gascooke, and W. D. Lawrance, J. Chem. Phys. **140**, 154310 (2014).

[15] J. R. Gascooke, E. A. Virgo, and W. D. Lawrance, J. Chem. Phys. **142**, 024315 (2015).

[16] J. R. Gascooke, E. A. Virgo, and W. D. Lawrance, J. Chem. Phys. **143**, 044313 (2015).

[17] J. R. Gascooke and W. D. Lawrance, J. Mol. Spectrosc. **318**, 53 (2015).

[18] V. L. Ayles, C. J. Hammond, D. E. Bergeron, O. J. Richards, and T. G. Wright, J. Chem. Phys. **126**, 244304 (2007).

[19] C. J. Hammond, V. L. Ayles, D. E. Bergeron, K. L. Reid, and T. G. Wright, J. Chem. Phys. **125**, 124308 (2006).

[20] J. A. Davies and K. L. Reid, J. Chem. Phys. **135**, 124305 (2011).

[21] A. M. Gardner, W. D. Tuttle, L. Whalley, A. Claydon, J. H. Carter, and T. G. Wright, J. Chem. Phys. **145**, 124307 (2016).

[22] J. R. Gascooke, L. D. Stuart, P. G. Sibley, and W. D. Lawrance, J. Chem. Phys. **149**, 074301 (2018), this work contains considerable extra information in its supplementary material. Note, however, that the excitation wavenumber axis is incorrect in Fig. S9.

[23] W. D. Tuttle, A. M. Gardner, L. E. Whalley, and T. G. Wright, J. Chem. Phys. **146**, 244310 (2017).

[24] A. M. Gardner, W. D. Tuttle, L. E. Whalley, and T. G. Wright, Chem. Sci. **9**, 2270 (2018).

[25] W. D. Tuttle, A. M. Gardner, L. E. Whalley, D. J. Kemp, and T. G. Wright, Phys. Chem. Chem. Phys. **21**, 14133 (2019).

[26] D. J. Kemp, A. M. Gardner, W. D. Tuttle, and T. G. Wright, "Unravelling overlaps and torsion-facilitated coupling using two-dimensional laser-induced fluorescence," Mol. Phys. (in press).

[27] D. J. Kemp, L. E. Whalley, A. M. Gardner, W. D. Tuttle, L. G. Warner, and T. G. Wright, J. Chem. Phys. **150**, 064306 (2019).

[28] A. M. Gardner, W. D. Tuttle, P. Groner, and T. G. Wright, J. Chem. Phys. **146**, 124308 (2017).

[29] W. D. Tuttle, A. M. Gardner, K. B. O'Regan, W. Malewicz, and T. G. Wright, J. Chem. Phys. **146**, 124309 (2017).

[30] J. R. Gascooke and W. D. Lawrance, Eur. Phys. J. D **71**, 287 (2017).

[31] W. T. Cave and H. W. Thompson, Faraday Soc. Trans. **9**, 35 (1950).

[32] T. Cvitaš and J. M. Hollas, Mol. Phys. **20**, 645 (1971).

[33] C. J. Seliskar, M. A. Leugers, M. Heaven, and J. L. Hardwick, J. Mol. Spectrosc. **106**, 330 (1984).

[34] K. Okuyama, N. Mikami, and M. Ito, J. Phys. Chem. **89**, 5617 (1985).

[35] J. A. Davies, L. E. Whalley, and K. L. Reid, Phys. Chem. Chem. Phys. **19**, 5051 (2017).

[36] E. B. Wilson, Jr., Phys. Rev. **45**, 706 (1934).

[37] G. Varsányi, *Assignments of the Vibrational Spectra of Seven Hundred Benzene Derivatives* (Wiley, New York, 1974).

[38] R. S. Mulliken, J. Chem. Phys. **23**, 1997 (1955).

[39] G. Herzberg, *Molecular Spectra and Molecular Structure. II. Infrared and Raman Spectra of Polyatomic Molecules* (Krieger, Malabar, 1991).

[40] A. M. Gardner and T. G. Wright, J. Chem. Phys. **135**, 114305 (2011).

[41] A. Andrejeva, A. M. Gardner, W. D. Tuttle, and T. G. Wright, J. Mol. Spectrosc. **321**, 28 (2016).

[42] P. J. Breen, J. A. Warren, E. R. Bernstein, and J. I. Seeman, J. Chem. Phys. **87**, 1917 (1987).

[43] E. Fermi, Z. Phys. **71**, 250 (1931).

[44] J. R. Gascooke and W. D. Lawrance, J. Chem. Phys. **138**, 134302 (2013).

[45] N. T. Whetton and W. D. Lawrance, J. Phys. Chem. **93**, 5377 (1989).

[46] Z.-Q. Zhao and C. S. Parmenter, Ber. Bunsenges. Phys. Chem. **99**, 536 (1995).

[47] J. A. Davies and K. L. Reid, Phys. Rev. Lett. **109**, 193004 (2012).

[48] D. J. Kemp, A. M. Gardner, W. D. Tuttle, J. Midgley, K. L. Reid, and T. G. Wright, J. Chem. Phys. **149**, 094301 (2018).

[49] W. D. Tuttle, A. M. Gardner, and T. G. Wright, Chem. Phys. Lett. **684**, 339 (2017).

[50] D. J. Kemp, L. E. Whalley, W. D. Tuttle, A. M. Gardner, B. T. Speake, and T. G. Wright, Phys. Chem. Chem. Phys. **20**, 12503 (2018).

[51] G. A. Bethardy, X. Wang, and D. S. Perry, Can. J. Chem. **72**, 652 (1994).

[52] D. S. Perry, G. A. Bethardy, and X. Wang, Ber. Bunsenges. Phys. Chem. **99**, 530 (1995).

[53] P. M. Felker and A. H. Zewail, J. Chem. Phys. **82**, 2294 (1985).

[54] D. B. Moss, C. S. Parmenter, and G. E. Ewing, J. Chem. Phys. **86**, 51 (1987).

13. Vibration-modified torsional potentials and vibration-torsion ("vibtor") levels in the *m*-fluorotoluene cation:

Contributions:

Title: Vibration-modified torsional potentials and vibration-torsion ("vibtor") levels in the m-fluorotoluene cation[44]

Authors: David J. Kemp, Elizabeth F. Fryer, Alexander R. Davies, and Timothy G. Wright

Submitted to: Journal of Chemical Physics, 25th June 2019; accepted 7th August 2019; published 30th August 2019

Reproduced from 'Vibration-modified torsional potentials and vibration-torsion ("vibtor") levels in the *m*-fluorotoluene cation', with the permission of AIP Publishing. This article can be located at https://aip.scitation.org/doi/10.1063/1.5116520

This work consists of a collection of REMPI and ZEKE spectra. These were collected through a combination of myself, as well as two masters project students under my supervision: Alexander Davies and Elizabeth Fryer.

The contribution I made was mostly involved in deducing the unfamiliar activity seen in the ZEKE spectra, as well as providing assignments and deductions about the numerous interactions noted. Numerous discussions were had between myself, Alexander and Elizabeth as well as with both Timothy Wright and Warren Lawrance (Flinders University, Australia) regarding the unusual intensity patterns seen related to the torsions.

Figure production and assignments was done purely by myself, with constant interaction occurring between myself and Timothy Wright.

Vibration-modified torsional potentials and vibration-torsion ("vibtor") levels in the m-fluorotoluene cation

View Online   Export Citation   CrossMark

David J. Kemp, Elizabeth F. Fryer, Alexander R. Davies, and Timothy G. Wright[a] [iD]

AFFILIATIONS

School of Chemistry, University of Nottingham, University Park, Nottingham NG7 2RD, United Kingdom

[a]Tim.Wright@nottingham.ac.uk

ABSTRACT

Zero-kinetic-energy (ZEKE) spectra are presented for m-fluorotoluene, employing different low-lying (<350 cm^{-1}) intermediate torsional and vibration-torsional ("vibtor") levels of the S_1 state. The adiabatic ionization energy (AIE) is found to be $71\,997 \pm 5$ cm^{-1} (8.9265 ± 0.0006 eV). It is found that the activity in the ZEKE spectra varies greatly for different levels and is consistent with the assignments of the S_1 levels deduced in the recent fluorescence study of Stewart et $al.$ [J. Chem. Phys. $\textbf{150}$, 174303 (2019)]. For cation torsional levels, the most intense band corresponds to changes in the torsional quantum number, in line with the known change in the phase of the torsional potential upon ionization. This leads to the observation of an unprecedented number of torsions and vibtor levels, with the pronounced vibtor activity involving out-of-plane vibrations. Interactions between levels involving torsions are discussed, with evidence presented, for the first time it is believed, for modification of a torsional potential induced by a vibration. Also, we discuss the possibility of distortion of the methyl group leading to a change from G_6 molecular symmetry to C_s point group symmetry.

$Published$ $under$ $license$ by AIP $Publishing.$ https://doi.org/10.1063/1.5116520

I. INTRODUCTION

The coupling of methyl torsion and vibrational motions has been the subject of a series of studies on toluene,[1-7] $para$-fluorotoluene (pFT),[8-18] and $para$-xylene (pXyl)[15,19,20] using a combination of fluorescence and photoionization spectroscopies. These studies have shown that such coupling can be examined and understood in detail in the low-wavenumber region and is likely to be prevalent to higher wavenumbers, driving the transition to statistical ("dissipative") intramolecular vibrational redistribution (IVR). This underpins the ability to understand energy dispersal, photostability, and photochemical control. Timbers et $al.$[21] have concluded that $meta$-fluorotoluene (mFT) undergoes IVR more than an order of magnitude faster than pFT, showing that the location of substituents is likely to be important in the coupling.

Recently, Stewart et $al.$[22] have examined the first 350 cm^{-1} of the $S_1 \leftarrow S_0$ transition of mFT, assigning the spectra with the use of two-dimensional laser-induced fluorescence (2D-LIF).[23] The spectra were assigned in terms of torsional and vibration-torsional

("vibtor") levels in the S_0 and S_1 states. In the present work, we shall use the same S_1 levels as intermediates in the recording of zero-kinetic-energy (ZEKE) spectra to obtain detailed information on the low-lying levels in the cation. The work of Stewart et $al.$[22] and the present study build on that of Ito and coworkers[24-27] who have recorded laser-induced fluorescence (LIF), dispersed fluorescence (DF), resonance-enhanced multiphoton ionization (REMPI), and ZEKE spectra of the low-wavenumber region of mFT. Additionally, Lu et $al.$[28] have put forward a rationalization of the torsional barrier heights in substituted toluenes. We also note that Feldgus et $al.$[29] have recorded REMPI and ZEKE spectra of m-chlorotoluene (mClT). We shall refer to these studies later.

Stewart et $al.$[22] reported that there is interaction between the torsional motion and low frequency vibrations in both S_0 and S_1 and postulated that such interactions may be present in the cation. Here, we explore the torsional and vibtor states of the cation with the aim of exploring the extent of such interactions in the mFT cation. It will be seen that mFT is an excellent molecule for investigating torsions

and vibtor interactions since the torsional levels in the S_0 state are close to freely rotating, while those in the S_1 state are moderately hindered and those in the cation are severely hindered. In the latter case, the lowest few torsional levels might be regarded as torsional vibrations. In addition, we find that numerous vibtor levels are seen involving the lowest-wavenumber vibrations.

II. EXPERIMENTAL

The REMPI/ZEKE apparatus was the same as that used in earlier work.[8] The focused, frequency-doubled outputs of two dye lasers (Sirah CobraStretch) were overlapped spatially and temporally and passed through a vacuum chamber coaxially and counterpropagating, where they intersected a free jet expansion of mFT (Sigma Aldrich, 98% purity) in 1.5 bars Ar. The excitation laser operated with Coumarin 503 and was pumped with the third harmonic (355 nm) of a Surelite III Nd:YAG laser, while the ionization laser operated with Pyrromethene 597, pumped with the second harmonic (532 nm) of a Surelite I Nd:YAG laser.

The jet expansion passed between two biased electrical grids located in the extraction region of a time-of-flight mass spectrometer, which was employed in the REMPI experiments. These grids were also used in the ZEKE experiments by application of pulsed voltages, giving typical fields of ~10 V cm^{-1} after a delay of up to 2 μs; this delay was minimized while avoiding the introduction of excess noise from the prompt electron signal. The resulting ZEKE bands had widths of ~5 to 7 cm^{-1}. Electron and ion signals were recorded on separate sets of microchannel plates.

III. RESULTS AND ASSIGNMENTS

A. Nomenclature and labeling

1. Vibrational and torsional labeling

Since neither Wilson[30]/Varsányi[31] nor Mulliken[32]/Herzberg[33] notations are appropriate for the vibrations of mFT,[34,35] we shall employ the D_i labels from Ref. 35, as used in the recent work by Stewart et $al.$[22] This C_s point group labeling scheme is based on the vibrations of the $meta$-difluorobenzene (mDFB) molecule, for which the $S_1 \leftarrow S_0$ transition has been investigated using LIF and DF spectroscopy.[36] (While mDFB has C_{2v} point group symmetry, the labeling scheme in Ref. 35 was developed to be applicable to both symmetric and asymmetric substitutions.) Although not pursued in the present work, we find that the vibrational activity in the corresponding electronic transition of mDFB is similar to that in mFT, consistent with comparisons made for the corresponding $para$-substituted molecules.[37]

Since the G_6 molecular symmetry group (MSG) is appropriate for vibtor levels in mFT, we shall use these symmetry labels throughout. In addition, torsional levels will be labeled via their m quantum number. (The reader may find it useful to refer to Refs. 19 or 22 if they are not familiar with these labels.) The correspondence between the C_s point group labels and the G_6 MSG ones is given in Table I. To calculate the overall symmetry of a vibtor level, it is necessary to use the corresponding G_6 label for the vibration and then find the direct product with the symmetry of the torsion (Table I), noting that a C_{3v}

TABLE I. Correspondence of the C_s point group symmetry classes with those of the G_6 molecular symmetry group. Also indicated are the symmetries of the D_i vibrations and the different pure torsional levels.[a]

C_s	G_6	D_i[b]	m
a'	a_1	D_1-D_{21}	0, 3(+), 6(+), 9(+)
a''	a_2	$D_{21}-D_{30}$	3(−), 6(−), 9(−)
	e		1, 2, 4, 5, 7, 8

[a]Symmetries of vibtor levels can be obtained by combining the vibrational symmetry (in G_6) with those of the pure torsional level, using the C_{3v} point group direct product table.

[b]The D_i labels are described in Ref. 35, where the vibration mode diagrams can also be found.

point group direct product table can be used, since the G_6 MSG and the C_{3v} point group are isomorphic.

Under the free-jet expansion conditions employed here, almost all of the molecules are expected to be cooled to their zero-point vibrational level, and thus, essentially all $S_1 \leftarrow S_0$ pure vibrational excitations are expected to be from this level. In contrast, owing to nuclear-spin and rotational symmetry, the molecules can be in one of the $m = 0$ or $m = 1$ torsional levels.

2. Coupling and transitions

When designating excitations, we shall generally omit the lower level since it will be obvious from the jet-cooled conditions. In the usual way, vibrational transitions will be indicated by the cardinal number, i, of the D_i vibration, followed by a super-/subscript specifying the number of quanta in the upper/lower states, respectively; torsional transitions will be indicated by m followed by its value. Finally, vibtor transitions will be indicated by a combination of the vibrational and torsional transition labels.

As has become common usage, we will generally refer to a level using the notation of a transition, with the level indicated by the specified quantum numbers, superscripts indicating levels in the S_1 state, and, when required, subscripts indicating levels in the S_0 state. Since we will also be referring to transitions and levels for the ground state cation, D_0^+, we shall indicate those as superscripts, but with an additional single preceding superscripted + sign. Relative wavenumbers of the levels will be given with respect to the relevant zero-point vibrational level with $m = 0$ in each electronic state.

For cases where the geometry and the torsional potential are both similar in the S_1 and D_0^+ states, the most intense transition is expected to be that for which no changes in the torsional and/or vibrational quantum numbers occur: these will be designated as $\Delta m = 0$, $\Delta v = 0$, or $\Delta(v, m) = 0$ transitions, as appropriate. However, as will be seen (and as reported in Ref. 27), the $\Delta m = 0$ and $\Delta(v, m) = 0$ transitions are almost always not the most intense bands in the ZEKE spectra for mFT, indicative of a significant change in the torsional potential upon ionization.

If two levels are close in wavenumber and have the same overall symmetry, then (except between vibrational fundamentals, to first order) interactions can occur, with the simplest example being the anharmonic interaction between two vibrational levels—the classic Fermi resonance.[38] For molecules that contain a hindered internal

rotor, and if vibration-torsional coupling occurs, then interactions can also involve torsional or vibtor levels. The end result of such interactions is the formation of eigenstates with mixed character. Such couplings are only expected to be significant for small changes, $\Delta v \approx 3$, of the vibrational quantum number, and also for changes, Δm, of 0, ± 3, or ± 6 in the torsional quantum number in descending order of likely strength.[39,40] Often the eigenstates will be referred to by the dominant contribution, with the context implying if an admixture is present.

3. Torsional energies

The energy levels of a hindered methyl rotor have been the subject of numerous studies, with the paper by Spangler[41] being a good starting point. For a hindered methyl rotor, the lowest couple of terms of the torsional potential may be expressed as

$$V(\alpha) = \frac{V_3}{2}(1 - \cos 3\alpha) + \frac{V_6}{2}(1 - \cos 6\alpha), \tag{1}$$

where α is the torsional angle. In the cases of toluene and pFT, the V_3 term is zero by symmetry, but in mFT, this is the largest term. If the V_6 term is small relative to V_3, which is usually the case, then its effect is simply to modify the shape of the potential. (For larger values of V_6, local minima appear in between the ones arising from the V_3 term.) Previous work[22,27,28] has shown that for mFT, V_3 has approximate values of 20 cm^{-1} for the S$_0$ state, 115 cm^{-1} for the S$_1$ state, and -300 cm^{-1} for the D$_0^+$ state. Thus, these three states of the same molecule are, respectively, close to a free rotor, a moderately hindered rotor, and a highly hindered rotor.

The effect of the magnitude of the V_3 term on the energies of the m levels may be seen in Fig. 1(a), where the V_6 term has been set at zero and the V_3 term varied. (Note that the sign of the V_3

parameter, which is a way of indicating the phase of the torsional potential, does not affect the energy levels, but it can be deduced from the calculated geometry.[42,43]) As described in Spangler,[41] as V_3 increases, deep within the potential well, the free-rotor m levels evolve into triply degenerate torsional vibrations, with each torsional vibration arising from one degenerate pair of $m \neq 3n$ levels, plus one $m = 3n$ level. These latter levels lose their degeneracy in V_{3n} potentials, and the resulting levels can be denoted $m = 3n(+)$ and $m = 3n(-)$, with the former being of a_1 and the latter of a_2 symmetry in G_6.[22,41] Thus, if the torsional barrier is high, we can expect low-lying e symmetry levels to be close-to-degenerate with an $m = 3n(+)$ or $m = 3n(-)$ level. As may be seen from Fig. 1(a), in G_6, the splitting between the $m = 3n(+)$ and $m = 3n(-)$ levels is largely an effect of V_3 but is also affected by (the smaller-valued) V_6—see Fig. 1(c). If V_3 is very small, or is zero as in a G_{12} molecule such as toluene or pFT [see Fig. 1(b)], then the sign of V_6 determines the energy ordering of the $m = 3n(+)$ and $m = 3n(-)$ levels, particularly for $n = 1$. It is also the case that the energies of the other m levels depend on both parameters, as well as the effective rotational constant for torsion of the -CH$_3$ group, denoted F, whose value is expected to be only slightly different in the three electronic states under consideration. As a consequence, it is not straightforward to deduce the values of the torsional parameters from the spectrum directly, and that difficulty is further exacerbated by possible interactions between torsional, vibtor, and vibrational levels.[22]

B. Overall comments on the spectra

1. The S$_1$ ← S$_0$ spectrum

The REMPI spectrum covering the first 350 cm^{-1} of the mFT S$_1$ ← S$_0$ spectrum is shown in Fig. 2. It is very similar in
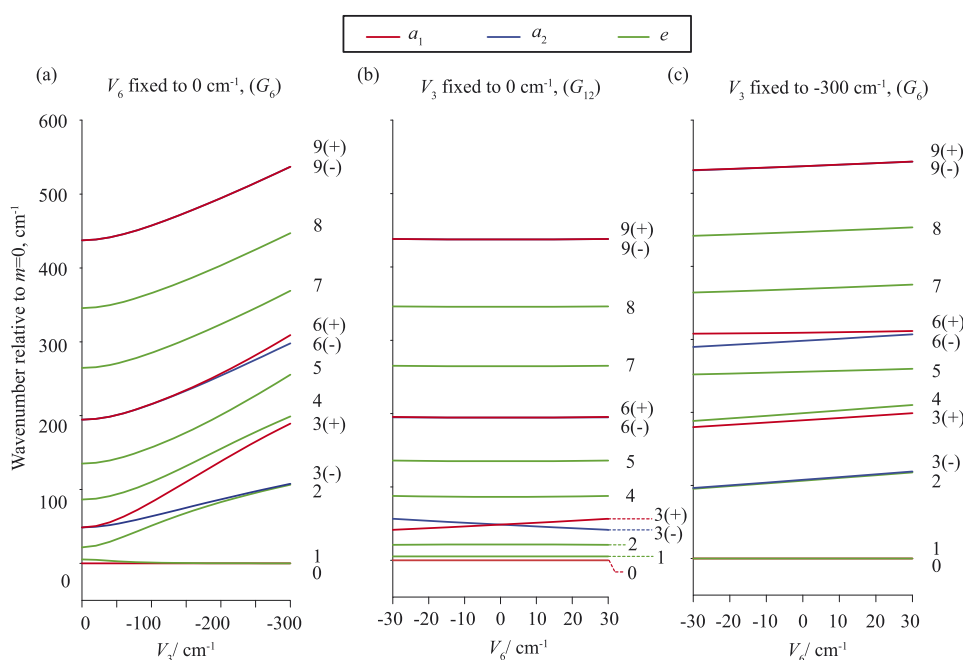
Note: The ordering of 3(+) and 3(−) on Figure 1(b) is displayed incorrectly and needs reversing

FIG. 1. (a) Evolution of the m levels as a function of V_3 when $V_6 = 0$ cm^{-1}, (b) evolution of the m levels as a function of V_6 when $V_3 = 0$ cm^{-1}, and (c) evolution of the m levels as a function of V_6 when $V_3 = -300$ cm^{-1}. In some cases, lines are superimposed, as can be deduced from the m labels.
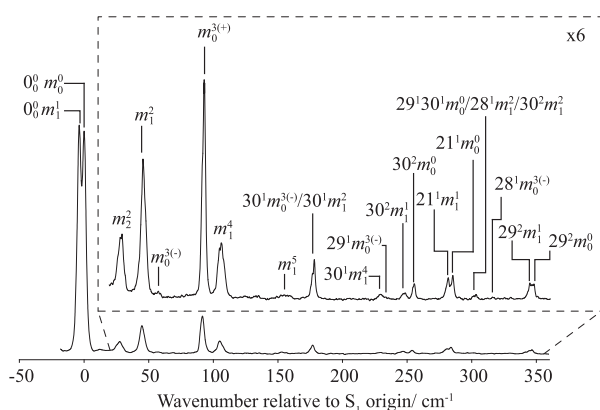
FIG. 2. REMPI spectrum of the 0–350 cm^{-1} region of the $S_1 \leftarrow S_0$ transition of m-fluorotoluene. The assignments have been reported in Ref. 22, and the ZEKE spectra in the present work are consistent with these.

appearance to the LIF spectra of Stewart $et\ al.$[22] and Okuyama $et\ al.$[24] Some of the assignments in Ref. 24 have been superseded by those in Ref. 22, and it is the latter that will be referred to in the present work and which are shown in Fig. 2. As will be seen, the activity observed in the ZEKE spectra is essentially consistent with the assignments of Ref. 22.

The $S_1\ 0^0 m^0 \leftrightarrow S_0\ m_0$ origin transition is located at 37 385.9 cm^{-1}, with the $S_1\ m^1 \leftrightarrow S_0\ m_1$ transition located 4.0 cm^{-1} below this (Ref. 22)—see Fig. 2. It may be seen that there are vibtor as well as "pure" torsional transitions observed in this region of the

spectrum. For each vibration of a_1 symmetry (fundamental, over-tone, or combination), it is expected to see transitions corresponding to both m^0 and m^1 transitions. Vibrations of a_2 symmetry are only expected as vibtors in combination with $m = 3(-)$, and perhaps weakly with $m = 6(-)$, when exciting from $S_0\ m = 0$, while weak $X^1 m^1 \leftarrow 0^0\ m^1$ transitions are also seen for X being a vibration of a_2 symmetry,[22] and their activity is likely induced by second order couplings.

2. ZEKE spectra via torsional levels of S_1

We shall now discuss the ZEKE spectra. In Table II, we have tabulated the wavenumbers of the vibtor levels relative to their respective ($m = 0$) vibrational fundamentals—these assignments will be deduced in Secs. III B 3–III B 7. In the figures, we have indicated the assignments of many of the bands, but for clarity, we have omitted the preceding superscript "+" on these. Note that in the figures, we have not indicated all of the observed weak transitions although many of these can be deduced from the values given in Table II.

We initially consider the first ~880 cm^{-1} of each of the ZEKE spectra recorded via $S_1 m^0$ and $S_1 m^1$, which are shown in Figs. 3(a) and 3(d), respectively. As may be seen, very different activity is seen in both cases with transitions from $S_1 m^1$ maintaining e symmetry in the final states, while transitions from $S_1 m^0$ lead to the most intense bands being of a_1 symmetry, but also some bands are associated with symmetry-forbidden levels whose activity is discussed further in Sec. IV. It is also clear in each spectrum that the $\Delta(v, m) = 0$ band is not the most intense feature. The spectra have been shifted so that the bands are on the same internal wavenumber scale.

TABLE II. Separations of vibtor levels built on different vibrations (cm^{-1}).[a]

					Vibrational level[b]				
Torsion[c]	$^{+}0^0$ [0]	$^{+}30^1$ [167]	$^{+}29^1$ [194][d]	$^{+}21^1$ [296]	$^{+}29^1 30^1$ [365]	$^{+}30^2$ [335]	$^{+}28^1$ [372]	$^{+}29^2$ [384]	$^{+}18^1$ [510]
$^{+}m^{0,1}$	0	0	0	0	0	0	0	0	0
$^{+}m^2$	101	99	98	102		91	(106)[e]	98	100
$^{+}m^{3(-)}$	103	97	100	(107)[e]		92	105	(97)[e]	102
$^{+}m^{3(+)}$	185	186	181	189	180	178		181	186
$^{+}m^4$	192	179	191	195	(187)[e]	(170)[e]	193	190	192
$^{+}m^5$	250	244	251	253	(249)[e]	236	252	246	250
$^{+}m^{6(-)}$	292	282	294	294		284	293	286	293
$^{+}m^{6(+)}$	311		311	317	304	299	313	306	311
$^{+}m^7$	368	366		369		369			366
$^{+}m^8$	442								
$^{+}m^{9(\pm)}$	526								

[a]Torsional spacings are given with respect to the band position of the $m = 0$ level of the indicated vibration.

[b]Values in square brackets in the column headers are the wavenumbers of the $m = 0$ level of the indicated vibration.

[c]The $^{+}m^0$ and $^{+}m^1$ levels are degenerate at our resolution. Levels with $m \neq 3n$ have degenerate + and—levels. The $^{+}m^{9(+)}$ and $^{+}m^{9(-)}$ levels are expected to be close to degenerate as they lie above the V_3 barrier; it is the $^{+}m^{9(+)}$ level that is seen in this work, via $m^{3(+)}$.

[d]The fundamental value for $^{+}29^1$ is tentative.

[e]These values in parentheses are weak, and/or their assignment/band center is uncertain.

FIG. 3. ZEKE spectra recorded via the following intermediate S_1 levels: (a) m^0, (b) $m^{3(-)}$, (c) $m^{3(+)}$, (d) m^1, (e) m^2, (f) m^4, and (g) m^5. The preceding superscripted "+" used in the text is omitted in the labels for clarity. To avoid congestion, only a selection of transitions is labeled—see text and Table II for further assignments and discussion.

In the cation, the $m = 0$ and $m = 1$ levels are close to being degenerate, as expected for a high value of V_3 (see Sec. III A 3, Fig. 1, and Ref. 41), and also the $m = 2$ and $m = 3(-)$ levels are expected to be very close in energy, as observed; in contrast, $m = 4$ and $m = 3(+)$ are noticeably separated. Since the top of the barrier is now being approached, the energies of $m = 5$ and $m = 6(-)$ are still somewhat separated, and the latter is quite close to $m = 6(+)$. Above the barrier, i.e., for $m > 7$, the $m = \pm 3n$ levels are calculated to be very close in energy.

We initially concentrate on the spectrum recorded from S_1 $m = 0$ in Fig. 3(a). The spectrum is dominated by the $^+m^{3(+)}$ band, with a sizeable $^+m^{6(+)}$ band; these correspond to $\Delta m = +3$ and $+6$, respectively. The greater intensity of the $\Delta m = +3$ band over that of the $\Delta m = 0$ band indicates a significant change in the torsional potential between the S_1 and D_0^+ states. We also clearly see the symmetry forbidden bands, $^+m^{3(-)}$ and $^+m^{6(-)}$, which arise from a_2 symmetry levels. We also see the $^+m^0$ band at an overall wavenumber of $71\,997 \pm 5$ cm^{-1} (8.9265 ± 0.0006 eV), which corresponds to the adiabatic ionization energy (AIE). (Note that we have not adjusted

this value for the pulsed electric field, owing to the well-known decay of the lower-lying Rydberg states accessed in the pulsed-field ionization process.[44]) Surprisingly, we also apparently see the $^+m^5$ band, whose activity will be discussed in Sec. IV C. To higher wavenumbers, we see the $^+18^1$ band, together with a series of vibtor bands that largely replicate the activity on the origin band, including the (apparent) $^+18^1m^5$ band.

We now move onto the ZEKE spectrum recorded via S_1 $m = 1$—see Fig. 3(d). Here, we see a very different intensity profile, with the $\Delta m = 3$ bands, $^+m^2$ and $^+m^4$ being more intense than the $\Delta m = 0$ band, $^+m^1$; furthermore, the most intense band is the $\Delta m = 6$ band, $^+m^5$, while the $^+m^7$ band is clearly seen and is of a similar intensity as $^+m^1$. (Note that the m levels are degenerate for $m \neq 3n$ and so, as an example, the $^+m^2$ band, $\Delta m = 3$, actually arises from a combination of $^+m^{-2} \leftarrow m^1$ and $^+m^2 \leftarrow m^{-1}$ transitions.) Although weak, a clear series of vibtor bands associated with each of $^+30^1$ and $^+29^1$ (not indicated—see Table II) can be seen, as well as several with $^+28^1$ (not indicated—see Table II). To higher wavenumbers, a very similar pattern of bands can be observed, arising from combinations with $^+18^1$.

Moving onto the ZEKE spectrum via m^2 [Fig. 3(e)], we note that this S_1 torsional level can be reached via two transitions, m_2^2 and m_1^2. The former is a hot band, caused by incomplete cooling of the S_0 $m = 2$ population into $m = 1$. Both ZEKE spectra are essentially the same, but the spectrum via the cold band is the more intense, and it is this one that is presented. Again, we note that the $\Delta m = 0$ band is not the most intense, with this being the $\Delta m = -3$ band, accessing $^+m^1$. Also, the $^+m^4$ band corresponding to $\Delta m = 6$ is more intense than the $\Delta m = 0$ band. The $\Delta m = 3$ band, $^+m^5$, is also clearly seen, as is the $\Delta m = 6$ band, $^+m^8$. As with the ZEKE spectra via m^0 and m^1, we also see combination bands involving $^+18^1$. There are also vibtor bands evident in this spectrum: $^+30^1m^1$, $^+30^1m^2$, $^+30^1m^4$, and $^+30^1m^5$ and (not indicated) $^+29^1m^2$, $^+29^1m^4$, and $^+29^1m^5$ are seen (noting that $^+29^1m^1$ is likely overlapped by the $^+m^4$ band)—see Table II.

The $m^{3(-)}$ band is extremely weak (see Fig. 2), but a ZEKE spectrum was obtained via this level, giving rise to $^+m^{3(-)}$ and $^+m^{6(-)}$ bands, with the latter slightly more intense—Fig. 3(b). The $^+m^{6(-)}$ band is a symmetry-allowed $\Delta m = 3$ band and has a similar intensity as the $\Delta m = 0$ band. A weak band assignable as $^+18^1m^{3(-)}$ is also evident.

The ZEKE spectrum recorded via $m^{3(+)}$—Fig. 3(c)—is interesting in that the $\Delta m = 0$ band is very weak, with the width of the feature suggesting that there is likely partial overlap with $^+29^1m^0$. The torsional region of the spectrum is dominated by the two $\Delta m = 3$ bands, $^+m^0$ and $^+m^{6(+)}$; the $\Delta m = 6$ band, $^+m^{9(+)}$ is also seen. There are also symmetry-forbidden torsional bands $^+m^{3(-)}$ and $^+m^{6(-)}$, as well as weak, symmetry-forbidden vibrational bands, $^+30^1m^0$ and (not indicated—see Table II) $^+29^1m^0$ and $^+28^1m^0$. Additionally, a symmetry-allowed vibrational band is seen for $^+18^1m^0$, with $^+21^1m^0$ likely overlapped by the $^+m^{6(-)}$ band; also, a weak $^+30^2m^0$ band (not indicated—see Table II) is seen. Above 500 cm^{-1}, there are the now-expected combinations of the earlier bands with $^+18^1$. There are several other weak features, for which there are possible, but not definitive, assignments, and so we refrain from discussing those. We do note that the symmetry-allowed $^+30^1m^{3(-)}$ band is clearly observed, while $^+29^1m^{3(-)}$ would be obscured by the $^+m^{6(-)}$ band.

The ZEKE spectrum recorded via m^4—Fig. 3(f)—exhibits a sizeable $\Delta m = 0$ band, but it is not the most intense, with this being the $^+m^1$ band, corresponding to $\Delta m = 3$, and the (also $\Delta m = 3$) $^+m^7$ band is also clearly seen. The $\Delta m = 6$ band, $^+m^2$, is also very intense, while the $\Delta m = 9$ band, $^+m^5$, is also clearly active. We also see generally weak bands corresponding to vibtor versions of these torsions in combination with $^+30^1$; the exception to this is the $^+30^1m^4$ band, which demonstrates a significant intensity—this is commented on in Subsection III B 3. A number of corresponding vibtor bands involving $^+29^1$ are also seen (not indicated—see Table II). Above 500 cm^{-1} are seen the $^+18^1$ band and vibtor bands involving this vibration.

The ZEKE spectrum recorded via m^5 is quite weak, see Fig. 3(g), but clear torsional bands can be seen. The $\Delta m = 0$ band is fairly intense but is slightly weaker than the most intense $\Delta m = 9$ band, $^+m^4$; the two $\Delta m = 3$ bands, $^+m^2$ and $^+m^8$, are also sizeable. The $^+30^1m^1$ band is also seen clearly. Above 500 cm^{-1}, vibtor bands built upon $^+18^1$ are seen.

3. Vibtor levels involving 30^1

In Fig. 4(a), we show the ZEKE spectrum recorded via the two overlapped vibtor transitions, 30^1m^2 and $30^1m^{3(-)}$. Transitions to
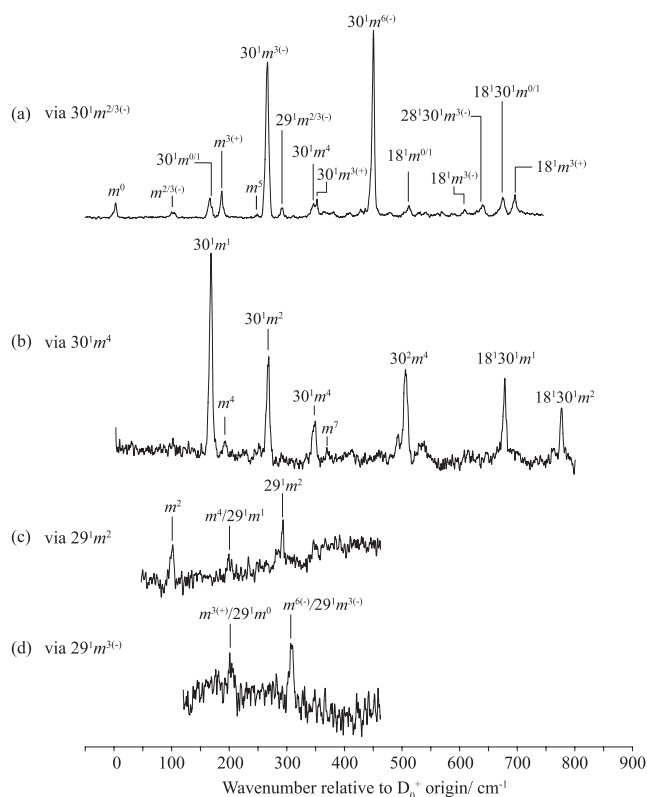

FIG. 4. ZEKE spectra recorded via the following intermediate S$_1$ levels: (a) the overlapped $30^1m^2/30^1m^{3(-)}$, (b) 30^1m^4, (c) 29^1m^2, and (d) $29^1m^{3(-)}$. The preceding superscripted "+" used in the text is omitted in the labels for clarity. See text for further discussion.

these levels are symmetry allowed from the S$_0$ $m = 1$ and $m = 0$ levels, respectively. It was shown in Ref. 22 that interactions in the S$_1$ state cause the 30^1m^2 and $30^1m^{3(-)}$ bands to be almost coincident, but the separate contributions could be extracted from the 2D-LIF spectrum; the latter band is significantly the stronger one. As a consequence, we expect the ZEKE spectrum to demonstrate bands arising from both levels but be dominated by bands arising from $30^1m^{3(-)}$. The two strongest bands can be assigned to the $\Delta(v, m) = 0$ band, $^+30^1m^{3(-)}$ and the $\Delta m = 3$ band, $^+30^1m^{6(-)}$. Furthermore, the presence of these two strong bands is consistent with the observation of the $^+m^{3(-)}$ and $^+m^{6(-)}$ bands seen when ionizing from $m^{3(-)}$—Fig. 3(b). Note that in the cation, the $^+30^1m^2$ band is expected to be very close in energy to the $^+30^1m^{3(-)}$ band, arising from the large V_3 value, and indeed the $\Delta v = -1$ bands, $^+m^2$ and $^+m^{3(-)}$, are very close in energy (Table II). On symmetry grounds, the observed weak $^+m^5$ could arise from 30^1m^2, but we note that $^+m^4$ and $^+m^2$ are not seen. An alternative source of activity would be a deviation of the symmetry away from G_6—see Sec. IV C. The $^+m^{3(+)}$ band can arise from $30^1m^{3(-)}$. Overall, therefore, there is support from this ZEKE spectrum for the REMPI feature to arise from an overlap of $30^1m^{3(-)}$ and 30^1m^2, consistent with the deductions of Ref. 22. Other assignments are noted in Fig. 4(a), with combinations involving $^+18^1$ being seen to higher wavenumbers.

Overall, a fairly complete set of vibtor levels built on $^+30^1$ is seen, and these are tabulated in Table II. As well as a possible "closing up" of the levels compared to the pure torsional levels, a key observation here is that the $^+30^1m^{3(-)}$ level lies *below* the $^+30^1m^2$ level. These two points suggest that the values of one or more of the torsional parameters may have changed in these vibtor levels and also that there are specific vibtor interactions between levels—further comment is made in Sec. IV D.

In the ZEKE spectrum recorded via 30^1m^4—Fig. 4(b)—we can see that the spectrum is dominated by the $\Delta m = 3$ band, $^+30^1m^1$, with the other symmetry-allowed vibtor levels also prominent. Interestingly, consistent with the strong $^+30^1m^4$ band seen when exciting via m^4—see Fig. 3(f)—we see a reasonably strong $^+30^2m^4$ band in the spectrum in Fig. 4(b); further discussion will be presented in Sec. IV D. To higher wavenumbers, we see combinations with $^+18^1$.

Via the 29^1m^2 band at 216 cm^{-1}, a weak ZEKE spectrum is seen, showing the $\Delta(v, m) = 0$ band [Fig. 4(c)], as well as $^+m^2$ and a band that likely arises from overlapped $^+m^4$ and $^+29^1m^1$ transitions. The activity is consistent with the assignment[22] of this band to 29^1m^2. Similarly, when exciting via the $^+29^1m^{3(-)}$ band at 234 cm^{-1} [Fig. 4(d)], we saw weak bands assignable as an overlapped $^+m^{3(+)}/^+29^1m^0$ pair of transitions, together with the $\Delta(v, m) = 0$ band. Although we might have expected to see $^+29^1m^{6(-)}$ by analogy with the ZEKE spectra recorded via $m^{3(-)}$ and $30^1m^{3(-)}$ (see Secs. III B 1 and III B 2), and as will be seen $28^1m^{3(-)}$ (Sec. III B 6), the signal in the higher wavenumber region of the spectrum via 29^1m^2 was too poor to be reliable.

4. Spectra via 30^2m^0 and 30^2m^1

The ZEKE spectra recorded via the 30^2m^0 and 30^2m^1 levels are shown in Fig. 5. The band intensity profile of the spectrum via 30^2m^1 [Fig. 5(b)] somewhat resembles that of the spectrum via 0^0m^1
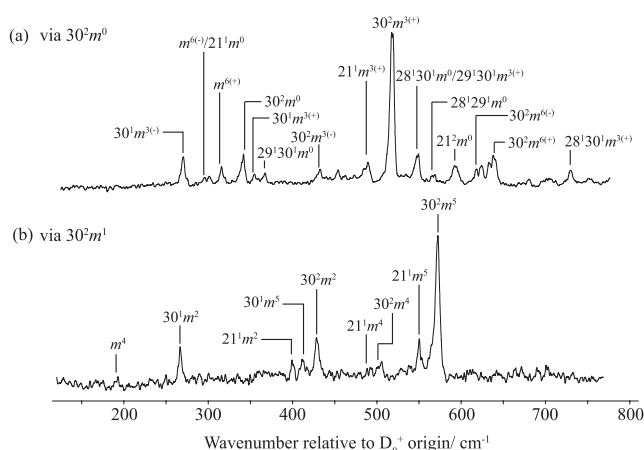
FIG. 5. ZEKE spectra recorded via the following intermediate S_1 levels: (a) $30^2 m^0$ and (b) $30^2 m^1$. The preceding superscripted "+" used in the text is omitted in the labels for clarity. See text for further discussion.

[Fig. 3(d)] in that the $\Delta(v, m) = 0$ band is extremely weak, but there are clear bands for the $\Delta m = 3$ band, $^+30^2 m^2$, with the $\Delta m = 6$ band, $^+30^2 m^5$, the most intense. With these bands seen, it might also be expected to observe clear $^+30^2 m^4$ and $^+30^2 m^7$ bands; however, the former is weak, and the latter is not obviously seen. Also evident are the $^+m^4$ and $^+30^1 m^2$ bands. Other weak bands can be assigned as the set of vibtors: $^+21^1 m^2$, $^+21^1 m^4$, and $^+21^1 m^5$.

When exciting via $30^2 m^0$ [Fig. 5(a)], again there is a strong similarity with the activity seen via $0^0 m^0$ [Fig. 3(a)] with a dominant $^+30^2 m^{3(+)}$ band and bands corresponding to $^+30^2 m^0$, $^+30^2 m^{3(-)}$, $^+30^2 m^{6(-)}$, and $^+30^2 m^{6(+)}$. There are also bands arising from $^+30^1 m^{3(-)}$ and $^+30^1 m^{3(+)}$ and (likely, unshown) $^+30^1 m^{6(-)}$ and $^+30^1 m^{6(+)}$, as well as the torsional bands $^+m^{6(-)}$ and $^+m^{6(+)}$. Additionally, overlapped bands arising from $^+21^1 m^0$ and $^+21^1 m^{3(+)}$ appear to be present, as well as a band assigned as $^+21^2 m^0$. Finally, bands that are assignable to the $^+29^1 30^1$, $^+28^1 30^1$(overlapped), and $^+28^1 29^1$ combination bands are evident, with the corresponding $^+m^{3(+)}$ vibtor levels seen for the first two of these in the range scanned.

Overall, a fairly complete set of vibtor levels built on $^+30^2$ is seen, and these are tabulated in Table II. As well as a distinct "closing up" of the levels compared to the pure torsional levels, it is interesting to note the change in ordering of the $^+30^2 m^{3(+)}$ and $^+30^2 m^4$ levels. As with the $^+30^1$ vibtor levels, this suggests that the values of one or more of the torsional parameters have changed, but also that there are specific vibtor interactions between levels. This is discussed further in Sec. IV D.

5. Spectra via $21^1 m^0$ and $21^1 m^1$

The ZEKE spectra recorded via the two lowest torsional levels of 21^1 are shown in Fig. 6. When exciting via $21^1 m^1$ [Fig. 6(b)], a fairly similar profile is seen to that observed when exciting via $0^0 m^1$ [Fig. 3(d)] with a strong activity in $^+21^1 m^2$, $^+21^1 m^4$, and $^+21^1 m^5$, and clear bands are also seen for $^+21^1 m^1$ and $^+21^1 m^7$. In addition, weak bands are seen for $^+m^2$ and $^+m^4$, $30^1 m^4$, $30^1 m^5$, and (overlapped) $^+30^1 m^7$. A similar set of vibtor bands is seen with $^+30^2$.
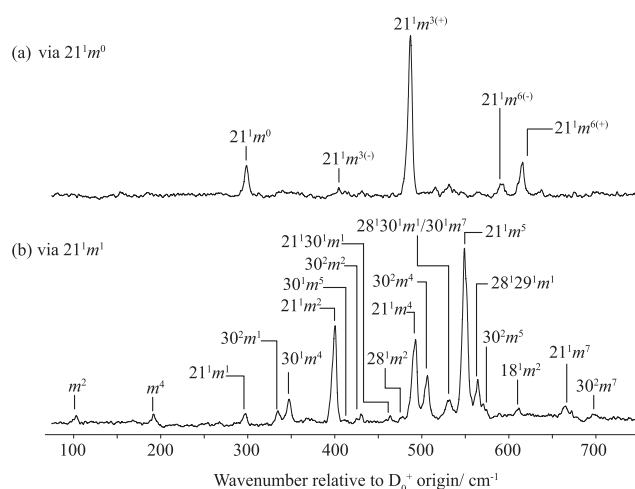

FIG. 6. ZEKE spectra recorded via the following intermediate S_1 levels: (a) $21^1 m^0$ and (b) $21^1 m^1$. The preceding superscripted "+" used in the text is omitted in the labels for clarity. See text for further discussion.

The ZEKE spectrum via $21^1 m^0$ [Fig. 6(a)] is somewhat more straightforward, with the spectrum resembling that recorded via $0^0 m^0$ [Fig. 3(a)] with the most-intense band being the sizeable $^+21^1 m^{3(+)}$ $\Delta m = 3$ band, together with the $\Delta m = 0$ band, $^+21^1 m^0$ and the $\Delta m = 6$ band, $^+21^1 m^{6(+)}$. Also see are the symmetry-forbidden bands, $^+21^1 m^{3(-)}$ and $^+21^1 m^{6(-)}$.

Although the recording of ZEKE spectra was attempted via $21^1 m^2$, no discernible structure was evident owing to the very weak transition.

6. Spectra via $29^1 30^1 m^0$, $28^1 m^2$, and $28^1 m^{3(-)}$

The recording of ZEKE spectra via $29^1 30^1 m^1$ was attempted, but no bands were evident.

The ZEKE spectrum via the overlapped[22] $29^1 30^1 m^0$, $28^1 m^2$, and $30^2 m^2$ transitions is shown in Fig. 7(a). From $29^1 30^1 m^0$, by comparison with the $0^0 m^0$ spectrum [Fig. 3(a)], the expected $^+29^1 30^1 m^{3(+)}$ band is seen, together with $^+29^1 30^1 m^{6(+)}$. From $28^1 m^2$, by comparison with the spectrum via m^2 [Fig. 3(e)], we only see the two most-intense features: $^+28^1 m^1$ and $^+28^1 m^4$. A very weak feature can be seen that is in the expected position for $^+30^2 m^2$, which is consistent with $30^2 m^2$ being a very weak feature overlapped by $29^1 30^1 m^0$ and $28^1 m^2$.

The spectrum via $28^1 m^{3(-)}$—Fig. 7(b)—is very similar to those via $m^{3(-)}$ and $30^1 m^{3(-)}$ in that both $^+28^1 m^{3(-)}$ and $^+28^1 m^{6(-)}$ bands are clearly seen. As noted above, we did see the $^+29^1 m^{3(-)}$ band when exciting via $29^1 m^{3(-)}$, but the signal was too poor to see the now-expected $^+29^1 m^{6(-)}$ band.

7. Spectra via $29^2 m^0$ and $29^2 m^1$

The ZEKE spectra via these two levels are shown in Fig. 8. When exciting via $29^2 m^1$ [Fig. 8(b)], expected bands are seen for $^+29^2 m^1$, $^+29^2 m^2$, $^+29^2 m^4$, and $^+29^2 m^5$. There are also clear bands associated with $^+29^1 30^1 m^1$, $^+28^1 29^1 m^1$, and some $^+29^1$ vibtor bands.
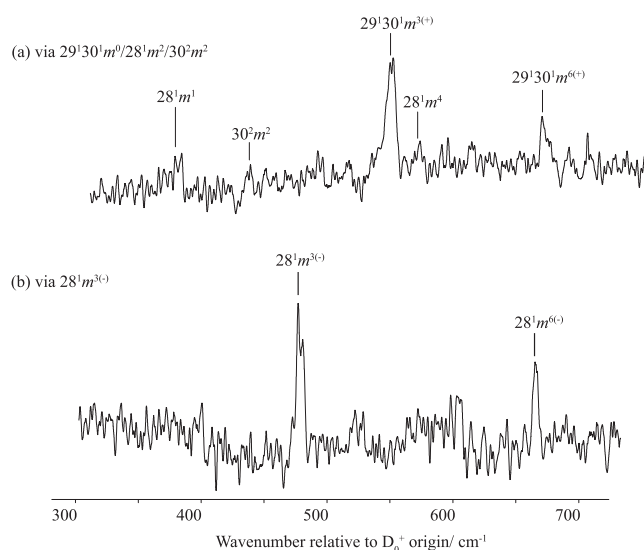
FIG. 7. ZEKE spectra recorded via the following intermediate S_1 levels: (a) the overlapped $29^1 30^1 m^0/28^1 m^2/30^2 m^2$ and (b) $28^1 m^{3(-)}$. The preceding superscripted "+" used in the text is omitted in the labels for clarity. See text for further discussion.

The ZEKE spectrum via $29^2 m^0$ [Fig. 8(a)] has the expected [by comparison with Fig. 3(a)] most-intense band as $^+29^2 m^{3(+)}$, with the other expected bands $^+29^2 m^0$, $^+29^2 m^{6(-)}$, and $^+29^2 m^{6(+)}$. We also observe the weak, symmetry-allowed vibtor band $^+29^1 m^{3(-)}$, noting that the symmetry-allowed vibtor band $^+29^1 m^{6(-)}$ could be overlapped with $^+29^2 m^{3(-)}$. Weak, symmetry-forbidden $^+29^1 m^{3(+)}$ (overlapped) and $^+29^1 m^{6(+)}$ bands are also tentatively assigned.
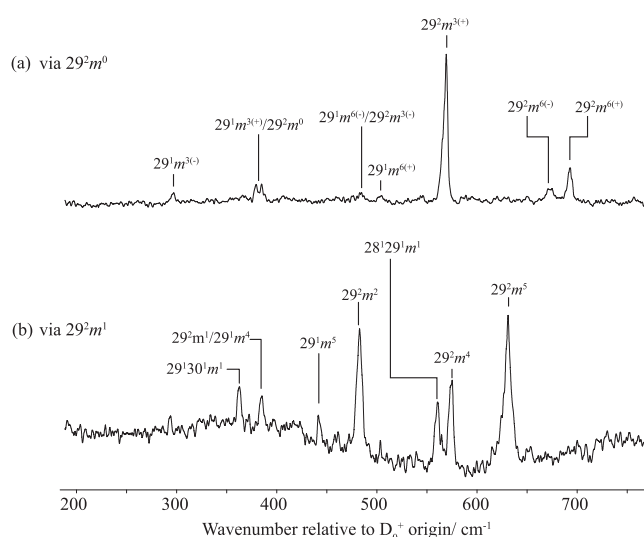

FIG. 8. ZEKE spectra recorded via the following intermediate S_1 levels: (a) $29^2 m^0$ and (b) $29^2 m^1$. The preceding superscripted "+" used in the text is omitted in the labels for clarity. See text for further discussion.

IV. DISCUSSION

A. The strong propensity away from $\Delta m = 0$ bands

One of the most prominent aspects of the spectra is that the $\Delta m = 0$ bands are not the most intense. Similar observations have been made in the mFT work of Ito et al.[25–27] and Weisshaar et al. on mClT.[29] This stems from the change in the global minimum from pseudo-trans in the S_1 state to pseudo-cis in the D_0^+ state;[28,29] these geometries are shown in Fig. 9. This implies that the phase of the torsional potential is different in the two states, which can be expressed as the sign of the V_3 parameter being different. Using the same convention as Lu et al.,[28] we use $\alpha = 0°$ to represent the pseudo-trans structure and V_3 positive and $\alpha = 180°$ for the pseudo-cis structure, where V_3 is negative. As noted above, the sign of the V_3 parameter does not change the energies or ordering of any of the torsional levels, and so the sign can only be directly deduced from the geometry.[42,43] However, the fact that there are different signs of V_3 between the S_1 and D_0^+ states is useful since it gives rise to a greater activity in the ZEKE spectra. Consequently, this gives more levels from which to deduce the torsional parameters.

Previous work has looked at both the form of the torsional potential in substituted benzenes with G_6 symmetry [Eq. (1)] and the values of the torsional parameters F, V_3, and V_6 in the three electronic states S_0, S_1, and D_0^+. Although an earlier microwave study[45] deduced values for these parameters in the S_0 state, two possible sets of values were offered. The recent study by Stewart et al.[22] has obtained revised values for these parameters, taking into account vibtor interactions, which are in reasonable agreement with one of the sets of values from Ref. 45 and with the low-level quantum chemical calculations by Lu et al.[28] Similarly, in the same study,[22] these parameters were deduced for the S_1 state and provide more robust values than those in the previous LIF study of Okuyama et al.,[24] where there were a number of misassignments.

As mentioned, Takazawa et al.[27] have deduced that the phases of the S_0 and S_1 torsional potentials are the same, but that they are out of phase with that for the D_0^+ state, in agreement with the geometries obtained in Ref. 28, and this is in agreement with the conclusions reached for mClT.[29] We have confirmed with B3LYP/aug-cc-pVTZ quantum chemistry calculations that, indeed, the S_0 and S_1 states have pseudo-trans global minima, while the D_0^+ state is pseudo-cis (see Fig. 9) so that V_3 in D_0^+ is negative. (Note that for the S_1 state, TD-B3LYP was employed, while for the D_0^+ state, UB3LYP was employed, $\langle S^2 \rangle = 0.76$.) This change in the phase between the S_1 and D_0^+ states was discussed in Refs. 27 and 29 in relation to the nondiagonal intensities seen in the spectra of mFT and mClT and seen in the present work.

As can be seen from Fig. 1(a), for m levels that are contained within the well, triplets of these move toward degeneracy as V_3 increases (see Sec. III B 3). Since previous work[27] has determined that V_3 in mFT$^+$ is around -300 cm^{-1}, we would expect this picture to hold here, as indeed is confirmed by the ZEKE spectra. As part of this evolution, V_3 leads to a separation of the $m = 3(\pm)$ levels, with $m = 3(+)$ moving toward the $m = 4$ level, and $m = 3(-)$ converging with the $m = 2$ level; thus, $m = 3(+)$ will lie above $m = 3(-)$ on the basis of this parameter alone. Since V_6 is generally very much smaller than V_3 for G_6 symmetry molecules, this ordering is not expected to change, as may be seen in Fig. 1(c); indeed, the variation of the energies of the m levels is rather small for V_6 values
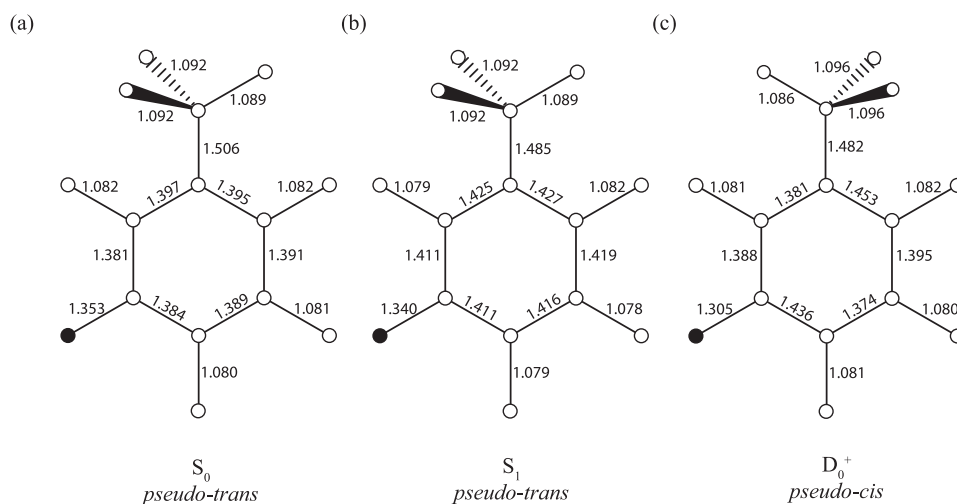
FIG. 9. Calculated geometries for the (a) S_0 (B3LYP/aug-cc-pVTZ), (b) S_1(TD-B3LYP/aug-cc-pVTZ), and (c) D_0^+ (UB3LYP/aug-cc-pVTZ) electronic states of m-fluorotoluene. The bond lengths are in Å. Note the differing conformation of the cation relative to the two neutral states. The filled circles represent the F atom, and the unfilled circles represent the C and H atoms.

of a few tens of cm^{-1}. (The value of F we employ here, 5.4 cm^{-1}, is significantly different to that employed by Ito and co-workers;[25–27] a similar value was used by the same group for the S_1 state[24–27] and this was discussed by Stewart et $al.$[22] and concluded to be physically unreasonable.) The principal differences between our assignments and those of Ref. 27 are the energies of the $^+m^{6(+)}$ and $^+m^7$ levels. The former is a slight difference that could result from estimating band centers, the second is a band that is reassigned in the present work to $^+30^1m^4$—i.e., a vibtor transition. In Refs. 24, 25, 26, and 27, vibtor transitions were not considered, and some similar reassignments were discussed in Ref. 22 for the S_1 state. For this reason, the present results and assignments are expected to be the more reliable.

B. Appearance of strong $^+m^{3(−)}$ and $^+m^{6(−)}$ bands, when exciting via m^0

Both the $m = 3(−)$ and $m = 6(−)$ levels have a_2 symmetry and are therefore symmetry forbidden when exciting via m^0. One explanation for the appearance of these symmetry-forbidden bands could be rotation-torsional coupling, which is the source of the weak activity for $m^{3(−)}$ in the S_1 state[21,22] [and this could also apply to the $m = 6(±)$ levels]. That the $m^{3(−)}$ REMPI band is very weak (see Fig. 2) in the present work is likely the result of the very cold rotational temperatures herein. In the cation, each of the $^+m^{3(±)}$ and $^+m^{6(±)}$ pairs of levels is more-separated energetically, and so we rule out a strong torsion-rotation coupling here and reject this as the main explanation for the appearance of the $^+m^{3(−)}$ and $^+m^{6(−)}$ ZEKE bands.

Since the S_1 $m = 0$ level is of a_1 symmetry, it is not expected to see the $^+m^{3(−)}$ and $^+m^{6(−)}$ bands in the ZEKE spectrum when exciting via this level; however, these bands are relatively strong. It is notable that vibrations with these corresponding symmetries are often seen in photoelectron spectra of relevant substituted benzenes. In our work on toluene[3] and pFT,[11] we also assigned the $^+m^{3(−)}$ band when exciting via S_1m^0. Recently, we discussed this issue in the D_{2h} molecule, pDFB,[46] where nontotally symmetric bands of b_{3u}, b_{2g},

and a_u symmetry were observed (these all correlate with a_2 symmetry in G_6). In that work, we argued that there were no excited cationic states of the correct symmetry to allow vibronic coupling to be the source of the intensity of these bands and we invoked a variant on the intrachannel coupling mechanism put forward by Poliakoff et $al.$,[47] adapting it to the production of the high-lying Rydberg states that are formed in the pulsed-field ionization ZEKE method.

Assuming that the corresponding excited states for mFT$^+$ are at relatively similar energies to those for pDFB$^+$ (Ref. 48) and then adapting the symmetries to G_6, it can be seen that it is now possible that vibronic coupling in mFT$^+$ is a mechanism for the observed torsional and vibrational activity as there are low-lying cation states of both a_1 and a_2 symmetry, albeit that it is unclear how strong this coupling would be.

Considering now the intrachannel coupling mechanism,[46,47] the basic idea is that the Rydberg electron interacts with the vibrations of the nuclear core and so does not require another electronic state to be involved, and we suggested in Ref. 46 that this was most likely for s and p Rydberg electrons, which are more penetrating. In the present G_6 case, the symmetries of these electrons are a_1 (s, p$_y$, and p$_z$) and a_2 (p$_x$), and so, when combining the electronic symmetry of the ground state cation (A_2) with that of the Rydberg electron, both a_1 and a_2 symmetry vibrations and torsions can be activated by this process. Hence, this also provides an explanation for the observation of symmetry-forbidden bands in the ZEKE spectra. It is plausible that both the vibronic and intrachannel coupling mechanisms are operating in mFT$^+$, with the intensity of each band depending on the strengths of these interactions.

Although we see symmetry-forbidden torsional levels of a_2 symmetry in the ZEKE spectra recorded when exciting via the S_1m^0 band, we do not see nontotally symmetric vibrations, suggesting that the coupling to the torsional motion is stronger than that to the low-frequency vibrations in mFT$^+$. That said, both $^+30^1m^0$ and $^+29^1m^0$ are seen weakly in the ZEKE spectrum recorded via $m^{3(+)}$ —see Fig. 3(c) and Table II, and $^+30^1m^1$ and $^+29^1m^1$ are seen weakly via S_1m^1 [Fig. 3(d) and Table II]. The fact that only low-frequency

vibrations or torsions are seen is consistent with these nuclear motions being on a time scale that allows interaction with the Rydberg electrons.

One final explanation would be movement of the CH_3 group off-axis as a result of interactions with vibrational motion, which is discussed further in Subsection IV C. In this case, the a_1 and a_2 classes combine, and this would make $^+m^{3(-)}$ and $^+m^{6(-)}$ transitions allowed.

C. The appearance of $^+m^5$ in the ZEKE spectrum via m^0

Under the normally strong selection rule of no change in torsional state symmetry, we expect to see transitions to only a_1 symmetry levels when exciting via m^0 and to only e symmetry levels when exciting via m^1. It is thus difficult to explain the observed activity of $^+m^5$ via S_1m^0, which involves an apparent change in nuclear symmetry. There are two possible explanations for this band.

Since we excite at wavenumbers where there is no significant overlap in the m^0 and m^1 band profiles, this excludes a dual excitation; furthermore, there are no obvious hot bands that would appear underneath m^0. One possibility is in terms of a coincident band, and among others, Lawrance and co-workers have shown that ^{13}C isotopologues of substituted benzenes give rise to features in the excitation spectrum that generally appear ~4 cm^{-1} to higher wavenumbers than the ^{12}C bands.[49] As such, by reference to Fig. 2, it may be seen that the ^{13}C-mFT m^1 band is expected to lie underneath the ^{12}C-mFT band, and as can be seen from Fig. 3(d), we expect a prominent $^+m^5$ band when exciting m^1. Since a $^{13}C/^{12}C$ substitution will not affect the torsional levels to an extent that will be discernible within the present resolution, we might expect to see a weak version of the m^1 ZEKE spectrum, arising from ^{13}C-mFT, to appear when exciting via ^{12}C-mFT m^0. To test if this is a possible explanation, in Fig. 10(a), we have overlaid the m^0 ZEKE spectrum with the m^1 ZEKE spectrum, scaled to match the intensities of the $^+m^5$ bands in the two spectra. As may be seen, both the $^+m^1$ and $^+m^2$ bands are not diagnostic since they are almost perfectly coincident with the $^+m^0$ and $^+m^{3(-)}$ bands, respectively, because of the large V_3 term (see Fig. 1). However, the $^+m^4$ band is displaced from the $^+m^{3(+)}$ band—see Fig. 3 and Table II—and from Fig. 10(a), it can be seen that there is no definitive evidence for the $^+m^4$ band in the m^0 ZEKE spectrum, although it is not possible to rule this out entirely.

We now highlight that no coupling with molecular motion can induce the activity for the $^+m^5$ transition in G_6, with translations, rotations, and vibrations all having a_1 or a_2 symmetry. In addition, there is no other vibtor level that can lead to the (e symmetry) $^+m^5$ activity via interactions, when exciting via the (a_1 symmetry) S_1 $m = 0$ level. It is possible to form localized e symmetry orbitals from the methyl H 1s orbitals,[25] and so it may be that such orbitals might give a mechanism for the activity of this band via torsion-electronic coupling.

Another explanation is a movement away from G_6 molecular symmetry, as has been discussed in relation to the precessing of the methyl group around the C_3 axis as it rotates.[28,50] Such geometric distortions have been termed "torsional flexing" and been shown to be described by the V_6 parameter.[51] This
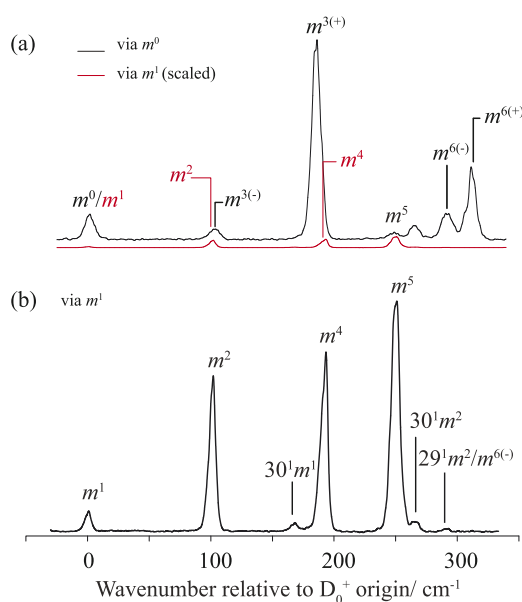

FIG. 10. (a) Overlay of the ZEKE spectrum via m^1 with that via m^0—the former spectrum has been scaled so that the $^+m^5$ bands have approximately the same intensity in both spectra. See text for discussion. (b) ZEKE spectrum via m^1 showing the band at ~292 cm^{-1} that can be assigned to $^+29^1m^2$ or $^+m^{6(-)}$. The preceding superscripted "+" used in the text is omitted in the labels for clarity. See text for further discussion.

would move the symmetry away from G_6, but if the methyl C–H bonds remained the same length, then the symmetry would become G_3, which would still retain e symmetry (with a_1 and a_2 combining to form a single a symmetry class, as mentioned in Subsection IV B).

A viable explanation requires the height of the torsional barrier to be sufficient to "lock" the torsional motion such that it is best described as a vibration of a C_s symmetry molecule. In these circumstances, the methyl C–H bond lengths would not be expected to be the same—as indeed they are not [Fig. 9(c)]. Then, the "torsions" could be described as a'' symmetry vibrations, which could gain an activity via vibronic or intrachannel coupling, as described in Sec. IV B. We agree that it is strange that we only see $^+m^5$, but this could be an intensity effect.

We also note that in the ZEKE spectra recorded via e symmetry levels in Figs. 3(d)–3(g), we see a band at ~292 cm^{-1}. One possible assignment of this is to $^+29^1m^2$, but it is also possible that this could be $^+m^{6(-)}$—see Fig. 10(b). If the latter were the case, then this would be an a_2 symmetry band observed via an e symmetry level, again breaking the a/e selection rule, and again being consistent with a geometric distortion away from G_6 symmetry. (Interestingly—see Fig. 1—the $^+m^5$ and $^+m^{6(-)}$ levels are the two levels that converge as V_3 increases, to form the third quantum of the torsion vibration.) We also comment that the $^+m^5$ band was seen in the ZEKE study of mFT by Takazawa et al.[27] although it was not commented upon—indeed, in their Appendix, they specifically note that no $a \leftrightarrow e$ symmetry transitions were observed even though this band is clearly in their spectrum.

In summary, there are two plausible explanations for the appearance of the $^+m^5$ band when exciting via m^0: an overlap with the ^{13}C-mFT m^1 band or a significant geometric distortion away from G_6 symmetry. Although not definitive, the significant magnitude of V_3 and no definitive evidence for the expected $^+m^4$ band in Fig. 10(a) lead us tentatively to favor the latter explanation. A mass-analyzed threshold ionization (MATI) experiment would be useful in deciding between the two interpretations discussed.

D. Interactions involving the $^+30^1$ and $^+30^2$ vibtor levels

One aspect of the ZEKE spectra that stands out is the activity of the D_{30} vibration via various vibtor levels, including both the fundamental and the first overtone. (The expectation that such a structure would be seen was expressed in Ref. 22.) This covers general activity as well as several unusually intense or weak bands. Because of this activity, we have been able to ascertain the band positions of many vibtor levels involving this vibration (see Table II). In so doing, we conclude that the torsional potential appears to be modified when this vibration is excited—see below.

In Fig. 3, it may be seen that there is the activity of $^+30^1 m^{3(-)}$ when exciting via m^0 and a weak $^+30^1 m^0$ band when exciting via $m^{3(+)}$; there is also a weak $^+29^1 30^1 m^0$ band observed when exciting via m^0. A series of e symmetry vibtor bands involving $^+30^1$ are seen when exciting via the four e symmetry torsional levels m^1, m^2, m^4, and m^5. Particularly noticeable is the abnormally intense $^+30^1 m^4$ band when exciting via m^4 [see Fig. 3(f)]; the activity of this band is echoed by the unexpectedly intense $^+30^2 m^4$ band, seen when exciting via $30^1 m^4$ [Fig. 4(b)]. We also see a number of vibtor bands involving both $^+30^1$ and $^+30^2$ when exciting via $21^1 m^1$ [Fig. 6(b)]; this richness in structure can be contrasted with the very simple spectrum observed via $21^1 m^0$. Also, such a $^+30^1$ activity is not seen when exciting via the 29^2 bands, except for $^+29^1 30^1 m^1$ [Fig. 8(b)]. We also see weak $^+21^1$ vibtor bands when exciting via the 30^2 levels—see Fig. 5.

In Fig. 11, we show portions of ZEKE spectra showing the a_1/a_2 torsional levels when exciting via m^0, together with the corresponding $^+30^1$ and $^+30^2$ vibtor levels, obtained when exciting through the $30^1 m^{3(-)}$ and $30^2 m^0$ intermediate levels. (Ideally, we would have recorded a ZEKE spectrum via the $30^1 m^0$ level; however, this transition is not seen in the REMPI spectrum.) The 30^1 spectra have been offset to align the $^+30^1 m^0$ and $^+30^2 m^0$ bands with the $^+m^0$ band. It may be seen that there is a slight shift in the $^+30^1$ vibtor bands to lower wavenumber with respect to the corresponding torsional ones and somewhat more so for the $^+30^2$ ones. In a similar way, in Fig. 12, we show portions of ZEKE spectra that show the e torsional levels when exciting via m^1, together with the corresponding $^+30^1$ and $^+30^2$ vibtor levels, obtained when exciting through the $30^1 m^4$ and $30^2 m^1$ intermediate levels. (Similar to the above comment, it would have been useful to have recorded a ZEKE spectrum via the $30^1 m^1$ level; however, this transition is not seen in the REMPI spectrum.) The 30^1 and 30^2 spectra have been offset to align the $^+30^1 m^1$ and $^+30^2 m^1$ bands with the $^+m^1$ band. The $^+30^1$ vibtor bands appear to have shifted with respect to the corresponding torsional ones, with the $^+30^2$ bands having shifted more so. It is also noticeable that the $^+30^1 m^4$ and $^+30^2 m^4$ bands appear to be shifted
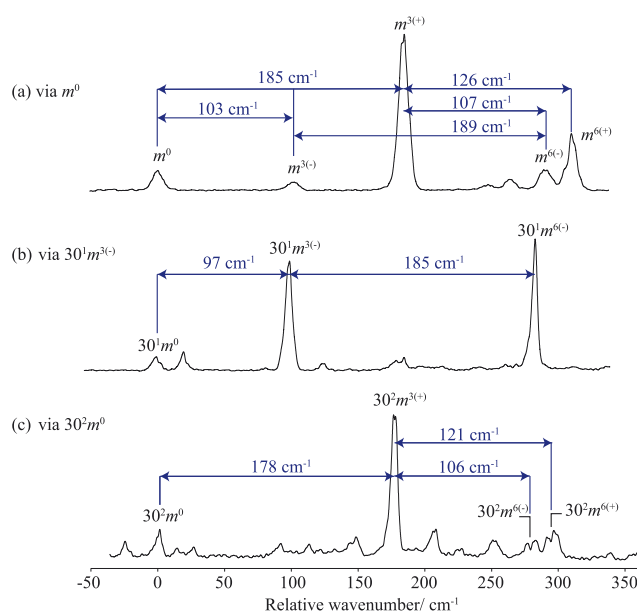

FIG. 11. Sections of ZEKE spectra recorded via the following a_1 symmetry intermediate S_1 levels: (a) $0^0 m^0$, (b) $30^1 m^{3(-)}$, and (c) $30^2 m^0$. The spectra in (b) and (c) have been shifted so that their respective $^+m^0$ vibtor transitions are aligned with $^+m^0$. Different spacings between the corresponding torsional levels are evident. The preceding superscripted "+" used in the text is omitted in the labels for clarity. See text for further discussion.

from the expected position—see Table II and comments below. We interpret these observations as suggesting that the torsional potential is modified from that of the vibrationless case; however, to gain quantitative information on this, a full analysis including anharmonicity, vibration-torsional coupling, and variation of the torsional parameters would be required—this is in progress by Lawrance and Gascooke (Flinders University, Adelaide) and will be the subject of a forthcoming publication. A vibration-modified potential can be rationalized by looking at the calculated vibrational mode diagram for D_{30} in Fig. 13. We can see that the motion involves the two *ortho* hydrogen atoms to the methyl group moving out of plane in sync, while the methyl group moves out-of-phase with this. In addition, it is clear that there is torsional motion of the methyl group also.

The significant activities of $^+30^1 m^4$ when exciting via m^4 and of $^+30^2 m^4$ when exciting via $30^1 m^4$ [see Figs. 3(f) and 4(b)] are in contrast to the corresponding $^+29^1$ vibtor bands. It may be seen from Fig. 13 that D_{29} also contains an element of torsional motion. Furthermore, $^+m^4$ is closer in wavenumber to $^+29^1$ than to $^+30^1$. Together, this suggests that the coupling of the vibrational and torsional motions is very specific. Indeed, in the S_1 state, it was also concluded that the D_{30} vibration coupled to the torsions more efficiently than did D_{29}.[22] In the case of mFT, the D_{30} motion appears to be key in coupling to the torsional motion although other vibrations such as D_{29} are also involved. In previous work, it has been noted that vibrations that involve motions close to the coordinate that demonstrates high-amplitude motion[52–54] are expected to show increased coupling. However, we have noted in very recent work[18]
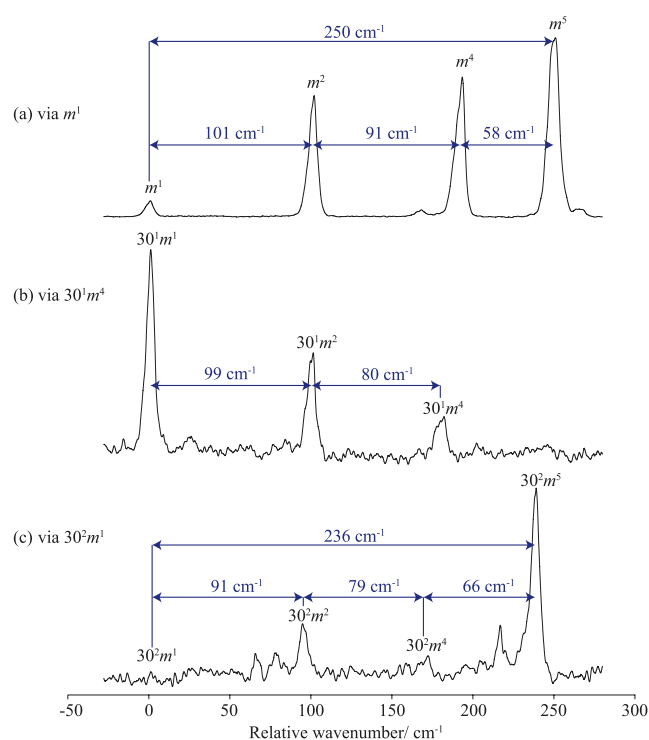
FIG. 12. Sections of ZEKE spectra recorded via the following e symmetry intermediate S_1 levels: (a) $0^0 m^1$, (b) $30^1 m^4$, and (c) $30^2 m^1$. The spectra in (b) and (c) have been shifted so that their respective $^+m^1$ vibtor transitions are aligned with $^+m^1$. Different spacings between the corresponding torsional levels are evident. The preceding superscripted "+" used in the text is omitted in the labels for clarity. See text for further discussion.
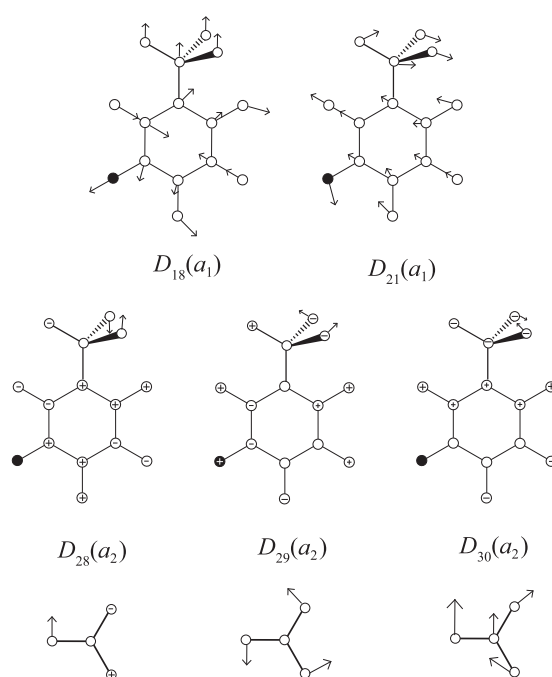

FIG. 13. Calculated vibrational mode diagrams for m-fluorotoluene$^+$. For the three out-of-plane (a_2 symmetry) vibrations at the bottom of the figure, the motion of the CH_3 group is indicated, as viewed along its C_3 axis.

that it is important to look at the whole motion of a vibration. The present work demonstrates that even then, there are subtleties as to which vibrations couple most efficiently.

Previous workers[28] have discussed the precession of the methyl group and variations in geometric parameters as a function of the torsional angle. Indeed, it has been shown that such precession may be equated with an altered V_6 contribution to the potential.[51] However, we have noted in the above that, for example, the observation of $^+m^5$ when exciting via the origin is inconsistent with the maintenance of equal C–H bond lengths in the methyl group. We have tentatively suggested that this is a result of the CH_3 geometry being distorted significantly in the cation [see Fig. 9(c)], relaxing selection rules based on the G_6 MSG, and moving toward selection rules based on the C_s point group. Since an infinitely high barrier fixes the methyl group, there must be a means by which the potential evolves fully from G_6 to C_s, and this cannot occur simply by variation of V_3 and V_6, which arise from a maintained C_3 rotational axis in the CH_3 group.

It can be seen from Table II that there is a change in the expected ordering of some of the vibtor levels. For example, $^+30^1 m^4$ appears too low (below $^+30^1 m^{3(-)}$). This could arise from an interaction with $^+m^7$, with the former being expected at 355–360 cm^{-1}, and the latter at ~368 cm^{-1}. Consistent with this, $^+m^7$ is seen in the

ZEKE spectrum in Fig. 4(b). Interestingly, m^7 is seen in emission in Ref. 22 although the m^7 band is not seen in the present REMPI, nor the fluorescence spectra of that work.

It can also be seen that the $^+30^2 m^4$ level has been pushed below the $^+30^2 m^{3(-)}$ level. Although we do not see the $^+30^1 m^7$ band, a possible $^+30^1 m^7 \dots ^+30^2 m^4$ interaction is plausible, as a counterpart to the $^+30^1 m^4 \dots ^+m^7$ interaction. It is likely that there are other weak vibtor interactions occurring throughout the region.

E. Other vibrations

In Table II, the relative wavenumbers of the torsional levels associated with a number of vibrations are tabulated. These have been extracted from our ZEKE spectra and cross-checked where possible. We have commented on the $^+30^1$ and $^+30^2$ levels in Subsection IV D and implied that there are shifts for the $^+29^1$ levels but that these are small. We also see small shifts for the $^+29^2$ and $^+29^1 30^1$ levels and note that all of these involve out-of-plane vibrations. On the other hand, no noticeable shifts are seen for the in-plane vibrations, $^+18^1$ and $^+21^1$. It can be seen from their mode diagrams (Fig. 13) and symmetry that there is no torsional aspect to their motions, which may underlie the lack of interaction between these vibrations and the torsion. Interestingly, there also seems to be no interaction between $^+28^1$ and the torsion, despite this being an out-of-plane mode; this is not unexpected when looking at its motion (Fig. 13), which also does not contain any obvious torsional motion.

TABLE III. Calculated and experimental wavenumbers for the vibrations pertinent to the present study.

Symmetry	D_i	S$_1$		D$_0^+$	
		Calculated[a]	Experimental	Calculated[b]	Experimental[c]
a_1	18	459		509	510
	21	281	284[d]	290	296
a_2	28	241	258[d,e]	373	372
	29	184	173[d]	190	194[f]
	30	122	127[d]	167	167

[a]TD-B3LYP/aug-cc-pVTZ, scaled by 0.97. Note that these values replicate those at an essentially identical level of theory published in Ref. 22.
[b]UB3LYP/aug-cc-pVTZ, scaled by 0.97; $\langle S^2 \rangle = 0.76$.
[c]Present work.
[d]From Ref. 22.
[e]From Ref. 24.
[f]The fundamental value for $^+29^1$ is tentative.

In Table III, we give the experimental and calculated wavenumbers for the vibrations discussed in the present work. Generally, the agreement between the two sets of values is good; similarly good agreement was found for the vibrations in the S$_0$[22,35] and S$_1$[22] states. Ongoing work in our group is focusing on higher-wavenumber vibrations.

F. Discussion of the origin of the barriers

Lu *et al.*[28] have discussed the barriers in various methyl-substituted benzenes, concentrating on the S$_0$ and D$_0^+$ states. They calculated the equilibrium geometries and barrier heights, finding relatively good agreement for the latter between calculated and experimental values; the calculations thus identified the sign of the V_3 barrier in many cases. In discussing the V_3 barriers in the S$_0$ state, it was the steric interaction between the methyl hydrogen atoms and the *ortho* hydrogen atoms that was key, and this was also the case for the V_6 barrier in molecules that belonged to the G_{12} MSG, which has been discussed previously.[18,55,56] When V_3 was large, the barrier was discussed in terms of asymmetry in the two C–C bonds that neighbored the C–CH$_3$ bond, with a relationship being found between the difference in bond order of the two C–C bonds and the barrier height. Furthermore, it was found that for mFT$^+$, the geometry was *pseudo-cis* in the cation, as we find—Fig. 9(c). As far as we can see, there was no explicit rationale as to the link between the bond order difference and the barrier height; however, it was implied that it was to do with the location of the positive charge following ionization of mFT. This charge is concentrated in one of the aforementioned C–C bonds neighboring the methyl group, with the other concentration being in a C–C bond neighboring the C–F bond; this is embodied in those bond lengths, as can be seen in Fig. 9(c). The *pseudo-cis* geometry has the in-plane methyl hydrogen on the opposite side to the C–C bond with the localized positive charge, thus reducing the Coulombic repulsion between the δ+ methyl H atoms and the positive charge localized in one of the adjoining C–C bonds; further-more, it is then intuitively clear then why the bond order difference of the two C–C bonds neighboring the methyl group, being linked

to the difference in charge density, is explicitly linked to the barrier height.

It is an interesting conclusion from previous work from Weisshaar's group[28,29] that for both mFT$^+$ and mClT$^+$, the equilibrium geometry was *pseudo-cis* and the barriers were very similar. It was concluded that the type of substituent determined the π electron density structure and this in turn dominated the sign and value of the V_3 parameter. It would be useful to explore this conclusion further.

Considering the interaction between some out-of-plane vibrations and the torsional motion, we note that in the cation, this lowers the barrier slightly for D_{30} vibtor levels. Since the barrier appears to originate predominantly from the asymmetry in the interaction with the π-electron charge density, it appears logical that moving the methyl group out of plane lowers this interaction somewhat.

V. CONCLUSIONS

In the present work, we have recorded ZEKE spectra via many of the S$_1$ levels below 350 cm^{-1}. These consist of torsions, low-frequency vibrations, and vibtor levels. The activity we see, which confirms the assignments deduced in Ref. 22 from 2D-LIF spectra, allows the largest number of torsion and vibtor levels to be observed for a single molecule to date. This has allowed detailed information to be deduced on the torsional and vibration-torsional levels in the cation. This provides persuasive evidence that the torsional potential itself is altered by particular vibrational motions. In addition, a number of vibtor levels are likely involved in more localized interactions, and this will be explored further in future work with the Lawrance group at Flinders University and will form part of a future publication. We also have discussed the possibility that the spectroscopy may be indicating a definitive shift away from G_6 molecular symmetry and that the molecule is starting to behave more like a C_s molecule. We have also reported values for five cationic vibrational wavenumbers.

Future ZEKE and 2D-LIF work will look at higher-lying vibrations, where we hope to gain insight into the explicit levels involved

in the switch to dissipative IVR and, by comparison to our work on pFT,[16,18] the differences that underpin the more-rapid IVR that occurs for mFT than pFT, as investigated by Timbers *et al.*[21] This comparison should provide further illumination into the substituent positional effect.

ACKNOWLEDGMENTS

REFERENCES

[1] J. A. Davies, A. M. Green, A. M. Gardner, C. D. Withers, T. G. Wright, and K. L. Reid, Phys. Chem. Chem. Phys. **16**, 430 (2014).

[2] A. M. Gardner, A. M. Green, V. M. Tamé-Reyes, K. L. Reid, J. A. Davies, V. H. K. Parkes, and T. G. Wright, J. Chem. Phys. **140**, 114308 (2014).

[3] A. M. Gardner, A. M. Green, V. M. Tamé-Reyes, V. H. K. Wilton, and T. G. Wright, J. Chem. Phys. **138**, 134303 (2013).

[4] E. A. Virgo, J. R. Gascooke, and W. D. Lawrance, J. Chem. Phys. **140**, 154310 (2014).

[5] J. R. Gascooke, E. A. Virgo, and W. D. Lawrance, J. Chem. Phys. **142**, 024315 (2015).

[6] J. R. Gascooke, E. A. Virgo, and W. D. Lawrance, J. Chem. Phys. **143**, 044313 (2015).

[7] J. R. Gascooke and W. D. Lawrance, J. Mol. Spectrosc. **318**, 53 (2015).

[8] V. L. Ayles, C. J. Hammond, D. E. Bergeron, O. J. Richards, and T. G. Wright, J. Chem. Phys. **126**, 244304 (2007).

[9] C. J. Hammond, V. L. Ayles, D. E. Bergeron, K. L. Reid, and T. G. Wright, J. Chem. Phys. **125**, 124308 (2006).

[10] J. A. Davies and K. L. Reid, J. Chem Phys. **135**, 124305 (2011).

[11] A. M. Gardner, W. D. Tuttle, L. Whalley, A. Claydon, J. H. Carter, and T. G. Wright, J. Chem. Phys. **145**, 124307 (2016).

[12] J. R. Gascooke, L. D. Stewart, P. G. Sibley, and W. D. Lawrance, J. Chem. Phys. **149**, 074301 (2018).

[13] W. D. Tuttle, A. M. Gardner, L. E. Whalley, and T. G. Wright, J. Chem. Phys. **146**, 244310 (2017).

[14] A. M. Gardner, W. D. Tuttle, L. E. Whalley, and T. G. Wright, Chem. Sci. **9**, 2270 (2018).

[15] W. D. Tuttle, A. M. Gardner, L. E. Whalley, D. J. Kemp, and T. G. Wright, Phys. Chem. Chem. Phys. **21**, 14133 (2019).

[16] D. J. Kemp, A. M. Gardner, W. D. Tuttle, and T. G. Wright, "Unravelling overlaps and torsion-facilitated coupling using two-dimensional laser-induced fluorescence," Mol. Phys. (in press).

[17] D. J. Kemp, L. E. Whalley, A. M. Gardner, W. D. Tuttle, L. G. Warner, and T. G. Wright, J. Chem. Phys. **150**, 064306 (2019).

[18] D. J. Kemp, W. D. Tuttle, A. M. Gardner, L. E. Whalley, and T. G. Wright, J. Chem. Phys. **151**, 064308 (2019).

[19] A. M. Gardner, W. D. Tuttle, P. Groner, and T. G. Wright, J. Chem. Phys. **146**, 124308 (2017).

[20] W. D. Tuttle, A. M. Gardner, K. B. O'Regan, W. Malewicz, and T. G. Wright, J. Chem. Phys. **146**, 124309 (2017).

[21] P. J. Timbers, C. S. Parmenter, and D. B. Moss, J. Chem. Phys. **100**, 1028 (1994).

[22] L. D. Stewart, J. R. Gascooke, and W. D. Lawrance, J. Chem. Phys. **150**, 174303 (2019).

[23] J. R. Gascooke and W. D. Lawrance, Eur. Phys. J. D **71**, 287 (2017).

[24] K. Okuyama, N. Mikami, and M. Ito, J. Phys. Chem. **89**, 5617 (1985).

[25] K. Takazawa, M. Fujii, T. Ebata, and M. Ito, Chem. Phys. Lett. **189**, 592 (1992).

[26] M. Ito, K. Takazawa, and M. Fujii, J. Mol. Struct. **292**, 9 (1993).

[27] K. Takazawa, M. Fujii, and M. Ito, J. Chem. Phys. **99**, 3205 (1993).

[28] K.-T. Lu, F. Weinhold, and J. C. Weisshaar, J. Chem. Phys. **102**, 6787 (1995).

[29] S. H. Feldgus, M. J. Schroeder, R. A. Walker, W.-K. Woo, and J. C. Weisshaar, Int. J. Mass Spectrom. Ion Processes **159**, 231 (1996).

[30] E. B. Wilson, Jr., Phys. Rev. **45**, 706 (1934).

[31] G. Varsányi, *Assignments of the Vibrational Spectra of Seven Hundred Benzene Derivatives* (Wiley, New York, 1974).

[32] R. S. Mulliken, J. Chem. Phys. **23**, 1997 (1955).

[33] G. Herzberg, *Molecular Spectra and Molecular Structure II. Infrared and Raman Spectra of Polyatomic Molecules* (Krieger, Malabar, 1991).

[34] A. M. Gardner and T. G. Wright, J. Chem. Phys. **135**, 114305 (2011).

[35] D. J. Kemp, W. D. Tuttle, F. M. S. Jones, A. M. Gardner, A. Andrejeva, J. C. A. Wakefield, and T. G. Wright, J. Mol. Spectrosc. **346**, 46 (2018).

[36] P. A. Graham and S. H. Kable, J. Chem. Phys. **103**, 6426 (1995).

[37] W. D. Tuttle, A. M Gardner, and T. G. Wright, Chem. Phys. Lett. **684**, 339 (2017).

[38] E. Fermi, Z. Phys. **71**, 250 (1931).

[39] J. R. Gascooke and W. D. Lawrance, J. Chem. Phys. **138**, 134302 (2013).

[40] N. T. Whetton and W. D. Lawrance, J. Phys. Chem. **93**, 5377 (1989).

[41] L. H. Spangler, Annu. Rev. Phys. Chem. **48**, 481 (1997).

[42] R. D. Gordon and J. M. Hollas, Chem. Phys. Lett. **164**, 255 (1989).

[43] J. D. Lewis, T. B. Malloy, Jr., T. H. Chao, and J. Laane, J. Mol. Struct. **12**, 427 (1972).

[44] X. Zhang, J. M. Smith, and J. L. Knee, J. Chem. Phys. **97**, 2843 (1992).

[45] H. D. Rudolph and A. Trankaus, Z. Naturforsh. A **23a**, 68 (1968).

[46] D. J. Kemp, A. M Gardner, W. D. Tuttle, J. Midgley, K. L. Reid, and T. G. Wright, J. Chem. Phys. **149**, 094301 (2018).

[47] G. J. Rathbone, E. D. Poliakoff, J. D. Bozek, and R. R. Lucchese, Can. J. Chem. **82**, 1043 (2004).

[48] S.-Y. Yu and M.-B. Huang, J. Mol. Struct.: THEOCHEM **822**, 48 (2007).

[49] J. R. Gascooke and W. D. Lawrance, Chem. Phys. Lett. **555**, 38 (2013).

[50] X.-Q. Tan and D. W. Pratt, J. Chem. Phys. **100**, 7061 (1994).

[51] R. M. Lees, J. Chem. Phys. **59**, 2690 (1973).

[52] G. A. Bethardy, X. Wang, and D. S. Perry, Can. J. Chem. **72**, 652 (1994).

[53] D. S. Perry, G. A. Bethardy, and X. Wang, Ber. Bunsengesellschaft Phys. Chem. **99**, 530 (1995).

[54] R. Pearman and M. Gruebele, Z. Phys. Chem. **214**, 1439 (2000).

[55] D. B. Moss, C. S. Parmenter, and G. E. Ewing, J. Chem. Phys. **86**, 51 (1987).

[56] J. A. Davies, L. E. Whalley, and K. L. Reid, Phys. Chem. Chem. Phys. **19**, 5051 (2017).

14. Torsions, low-frequency vibrations and vibration-torsion ("vibtor") levels in the *m*-chlorotoluene cation:

Contributions:

This work consists of a series of analysed REMPI and ZEKE spectra. These were collected by myself as well as an undergraduate project student under my supervision: Lewis Warner.

My contributions were mainly through comparison of spectra between the series of data in this work, and those from our recent *m*-fluorotoluene study, and deducing and understanding the differences. Many discussions were had between myself and Timothy Wright regarding the electronic and vibrational activity seen.

Figure production and assignments was done by myself. Deliberation and communication regarding what to put on figures and how to best present the content was had with Timothy Wright.

Torsions, low-frequency vibrations, and vibration–torsion ("vibtor") levels in the *m*-chlorotoluene cation

View Online   Export Citation   CrossMark

David J. Kemp, Lewis G. Warner, and Timothy G. Wright[a]   iD

AFFILIATIONS

School of Chemistry, University of Nottingham, University Park, Nottingham NG7 2RD, United Kingdom

[a]Author to whom correspondence should be addressed: Tim.Wright@nottingham.ac.uk

ABSTRACT

Zero-electron-kinetic-energy (ZEKE) spectra are presented for *m*-chlorotoluene (*m*ClT), employing different low-lying torsional and vibration–torsional ("vibtor") levels of the S_1 state as intermediates. The adiabatic ionization energy is determined to be 71 319 cm^{-1} ± 5 cm^{-1} (8.8424 ± 0.0006 eV). It is found that the activity in the ZEKE spectra varies greatly for different levels and is consistent with the assignments of the S_1 levels of *m*-fluorotoluene (*m*FT) deduced in the recent fluorescence study of Stewart *et al.* [J. Chem. Phys. **150**, 174303 (2019)] and the ZEKE study from Kemp *et al.* [J. Chem. Phys. **151**, 084311 (2019)]. As with *m*FT, the intensities in the ZEKE spectra of *m*ClT are consistent with a phase change in the torsional potential upon ionization, allowing a large number of torsions and vibtor levels to be observed for the cation. Vibration-induced modifications of the torsional potential are discussed. Calculated vibrational wavenumbers for the S_0, S_1, and $D_0{}^+$ states are also presented.

Published under license by AIP Publishing. https://doi.org/10.1063/1.5142992

I. INTRODUCTION

Energy flow in molecules is now generally accepted as being facilitated by the coupling of both methyl torsion and vibrational motions and so is important for understanding the photophysics of molecules.[1,2] A very recent example highlights the role vibrational excitation has in light harvesting.[3] Understanding the processes occurring in complicated molecules is greatly aided by detailed studies on small molecules, and recent examples from our and Reid and Lawrance groups have looked at toluene,[4–6] *para*-fluorotoluene (*p*FT),[7–15] and *para*-xylene (*p*Xyl),[10,16,17] using a combination of fluorescence and photoionization spectroscopies. These studies elucidated how vibration–vibration and vibration–torsion coupling can drive the transition to statistical ("dissipative") intramolecular vibrational redistribution (IVR), underpinning energy dispersal and photostability.[10,12]

Timbers *et al.*[18] concluded that *meta*-fluorotoluene (*m*FT) undergoes IVR more than an order of magnitude faster than *p*FT, showing that the location of substituents is likely to be important in the coupling. Recently, Stewart *et al.*[19] examined

the first 350 cm^{-1} of the $S_1 \leftarrow S_0$ transition of *m*FT, assigning the spectra with the use of two-dimensional laser-induced fluorescence (2D-LIF), and in a follow-up study,[20] we studied the same S_1 energy levels using zero-electron-kinetic-energy (ZEKE) spectroscopy. The spectra were assigned in terms of torsional and vibration–torsional ("vibtor") levels in the S_0, S_1, and $D_0{}^+$ states.

Stewart *et al.*[19] concluded that there are interactions between the torsional motion and low frequency vibrations in both the S_0 and the S_1 states of *m*FT and postulated that such interactions may be present in the cation. In Ref. 20, we confirmed the latter suggestion, and highlighted that in the cation, the torsional potential was being altered by the vibrational motion. In the present work, we wish to explore whether the same interactions occur in *m*-chlorotoluene (*m*ClT). Of course, vibrational wavenumbers may alter with a different substituent and this is likely to affect vibtor interactions. The present work on *m*ClT builds upon the work of Ichimura *et al.*,[21] who recorded laser-induced fluorescence (LIF) and dispersed fluorescence (DF) spectra, and of Feldgus *et al.*,[22] who reported a resonance-enhanced multiphoton ionization (REMPI)

spectrum and zero-electron-kinetic-energy (ZEKE) spectra via a handful of the lowest-wavenumber S_1 levels.

II. EXPERIMENTAL

The REMPI/ZEKE apparatus employed was the same as that used in earlier work.[23] The focused, frequency-doubled outputs of two dye lasers (Sirah CobraStretch) were overlapped spatially and temporally, and passed through a vacuum chamber coaxially and counterpropagating, where they intersected a free jet expansion of mClT (Alfa Aesar, 98% purity) in 1.5 bar Ar. The sample container and nozzle were heated to ~50 °C to obtain a high enough vapor pressure to give a strong signal. The excitation laser operated with Coumarin 540A and was pumped with the third harmonic (355 nm) of a Surelite III Nd:YAG laser, while the ionization laser operated with Pyrromethene 597, pumped with the second harmonic (532 nm) of a Surelite I Nd:YAG laser. All spectra presented in the present work were recorded in the ^{35}Cl isotopologue mass channel, although spectra were also recorded separately in the ^{37}Cl isotopologue mass channel, but no significant shifts were seen over the spectral range scanned herein.

The jet expansion passed between two biased electrical grids located in the extraction region of a time-of-flight mass spectrometer, which was employed in the REMPI experiments. These grids were also used in the ZEKE experiments by application of pulsed voltages, giving typical fields of ~10 V cm^{-1}, after a delay of up to 2 μs; this delay was minimized while avoiding the introduction of excess noise from the prompt electron signal. The resulting ZEKE bands had widths of ~5 cm^{-1} to 7 cm^{-1}. Electron and ion signals were recorded on separate sets of microchannel plates.

III. RESULTS AND ASSIGNMENTS

A. Nomenclature and labeling

1. Vibrational and torsional labeling

We employ the D_i labels from Ref. 24 for the vibrations of mClT as used in the recent work by Stewart *et al.*[19] and ourselves for mFT[20]—see Table I. This C_s point group labeling scheme[24] is based on the vibrations of the *meta*-difluorobenzene (mDFB) molecule, developed to be applicable to both symmetric and asymmetric substitutions. We note that Ichimura *et al.*[21] employed Wilson labels in their jet-cooled fluorescence study, which do not describe the motions very well.[24] Therefore, in Table I, we "translated" these into the D_i labels for both the S_0 and the S_1 states. It may be seen that the gas phase DF values[21] for the S_0 state agree well with earlier infrared and Raman values (discussed in depth in Ref. 24). Both the DF and the LIF values for the S_0 and S_1 states are in good agreement with the calculated values.

Since the G_6 molecular symmetry group (MSG) is appropriate for vibtor levels in mClT, we shall use these symmetry labels throughout. In addition, torsional levels will be labeled via their m quantum number—see Ref. 16 or 19. The correspondence between the C_s point group labels and the G_6 MSG ones is given in Table II. To calculate the overall symmetry of a vibtor level, it is necessary to use the corresponding G_6 label for the vibration, and then find the direct product with the symmetry of the torsion (Table II), noting

that a C_{3v} point group direct product table can be used, since the G_6 MSG and the C_{3v} point group are isomorphic.

Under the free-jet expansion conditions employed here, almost all of the molecules are expected to be cooled to their zero-point vibrational level, and thus essentially all $S_1 \leftarrow S_0$ pure vibrational excitations are expected to be from this level. In contrast, owing to nuclear-spin and rotational symmetry,[16] the molecules can be in one of either the $m = 0$ or $m = 1$ torsional levels in the S_0 state.

2. Transitions and coupling

When designating excitation transitions, we shall generally omit the lower level, since it will be obvious from the jet-cooled conditions. In the usual way, vibrational transitions will be indicated by the cardinal number, i, of the D_i vibration, followed by a super-/subscript specifying the number of quanta in the upper/lower states, respectively; torsional transitions will be indicated by m followed by its value. Finally, vibtor transitions will be indicated by a combination of the vibrational and torsional transition labels (see Ref. 20, and below, for specific examples).

As has become common usage, we will generally refer to a level using the notation of a transition, with the level indicated by the specified quantum numbers, with superscripts indicating levels in the S_1 state and, when required, subscripts indicating levels in the S_0 state. Since we will also be referring to transitions and levels for the ground state cation, D_0^+, we shall indicate those as superscripts in the text, but with an additional single preceding superscripted + sign. (These signs are omitted in the figures for clarity.) Relative wavenumbers of the levels will be given with respect to the $m = 0$ zero-point vibrational level in each electronic state (again, see Ref. 20, and below, for specific examples.).

For cases where the geometry and the torsional potential are similar in both the S_1 and the D_0^+ states, the most intense transition is expected to be that for which no changes in the torsional and/or vibrational quantum numbers occur: these will be designated as $\Delta m = 0$, $\Delta v = 0$, or $\Delta(v, m) = 0$ transitions, as appropriate. However, as will be seen, and as was reported for mFT,[20] the $\Delta m = 0$ and $\Delta(v, m) = 0$ transitions are almost always not the most intense bands in the ZEKE spectra, suggesting a significant change in the torsional potential upon ionization.

If two levels are close in wavenumber and have the same overall symmetry, then (except between vibrational fundamentals, to first order) interactions can occur, with the simplest example being the anharmonic interaction between two vibrational levels—the classic Fermi resonance.[25] For molecules that contain a hindered internal rotor then, if vibration–torsional coupling is present, interactions can also involve torsional or "vibtor" levels. The end result of such interactions is the formation of eigenstates with mixed character. Such couplings are only expected to be significant for small changes, $\Delta v \approx 3$, of the vibrational quantum number, and also for changes, Δm, of 0, ±3, or ±6 in the torsional quantum number in the descending order of likely strength.[26,27] Often the eigenstates will be referred to by the dominant contribution, with the context implying if an admixture is present.

3. Torsional energies

The energy levels of a hindered methyl rotor have been the subject of numerous studies, with the paper by Spangler[28] being a

TABLE I. Calculated and experimental vibrational wavenumbers (cm^{-1}) for mClT in the S_0, S_1, and D_0^+ states.[a]

D_i [b]	S_0		S_1		D_0^+	
	Calculated	Experiment	Calculated	Experiment	Calculated	Experiment
			a$_1$			
D_1	3109	3085	3127		3119	
D_2	3089	3064	3113		3109	
D_3	3087		3122		3110	
D_4	3071		3080		3089	
D_5	1562	1578	1489		1539	
D_6	1588	1604	1473		1370	
D_7	1468	1478	1391		1429	
D_8	1404	1467	1337		1354	
D_9	1298	1296	1259		1340	
D_{10}	1194	1221	1187		1203	
D_{11}	1270	1272	1403		1263	
D_{12}	1155	1164	1127		1121	
D_{13}	1069	1096	1013		1059	
D_{14}	1086	1079	1038		1082	
D_{15}	989	1002	955	[962][c]	983	
D_{16}	835	858 [865][c]	817	[823][c]	840	
D_{17}	675	684 [687][c]	636	[635][c]	665	
D_{18}	513	522 [524][c]	446	[454][c]	455	457[d]
D_{19}	402	416 [409][c]	373	[374][c]	391	396[d]
D_{20}	376	387 [387][c]	368		377	
D_{21}	226	221	226	231[d]	233	240[d]
			a$_2$			
D_{22}	970	976	782		991	
D_{23}	894	898	714		926	
D_{24}	871	869	535		863	
D_{25}	770	776	584		781	
D_{26}	683	684	468		589	
D_{27}	526	522	376		495	
D_{28}	432	431	241		366	
D_{29}	213	234	159	151[d]	176	176[d]
D_{30}	171	185	80	107[d]	150	149[d]

[a]Frequencies calculated at the optimized geometries. For the S_0 state, the level of calculation was B3LYP/aug-cc-pVTZ (values very similar to those in Ref. 24); for the S_1 state, TD-B3LYP/aug-cc-pVTZ; and for the D_0^+ state, UB3LYP/aug-cc-pVTZ. In all cases, the calculated harmonic vibrational wavenumbers were scaled by 0.97. Values reported are for the ^{35}Cl isotopologue.
[b]The D_i labels are described in Ref. 24, where the vibration mode diagrams can also be found.
[c]Values taken from the fluorescence study of Ichimura et al.[21]
[d]Present work. The S_1 values for D_{29} and D_{30} are estimated from the respective overtone bands.

good starting point. For a hindered methyl rotor, the lowest couple of terms of the torsional potential may be expressed as

$$V(\alpha) = \frac{V_3}{2}(1 - \cos 3\alpha) + \frac{V_6}{2}(1 - \cos 6\alpha), \qquad (1)$$

where α is the torsional angle. If the V_6 term is small relative to V_3, which is usually the case, then its effect is simply to modify the shape of the potential. Recent work[22] has deduced that for mClT, V_3 has approximate values of: 2 cm^{-1} for the S_0 state, 110 cm^{-1} for the S_1

state, and −285 cm^{-1} for the D_0^+ state. (The sign of the V_3 parameter is a way of indicating the phase of the torsional potential, and does not affect the energy levels, but it can be deduced from the calculated geometry.[29,30]) Thus, these three states of the same molecule are, respectively, very close to a free rotor; a moderately-hindered rotor; and a highly-hindered rotor.

In Ref. 20, we illustrated how the magnitude of the V_3 term affected the energies of the m levels for mFT. As described in Spangler,[28] as V_3 increases, deep within the potential well the

TABLE II. Correspondence of the C_s point group symmetry classes with those of the G_6 molecular symmetry group. Also indicated are the symmetries of the D_i vibrations and the different pure torsional levels.[a]

C_s	G_6	D_i [b]	m
a'	a_1	D_1–D_{21}	$0, 3(+), 6(+), 9(+)$
a''	a_2	D_{21}–D_{30}	$3(-), 6(-), 9(-)$
	e		$1, 2, 4, 5, 7, 8$

[a]Symmetries of vibtor levels can be obtained by combining the vibrational symmetry (in G_6) with those of the pure torsional level, using the C_{3v} point group direct product table.
[b]The D_i labels are described in Ref. 24, where the vibration mode diagrams can also be found.

free-rotor m levels evolve into triply degenerate torsional vibrations, with each torsional vibration arising from one degenerate pair of $m \neq 3n$ levels, plus one $m = 3n$ level. These latter levels lose their degeneracy in V_{3n} potentials and the resulting levels can be denoted $m = 3n(+)$ and $m = 3n(-)$, with the former being of a_1 and the latter of a_2 symmetry in G_6.[19,28] Thus, if the torsional barrier is high, we expect low-lying e symmetry levels to be close-to-degenerate with an $m = 3n(+)$ or $m = 3n(-)$ level. The splitting between the $m = 3n(+)$ and $m = 3n(-)$ levels is largely an effect of V_3, but is also affected by (the smaller-valued) V_6.[20] Although for a G_{12} symmetry molecule such as toluene or pFT, the sign of V_6 determines the energy ordering of the $m = 3n(+)$ and $m = 3n(-)$ levels, particularly for $n = 1$. For a G_6 symmetry molecule, the energies of the m levels depend on both parameters, as well as the effective rotational constant for torsion of the $-CH_3$ group, denoted as F, whose value is expected to be only slightly different in the three electronic states under consideration. As a consequence, it is not straightforward to deduce the values of the torsional parameters from the spectrum directly, and that difficulty is further exacerbated by possible interactions between torsional, vibtor, and vibrational levels.[19]

B. Spectra and assignments

1. Overview of the $S_1 \leftarrow S_0$ spectrum

The REMPI spectrum covering the first 350 cm^{-1} of the mClT $S_1 \leftarrow S_0$ spectrum is shown in Fig. 1; the assignments shown have been deduced in this work. Also shown is a comparison with the 0–350 cm^{-1} region of mFT, with assignments given for the latter that have been discussed recently.[19,20] As may be seen, these low-wavenumber regions consist of a series of bands that can be associated with torsions, vibtor, and low-frequency vibrational levels. A laser-induced fluorescence (LIF) spectrum has been presented in Ref. 21 that shows transitions up to 1000 cm^{-1} above the origin, although assignments are only given for some of the bands up to 860 cm^{-1}. The calculated wavenumbers for the D_i vibrations of the S_0, S_1, and $D_0{}^+$ states are given in Table I. In the present work, we shall make use of these quantum chemical calculations and the activity seen in the ZEKE spectrum, to deduce assignments in both the S_1 and the $D_0{}^+$ states, and will comment on the previous mClT assignments and values given in Refs. 21 and 22.

We note particularly that a number of the REMPI bands appear as doublets—see Fig. 1. This attribute of the spectra arises from the
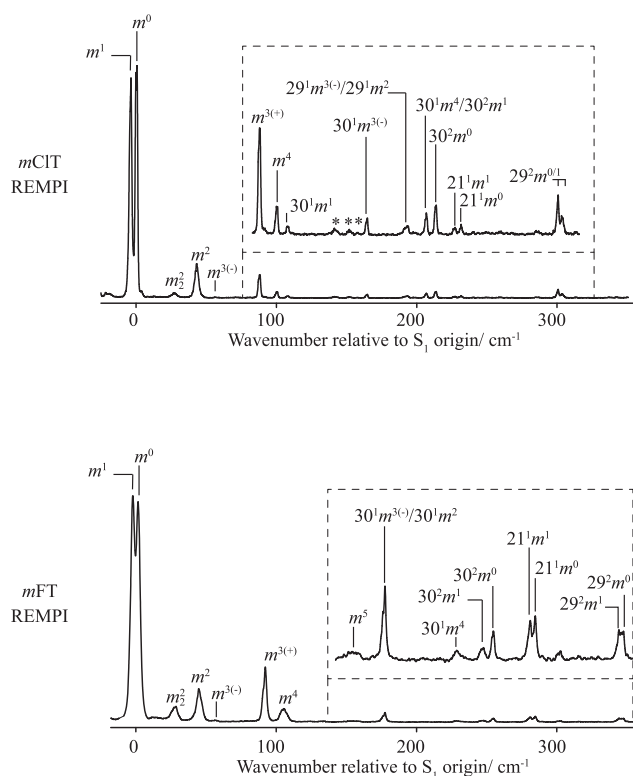

FIG. 1. Comparison between the 0–350 cm^{-1} regions above the origins of the $S_1 \leftarrow S_0$ transitions in m-chlorotoluene and m-fluorotoluene. The assignments for the latter have been discussed in Refs. 19 and 20, and there is a high degree of consistency between the two sets of spectra. The asterisked bands are thought to arise from complexes. See the text for further discussion of the assignments.

population of both the $m = 0$ and the $m = 1$ levels in the S_0 state owing to nuclear spin symmetry.[16] The lower wavenumber band is assigned to the m_1^1 transition, so that for the first intense doublet band in the spectrum, the true origin is the second of those two bands, which corresponds to the m_0^0 transition. Symmetry-allowed transitions from $m = 1$ in the S_0 state will be to S_1 levels of e symmetry, while those from $m = 0$ will be to those of a_1 symmetry, so that we expect very different ZEKE activity from these two levels.

2. Torsional levels

In Figs. 2 and 3, we show the ZEKE spectra recorded via the torsional levels of the S_1 state, separating these into a_1 and e symmetry, respectively. For the a_1 symmetry levels, we record spectra via m^0 and $m^{3(+)}$, while for the e levels we record spectra via the m^1, m^2, and m^4 levels. In contrast to mFT, we were unable to record spectra via the $m^{3(-)}$ and m^5 levels. As with mFT, we could record spectra via $m = 2$ accessed via both the m_1^2 and the m_2^2 transitions, with the activity looking similar, but with the former having the better signal to noise, and so is the one presented herein.

In Fig. 2, the ZEKE spectra via the a_1 symmetry m levels, m^0 and $m^{3(+)}$ are presented; the low wavenumber regions of these are
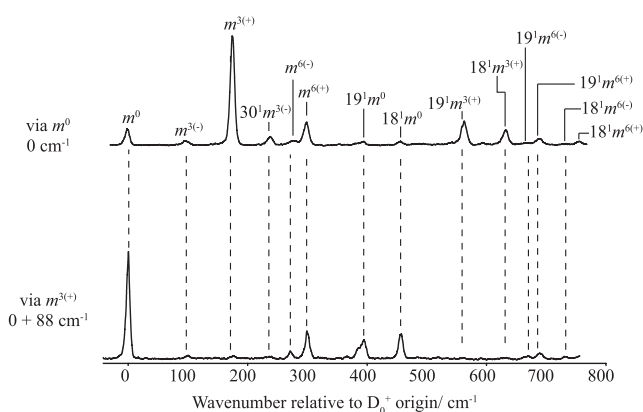
FIG. 2. ZEKE spectra recorded via two a_1 symmetry torsional levels of the S_1 state. The preceding superscripted "+" used in the text is omitted in the labels for clarity. See the text for further discussion of the assignments.

similar to the spectra reported by Feldgus *et al.*,[22] although the current spectra span a wider range. It may immediately be seen that the most intense transition does not correspond to $\Delta m = 0$, but to $|\Delta m| = 3$ in both cases. In the case of $m = 0$, the intensity of the $^+m^{6(+)}$ band is also sizable. These are consistent with a change in the phase of the torsional potential upon ionization, as seen for mFT.[20] Alongside, the $^+m^{3(+)}$ and $^+m^{6(+)}$ are the symmetry-forbidden $^+m^{3(-)}$ and $^+m^{6(-)}$ bands, respectively; the activities of these could arise from rotation–torsion coupling[19,20] or vibronic/intrachannel coupling.[20]

We also see the symmetry-allowed $^+30^1m^{3(-)}$ band when ionizing via m^0, which was also seen for mFT.[20] To higher wavenumber, vibtor combinations, involving $^+18^1$ and $^+19^1$ can be seen, with

largely the same relative intensities as the lower wavenumber bands. These observations are very similar to those in our previous work on mFT,[20] except that only combinations with $^+18^1$ were observed. This could suggest that there are slightly different geometry changes upon ionization between the mFT and mClT molecules, or that there is different Duschinsky mixing of the vibrations—this is the subject of ongoing work.

The $^+m^0$ band can be used to determine the adiabatic ionization energy (AIE), which is derived as 71 319 cm^{-1} ± 5 cm^{-1}. This value is slightly lower than the value of 71 333 cm^{-1} ± 5 cm^{-1} deduced by Feldgus *et al.*,[22] which we assume has been increased to reflect the lowering of the AIE by the applied electric field. However, we do not apply such a correction since the forced ionization of Rydberg states solely would lead to a very wide ZEKE band of ~15 cm^{-1}, with the actual AIE toward the high wavenumber end of the band. This is because of the well-known decay of the lower-lying Rydberg states accessed in the pulsed-field ionization process,[31] and this is confirmed by the fact that the ZEKE bands had widths of ~5 cm^{-1} to 7 cm^{-1}, some of which is due to unresolved rotational structure.

In Fig. 3, the ZEKE spectra recorded via three e symmetry levels, m^1, m^2, and m^4 are presented. The low wavenumber sections of those recorded via m^1 and m^2 are similar to the spectra reported by Feldgus *et al.*,[22] but the range here is larger; the spectrum recorded via m^4 is reported here for the first time. Across these three spectra, again, it is clear that the most intense transitions correspond to $|\Delta m| = 3$, rather than $\Delta m = 0$. Also, combinations with $^+18^1$ and $^+19^1$ are seen to higher wavenumber in all cases. Looking first at the ZEKE spectrum recorded via m^1, it can be seen that the $\Delta m = 3$ transitions to $^+m^2$ and $^+m^4$ (remembering that the m quantum number is signed for $m \neq 3n$) are intense; however, the transition to $^+m^5$ is also very intense, which is a $\Delta m = 6$ transition (in the case of mFT,[20] this was the most intense band). We also observe the $^+m^7$ band ($\Delta m = 6$) and the $^+m^8$ band ($\Delta m = 9$).
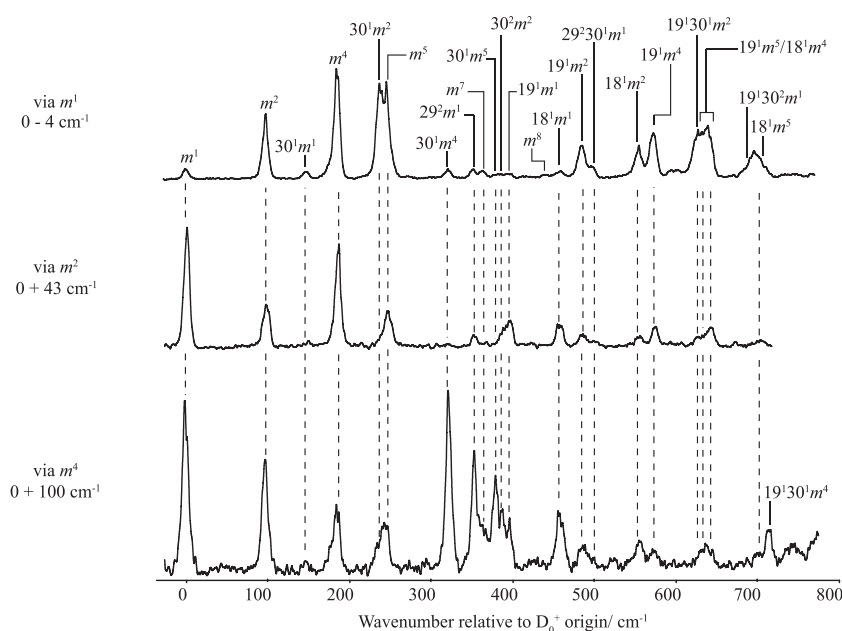

FIG. 3. ZEKE spectra recorded via three e symmetry torsional levels of the S_1 state. The preceding superscripted "+" used in the text is omitted in the labels for clarity. See the text for further discussion of the assignments.

Of note is the strong activity of $^+30^1m^2$ when exciting via m^1. This band is so strong that Feldgus *et al.*[22] understandably suggested that there was a Fermi resonance between $^+m^5$ and $^+30^1m^2$. However, the relative intensities of the two corresponding bands when exciting via different intermediate levels (see Fig. 3 and Sec. III B 3) does not seem to support this. Rather, it appears that there is an anomalously strong transition intensity associated with the $^+30^1m^2 \leftarrow m^1$ ionization. This is analogous to the strong intensity of the $^+30^1m^4 \leftarrow m^4$ transition seen in the case of *m*FT.[20] In that work, we did see vibtor transitions associated with $^+30^1$ when exciting via m^1; however, these were relatively weak compared to the main $^+m^x$ bands; certainly the $^+30^1m^2$ band was significantly weaker than that in the present case.

When exciting via m^2, there are strong transitions to $^+m^1$ ($\Delta m = 3$), $^+m^4$ ($\Delta m = 6$) and, to a lesser extent, $^+m^5$ ($\Delta m = 3$). Notably, the relative intensity of the $^+30^1m^2$ band seems to be significantly less than that when exciting via m^1; indeed, this also seems to be the case when exciting via m^4. In contrast, the $^+30^1m^4$ band is very intense when exciting via m^4, and this behavior is similar to that observed for *m*FT,[20] although the $^+30^1m^5$ transition is much stronger for *m*ClT here. The ZEKE spectrum via m^4 is compared to the spectra obtained via m^1 and m^2. It can be seen that the $^+m^1$ band is intense, while the expected $^+m^7$ band is overlapped (both $|\Delta m| = 3$). The $|\Delta m| = 6$ band, $^+m^2$ is also intense. We show the same spectrum again in Fig. 4, where its activity is compared to the spectra obtained via 30^1m^x vibtor levels (see Sec. III B 3).

3. Vibtor levels involving 30^1

In Fig. 4, we show the ZEKE spectra recorded via 30^1m^1, 30^1m^4 (overlapped with 30^2m^1), and $30^1m^{3(-)}$, and compare to the spectrum obtained via m^4 (also shown in Fig. 3, where it is compared to ZEKE spectra recorded by other *e* symmetry torsional levels).

We note that the 30^1m^1 and m^4 transitions are relatively close to each other and are each of *e* symmetry; as such, there is the possibility of interaction between these two levels. The ZEKE spectrum via the former level is the second trace in Fig. 4, where it can be compared with that via m^4 (top trace). (The appearance of the 30^1m^1 ZEKE spectrum is clearly that of an $m = 1$ level.) It can be seen that there is a significant amount of cross-activity between the two spectra. This is of interest as it is not clear where the transition strength for the 30^1m^1 level originates. The usual vibronic interaction for substituted benzenes in the S_1 state would involve in-plane vibrations that are of a_1 symmetry, while the D_{30} vibration is an out-of-plane vibration of a_2 symmetry. Despite the weakness of the $^+30^1m^4$ band, which might be expected to be stronger, the appearance of the 30^1m^1 ZEKE spectrum is suggestive of a $m^4 \ldots 30^1m^1$ interaction in the S_1 state. The absence of nearby levels of a_2 symmetry to interact with it, and the absence of the corresponding 30^1m^0 band, either here or in the spectra in Fig. 2, supports an interaction of 30^1m^1 with an *e* symmetry torsional level.

The ZEKE spectrum recorded via the REMPI band at 206 cm^{-1} has significant activity in $^+30^1m^x$ and $^+30^2m^x$ bands. This leads to the deduction that it arises from two overlapped transitions, 30^1m^4 and 30^2m^1. The picture is slightly complicated by the strong $^+30^2m^4$ band observed when exciting via 30^1m^4 and the strong $^+30^1m^5$ band seen when exciting via 30^2m^1 in *m*FT.[20] Similar activity is seen here via the 206 cm^{-1} band but, given the unusual intensities noted for *m*FT, it is difficult to state confidently which transitions have dominant contributions from 30^1m^4 or 30^2m^1, as it is likely that most transitions have contributions from both. Further comment on the 30^2m^1 contributions will be given in Sec. III B 5.

The appearance of the spectrum via $30^1m^{3(-)}$ is reminiscent of the corresponding and related spectra recorded for *m*FT,[20] with a strong $\Delta m = 0$ band and a significant $|\Delta m| = 3$ band, although the $^+30^1m^0$ was not clearly visible here.
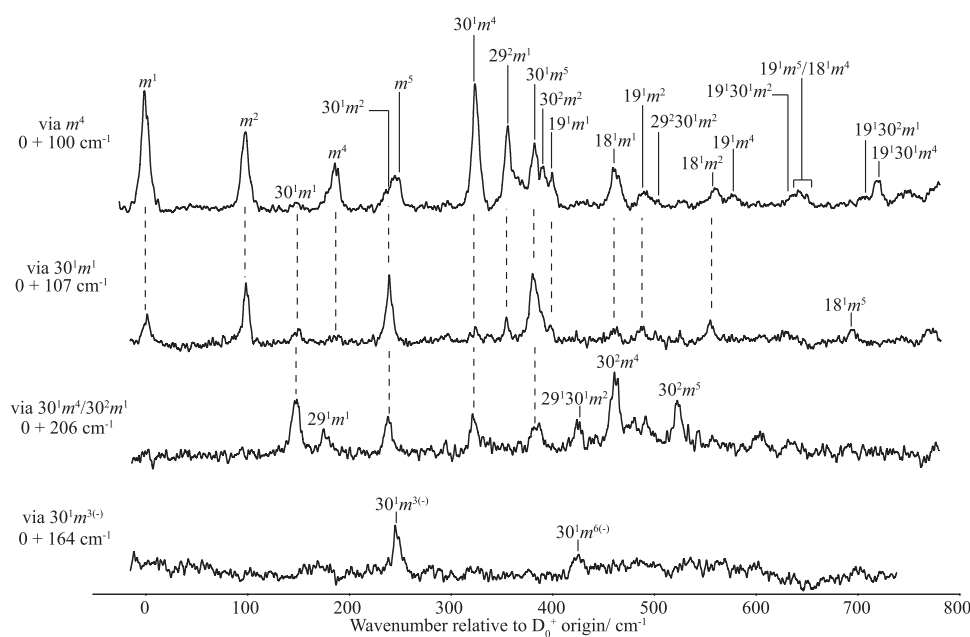
FIG. 4. ZEKE spectra recorded via vibtor levels of the S_1 state involving the 30^1 vibration; the ZEKE spectrum via m^4 is shown for comparison. It is concluded that there are two overlapped transitions at the excitation energy used for the third trace; comparison is made here for the 30^1m^4 contribution, with the 30^2m^1 contributions being highlighted in Fig. 6. The preceding superscripted "+" used in the text is omitted in the labels for clarity. See the text for further discussion of the assignments.

4. The band at 192 cm^{-1}

In Fig. 5, we show the ZEKE spectrum recorded via the REMPI transition at 192 cm^{-1} above the origin. This spectrum is a little puzzling since if the first band is situated at 0 cm^{-1}, then the resulting cation internal wavenumber scale is not consistent with the number of the band positions; however, if some of their band positions are moved up by ~5 cm^{-1}, then many of these bands can be clearly assigned. We conclude that this spectrum consists of two sets of transitions, one involving a_1 symmetry levels and one e symmetry (the latter will be on an energy scale that differs by the $m = 1$ to $m = 0$ energy spacing in the S_0 state). As such, the REMPI band must be an overlap of two features: one involving levels of a_1 symmetry, commencing at the S_0 $m = 0$ level and one involving levels of e symmetry, originating from the S_0 $m = 1$ level. The first band is seen to arise from the $^+m^0$ transition, with the $^+m^1$ transition being too weak to see definitively. A perusal of the possible S_1 levels that could give rise to these two overlapped features suggests that one is 29^1m^2 and the other is $29^1m^{3(-)}$. Thus, the main bands arise from $^+29^1m^x$ transitions, of both a_1 and e symmetry. The wavenumber, and additionally since we do not expect the $\Delta(v, m) = 0$ band to be the most intense, indicates that it is more prudent to assign the most intense band at 273 cm^{-1} to $^+29^1 m^{3(-)}$, with a contribution from $^+29^1m^2$. This is consistent with the feature at 173–178 cm^{-1} being an overlap of $^+29^1m^0$ and $^+29^1m^1$ contributions. Furthermore, the band at ~455 cm^{-1} can be assigned as the $\Delta m = 3$ transition, $^+29^1m^{6(-)}$. A band at ~239 cm^{-1} seems most sensibly assignable to $^+30^1m^{3(-)}$, the bands at 300 cm^{-1} and 321 cm^{-1} to $^+m^{6(+)}$ and $29^130^1m^0$, respectively.

For these REMPI bands to overlap, at least one of them must be subject to an interaction in the S_1 state. In fact, the 29^1m^2 level is expected close to 199 cm^{-1}, while the $29^1m^{3(-)}$ level is expected at about 207 cm^{-1}. Possible interactions involving these levels are $29^1m^{3(-)} \ldots 30^2m^0$ and $29^1m^2 \ldots 30^2m^1$, which would provide some explanation for the larger-than-expected separation between 30^2m^0 and 30^2m^1—see Sec. III B 5, notwithstanding the lack of cross activity in the respective spectra. It is seen that the ZEKE band at ~300 cm^{-1} is slightly too high in wavenumber to be assigned to a $^+30^2$ band to support this; an alternative is that this ZEKE band is $^+m^{6(+)}$, and so indicative of a $29^1m^{3(-)} \ldots m^{6(+)}$ interaction, which would imply that the unperturbed $m^{6(+)}$ level lies above $29^1m^{3(-)}$. We do not see a $m^{6(+)}$ band in the REMPI spectrum, so cannot confirm this hypothesis, although it seems reasonable. It is clear that there are a number of possible interactions involving the 29^1m^2 and $29^1m^{3(-)}$ levels.

5. Vibtor levels involving 30^2

ZEKE spectra recorded via the bands at 206 cm and 213 cm are shown in Fig. 6. The REMPI band at 213 cm^{-1} is straightforwardly assigned to 30^2m^0 on the basis of its ZEKE spectrum, in particular, the strong $^+30^2m^{3(+)}$ band. It is interesting that there is activity in several vibtor bands involving $^+21^1$, which was also the case for mFT.[20] We have noted above that a distinct 30^2m^1 REMPI band was not observed for mClT, but it is believed that this is overlapped by the 30^1m^4 transition (see Fig. 4 and Sec. III B 3). That ZEKE spectrum is presented again in Fig. 6 for completeness and for more-facile comparison with that of 30^2m^0. The separation between 30^2m^1 and 30^2m^0 is ~7 cm^{-1}, which is greater than the ~4 cm^{-1} for the m^1 and m^0 bands, confirming that vibtor interactions are occurring for at least one of these levels, and in Sec. III B 4, we have suggested that this is possibly with $29^1m^{3(-)}$; a similarly larger-than-anticipated separation was seen for mFT,[19,20] although a specific interaction was not identified. We also find that there is no discernible activity for $^+21^1$ vibtor levels in the 30^2m^1 ZEKE spectrum, and indeed, only very weak $^+21^1m^x$ bands were seen in the corresponding ZEKE spectrum for mFT.[20]

6. Vibtor levels involving 21^1

Much more straightforward is the pair of ZEKE spectra recorded for 21^1m^1 and 21^1m^0, Fig. 7, where the vibtor activity is similar to that observed for the m^1 and m^0 levels. The $^+30^2m^{3(+)}$
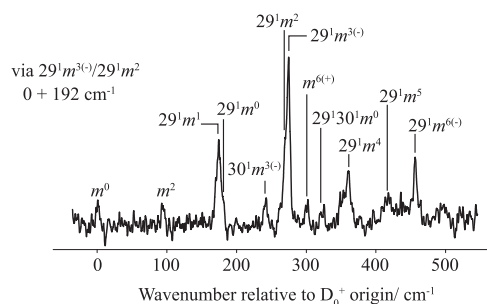

FIG. 5. ZEKE spectrum recorded via the $29^1m^{3(-)}/29^1m^2$ overlapped transitions of the S_1 state. The preceding superscripted "+" used in the text is omitted in the labels for clarity. Note that bands arising from transitions involving e symmetry bands are actually 5 cm^{-1} higher than those indicated on the scale in this particular spectrum. See the text for further discussion of the assignments.
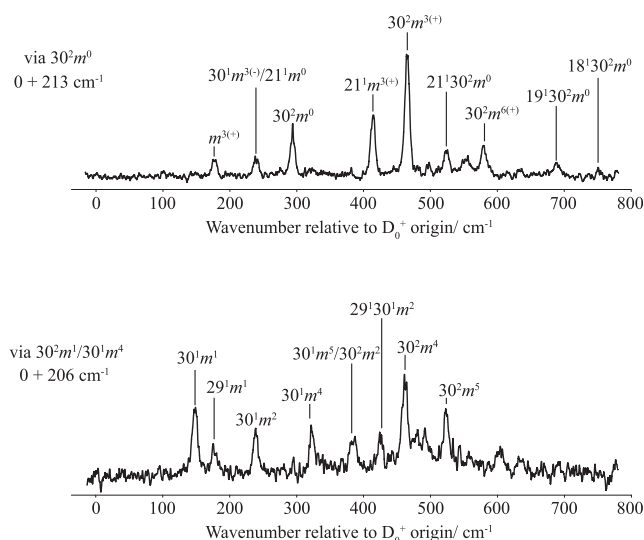

FIG. 6. ZEKE spectra recorded via the 30^2m^0 and 30^2m^1 levels of the S_1 state. In the latter case, the transition is overlapped with the 30^1m^4 level. The preceding superscripted "+" used in the text is omitted in the labels for clarity. See the text for further discussion of the assignments, and also Fig. 4.
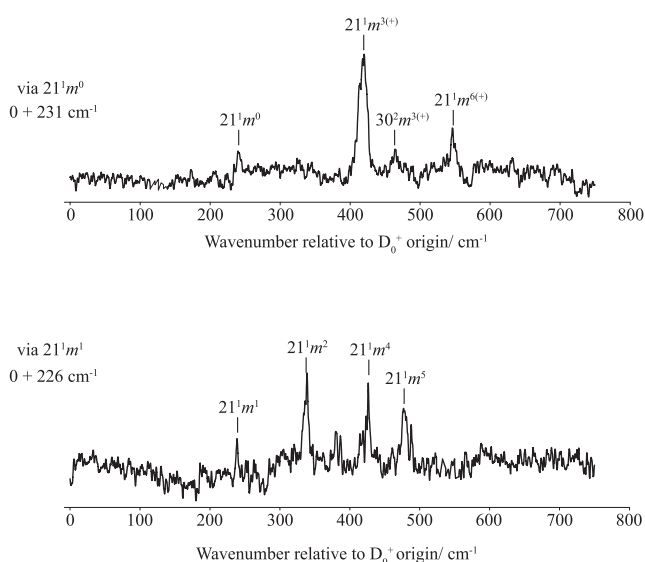
FIG. 7. ZEKE spectra recorded via the 21^1m^0 and 21^1m^1 levels of the S_1 state. The preceding superscripted "+" used in the text is omitted in the labels for clarity. See the text for further discussion of the assignments.

vibtor band is seen, mirroring the $^+21m^x$ activity seen in the 30^2m^0 ZEKE spectrum (Sec. III B 5), and consistent with observations for mFT.[20]

7. Vibtor levels involving 29^2

The pair of ZEKE spectra recorded for 29^2m^0 and 29^2m^1 contains activity that is largely as expected—see Fig. 8. This confirms their assignment, but shows that the REMPI bands are in the reverse order to that expected, with the 29^2m^0 band lying *below* that of 29^2m^1; moreover, the higher-wavenumber band is broader than expected (see the top trace in Fig. 8). For the ZEKE spectrum recorded via 29^2m^1, there are the expected $^+29^2m^x$ e symmetry vibtor bands, but in addition $^+29^1m^1$, $^+29^1m^4$, and $^+29^1m^5$ bands (unexpectedly, however, there is no $^+29^1m^2$ band). The ordering of the REMPI bands, the $^+29^1m^x$ activity, the broader profile of the higher wavenumber band (more consistent with a higher, e symmetry m level) and the expected energies of vibtor levels suggests a $29^2m^1 \ldots 29^1m^5$ interaction. Although too weak to record a ZEKE spectrum to confirm its assignment, there is a weak REMPI band at 287 cm^{-1} that can reasonably be associated with the partner level from this interaction (see the top trace in Fig. 8). We thus conclude that this $29^2m^1 \ldots 29^1m^5$ interaction has led to a shift in the expected band ordering of the 29^2m^0 and 29^2m^1 pair.

C. Torsional potentials

A full fit of the torsional and vibtor levels, including vibtor interactions, has not been carried out in this work, since the precision does not merit it. However, significant insight can be obtained from the band separations, and these are tabulated in Table III. We first note that for the pure torsional levels, we have calculated
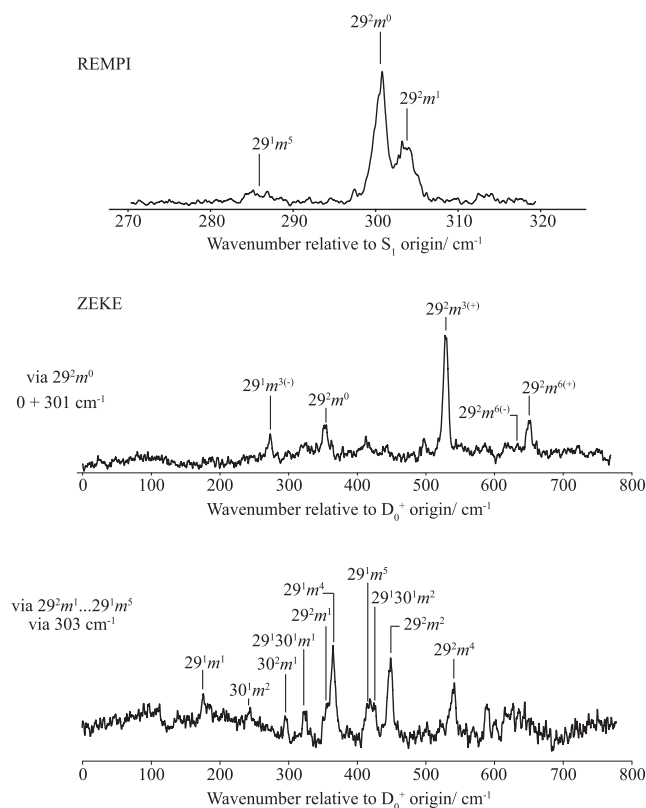

FIG. 8. In the top trace, an expansion of the 270–320 cm^{-1} region of the REMPI spectrum of the $S_1 \leftarrow S_0$ transition of m-chlorotoluene is shown. Below this are ZEKE spectra recorded via the 29^2m^0 and 29^2m^1 levels of the S_1 state. In the case of the latter, there is some evidence for an interaction with the 29^1m^5 state. See the text for further discussion of the assignments.

TABLE III. Calculated and experimental torsional levels for mClT.

m	S_1[a]		D_0^+[b]	
	Calculated	Observed	Calculated	Observed
0	0	0	0	0
1	0.79	1	0.1	0
2	48.2	48	96.4	98
3(−)	56.3	56	97.7	98
3(+)	86.2	88	177.2	175
4	107.5	106	186.9	186
5	150.6		246.0	246
6(−)	203.2		286.9	284
6(+)	204.8		301.1	300
7	268.3		359.8	363
8	342.8		437.8	439
9(−)	427.5		530.9	
9(+)	427.5		531.1	

[a]S_1 $V_3 = 110$ cm^{-1}; $V_6 = -20$ cm^{-1}; and $F = 5.0$ cm^{-1}.
[b]D_0^+ $V_3 = -287.5$ cm^{-1}; $V_6 = -20$ cm^{-1}; and $F = 5.4$ cm^{-1}.
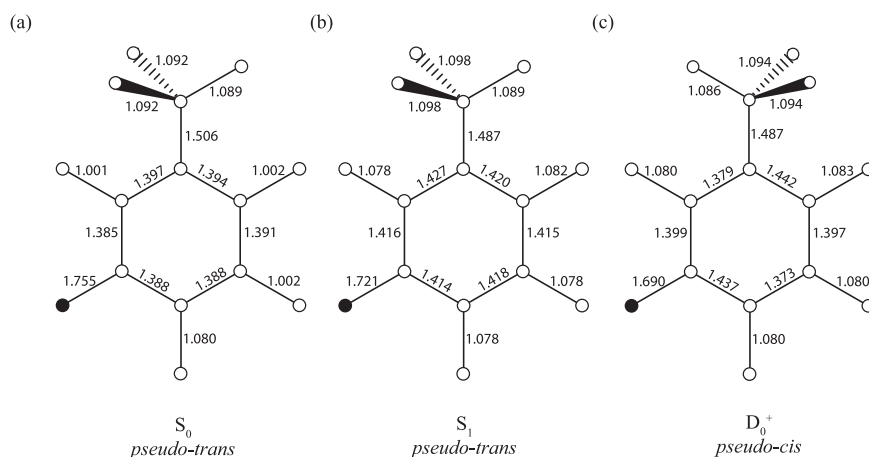
FIG. 9. Calculated geometries for the (a) S_0 (B3LYP/aug-cc-pVTZ), (b) S_1 (TD-B3LYP/aug-cc-pVTZ), and (c) D_0^+ (UB3LYP/aug-cc-pVTZ) electronic states of m-chlorotoluene. The bond lengths are in Å. Note the differing conformation of the cation relative to the two neutral states. The filled circle represents the Cl atom, the C and H atoms are both unfilled circles.

the energies of the m levels by varying the V_3 parameter, to obtain reasonable agreement with the experimental observations. Our best values are +110 cm^{-1} for V_3 for the S_1 state and −287.5 cm^{-1} for the cation. These values are close to the values reported by Feldgus et al.,[22] and indeed, the present positions of the bands are in excellent agreement with those reported therein. (We fixed the V_6 and F values to those given by Feldgus et al.[22]) Because of the need to vary three parameters, and the neglect of vibtor interactions, these values should be viewed as merely reasonable estimates. That said, the V_3 parameters for mClT seem to be about 5 cm^{-1} and between 10 cm^{-1} and 15 cm^{-1} lower than those for mFT, for the S_1 and D_0^+ states, respectively, i.e., the torsional motion is less hindered in mClT than that in mFT. We note that the sign of V_3 cannot be established from the spectrum, and comes from optimized geometries. In agreement with Feldgus et al.,[22] the calculated geometries

position the methyl group in the *pseudo*-trans orientation in the S_0 and S_1 states, i.e., the in-plane methyl hydrogen points away from the chlorine substituent, and *pseudo*-cis in the D_0^+ state— see Fig. 9. This confirms the change in the phase of the torsional potential, consistent with the significant torsion and vibtor activity seen in the spectrum, and the observation that the $\Delta(v, m) = 0$ band is mostly not the most intense feature.

Taking into account experimental uncertainties in measuring band centers, Table IV indicates that several of the vibrations of the cation have vibtor levels that have about the same spacings as those built upon the torsional levels associated with the vibrational origin: $^+18^1$, 19^1, $^+21^1$, $^+29^1$, and $^+29^2$. On the other hand, those built upon $^+30^1$ and $^+30^2$ appear to have potentials that are less hindered, since the spacings are less than those associated with the vibrational origin. A similar picture was seen for mFT,[19,20] where it

TABLE IV. Separations of vibtor levels built on different vibrations (cm^{-1}).[a]

	Vibrational level[b]							
Torsion[c]	$^+0°$ [0]	$^+30^1$ [149]	$^+29^1$ [176]	$^+21^1$ [240]	$^+30^2$ [294]	$^+29^2$ [354]	$^+19^1$ [396]	$^+18^1$ [456]
$^+m^{0,1}$	0	0	0	0	0	0	0	0
$^+m^2$	98	89 (238)	101 (277)	99 (339)	87 (381)	94 (448)	90 (486)	97 (555)
$^+m^{3(-)}$	98	89 (238)	98 (273)					
$^+m^{3(+)}$	175			176 (416)	172 (466)	175 (529)	167 (563)	177 (633)
$^+m^4$	186	173 (322)	182 (358)	187 (427)	168 (462)	184 (538)	177 (573)	186 (642)
$^+m^5$	246	230 (379)	240 (416)	239 (479)	229 (523)	247 (601)	246 (642)	248 (704)
$^+m^{6(-)}$	284						272 (668)	278 (734)
$^+m^{6(+)}$	300			307 (547)	286 (580)	298 (652)	295 (691)	300 (756)
$^+m^7$	363							
$^+m^8$	439							

[a]Torsional spacings are given with respect to the band position of the $^+m = 0$ or $^+m^1$ level of the indicated vibration.
[b]Values in square brackets in the column headers are the wavenumbers of the $^+m = 0$ level of the indicated vibration. Values in parentheses are the vibtor band positions, while the values outside parentheses are the spacings between the vibtor levels for the particular vibration. For weak bands and overlapped features, we have given our best estimate of the band position.
[c]The $^+m^0$ and $^+m^1$ levels are degenerate at our resolution (see Table III). Levels with $^+m \neq 3n$ have degenerate + and − levels.

was noted that the out-of-plane D_{30} vibration coupled to the torsional motion more effectively than did the (also out-of-plane) D_{29} vibration, in both the S_1 and the D_0^+ states. It was also noted in Ref. 20 that the in-plane D_{18} and D_{21} vibrations did not appear to couple significantly with the torsional motion and also is consistent with the data in Table IV. (See Ref. 20 for mode diagrams for these vibrations.) Although the $^+19^1m^x$ vibtor levels are mostly in the expected positions for mClT$^+$ (see Table IV), both $^+19^1m^{3(+)}$ and $^+19^1m^4$ are significantly lower than expected, suggesting (currently unidentified) vibronic interactions in the cation for these levels.

We calculated the torsional barrier in the mClT$^+$ cation when we distort the geometry of the molecule along the D_{30} vibrational coordinate. Indeed, for small distortions along that coordinate, in line with that expected for the fundamental and first overtone levels, there is a lowering of the barrier by a few tens of cm^{-1}, in line with the experimental observations for both mFT$^+$ and mClT$^+$.

IV. CONCLUDING REMARKS

In the present work, we have recorded a significant number of ZEKE spectra via different S_1 torsional and vibtor levels, allowing confirmation of the assignment of the intermediate levels, and also obtaining both vibrational and torsional information on the cation. Furthermore, as with mFT,[20] we have again found clear evidence of changes in torsional potentials, particularly involving the D_{30} vibration and its overtone, in the cation. Additionally, the anomalous intensity of the $^+30^1m^2$ band when exciting via m^1 and, more generally, the activity of $^+30^1m^x$ bands in the spectra for mFT and mClT, confirm that certain out-of-plane vibrational motions are intricately linked to torsional motion. Overall, we conclude that it is unlikely that one can express the vibtor levels of $^+30^1$ and $^+30^2$ as simply products of torsional and vibrational wavefunctions.

The observation of activity for the out-of-plane 30^1 vibration in the $S_1 \leftarrow S_0$ transition is unexpected since it is symmetry forbidden, and we have suggested that its activity here arises from a $m^4 \ldots 30^1m^1$ interaction. It is interesting to note that the intensity of the $^+30^1m^4$ band is much lower than might be expected when exciting via the 30^1m^1 band, and similar anomalies were seen for $m = 4$ vibtor levels in ZEKE spectra via 30^1m^4 and 30^2m^4 levels in mFT.[20] We have also concluded that the 29^2m^0 and 29^2m^1 levels are not in the expected order and hypothesized that there is a $29^1m^5 \ldots 29^2m^1$ interaction that caused the latter level to move up in wavenumber. We have also highlighted that the spacing between the 30^2m^0 and 30^2m^1 levels is greater than the expected 4 cm^{-1}, as seen for the origin bands, and suggested various interactions.

We have also discussed the suggestion in Ref. 22 that there is an interaction between $^+m^5$ and $^+30^1m^2$ (denoted b^{1}m^2 therein). This hypothesis was based on the appearance of the ZEKE spectrum recorded via m^1 (see Fig. 3), where, as well as the expected m^5 band, a very strong $^+30^1m^2$ band is seen. However, we note that the $^+m^5$ band is in the expected position (see Table III) and, furthermore, there is no such strong $^+30^1m^2$ band when exciting via m^2 (Fig. 3), with this being a shoulder on the side of the $^+m^5$ band in the spectrum seen when exciting via m^4 (Fig. 3). Moreover, the $^+m^5$ band is not seen when exciting via 30^1m^1, while the $^+30^1m^2$ band is relatively intense (Fig. 4). While we concur that the $^+30^1$ vibration

is interacting with the torsional motion, this is not a 1:1 interaction with a particular $^+m^x$ level, but a more general phenomenon, causing a change to the intermolecular potential. Clearly, the coupled motion of the $^+30^1$ vibration with the torsion is also leading to wavefunction changes that have an unusual affect on photoionization intensities. With mFT,[20] we noted the surprisingly intense $^+30^1m^4$ band, when exciting via m^4, and the intense $^+30^2m^4$ band when exciting via 30^1m^4; on the other hand, the $^+30^2m^4$ band was anomalously weak when exciting via 30^2m^1. In the present work on mClT, partly owing to overlapped bands, it is not possible to say definitively that these particular intensities are anomalous, although we do see prominent $^+30^1m^x$ bands when exciting via m^4, for example.

We now comment on the V_3 barriers in the S_0, S_1, and D_0^+ states. By reference to the geometries of mFT in these three states[20] and Fig. 9 for mClT, there is not the marked asymmetry in the C–C bond lengths in the S_1 state as there is in the D_0^+ state. Thus, the explanation of the significantly larger barrier in the S_1 state cannot be solely attributed to asymmetric charge distributions, as suggested by Feldgus et al.[22] On the other hand, there is a reasonably significant shortening of the C–CH$_3$ bond length, $S_1 \leftarrow S_0$, which would increase the "vdW" interaction with the "ortho" hydrogens, and this would be a plausible explanation of the increase in the barrier height. For $D_0^+ \leftarrow S_1$, the C–CH$_3$ bond length is about the same in the two states, but now we have the asymmetry in charge distribution (see the next paragraph and Refs. 20 and 22), and this both increases the barrier and switches the equilibrium geometry from $pseudo$-trans (for S_0 and S_1) to $pseudo$-cis (for D_0^+).

Also, in agreement with Feldgus et al.,[22] we find that the main V_3 torsional barrier in mClT is slightly lower than that in mFT. This barrier appears to be associated with an asymmetry in the charge distribution in the carbon–carbon bonds closest to the C–CH$_3$ bond, indicated by the C–C bond lengths (see Fig. 9), and has been discussed by Weisshaar's group[22,32] and ourselves.[20] This asymmetry is largely due to the electron density distribution of the highest occupied molecular orbital (HOMO) of the S_0 state of the substituted benzene, which has electron density concentrated in two C–C bonds on opposite sides of the benzene ring adjacent to each of the substituents. Once the molecule is ionized, this leads to two regions of more-concentrated positive charge in these positions. Further modifications of the electron density occur depending on the characteristics of substituents, such as their electronegativity. Hence, the lower barrier for the less electronegative Cl substituent makes sense, since it can tolerate the neighboring positive charge better than the more electronegative F atom can. This difference is consistent with the difference in the C–C bond lengths on either side of the methyl substituent, which Feldgus et al.[22] have noted is related to the difference in the natural bond order. For mFT, the difference is 0.072 Å, while in mClT it is 0.063 Å, in line with the somewhat smaller V_3 barrier for mClT. Furthermore, the removal of the electron is expected to be easier for mClT than mFT, and this is in line with the lower AIE for mClT (71 319 cm^{-1}) than that for mFT (71 997 cm^{-1}).[20]

Last, we note that the high barrier in the D_0^+ state suggests that the lower torsional levels are close to being vibrational levels. This would mean that the rotor motion is significantly localized and would suggest that the methyl group C–H bonds would not all be of equal lengths. Under these circumstances, as suggested for mFT,[20] there would be a movement away from molecular group symmetry toward point group symmetry.

We note that other explanations for barrier height variation have been put forward, including π^*/σ^* interactions that underlie hyperconjugation.[33,34] The idea is that variations in orbital energies suggest that the LUMO is the key factor in determining barrier heights and correlations with the Hammett constant suggested. However, we note that this explanation has been challenged by Suzuki *et al.*[35] and does not seem to explain the high barriers in the cation, where the orbital corresponding to the LUMO of the neutral molecule is unoccupied; thus, for the cation, we prefer the explanations of Weisshaar and co-workers discussed in the present work. We also note that for molecules such as toluene and *p*FT, the barrier will be a V_6 term, while for *ortho* and *meta* molecules, the barriers will be V_3 terms; furthermore, determining such barriers directly from spectra can be problematic because of vibtor interactions, as discussed herein, and the reliable determination of barrier heights from quantum chemistry likely requires a more-systematic study of electron correlation effects and basis set requirements.

The *m*FT and *m*ClT molecules represent very interesting molecules owing to the very different barrier heights in the three electronic states studied. In particular, this provides access to a significant number of torsional and vibtor levels in the cation. This has provided fruitful ground for investigating the interactions between torsional and vibrational motion, which is widely accepted as being a key aspect of internal energy flow and changes in photophysical behavior.

REFERENCES

[1] R. Improta, F. Santoro, and L. Blancafort, Chem. Rev. **116**, 3540 (2016).
[2] R. Barata-Morgado, M. L. Sanchez, A. Munoz-Losa, M. E. Martin, F. J. O. del Valle, and M. Aguilar, J. Phys. Chem. A **122**, 3096 (2018).
[3] Y. K. Kosenkov and D. Kosenkov, J. Chem. Phys. **151**, 144101 (2019).
[4] J. A. Davies, A. M. Green, A. M. Gardner, C. D. Withers, T. G. Wright, and K. L. Reid, Phys. Chem. Chem. Phys. **16**, 430 (2014).
[5] A. M. Gardner, A. M. Green, V. M. Tamé-Reyes, V. H. K. Wilton, and T. G. Wright, J. Chem. Phys. **138**, 134303 (2013).
[6] J. R. Gascooke, E. A. Virgo, and W. D. Lawrance, J. Chem. Phys. **143**, 044313 (2015).
[7] A. M. Gardner, W. D. Tuttle, L. Whalley, A. Claydon, J. H. Carter, and T. G. Wright, J. Chem. Phys. **145**, 124307 (2016).
[8] J. R. Gascooke, L. D. Stewart, P. G. Sibley, and W. D. Lawrance, J. Chem. Phys. **149**, 074301 (2018).
[9] A. M. Gardner, W. D. Tuttle, L. E. Whalley, and T. G. Wright, Chem. Sci. **9**, 2270 (2018).
[10] W. D. Tuttle, A. M. Gardner, L. E. Whalley, D. J. Kemp, and T. G. Wright, Phys. Chem. Chem. Phys. **21**, 14133 (2019).
[11] D. J. Kemp, A. M. Gardner, W. D. Tuttle, and T. G. Wright, Mol. Phys. **117**, 3011 (2019).
[12] D. J. Kemp, W. D. Tuttle, A. M. Gardner, L. E. Whalley, and T. G. Wright, J. Chem. Phys. **151**, 064308 (2019).
[13] J. A. Davies, L. E. Whalley, and K. L. Reid, Phys. Chem. Chem. Phys. **19**, 5051 (2017).
[14] A. M. Gardner, L. E. Whalley, D. J. Kemp, W. D. Tuttle, and T. G. Wright, J. Chem. Phys. **151**, 154302 (2019).
[15] C. J. Hammond, V. L. Ayles, D. E. Bergeron, K. L. Reid, and T. G. Wright, J. Chem. Phys. **125**, 124308 (2006).
[16] A. M. Gardner, W. D. Tuttle, P. Groner, and T. G. Wright, J. Chem. Phys. **146**, 124308 (2017).
[17] W. D. Tuttle, A. M. Gardner, K. B. O'Regan, W. Malewicz, and T. G. Wright, J. Chem. Phys. **146**, 124309 (2017).
[18] P. J. Timbers, C. S. Parmenter, and D. B. Moss, J. Chem. Phys. **100**, 1028 (1994).
[19] L. D. Stewart, J. R. Gascooke, and W. D. Lawrance, J. Chem. Phys. **150**, 174303 (2019).
[20] D. J. Kemp, E. F. Fryer, A. R. Davies, and T. G. Wright, J. Chem. Phys. **151**, 084311 (2019).
[21] T. Ichimura, A. Kawana, T. Suzuki, T. Ebata, and N. Mikami, J. Photochem. Photobiol., A **80**, 145 (1994).
[22] S. H. Feldgus, M. J. Schroeder, R. A. Walker, W.-K. Woo, and J. C. Weisshaar, Int. J. Mass Spectrom. Ion Processes **159**, 231 (1996).
[23] V. L. Ayles, C. J. Hammond, D. E. Bergeron, O. J. Richards, and T. G. Wright, J. Chem. Phys. **126**, 244304 (2007).
[24] D. J. Kemp, W. D. Tuttle, F. M. S. Jones, A. M. Gardner, A. Andrejeva, J. C. A. Wakefield, and T. G. Wright, J. Mol. Spectrosc. **346**, 46 (2018).
[25] E. Fermi, Z. Phys. **71**, 250 (1931).
[26] J. R. Gascooke and W. D. Lawrance, J. Chem. Phys. **138**, 134302 (2013).
[27] N. T. Whetton and W. D. Lawrance, J. Phys. Chem. **93**, 5377 (1989).
[28] L. H. Spangler, Annu. Rev. Phys. Chem. **48**, 481 (1997).
[29] R. D. Gordon and J. M. Hollas, Chem. Phys. Lett. **164**, 255 (1989).
[30] J. D. Lewis, T. B. Malloy, Jr., T. H. Chao, and J. Laane, J. Mol. Struct. **12**, 427 (1972).
[31] X. Zhang, J. M. Smith, and J. L. Knee, J. Chem. Phys. **97**, 2843 (1992).
[32] K.-T. Lu, F. Weinhold, and J. C. Weisshaar, J. Chem. Phys. **102**, 6787 (1995).
[33] H. Nakai and M. Kawai, Chem. Phys. Lett. **307**, 272 (1999).
[34] H. Nakai and M. Kawai, J. Chem. Phys. **113**, 2168 (2000).
[35] K. Suzuki, S.-I. Ishiuchi, M. Sakai, and M. Fujii, J. Electron Spectrosc. Relat. Phenom. **142**, 215 (2005).

15.   Summary and conclusions:

This work has focused on a series of spectra recorded with five techniques: resonance-enhanced multiphoton ionisation (REMPI), zero-electron-kinetic-energy (ZEKE), laser-induced fluorescence (LIF), dispersed fluorescence (DF) and two-dimensional laser-induced fluorescence (2D-LIF) spectroscopies.

Our primary focus has been the deduction of the role of the methyl rotor in aiding the mechanism of energy redistribution, through generalisations of Fermi resonances, complex Fermi resonances and more widespread IVR mechanisms; with the emphasis on interactions occurring between modes within the S_1 electronic state. Here, our objective has been to determine which are the dominant factors behind the interactions seen, *i.e.* whether interactions are caused purely by symmetry, and density of states; or if a degree of specificity between modes, in the form of a small difference in quantum numbers, is required for efficient coupling to be observed.

A further objective, specifically applying to the *meta*-disubstituted molecules, has been to understand the effect on torsional structure and torsion-related interactions through modification of the location of the substituent, as well as changing the substituent itself. These are expected to affect the height and phase of the torsional barrier, which can manifest as an energetic shift of the torsional energy levels; this may then lead to the torsional and vibtor levels moving closer, or further apart, from other internal energy levels, thus influencing the extent of any interactions seen. Further to this, modifying the halogen substituent itself will allow deduction of the influence of mass and electronic differences on the magnitude of coupling seen, as the energetic positions of the vibrations and torsions are expected to move as a result of the differences in physical and chemical properties.

Spectra have been collected using a large number of intermediates from each of the three different molecules in question, with multiple energetic regions of pFT initially being discussed. Across these regions, the density of vibrational states is expected to increase greatly, allowing one to probe and understand the types of coupling seen as a function of energy. Through the projection of the intermediates onto different electronic states, namely the S_0 and D_0^+ states, it was inferred that manyfold interactions were occurring; complementary information was gained *via* each technique allowing one to come to a conclusion regarding the assignments of the levels involved in the interactions, and thus the nature, as well as the extent, of the coupling seen. Further to this, from the sheer number of

possible intermediates studied, it was also possible, to a degree, to deduce whether interactions are occurring in the S_0 and D_0^+ states.

The initial set of publications on pFT (Chapters 10, 11 and 12) from this work has helped expand upon previously published details, with these chapters being contributions to a long term, overarching research objective. Initial assignments completed by Lawrance and coworkers[34] have contributed in-depth studies of the low-energy vibrational and torsional structure for the corresponding $S_1 \rightarrow S_0$ transition in pFT, as well as earlier work by the Wright group[11,12,28–30,43] (ZEKE) and the Reid group[11,13–15] (tr-PES), who performed a complimentary analysis of the structure accompanying the $D_0^+ \leftarrow S_1$ transition. Here, we have focussed on three localised regions of the S_1 excited state, namely the 400, 800 and 1200 cm^{-1} internal energy regions.

Chapter 10 began with an in-depth analysis of the S_0 structure *via* a number of S_1 intermediates localised around 400 cm^{-1}, mainly through 2D-LIF and DF spectroscopy, although with comparison from earlier ZEKE studies.[29] Using the assignments and expectations from the earlier work mentioned above, we noted that there were three bright states, 14^2, 29^1 and 11^1, all fairly close in energy. Noticeably, no obvious cross-activity was seen between these modes indicating a lack of significant interactions. With reference to work from Gascooke *et al.*[34] we noted that an intermediate was located coincident with 14^2: the vibtor level, $14^1m^{6(-)}$. We observed that certain fluorescence features in the 2D-LIF spectrum had an unusual rotational profile not seen *via* the large majority of other bands. It was hypothesised by Gascooke *et al.*[34] that interaction between these could be taking the form of a Coriolis-like interaction, where a rotationally-dependent vibration-torsion perturbation was occurring, inducing a distortion of the rotational profile of the band. Further, we demonstrated that three, and potentially more, intermediates were occurring roughly coincident with the $14^2/29^1$ overlapped band, with $20^2m^{6(+)}$, $14^120^2m^2$ and $14^120^2m^1$ all suggested as gaining S_1 intensity *via* coupling to one of the bright states, although the fact that these intermediates were close to coincident, *i.e.* that their energies had not shifted, indicated that the strength of the coupling was likely low. Here, only a small number of restricted IVR interactions were noted, with no obvious indication of widespread coupling.

We then, in Chapter 11, began to look at a series of intermediates appearing at 800 cm^{-1} in the S_1 state. Previous work by Parmenter,[78] in a comparison between pDFB.Ar and pFT.Ar, noted that it was likely that this region was composed mainly of two features that are strongly coupled, with these being the 9^1 fundamental and 29^2 overtone bands located at

797 cm^{-1} and 804 cm^{-1} respectively. This work initially went unseen, with the activity being independently deduced later by Reid *et al*. using picosecond tr-PES.[15] Further to this, high resolution studies of these, as well as other nearby intermediates, were completed by Wright *et al.*[30] employing ZEKE spectroscopy. Here, we used 2D-LIF to further probe this region in order to confirm these assignments, and to elucidate any further interactions that may have gone unnoticed, as the strengths of the 2D-LIF technique allow the discerning of interactions that may have been more difficult to see with tr-PES and ZEKE.

In our 2D-LIF spectrum *via* the 9^1 and 29^2 features, we initially noted that the misleading fluorescence structure of 9_1 leads one to believe that both eigenstates have similar compositions. We observed, however, that non-diagonal FCFs caused this illusion, with us observing a significantly larger 9_2 band *via* the 797 cm^{-1} eigenstate. This indicated that the majority of the fluorescence was indeed located in the D_9 coordinate, thus the 797 cm^{-1} band had a larger contribution from D_9, with the 804 cm^{-1} eigenstate corresponding mostly to $2D_{29}$. Furthermore, 9_1 and 29_2 are energetically close-by in S_0, thus we hypothesised that an interaction was also occurring in the ground state which further complicated the fluorescence intensity distribution between these bands. We argued that the character of the 9^1 and 29^2 intermediates could also be characterised by looking at Herzberg-Teller active fluorescence transitions which are expected to be induced *via* symmetric in-plane vibrations, such as 9^1. We therefore used the presence of stronger transitions to b_2 vibrational levels, such as 29_1 and 28_1, *via* the 797 cm^{-1} intermediate to come to the same conclusion as above that the 797 cm^{-1} eigenstate contained more 9^1 than 29^2 character, and *vice versa* for the 804 cm^{-1} eigenstate.

We also discussed the presence of many other intermediates, several of which were expected in the form of combination and overtone bands from those seen *via* the 400 cm^{-1} region previously discussed in Chapter 10. A number of vibrational and vibtor intermediates appeared energetically coincident with the 29^2 eigenstate and a large amount of this activity specifically included 14^x vibrations. A number of these were expected lower in energy than we observed, indicating that multiple interactions were likely occurring, potentially with 9^1, effectively shifting the intermediates upwards in wavenumber. Further to this, we considered the interpretation of the picosecond tr-PES data examined by Davies and Reid[15] which suggested that upon exciting the $9^{1\cdots}29^2$ Fermi resonance with a ~13 cm^{-1} wide ps laser pulse, rapid decay of only one of the torsional components was seen. This was hypothesised as arising from a rotation-dependent interaction between two coherently excited levels, such that a mismatch in rotational constants is created; this caused an *m*-specific destructive

interference between those excited levels, known as rotational dephasing. However, we noted that our ns data did not demonstrate such a loss of signal for one of the levels, and thus it was concluded that this must occur in the tr-PES study as a result of the wavepacket dynamics arising from preparing the states in a coherent fashion. We observed, however, that there were only two vibtors, that we can detect, that could undergo the m-specific interactions that may have led to rotational dephasing, with the candidates being the $14^3m^{6(-)}$ and $14^320^2m^x$ intermediates. By analogy with the 400 cm^{-1} region, in which we saw a rotationally dependent interaction between $14^1m^{6(-)}$ and 14^2m^0, we suggested that this interaction was likely between the $14^3m^{6(-)}$ and 14^4 intermediates, for both of which we observed activity. Notably, evidence for restricted IVR was observed within this region despite the increasing density of states. Further to this, interactions that were seen in this region involved similar levels that were involved in the hypothesised couplings *via* the 400 cm^{-1} region, which indicated that the specific nature of the levels involved may be important in deducing whether or not they can couple to the nearby bright states.

In Chapter 12 we explored the final part of our study of pFT: the 1200 cm^{-1} region. This region exhibited two totally-symmetric, in-plane vibrations, D_6 and D_5 at 1195 cm^{-1} and 1231 cm^{-1}, which appeared with roughly similar intensities in the REMPI spectrum. Both the 2D-LIF spectrum and the ZEKE spectra, however, were starkly different in that those recorded *via* D_5 were seen to be significantly less intense than those seen when exciting *via* D_6, indicating widespread dissipative IVR *via* D_5 only. A number of the intermediates expected within this region were from mixtures of overtones and combinations that appeared in the 400 cm^{-1} and 800 cm^{-1} wavenumber regions, thus the number of possible states which could couple was expected to be high; it is, then, somewhat unsurprising that widespread IVR should be occurring here, but surprising that the difference in the magnitude of coupling of D_5 was so different to that of D_6. Similarly, we compared our structure to that of the tr-PES study of Reid and coworkers,[12] where they prepared each of the 5^1 and 6^1 dominated eigenstates separately (as they are too far apart to excite coherently). They noted that their signal *via* the 6^1 dominated eigenstate decayed to roughly 50% within 100 ps, and the 5^1 dominated eigenstate had decayed to 10% within the same range of time. Their interpretation was that only one of the torsional components of the 6^1 eigenstate decayed, similar to the decay mechanism previously seen *via* the 800 cm^{-1} eigenstates. However, both our ZEKE and 2D-LIF spectra did not agree with this; we observed highly structured spectra that was not indicative of notable decay of either m component. Once again, evidence of two possible intermediates that could induce torsion-specific interactions were noted ($9^120^2m^{6(+)}$ and $17^119^129^1m^{3(+)}$),

which could both lead to rotational dephasing in the tr-PES study. We suggested that $9^1 20^2 m^{6(+)}$ could potentially mirror the same vibtor interaction we saw in the 400 cm^{-1} region *via* $20^2 m^{6(+)}$, and that this was the cause of the rotation dependent interaction seen in the tr-PES study. This, once again, promotes the idea that a degree of specificity between modes of the same symmetry is required for efficient coupling to be observed. Similarly, with D_5, we noted that there was a fluorescence feature corresponding to $18_1 m_2$ which had previously been demonstrated to be a signature of doorway state IVR.[43] Here, it is possible that population of the bright state, in this case $5^1 m^1$, is lost through to a bath of states through an indirect coupling mechanism *via* the $9^1 18^2 m^1$ doorway state, which is expected to be close in energy to 5^1. We discussed this interaction as an explanation for lack of intensity of the features seen in the 2D-LIF and ZEKE spectra *via* this eigenstate, as well as a further argument for the rotational dephasing seen in the tr-PES study. We did not detect any further vibtor interactions that could perturb $5^1 m^0$, although it is clear that some interaction must be occurring to cause the further dephasing observed in the time-resolved spectra. Notably, we saw the total number of symmetry allowed states that can couple was greater nearer D_5 than it was D_6, but not by a large margin. This suggests that the original idea that the rate of coupling is related purely to the density of states[5–10] is not strictly true, and that the nature of both the bright and dark states is important in determining the efficiency of the observable coupling interactions.

Although not a featured publication in this work, analysis of a number of ZEKE and 2D-LIF spectra in the 1015 cm^{-1} region of *p*FT[41] was undertaken, concurrent with other regions presented in this work, and is outlined briefly here. This work focused on S$_1$ intermediates occurring in a narrow range at about 1015 cm^{-1}, *i.e.* between the 800 and 1200 cm^{-1} regions. We noted that the 800 cm^{-1} region is within the restricted IVR regime, whereas the 1200 cm^{-1} contains elements of statistical IVR, thus it is of interest to see what character this feature exhibited. The 1015 cm^{-1} feature appeared broad in the REMPI spectrum, suggesting that there were multiple contributions. We noted that there was a great deal of fine structure, starting to appear at 1000 cm^{-1} in the 2D-LIF spectrum which looked relatively broad, indicating that a significant amount of IVR was likely occurring. Upon assignment of the plethora of bands in the 2D-LIF spectrum, we noted that there were at least 15 contributing intermediates, with the main bright states being identified as 17^2 and 13^2 with the presence of other, less intense, bright states: $29^1 30^2$ and $14^1 18^1 29^1$. It was notable that there was no evidence for direct coupling of the bright states, despite the intermediates being very close in wavenumber, but in fact each was coupled to an independent set of dark states, indicating

a situation approaching a statistical IVR description. Similarly, each of the states that were coupled together had a change in vibrational and/or torsional quantum number of three, consistent with the states needing to be close in quantum number, and having similar character, to interact. Although it is not straightforward to ascertain the explicit motion of these heavily mixed vibration/torsional combinations, this adds weight to the conclusions previously discussed above in that the magnitude of coupling must be strongly related to the relative motions of the states involved.

Previous ideas, seen in the literature,[79–81] suggested that symmetry was the key factor influencing IVR rate. These suggestions, however, did not consider jet-cooled molecules and/or used ultrafast techniques with a broad laser pulse, thus other factors may be expected to contribute to the activity seen in those studies. The conclusions from this work matches those from previous studies published within this project[31], which compared the activity from a range of intermediates across four similar molecules, *para*-difluorobenzene (*p*DFB), *para*-chlorofluorobenzene (*p*ClFB), *para*-fluorotoluene (*p*FT) and *para*-xylene (*p*Xyl). This comparison allowed for independent identification of the influence of point group symmetry and the presence of methyl groups on the IVR rates observed; notably, it was demonstrated that *p*Xyl had more extensive coupling than both *p*FT and *p*ClFB, despite being represented by a higher-symmetry point group. The presence of the double rotor was also shown to greatly increase the extent of IVR with respect to both single rotor and rotorless systems. This demonstrated that density of states, but not necessarily the point group, does play an important role in the facilitating of coupling, although it was also noted that the build-up of the density of states is erratic due to differences on a molecular basis, meaning that the presence of a significant number of bath states in proximity to the ZOB can be viewed as being serendipitous.

In conclusion, we know, as has previously been demonstrated,[29,34] that methyl-dependent coupling appears lower than 400 cm^{-1} in *p*FT where, compared to molecules without a rotor such as *p*DFB and *p*ClFB, no obvious coupling is seen in that energetic region. We demonstrated that as one starts to move up in energy, the extent of coupling in *p*FT facilitated by vibration-torsion interactions increases, with the number of interactions seen *via* the 800 cm^{-1} region being higher than that at 400 cm^{-1}, and then this increases again by the 1015 and 1200 cm^{-1} regions; this is, in part, related to the density of states, although is not purely related to the point group as previously suggested. We saw that both D_5 and D_6 have a relatively similar number of symmetry-allowed vibtors close-by that may interact with them, but widespread IVR is only seen *via* D_5. Similarly, in the 1015 cm^{-1} region, we saw that

a number of ZOBS appear coincident with one another, but with no evidence for them interacting together. Instead, they interacted exclusively through an independent set of dark states, of which the states were related by relatively small changes in the torsional and vibrational quantum numbers. We then demonstrated that there is a distinct repetition of 'signature indications' of torsion-related coupling, specifically the presence of the $18_1 m_2$ band previously discussed in the 845 cm^{-1} region of pFT[43] was also seen *via* D_5, which has been shown to be an indication of doorway state IVR, and which we believe is also a contributing factor in the widespread coupling seen *via* D_5. Once again, these points all indicate that the efficiency of the coupling between states is likely linked to their characters, as well as the density of states, with these being the key factors in determining the form of IVR that is observed.

Further to this point, we commented on the use of tr-PES as a technique for elucidating torsion specific coupling pathways, and we noted that rotation-dependent interactions may cause a dephasing effect, and this can be incorrectly interpreted as widespread dissipative IVR. We noted that the loss of signal was only seen in the time-resolved experiment, and not reflected in our work, and was concluded to occur as a result of rotation-dependent perturbations. Such interactions influenced the spacing between the interacting vibtor levels within the wavepacket, enough to cause a destructive interference effect which dramatically reduced the signal. Thus, we suggest that caution is merited if one is purely using time-resolved experimentation, and comparison to frequency-resolved experiment is desirable if available.

Following this, we identified and analysed the low-energy (0-350 cm^{-1}) regions for both mFT and mClT. This work was a foray into the study of *meta*-disubstituted systems that has largely gone untouched in the literature. mFT and mClT both belong to lower symmetry groups with respect to pFT. The result of this is that the density of same-symmetry states is expected to significantly increase which should have, given the conclusions of previous work, led to a greater rate of vibration and torsion facilitated coupling. Symmetry aside, the positioning of the substituent is expected to directly affect the electronic properties and mass distribution of the molecule, such that vibrational modes are expected to change in both motion as well as energetically. Furthermore, upon excitation and (especially) ionisation, geometric distortions are expected, with the effects of this on the rotor levels being anticipated to be much greater than seen in pFT due to the significantly heightened torsional barrier. These factors are all likely to directly modify the extent of vibration and torsion-enabled interactions, originally noted by Parmenter *et al.*[5]

In Chapters 13 and 14, we initially commented on the vibrational and torsional structure seen *via* both *m*FT and *m*ClT, noting that electronic and mass differences between the two induces a modification to the vibrational modes, such that different interactions may be expected to be observed. We noted that within the 0-350 cm^{-1} region, the majority of the structure is seen to be the same for both molecules, albeit with slight changes in geometry occurring upon excitation and ionisation, which manifested as a modification to the FCFs. A particular example was $^{+}m^5$ and $^{+}30^1m^2$ in *m*ClT which Feldgus *et al.*[45] suggested were in Fermi resonance in the cation, whereas analysis of a variety of other intermediates showed that this was not the case, further evincing that changes in electronic properties can induce varying intensity patterns and, thus, care is required when interpreting such structure. Furthermore, interactions in *m*ClT were more prevalent than in *m*FT, where at least 3 restricted interactions were confirmed – demonstrating that simply changing the substituent can perturb the energy levels enough such that distinctly different interactions can be induced. Additionally, the extent of coupling seen within this energetic region for the G_6 molecules, *m*FT and *m*ClT, compared to the G_{12} molecule, *p*FT, was not significantly different. Both the Lawrance[34] and Wright[29] groups have previously discussed that two out-of-plane vibrational modes coupled strongly to the rotor in *p*FT. Here, it was seen that there were two, perhaps three, vibrational modes that couple to the torsion in both *m*FT and *m*ClT, with two of these also being out-of-plane vibrational modes. If the argument related to increased coupling as a result of a reduction in symmetry were to hold, then one would expect the extent of coupling seen in the G_6 molecules to be higher which, in this energetic region at least, does not seem to be the case. Comparing the forms of vibrations that couple to the torsion, however, adds weight to the idea that the nature of the vibration, in this case high amplitude out-of-plane bends, is important in deducing whether or not efficient coupling is expected.

We noted that for the G_6 MSG molecules, *m*FT and *m*ClT, the V_3 barrier heights in both S$_1$ and D$_0^+$ are notably higher than the V_6 value for the G_{12} molecule, *p*FT, and we discussed the origin of the barrier as well as the implications of it. We noted that upon excitation to the S$_1$ state, there is a near 10-fold increase in barrier height for both the *m*FT and *m*ClT molecules. The reasoning behind this, though, is unclear as a fine balance of electronic and steric effects can be seen to impact this property. We noted that in our ZEKE spectra, we saw an intensity pattern related to the vibtors that we had not previously seen, in that the Δm=0 transitions were no longer the most intense with the Δm=3 transitions becoming so. This was rationalised as arising from a change in the phase of the torsional potential, linked to a

change in preferred conformation of the methyl rotor upon ionisation. Further to this, the energy gaps between the torsions indicated an additional 3-fold increase in barrier height upon ionisation. It can be seen that, upon ionisation, two regions of localised positive charge adjacent to the C-CH$_3$ and C-F (or C-Cl) bonds are created. We hypothesised that it is likely that the δ+ charge of the hydrogen atoms in the C-H bonds of the methyl rotor orient themselves in a position to minimise coulombic repulsion with the localised positive charges within the ring, although this cannot be the sole factor that induced such a large barrier as the height was also large in the S$_1$ state, albeit without the localised regions of charge. We also noted that the cationic barrier in *m*ClT was seen to be slightly lower than in *m*FT, likely due to the decreased inductive effect of the Cl atom, which destabilises the ring to a lesser extent than the F atom.

Further, for both *m*FT and *m*ClT molecules, we noted a series of cationic vibtor transitions involving the D_{30} out-of-plane vibration were all on the order of 10 cm^{-1} lower than expected, and the FCFs involving transitions to these levels had a different intensity pattern to other vibtor levels seen. We hypothesised that a coupling of the ring-localised vibration with the torsional levels occurs such that the torsional hindrance is lowered as a result of the vibrational motion, leading to a decrease in torsional potential as a function of the vibration – this has not previously been explicitly demonstrated to our knowledge, but is a further factor affecting the serendipitous nature of the positions of the energy levels.

In conclusion, this work has demonstrated that the presence of torsions often complicates the individual structure seen within experimental spectra. We note that the degree of torsion-related interactions depends mainly on two factors:

(i) The density of states: This is expected to rise greatly as a function of energy, thus coupling may be expected to be more prevalent towards higher internal energy. Additionally, mass and electronic effects caused by modifying the substituent can serendipitously cause a large number of compatible levels to appear close enough in energy to interact. Further to this, the barrier height can 'reposition' torsional energy levels, such that coupling interactions do not always occur in the same energetic region for different molecules, where there is also the added complication that there may be a vibrational dependence on the barrier height, and hence some vibration-torsion levels will also not appear where they are expected; (ii) the nature of the energy levels, whereby these do not always interact significantly to first order, even if close in energy and of the correct symmetry. The levels observed to couple in this work, particularly where strong coupling is seen, are often seen multiple times in slightly

modified forms across many spectra, with a number of the interacting states only having relatively small changes in quantum numbers between them, further adding weight to the idea that coupling is very specific to the modes involved.

16.   Future Work:

Over the last 50 years, substituted benzenes have been subjected to a large amount of work using a variety of spectroscopic techniques. We introduced this work by suggesting that the end goal was to understand the photophysics of larger biomolecules, particularly those that occur commonly in nature, such as the amino acids: tyrosine and phenylalanine. The methodology behind this was to use a bottom-up approach, beginning with simple substituted systems, to study interactions as a function of both the location of the substituent, as well as the nature of certain functional groups. A natural extension to our studies, then, would involve moving to other forms of molecules, where we began in this work to look at the *meta*-counterparts of molecules that are relative well understood. More challenging molecules of the same variety could also be studied, such as *meta*-xylene; this could be compared to previous work on *para*-xylene[25,26] where, here, a large increase in the density of states, as well as the influence of increased torsional barrier height could be further explored. It is, perhaps, expected that the rate of coupling seen here would dramatically increase with respect to *meta*-fluorotoluene, but the anticipated changes to the torsional energy level positions is also expected to have an impact on where, and how, the coupling is manifested.

Alternatively, one can also begin to look towards other classes of molecules such as pyrroles and their methylated counterparts. Several pyrrole analogues have forbidden electronic transitions to the S_1 state, thus the vibrational structure that is seen must gain intensity by other means. It would, therefore, be interesting to see how FC forbidden levels interact with one another, and to what extent this is seen. Further to this point, and discussed earlier, the use of two-photon excitation can allow one to modify the vibrational selection rules and see transitions that are nominally forbidden. From this, one can gain insight into the differences in the forms of coupling seen between two different forms of transitions. Ideally, this would be done with a combination of frequency and time-resolved experimentation to yield a more complete picture of the interactions occurring. Notably, data has already been collected for *N*-methylpyrrole within this project. There is a small amount of analysis of this molecule in the literature, with earlier work on the energetics of the excited states[82,83] being completed although, in more recent times, research has particularly focused on the excited state

structure[84–86] and dynamics[87,88], as well as low internal energy fluorescence studies.[86] Notably, high-resolution studies of the cation have not yet been tackled, thus is currently being worked on by us. Additionally, one would eventually like to try more complicated molecules, although there is the difficulty in that many of these have particularly low vapor pressures and can be difficult to get into the gas phase, thus some thought must be given on how to proceed with this. A possibility is to rework the nozzle/valve combination such that heating to high temperature is allowed; this has been employed by the Leutwyler in order to perform REMPI spectroscopy on a number of different bioanalogues,[89–93] but it is unclear whether or not this would yield enough vapour for one to perform ZEKE spectroscopy, for which signal is often more difficult to attain compared to REMPI spectroscopy.

The majority of studies on systems similar to those discussed in this work occur in the gas phase, whereby the energy levels and dynamics related to a large number of coupled states are now reasonably well understood. As such, it may be time to advance these concepts to include the effects of solvation. The literature contains various examples of complexes formed with some of the molecules discussed here, namely the work by Parmenter *et al.* on *p*DFB.Ar/He[94–97] and *p*FT-Ar complexes[78,98]. Furthermore, as this work is the basis of a biological study, it makes some sense to investigate the effects of naturally occurring solvents where, the most common of which, especially within our bodies, is water. Examples of this can be seen in the literature, with LIF studies of *para*-fluorophenol.H_2O by Chakraborty,[99] as well as the REMPI/IR-UV hole burning study on anisole.H_2O by Brutschy and Tarakeshwar[100], with further high-resolution work from Demtroeder *et al.*[101] In the literature, studies involving complexation between two molecules are the most commonly seen, thus probing complexes involving multiple molecules would be an ideal direction for this research. This would allow one to see the influence of the van der Waals' interactions on both intermolecular and intramolecular energy redistribution as a function of the number of molecules in the complex. It is worth noting, however, that it is especially difficult to obtain appreciable number densities of these in a jet-expansion, thus signal is often too low to yield any meaningful information. Furthermore, it is sometimes difficult to elucidate transitions from complexes as they are expected to be weaker, and sometimes overlapped, with their non-complexed counterparts. It is possible that one could use a mass-resolved experiment such as REMPI to first map out the internal energy levels of the complex and, following this, photoelectron spectroscopy techniques, both in the time and frequency domain, and/or fluorescence spectroscopy can be used to probe the intermediate levels.

Ideally, this work has provided a foundation which may be used as a basis for understanding a wide number of molecules within the domain of aromatic systems, where the future path of this field of work is seemingly unending with the large number of possible routes that can be taken.

17. References:

1   S. E. Whitmore, C. S. Potten, C. A. Chadwick, P. T. Strickland and W. L. Morison, *Photodermatol. Photoimmunol. Photomed.*, 2001, **17**, 213–217.

2   D. Herring, Formation of thymine dimer lesion in DNA., https://en.wikipedia.org/wiki/Pyrimidine_dimer#/media/File:DNA_UV_mutation.svg

3   A. Besaratinia, J. Yoon, C. Schroeder, S. E. Bradforth, M. Cockburn and G. P. Pfeifer, *FASEB J.*, 2011, **25**, 3079–3091.

4   R. Losantos, I. Funes-Ardoiz, J. Aguilera, E. Herrera-Ceballos, C. García-Iriepa, P. J. Campos and D. Sampedro, *Angew. Chemie - Int. Ed.*, 2017, **56**, 2632–2635.

5   P. J. Timbers, C. S. Parmenter and D. B. Moss, *J. Chem. Phys.*, 1994, **100**, 1028–1034.

6   R. A. Coveleskie, D. A. Dolson and C. S. Parmenter, *J. Phys. Chem.*, 1985, **89**, 645–654.

7   R. A. Coveleskie, D. A. Dolson and C. S. Parmenter, *J. Phys. Chem.*, 1985, **89**, 655–665.

8   K. W. Holtzclaw and C. S. Parmenter, *J. Chem. Phys.*, 1986, **84**, 1099–1118.

9   D. A. Dolson, K. W. Holtzclaw, D. B. Moss and C. S. Parmenter, *J. Chem. Phys.*, 1986, **84**, 1119–1132.

10   D. B. Moss and C. S. Parmenter, *J. Chem. Phys.*, 1993, **98**, 6897–6905.

11   J. A. Davies, A. M. Green, A. M. Gardner, C. D. Withers, T. G. Wright and K. L. Reid, *Phys. Chem. Chem. Phys.*, 2014, **16**, 430–443.

12   C. J. Hammond, V. L. Ayles, D. E. Bergeron, K. L. Reid and T. G. Wright, *J. Chem. Phys.*, 2006, **125**, 1–8.

13   J. A. Davies and K. L. Reid, *J. Chem. Phys.*, 2011, **135**, 1–15.

14   J. A. Davies, K. L. Reid, M. Towrie and P. Matousek, *J. Chem. Phys.*, 2002, **117**, 9099–9102.

15   J. A. Davies and K. L. Reid, *Phys. Rev. Lett.*, 2012, **109**, 193004.

16   K. Okuyama, N. Mikami and M. Ito, *J. Phys. Chem.*, 1985, **89**, 5617–5625.

17   K. Takazawa, M. Fujii and M. Ito, *J. Chem. Phys.*, 1993, **99**, 3205–3217.

18   M. Ito, K. Takazawa and M. Fujii, *J. Mol. Struct.*, 1993, **292**, 9–16.

19   K. T. Lu, G. C. Eiden and J. C. Weisshaar, *J. Phys. Chem.*, 1992, **96**, 9742–9748.

20   R. A. Walker, E. Richard, K. T. Lu, E. L. Sibert and J. C. Weisshaar, *J. Chem. Phys.*, 1995, **102**, 8718–8724.

21   K. T. Lu, F. Weinhold and J. C. Weisshaar, *J. Chem. Phys.*, 1995, **102**, 6787–6805.

22   K.-T. Lu and J. C. Weisshaar, in *Laser Techniques for State-Selected and State-to-State Chemistry II*, ed. Hepburn, JW, 1994, vol. 2124, pp. 348–359.

23   A. M. Gardner, A. M. Green, V. M. Tamé-Reyes, V. H. K. Wilton and T. G. Wright, *J. Chem. Phys.*, 2013, **138**, 134303.

24   A. M. Gardner, A. M. Green, V. M. Tamé-Reyes, K. L. Reid, J. A. Davies, V. H. K. Parkes and T. G. Wright, *J. Chem. Phys.*, 2014, **140**, 114308.

25   W. D. Tuttle, A. M. Gardner, K. B. O'Regan, W. Malewicz and T. G. Wright, *J. Chem. Phys.*, 2017, **146**, 124309.

26   A. M. Gardner, W. D. Tuttle, P. Groner and T. G. Wright, *J. Chem. Phys.*, 2017, **146**, 124308.

27   D. E. Bergeron, V. L. Ayles, O. J. Richards and T. G. Wright, *Chem. Phys. Lett.*, 2006, **430**, 282–286.

28   V. L. Ayles, C. J. Hammond, D. E. Bergeron, O. J. Richards and T. G. Wright, *J. Chem. Phys.*, 2007, **126**, 244304.

29   A. M. Gardner, W. D. Tuttle, L. Whalley, A. Claydon, J. H. Carter and T. G. Wright, *J. Chem. Phys.*, 2016, **145**, 0–23.

30   W. D. Tuttle, A. M. Gardner, L. E. Whalley and T. G. Wright, *J. Chem. Phys.*, 2017, **146**, 244310.

31   W. D. Tuttle, A. M. Gardner, L. E. Whalley, D. J. Kemp and T. G. Wright, *Phys. Chem. Chem. Phys.*, 2019, **21**, 14133–14152.

32   J. R. Gascooke, E. A. Virgo and W. D. Lawrance, *J. Chem. Phys.*, 2015, **142**, 0–13.

33   J. R. Gascooke and W. D. Lawrance, *J. Chem. Phys.*, 2013, **138**, 134302.

34   J. R. Gascooke, L. D. Stewart, P. G. Sibley and W. D. Lawrance, *J. Chem. Phys.*, 2018, **149**, 074301.

35   J. R. Gascooke, E. A. Virgo and W. D. Lawrance, *J. Chem. Phys.*, 2015, **143**, 044313.

36   J. R. Gascooke and W. D. Lawrance, *J. Mol. Spectrosc.*, 2015, **318**, 53–63.

37   E. A. Virgo, J. R. Gascooke and W. D. Lawrance, *J. Chem. Phys.*, 2014, **140**, 154310.

38   L. D. Stewart, J. R. Gascooke and W. D. Lawrance, *J. Chem. Phys.*, 2019, **150**, 174303.

39   D. J. Kemp, A. M. Gardner, W. D. Tuttle and T. G. Wright, *Mol. Phys.*, 2019, **117**, 3011–3026.

40   D. J. Kemp, L. E. Whalley, A. M. Gardner, W. D. Tuttle, L. G. Warner and T. G. Wright, *J. Chem. Phys.*, 2019, **150**, 064306.

41   A. M. Gardner, L. E. Whalley, D. J. Kemp, W. D. Tuttle and T. G. Wright, *J. Chem. Phys.*, 2019, **151**, 154302.

42   D. J. Kemp, W. D. Tuttle, A. M. Gardner, L. E. Whalley and T. G. Wright, *J. Chem. Phys.*, 2019, **151**, 064308.

43   A. M. Gardner, W. D. Tuttle, L. E. Whalley and T. G. Wright, *Chem. Sci.*, 2018, **9**, 2270–2283.

44 D. J. Kemp, E. F. Fryer, A. R. Davies and T. G. Wright, *J. Chem. Phys.*, 2019, **151**, 084311.

45 S. H. Feldgus, M. J. Schroeder, R. A. Walker, W. K. Woo and J. C. Weisshaar, *Int. J. Mass Spectrom. Ion Process.*, 1996, **159**, 231–244.

46 G. Herzberg, *Electronic Spectra and Electronic Structure of Polyatomic Molecules‵Van*, Van Nostrand, 1966.

47 G. Herzberg and S. Mrozowski, *Molecular Spectra and Molecular Structure. I. Spectra of Diatomic Molecules*, Van Nostrand, 1951, vol. 19.

48 J. M. Hollas, *Modern Spectroscopy*, Wiley, Fourth Edi.

49 F. Hund, *Z. Phys.*, 1925, **33**, 345–371.

50 A. Jablonski, *Nature*, 1933, **131**, 839–840.

51 M. Kasha, *Discuss. Faraday Soc.*, 1950, **9**, 14–19.

52 M. Born and R. Oppenheimer, *Ann. Phys.*, 1927, **389**, 457–484.

53 G. Herzberg and E. Teller, *Z. Phys. Chem*, 2017, **21B**, 410–446.

54 D. J. Kemp, A. M. Gardner, W. D. Tuttle, J. Midgley, K. L. Reid and T. G. Wright, *J. Chem. Phys.*, 2018, **149**, 094301.

55 J. Scott Miller and E. D. Poliakoff, *J. Chem. Phys.*, 2000, **113**, 899–902.

56 G. J. Rathbone, E. D. Poliakoff, J. D. Bozek and R. R. Lucchese, *Can. J. Chem.*, 2004, **82**, 1043–1051.

57 J. S. Miller, E. D. Poliakoff, T. F. Miller, A. P. P. Natalense and R. R. Lucchese, *J. Chem. Phys.*, 2001, **114**, 4496–4504.

58 E. Fermi, *Z. Phys.*, 1931, **71**, 250–259.

59 B. T. Darling and D. M. Dennison, *Phys. Rev.*, 1940, **57**, 128–139.

60 W. D. Tuttle, *Ph.D Thesis*, University of Nottingham, 2018.

61 G. Herzberg, *Molecular Spectra and Molecular Structure II: Infrared and Raman of Polyatomic Molecules*, Van Nostrand, 1956.

62 F. Duschinsky, *Acta Physicochim. URSS*, 1937, **7**, 551–566.

63 K. P. Huber and G. Herzberg, *Molecular Spectra and Molecular Structure*, Springer US, Boston, MA, 1979.

64 R. S. Mulliken, *Phys. Rev.*, 1930, **36**, 611–629.

65 E. B. Wilson, *Phys. Rev.*, 1934, **45**, 706–714.

66 G. Varsányi, *Assignments for Vibrational Spectra of 700 Benzene Derivatives*, Wiley, 1974.

67 A. M. Gardner and T. G. Wright, *J. Chem. Phys.*, 2011, **135**, 114305.

68   A. Andrejeva, A. M. Gardner, W. D. Tuttle and T. G. Wright, *J. Mol. Spectrosc.*, 2016, **321**, 28–49.

69   W. D. Tuttle, A. M. Gardner, A. Andrejeva, D. J. Kemp, J. C. A. Wakefield and T. G. Wright, *J. Mol. Spectrosc.*, 2018, **344**, 46–60.

70   D. J. Kemp, W. D. Tuttle, F. M. S. Jones, A. M. Gardner, A. Andrejeva, J. C. A. Wakefield and T. G. Wright, *J. Mol. Spectrosc.*, 2018, **346**, 46–59.

71   L. H. Spangler, *Annu. Rev. Phys. Chem.*, 1997, **48**, 481–510.

72   E. C. Richard, R. A. Walker and J. C. Weisshaar, *J. Chem. Phys.*, 1996, **104**, 4451–4469.

73   D. J. Kemp, L. E. Whalley, W. D. Tuttle, A. M. Gardner, B. T. Speake and T. G. Wright, *Phys. Chem. Chem. Phys.*, 2018, **20**, 12503–12516.

74   H. C. Longuet-Higgins, *Mol. Phys.*, 1963, **6**, 445–460.

75   P. R. Bunker and P. Jensen, *Molecular Symmetry and Spectroscopy*, NRC Research Press, 2006.

76   M. J. Frisch, et al, G. W. Trucks, H. B. Schlegel, G. E. Scuseria, M. A. Robb, J. R. Cheeseman, G. Scalmani, V. Barone, G. A. Petersson, H. Nakatsuji, X. Li, M. Caricato, A. V Marenich, J. Bloino, B. G. Janesko, R. Gomperts, B. Mennucci, H. P. Hratchian, J. V Ortiz, A. F. Izmaylov, J. L. Sonnenberg, D. Williams-Young, F. Ding, F. Lipparini, F. Egidi, J. Goings, B. Peng, A. Petrone, T. Henderson, D. Ranasinghe, V. G. Zakrzewski, J. Gao, N. Rega, G. Zheng, W. Liang, M. Hada, M. Ehara, K. Toyota, R. Fukuda, J. Hasegawa, M. Ishida, T. Nakajima, Y. Honda, O. Kitao, H. Nakai, T. Vreven, K. Throssell, J. A. Montgomery Jr., J. E. Peralta, F. Ogliaro, M. J. Bearpark, J. J. Heyd, E. N. Brothers, K. N. Kudin, V. N. Staroverov, T. A. Keith, R. Kobayashi, J. Normand, K. Raghavachari, A. P. Rendell, J. C. Burant, S. S. Iyengar, J. Tomasi, M. Cossi, J. M. Millam, M. Klene, C. Adamo, R. Cammi, J. W. Ochterski, R. L. Martin, K. Morokuma, O. Farkas, J. B. Foresman and D. J. Fox, *Gaussian16*, Wallingford CT, Revision C., 2016.

77   D. J. Kemp, L. G. Warner and T. G. Wright, *J. Chem. Phys.*, 2020, **152**, 064303.

78   Z.-Q. Zhao and C. S. Parmenter, *Ber. Bunsenges. Phys. Chem.*, 1995, **99**, 536–543.

79   L. W. Peng, B. W. Keelan, D. H. Semmes and A. H. Zewail, *J. Phys. Chem.*, 1988, **92**, 5540–5549.

80   M. Hippler, R. Pfab and M. Quack, *J. Phys. Chem. A*, 2003, **107**, 10743–10752.

81   R. S. von Benten, Y. Liu and B. Abel, *J. Chem. Phys.*, 2010, **133**, 134306.

82   R. McDiarmid and X. Xing, *J. Chem. Phys.*, 1996, **105**, 867–873.

83   C. D. Cooper, A. D. Williamson, J. C. Miller and R. N. Compton, *J. Chem. Phys.*, 1980, **73**, 1527–1537.

84   J. G. Philis, *Chem. Phys. Lett.*, 2002, **353**, 84–88.

85   J. G. Philis, *J. Mol. Struct.*, 2003, **651**–**653**, 567–570.

86   N. Biswas, S. Wategaonkar and J. G. Philis, *Chem. Phys.*, 2003, **293**, 99–109.

87   G. Wu, S. P. Neville, O. Schalk, T. Sekikawa, M. N. R. Ashfold, G. A. Worth and A. Stolow, *J. Chem. Phys.*, 2016, **144**, 014309.

88   A. G. Sage, M. G. D. Nix and M. N. R. Ashfold, *Chem. Phys.*, 2008, **347**, 300–308.

89   S. Lobsiger, H.-M. Frey, S. Leutwyler, P. Morgan and D. Pratt, *J. Phys. Chem. A*, 2011, **115**, 13281–13290.

90   S. Lobsiger, M. A. Trachsel, T. Den and S. Leutwyler, *J. Phys. Chem. B*, 2014, **118**, 2973–2984.

91   M. A. Trachsel, T. Wiedmer, S. Blaser, H.-M. Frey, Q. Li, S. Ruiz-Barragan, L. Blancafort and S. Leutwyler, *J. Chem. Phys.*, 2016, **145**, 134307.

92   M. A. Trachsel, S. Lobsiger, T. Schär, L. Blancafort and S. Leutwyler, *J. Chem. Phys.*, 2017, **146**, 244308.

93   M. A. Trachsel, S. Blaser, L. Siffert, T. Wiedmer and S. Leutwyler, *J. Chem. Phys.*, 2019, **151**, 124301.

94   O. Hye-Keun, C. S. Parmenter and M. C. Su, *Ber. Bunsenges. Phys. Chem*, 1988, **92**, 253–258.

95   K. W. Butz, D. L. Catlett, G. E. Ewing, D. Krajnovich and C. S. Parmenter, *J. Phys. Chem.*, 1986, **90**, 3533–3541.

96   B. D. Gilbert, C. S. Parmenter and H.-K. Oh, *J. Phys. Chem.*, 1995, **99**, 2444–2458.

97   M.-C. Su, H.-K. O and C. S. Parmenter, *Chem. Phys.*, 1991, **156**, 261–280.

98   Z.-Q. Zhao and C. S. Parmenter, *Ber. Bunsenges. Phys. Chem*, 1995, **99**, 536–543.

99   D. P. Mukhopadhyay, S. Biswas and T. Chakraborty, *J. Phys. Chem. A*, 2016, **120**, 9159–9169.

100   B. Reimann, K. Buchhold, H.-D. Barth, B. Brutschy, P. Tarakeshwar and K. S. Kim, *J. Chem. Phys.*, 2002, **117**, 8805–8822.

101   M. Becucci, G. Pietraperzia, M. Pasquini, G. Piani, A. Zoppi, R. Chelli, E. Castellucci and W. Demtroeder, *J. Chem. Phys.*, 2004, **120**, 5601–5607.